

**1,2-Diarylethene Molecular Switches Connecting Cobalt and Iron
Metallocenes**

Dissertation

with the aim of achieving a doctoral degree
at the Faculty of Mathematics, Informatics and Natural Sciences
Department of Chemistry
of Universität Hamburg

submitted by

Alejandra Escribano Sanvicente

from Vitoria-Gasteiz, Spain

Hamburg 2015

Declaration on oath

I hereby declare on oath, that I have written the present dissertation by my own and have not used other than the acknowledged resources and aids. I hereby declare that I have not previously applied or pursued for a doctorate (Ph.D. studies).

Hamburg, 19.05.2015

The present work was carried out in the period from October 2009 to May 2015 in the Institute of Inorganic and Applied Chemistry of the University of Hamburg in the research group of Prof. Dr. Jürgen Heck.

Day of the oral defense: 3rd July, 2015

The following evaluators recommend the admission of the dissertation:

Prof. Dr. Jürgen Heck

Prof. Dr. Carmen Herrmann

“Titanic projects precise of unwearing wills”

“Los proyectos titánicos requieren voluntades inquebrantables”

Enrique Serrano

Acknowledges

My particular thanks go to Prof. Dr. Jürgen Heck, my doctor father, for providing me the opportunity of studying in Germany, accepting me in his research group and leading me all the way through this dissertation. In our first meeting he asked me if I was sure I wanted to undertake my doctor thesis in Germany. My answer was “yes” and I have never regretted my decision.

I would also like to thank Prof. Dr. Carmen Herrmann for the second evaluation of this work, and Dr. Michael Steiger and Prof. Dr. Christian Klinke for the participation in the disputation Colloquium.

Thanks to the members and former members of the research group: Katrin Brüggmann, Dr. Markus Dede, Dr. Christian Wittenburg, Thomas Schuld, Beate Hoppe, Anne-Kathrin Baum, Dr. Matthias Böge, Dr. Marina Büchert, Dr. Sabrina Dircks, Dr. Christian Fowelin, Dr. Reentje Harms, Dr. Jan Holtman, Dr. Peter Kitaev, Anne Ladisch, Christoph and Nadine Lindström, Christian Lukaschek, Enno Meyer, Dr. Nils Pagels, Sarah Puhl, Philip Saul, Dr. Tiago Silva, Dr. Michael Schmidt, Dr. Dirk Schwidom, Dr. Sebastian Tschersich, Sebastian Triller, Marie Wolff, Anne Wolter-Steingrube and Dr. Elisabeth Ziemann, for the good work atmosphere, for their understanding and help with my German and for being my German family.

My special thanks go to my lab-mate and friend Elli, who laughed with me in the good times, supported me in the bad and knew how to tolerate my bad temper in the worst. She knows that without her, it would have been much more difficult for me to achieve this goal.

I would also like to convey my gratitude to my students in practice Sarah Puhl, Misin Zornic, André Albrecht, Julian Koch, Marcel Fassbender, Lisa-Natasha Unckel and Marijan Erzegovac.

Prof. Dr. Christian Klinke and Prof. Dr. Malte Brasholz: thanks for the support during the irradiation experiments by letting me use the equipment of their research groups.

For reading and correcting this work, I would like to express my gratitude to Dr. Boris Üfer, Juan Pablo Sánchez, Rosa Rodriguez, Sarah Puhl, Florian Hatesuer and Juan Navarro.

Important thanks to Torben Steenbock and Prof. Dr. Carmen Herrmann: thanks for your important collaboration in this project.

I cannot forget the help by the NMR-department (Dr. Erhard Haupt, Gabriele Eggers, Ute Gralla and Claudia Wontorra) and the X-ray service (Prof. Dr. Ulrich Behrens, Dr. Frank Hoffmann and Isabelle Nevoigt). I thank them the cooperation during these years.

For funding this work, thanks to the Sonderforschungsbereich 668 and the Free Hanseatic City of Hamburg in the context of the Landesexcellentinitiative Hamburg "Nanospintronics".

I would also like to thank the people who have accompanied me through this long way: my school friends from Vitoria, my classmates from the University of Zaragoza, my "roomies" from the *Colegio Mayor Santa Isabel*, especially Elena, who has taken care of me and supported me since back then. Finally, thanks to all friends I have made in Hamburg, who have made me feel at home: Isabel, Clara, Gloria, Nico, but also the other ones from Spain, Germany, Mexico, Colombia...

My last but not least thanks go to my family: my mother Mercedes, my father Fernando, my sister Marta and my brother Nano, but also Alfonso, Begoña and Pepón, who are like parents and brother to me. They have always loved me and supported me. Without them, I could not have come this far. *Gracias!*

For my father, Fernando Escibano Ruiz

Table of Context

1. Introduction.....	1
2. Theoretical Background	3
2.1. Molecular Switches	3
2.1.1. Photochromic molecular switches.....	8
2.1.1.1. Spiropyrane and Spirooxazine	10
2.1.1.2. Fulgides	12
2.1.1.3. Azo-derivatives	14
2.1.1.4. 1,2-Diarylethylenes.....	17
2.1.1.5. 1,2-Diarylethenes	21
2.1.2. Metal complexes containing diarylethene molecular switches	30
2.2. Magnetism	41
2.2.1. Diamagnetism	41
2.2.2. Paramagnetism	42
2.2.3. Collective Phenomena	44
2.2.3.1. Ferromagnetism	44
2.2.3.2. Antiferromagnetism	46
2.2.3.3. Ferrimagnetism.....	46
2.2.3.4. Mechanisms of Spin Coupling	47
2.3. Cobaltocene	49
2.4. Analytical methods	55
2.4.1. Cyclic Voltammetry	55
2.4.2. NMR-Spectroscopy	60
2.4.2.1. VT- ¹ H-NMR-Spectroscopy.....	62
2.4.3. UV-vis Spectroscopy.....	63
3. Motivation and Task-settings	66

4. Results and Discussion	69
4.1. Synthesis	69
4.1.1. Synthesis of the organic molecular switches.....	69
4.1.1.1. Synthesis of the organic cyclopentene-derivatives 1 and 2	69
4.1.1.2. Synthesis of the organic cyclohexene-derivatives 5 and 6	70
4.1.2. Synthesis of the organometallic complexes	72
4.1.2.1. Synthesis of the cobalt complexes 9-14 and 16	72
4.1.2.2. Synthesis of the iron complexes 17-19	75
4.1.2.3. Alternative synthesis path	79
4.2. NMR-spectroscopic experiments of the paramagnetic complexes.....	82
4.2.1. NMR-spectroscopic experiments mit complexes 13 and 14	82
4.2.1.1. VT- ¹ H-NMR Measurements from complexes 13 and 14	90
4.2.2. NMR-spectroscopic experiments of the ferrocenium-complex 19	95
4.3. Molecular Structures.....	96
4.3.1. Molecular crystal structures of the organic molecular switches.....	96
4.3.2. Molecular crystal structures of the cobalt complexes 9-12	100
4.3.3. Molecular crystal structures of the iron complexes 17-19	104
4.3.4. Conclusions (I)	107
4.4. Redox behaviour and irradiation experiments monitored <i>via</i> CV.....	108
4.4.1. Redox behavior of the cobaltocenium complexes 11 and 12	108
4.4.1.1. Irradiation experiments monitored by means of CV with complex 12	109
4.4.1.2. Irradiation experiments monitored by means of CV with complex 11	112
4.4.2. Redox behavior of the ferrocene complexes 17 and 18	115
4.4.2.1. Irradiation experiments monitored by means of CV with complex 17	116
4.4.2.2. Irradiation experiments monitored by means of CV with complex 18	118
4.4.3. Conclusions (II)	120

4.5. Irradiation experiments monitored by means of spectroscopic methods.....	122
4.5.1. Organic dithienylethene molecular switches	122
4.5.1.1. Conclusions (III).....	139
4.5.2. Irradiation experiments with the metal complexes 9-14, 17, 18	141
4.5.2.1. Irradiation experiments with the cobalt complexes 9-14	141
4.5.2.2. Irradiation experiments with the iron complexes 17 and 18	155
4.5.2.3. Conclusions (IV)	164
5. Summary	166
6. Zusammenfassung	169
7. Experimental Section	172
7.1. General.....	172
7.2. Analytical methods	172
7.3. Synthesis and characterization	174
7.3.1. 1,2-Bis(5-bromo-2-methylthien-3-yl)cyclopentene (2)	174
7.3.2. 1,2-Bis(5-chloro-2-methylthien-3-yl)cyclohexene (5).....	174
7.3.3. 1,2-Bis(5-iodo-2-methylthien-3-yl)cyclohexene (6).....	175
7.3.4. 1,2-Bis{2'-methyl-5'-[(η^5 -cyclopentadienyl)(η^4 -1'',3''-cyclopentadien-5''-yl)-cobalt(I)]-thiophen-3'-yl}cyclopent-1-en (9)	176
7.3.5. 1,2-Bis{2'-methyl-5'-[(η^5 -cyclopentadienyl)(η^4 -1'',3''-cyclopentadien-5''-yl)-cobalt(I)]-thiophen-3'-yl}cyclohexen-1-en (10).....	177
7.3.6. 1,2-Bis{2'-methyl-5'-[bis(η^5 -cyclopentadienyl)cobalt(III)]-thiophen-3'-yl}-cyclopent-1-en-bis(tetrafluoroborate) (11).....	178
7.3.7. 1,2-Bis{2'-methyl-5'-[bis(η^5 -cyclopentadienyl)cobalt(III)]-thiophen-3'-yl}-cyclohexen-1-en-bis(tetrafluoroborate) (12)	179
7.3.8. 1,2-Bis{2'-methyl-5'-[bis(η^5 -cyclopentadienyl)cobalt(III)]-thiophen-3'-yl}-cyclohexen-1-en-bis(hexafluorophosphate) (12b).....	180
7.3.9. 1,2-Bis{2'-methyl-5'-[bis(η^5 -cyclopentadienyl)cobalt(II)]-thiophen-3'-yl}-cyclopent-1-en (13)	180

7.3.10. 1,2-Bis{2'-methyl-5'-[bis(η^5 -cyclopentadienyl)cobalt(II)]-thiophen-3'-yl}-cyclohex-1-en (14)	181
7.3.11. Attempt to the synthesis of 1,2-bis{2'-methyl-5'-[(η^5 -cyclopentadienyl)(η^4 -1'',3''-cyclopentadien-5''-yl)cobalt(I)]-thiophen-3'-yl}perfluorocyclopent-1-en (16)	182
7.3.12. 1,2-Bis{2'-methyl-5'-[bis(η^5 -cyclopentadienyl)iron(II)]-thiophen-3'-yl}-cyclopent-1-en (17)	183
7.3.13. 1,2-Bis{2'-methyl-5'-[bis(η^5 -cyclopentadienyl)iron(II)]-thiophen-3'-yl}-cyclohex-1-en (18)	184
7.3.14. 1,2-Bis{2'-methyl-5'-[bis(η^5 -cyclopentadienyl)eisen(III)]-thiophen-3'-yl}-cyclopent-1-en-bis(tetrafluoroborate) (19).....	185
7.3.15. 1,2-Bis(2,3,4,5-tetramethylcyclopentadienyl)-cyclopent-1-en (22)	186
8. Literature.....	187
9. List of Chemicals	198
10. Supporting Information.....	203
10.1. ^1H - and ^{13}C -Spectra of the synthesized compounds	203
10.2. Crystallographic Data	212
11. Curriculum Vitae.....	217

List of Figures

Figure 1: Possible states of phenolphthalein, depending on the pH-value.....	4
Figure 2: Water-stimulated reversible isomerization.....	5
Figure 3: Retinoid Visual Cycle.....	5
Figure 4: Schematic representation of the substrate binding and releasing process.	6
Figure 5: Hapticity-switching reaction. ^[22]	7
Figure 6: Positive photochromism. ^[25]	9
Figure 7: Reversible switching reactions of spiropyran- and spirooxazine-derivatives.....	12
Figure 8: Fulgide molecular switch and qualitative UV-vis spectra.	13
Figure 9: Reversible switching reaction of azobenzene.....	14
Figure 10: Shinkai's supramolecular switching system. ^[60]	15
Figure 11: Azoferrocene switching reaction and cyclic voltammetric experiments.	16
Figure 12: Reversible switching cycle of Propofol. ^[10]	16
Figure 13: Photocyclization and dehydrogenation of stilbene. ^[65]	17
Figure 14: Photoreaction of a methyl-substituted stilbene.....	17
Figure 15: Cyano and maleic anhydride derivatives.	18
Figure 16: Diarylethene derivatives with different groups connecting the aromatic rings. ...	22
Figure 17: Diarylethene closed isomers with different substituents at positions 5 and 5'.....	23
Figure 18: Diarylethene derivative after Gilat <i>et al.</i> ^[81,82]	24
Figure 19: Possible conformations of a diarylethene derivative and switching reaction.	24
Figure 20: Switching reaction in presence of cyclodextrins.	25
Figure 21: Increase of the antiparallel conformation and consequent quantum yield.....	25
Figure 22: Diarylethene molecules incorporated in a polymer backbone.	26
Figure 23: Cyclophane diarylethene derivative.	27
Figure 24: Diarylethene cyclophane compound after Hossein. ^[88]	27
Figure 25: Diarylethene derivative synthesized by Hecht in 2012. ^[89]	27

Figure 26: Quantum yield of the photochromic and side reactions.....	28
Figure 27: Diarylethene derivatives.	28
Figure 28: Side product of the photocyclization reaction.	29
Figure 29: Tungsten photochromic complexes by Lehn. ^[107]	31
Figure 30: Dinuclear ruthenium complex.	32
Figure 31: Organic dithienylethene molecular switch and rhenium(I) complex.	33
Figure 32: Bis(ethynylferrocene) - DTE complexes synthesized by Guirado <i>et al.</i> ^[78]	33
Figure 33: Ruthenium(II)-complexes after Uchida <i>et al.</i> ^[112]	35
Figure 34: Ru(bipy) ₂ (phenylpyridyl) complex in its open form.....	35
Figure 35: Iron and ruthenium complexes after Akita. ^[114,115]	37
Figure 36: First M-C direct σ -bound complexes.....	37
Figure 37: DTE-M-DTE complexes by Abruña <i>et al.</i> ^[102]	39
Figure 38: Organic ligands and cobalt complexes prepared by Harvey in 2014. ^[119]	40
Figure 39: Curie and Curie-Weiss paramagnetic behaviour.	43
Figure 40: Ferromagnetic, antiferromagnetic and ferrimagnetic materials.....	44
Figure 41: Hysteresis loop of a ferromagnetic compound.	45
Figure 42: χ vs. T for paramagnetic, ferromagnetic, and antiferromagnetic materials.	46
Figure 43: Spin polarization.	47
Figure 44: „Super Exchange“ spin interaction..	48
Figure 45: „Double Exchange“ spin interaction. ^[126]	48
Figure 46: Direct spin interaction.	48
Figure 47: ¹ H- and ¹³ C-NMR measurements of cobaltocene derivatives.	50
Figure 48: ¹³ C-NMR chemical shifts of metallocenes at different temperatures.....	51
Figure 49: Non-rigid structure of cobaltocene and ¹³ C-NMR at different temperatures.....	52
Figure 50: Biscobaltocenes with a fulvalene-, pentalene-, and indacene-bringing ligand.....	53
Figure 51: Bis(cobaltocenyl)benzene complexes.....	54

Figure 52: Bis(cobaltocenyl)naphthalene complexes after Pagels. ^[166]	54
Figure 53: Cyclic voltammogram of a reversible process.	56
Figure 54: Cyclic voltammogram of reversible, quasireversible and irreversible processes....	58
Figure 55: Robin-Day classification.	60
Figure 56: Energy levels of a molecule in electronic, vibrational and rotational states.....	64
Figure 57: Switching reaction and magnetic coupling.	68
Figure 58: Nitronyl nitroxide radical units connected by a dithienylethene switch.....	68
Figure 59: Molecular structure of 4	71
Figure 60: ¹ H-NMR Spectrum of the diferrocenium complex 19	79
Figure 61: ¹ H-NMR-spectrum of complex 13 in benzene-d ₆	82
Figure 62: ¹ H-NMR-spectrum of complex 14 in toluene-d ₈	83
Figure 63: ¹³ C-NMR-spectrum of complex 14 in toluene-d ₈	84
Figure 64: Dihedral angle.	86
Figure 65: Over-time structural change (14) observed within ¹³ C-NMR spectroscopy.....	87
Figure 66: Several cuts from the ¹³ C-NMR spectra of complex 14	88
Figure 67: Possible conformations (complex 14).....	88
Figure 68: Different conformations for the cyclohexene ring.	89
Figure 69: VT- ¹ H-NMR of the cobalt complex 13 in toluene-d ₈	91
Figure 70: Temperature dependence of the proton signals (complex 13).....	92
Figure 71: Temperature dependence of the protons signals at position α/β (complex 13)...	92
Figure 72: Alkyl-cobaltocene complex and “Cobaltocene Anomaly”	92
Figure 73: VT- ¹ H-NMR of the cobalt(II) complex 14 in toluene-d ₈	94
Figure 74: Temperature dependence of the proton signals (complex 14).....	94
Figure 75: Temperature dependence of the signals at positions α and β (complex 14).	95
Figure 76: Crystal packing of 6	97
Figure 77: Molecular structures of 6	98

Figure 78: Molecular switch derivatives	99
Figure 79: Molecular structures of complex 9	101
Figure 80: Molecular structure of 10	101
Figure 81: Molecular structures of the dicationic complexes 11 and 12	103
Figure 82: Molecular structures of the neutral complexes 17 and 18	104
Figure 83: Molecular structures of complexes 17 and 18	105
Figure 84: “In” and “out” isomers of complex 18	106
Figure 85: Molecular structure of the dicationic complex 19	107
Figure 86: Cyclic voltammogram of complexes 11 and 12	109
Figure 87: Cyclic voltammogram of complex 12 before and after the UV irradiation.	111
Figure 88: Cyclic voltammogram of complex 11 before and after the UV irradiation.	113
Figure 89: Cyclic voltammogram of complex 11 before and after the UV irradiation	115
Figure 90: Cyclic voltammogram of complexes 17 and 18	116
Figure 91: Cyclic voltammogram of complex 17 before and after the UV irradiation.	117
Figure 92: Cyclic voltammogram of complex 17 before and after the UV irradiation.	118
Figure 93: Cyclic voltammogram of complex 18 before and after the UV irradiation.	119
Figure 94: Cyclic voltammogram of ferrocene before and after the UV irradiation.	121
Figure 95: Molecular switches under study.....	122
Figure 96: Irradiation experiments with compounds 1 and 5	124
Figure 97: Calculated UV-vis spectra of compounds 1 and 5	125
Figure 98: UV-vis spectra of compound 5 after two switching cycles	127
Figure 99: Orbital excitations, oscillator strengths, molecular orbital energies (5 -open).....	130
Figure 100: Orbital excitations, oscillator strengths, molecular orbital energies (5 -closed).131	
Figure 101: HOMOs and LUMOs for both switches and both states (BP86/def-TZVP).....	132
Figure 102: HOMOs and LUMOs for both switches and both states (B3LYP-D/def-TZVP). ..	132
Figure 103: Different types of photoreactions. ^[230,233]	135

Figure 104: Potential energy surface (PES) of 5 and 1	136
Figure 105: Irradiation experiment (5) monitored <i>via</i> ^1H -NMR-spectroscopy.....	139
Figure 106: Irradiation experiments monitored <i>via</i> UV-vis spectroscopy (9 and 10).	143
Figure 107: Irradiation experiments (350 nm, visible light) with 11 solved in acetonitrile. .	145
Figure 108: Irradiation experiments (385 nm, 532 nm) with 11 solved in acetonitrile.	146
Figure 109: Irradiation experiments (366 nm) with 11 solved in ethanol.....	147
Figure 110: Irradiation experiments (366 nm) with 12 solved in ethanol.....	148
Figure 111: Irradiation experiments (366 nm, visible light) with 12 solved in acetone.....	149
Figure 112: Irradiation experiments (350 nm, visible light) with 13 solved in pentane.....	151
Figure 113: Irradiation experiments (mercury lamp TQ-150) with 13 solved in pentane.....	152
Figure 114: Irradiation experiments (XBO lamp 450 W/4) with 13 solved in pentane.	153
Figure 115: UV-vis spectrum of 14 in solved pentane.	154
Figure 116: Irradiation experiments (366 nm) with 14 solved in pentane.....	154
Figure 117: Irradiation of complex 17 in hexane with UV light....	156
Figure 118: Irradiation of complex 18 in hexane with UV light....	156
Figure 119: Irradiation of complex 17 in hexane with UV light....	157
Figure 120: Irradiation of complex 17 in hexane with UV light....	159
Figure 121: Switching cycle of complex 17 in hexane.....	159
Figure 122: Irradiation of complex 18 in hexane with UV light.....	160
Figure 123: Switching cycle of complex 18 in hexane.	160
Figure 124: Calculated UV-vis spectra of compounds 17 and 18	161
Figure 125: Potential energy surface (PES) of 1 and 17	162
Figure 126: Ring closure mechanism for the ferrocenyl-complex 17	164
Figure 127: Synthesized metal complexes.....	166
Figure 128: ^1H -NMR-spectrum of 5 in chloroform- d_1 (S = solvent).	203
Figure 129: ^{13}C -NMR-spectrum of 5 in chloroform- d_1 (S = solvent)	203

Figure 130: ^1H -NMR-spectrum of 6 in chloroform- d_1 (S = solvent).	203
Figure 131: ^{13}C -NMR-spectrum of 6 in chloroform- d_1 (S = solvent).	204
Figure 132: ^1H -NMR-spectrum of 9 in benzene- d_6 (S = solvent).	204
Figure 133: ^{13}C -NMR-spectrum of 9 in benzene- d_6 (S = solvent).	205
Figure 134: ^1H -NMR-spectrum of 10 in toluene- d_8 (S = solvent).	205
Figure 135: ^{13}C -NMR-spectrum of 10 in pyridine- d_5 (S = solvent).	206
Figure 136: ^1H -NMR-spectrum of 11 in acetonitrile- d_3 (S = solvent).	206
Figure 137: ^{13}C -NMR-spectrum of 11 in acetonitrile- d_3 (S = solvent).	207
Figure 138: ^1H -NMR-spectrum of 12 in acetonitrile- d_3 (S = solvent).	207
Figure 139: ^{13}C -NMR-spectrum of 12 in acetonitrile- d_3 (S = solvent).	208
Figure 140: Cuts from the HMQC-spectrum of complex 14 in toluene- d_8	208
Figure 141: Cuts from the HMBC-spectrum of complex 14 in toluene- d_8	209
Figure 142: ^1H -NMR-spectrum of 17 in chloroform- d_1 (S = solvent).	209
Figure 143: ^{13}C -NMR-spectrum of 17 in chloroform- d_1 (S = solvent).	210
Figure 144: ^1H -NMR-spectrum of 18 in benzene- d_6 (S = solvent).	210
Figure 145: ^{13}C -NMR-spectrum of 18 in benzene- d_6 (S = solvent).	211

List of Schemes

Scheme 1: Molecular Switches.	3
Scheme 2: Switching cycle.	8
Scheme 3: Two orthogonal parts of the molecule in planes P and P'	10
Scheme 4: Switching reaction of spiropyranes and spirooxazines. ^[35]	11
Scheme 5: Switching reaction of fulgides (X = O) and fulgimides (X = NR).....	12
Scheme 6: Electrocyclic reaction.	19
Scheme 7: Possible modes to electrocyclic reactions. ^[68]	20
Scheme 8: General pattern of diarylethene molecular switches.	22
Scheme 9: Mechanism of the electrochromic reaction.....	38
Scheme 10: Oxidation and reduction reactions.....	56
Scheme 11: Molecular switches under study.	66
Scheme 12: Molecular switches employed in this work.....	69
Scheme 13: Retrosynthetic scheme for the molecular switch 1	69
Scheme 14: Synthesis of 2	70
Scheme 15: Synthesis of 5	72
Scheme 16: Synthesis of the Co(I)-complexes 9 and 10	73
Scheme 17: Hydride abstraction and subsequent reduction.	74
Scheme 18: Proposed synthesis of 16	75
Scheme 19: Unsuccessful Suzuki cross-coupling reaction.	76
Scheme 20: Synthesis of the ferrocene complexes 17 and 18	77
Scheme 21: Oxidation of the iron(II) centers of complex 17 to iron(III) (complex 19).....	77
Scheme 22: Synthesis of the organic compound 22	81
Scheme 23: Proposed metalation of 22	81
Scheme 24: Switching cycle.	122
Scheme 25: Switching reaction of Co(I)-complexes 9 and 10	141

Scheme 26: Switching reaction of the metallocene complexes.....	142
Scheme 27: Switching reactions for the diarylethene molecular switches.....	167

List of Tables

Table 1: Woodward-Hoffmann Rules. ^[68,69]	21
Table 2: Repeatable cycle number (RCN) under different conditions (Figure 27).	28
Table 3: Complexes XIX-XXIII	37
Table 4: Chemical shift of the protons at position 4'.	70
Table 5: Formal Potentials (V vs. FcH/FcH ⁺). ^[194]	74
Table 6: ¹ H-NMR signal shifts for complexes 13 and 14 in toluene-d ₈	83
Table 7: ¹ H-NMR signal shifts for complexes 13 , 14 and 19	95
Table 8: Distances between the methylated carbon atoms.	99
Table 9: Torsion angles.	99
Table 10: Selected distances and torsional angles in complexes 9 , 9' and 10	102
Table 11: Selected distances and torsional angles in complexes 11 and 12	103
Table 12: Selected distances and torsion angles in complexes 17 and 18	106
Table 13: Cyclic voltammetric data (11 and 12).	108
Table 14: Cyclic voltammetric data (12) before and after the irradiation with UV light.	109
Table 15: Cyclic voltammetric data (11) before and after the irradiation with UV light.	112
Table 16: Cyclic voltammetric data (11) before and after the irradiation with UV light.	114
Table 17: Cyclic voltammetric data of 17 and 18	115
Table 18: Cyclic voltammetric data (17) before and after the irradiation with UV light.	117
Table 19: Cyclic voltammetric data (18) before and after the irradiation with UV light.	119
Table 20: Calculated energy differences between the closed and the open isomers.	123
Table 21: Experimental UV-vis absorption spectroscopic data for 1 and 5 in hexane.	126
Table 22: Transition dipole moments for the HOMO-LUMO transition (1 and 5).	133
Table 23: Estimated activation barriers for switches 1 and 5	137
Table 24: UV-vis absorption spectroscopic data for complexes 9 and 10 in hexane.	144
Table 25: UV-vis absorption spectroscopic data for complexes 17 and 18 in hexane.	158

Table 26: Employed chemical products. ^[243]	198
Table 27: Crystallographic data for compounds 4 and 6	212
Table 28: Crystallographic data for compounds 9 and 10	213
Table 29: Crystallographic data for compounds 11 and 12	214
Table 30: Crystallographic data for compounds 17 and 18	215

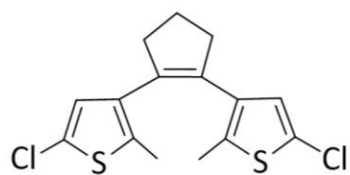
List of Abbreviations

Å	Ångstrom
acac	acetylacetonate
<i>n</i> -BuLi	<i>n</i> -butyllithium
^t Bu	<i>tert</i> -butyl
<i>t</i> -BuLi	<i>tert</i> -butyllithium
C	Curie constant
COSY	correlated spectroscopy
Cp	cyclopentadienyl
Cp*	pentamethylcyclopentadienyl
CV	cyclic voltammetry
χ	magnetic susceptibility
χ^D	magnetic susceptibility of diamagnetic materials
χ^{Exp}	experimental susceptibility
χ^P	magnetic susceptibility of paramagnetic materials
d	doublet, day
dppe	1,2-bis(diphenylphosphino)ethane
δ	chemical shift
δ_T^{dia}	diamagnetic chemical shift
δ_T^{exp}	experimental chemical shift
δ_T^{para}	paramagnetic chemical shift
TL	thin-layer chromatography
DCM	dichloromethane
DFT	density functional theory
DME	dimethoxyethane
DTE	dithienylethene
EI	electron ionization
ESI	electrospray ionization
ESR	electron-paramagnetic-resonance
Et	ethyl
<i>et al.</i>	in latin: <i>et alii</i> (and others)

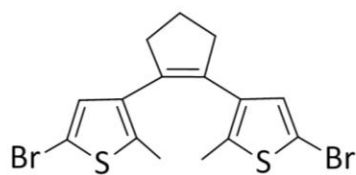
Et ₂ O	diethylether
F	Faraday constant
FAB	fast atom bombardment
FcH	ferrocene
FcH ⁺	ferrocenium
g	gramm, <i>g</i> -Factor
GS	ground state
h	hour
H	magnetic field
H _c	coercivity
HMBC	heteronuclear multiple-bond correlation
HMQC	heteronuclear multiple-quantum correlation
HOMO	highest occupied molecular orbital
Hz	hertz
η	haptivity
K	kilo, kelvin
L	liter
LUMO	lowest unoccupied molecular orbital
J	coupling constant
m	multiplet, meter, milli
M	molar, molecular weight, magnetization
M _R	remanence
Me	methyl
min	minute
MO	molecular orbital
MS	mass spectroscopy
m/z	mass per charge
NLO	nonlinear optics
NMR	nuclear magnetic resonance
Nr	number
<i>p</i>	para
PCH	dithienylcyclopentene-derivative

PCF	dithienylperfluorocyclopentene-derivative
PE	petroleum ether
PES	potential energy surfaces
Ph	phenyl
pm	picometer
PSS	photostationary state
q	quartet
quin	quintuplet
RCN	repeatable cycle number
RT	room temperature
s	singlet
SCE	saturated calomel electrode
T	temperature
T_c	Curie temperature
T_N	Néel temperature
t	<i>tert</i> -, time, triplet
θ	Weiss constant
THF	tetrahydrofurane
TMS	tetramethylsilane
TS	transition state
UV	ultraviolet
UV-vis	ultraviolet-visible
μ	magnetic moment
V	volume
vis	visible
vs.	in latin: <i>versus</i> (against, in contrast with)

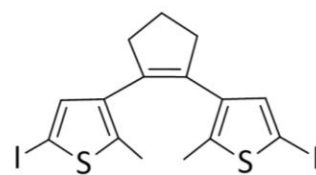
Compound Index



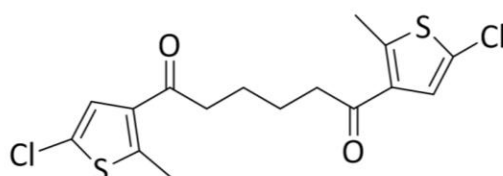
1



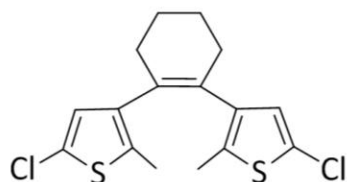
2



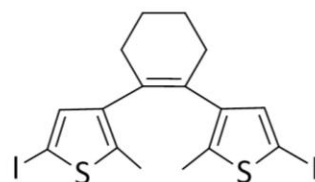
3



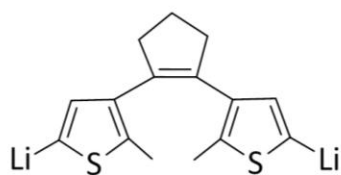
4



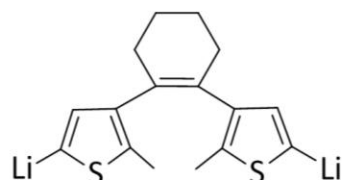
5



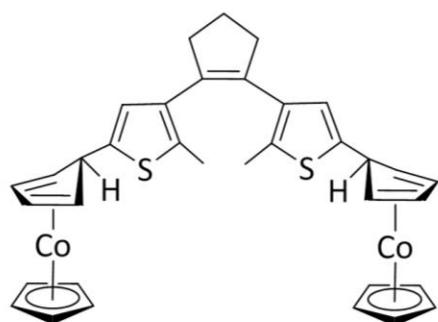
6



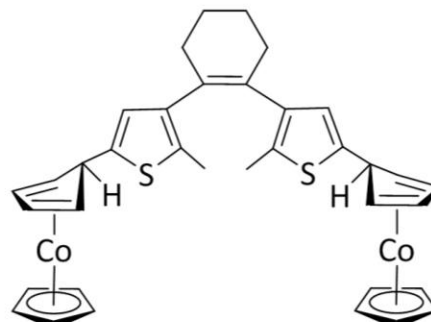
7



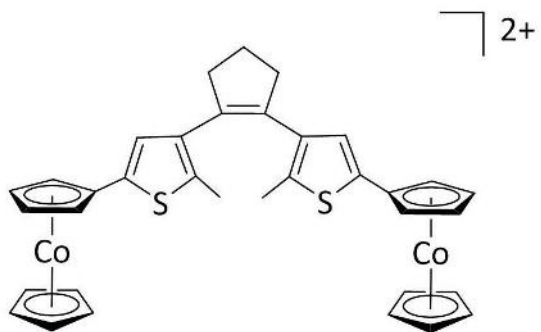
8



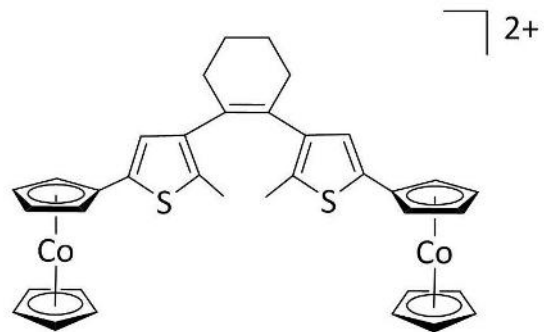
9



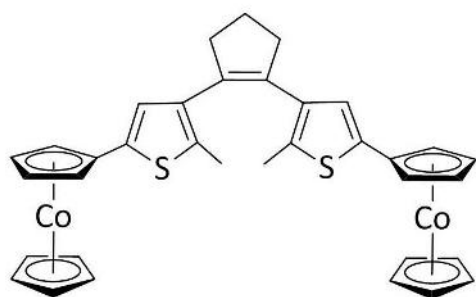
10



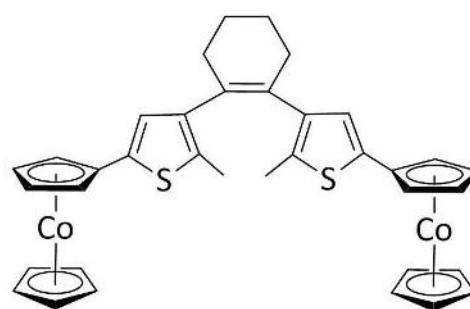
11



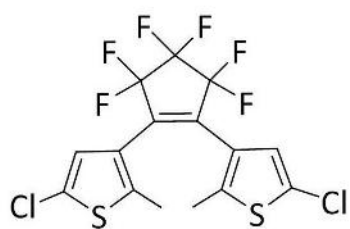
12



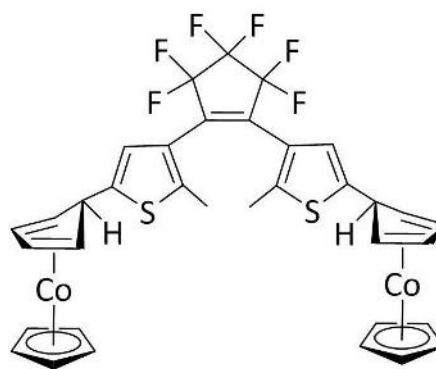
13



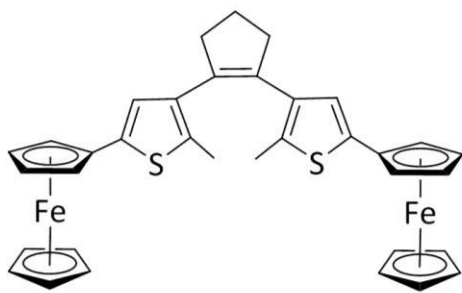
14



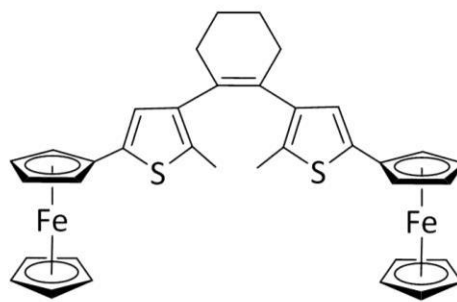
15



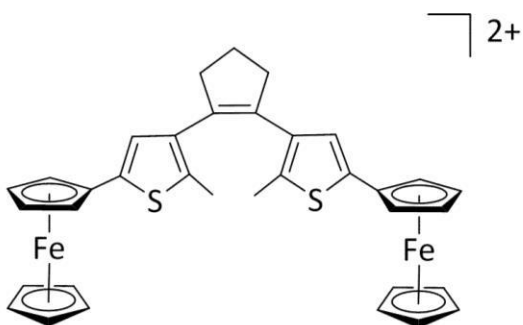
16



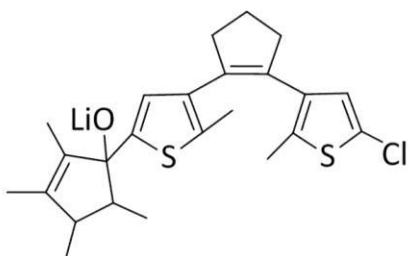
17



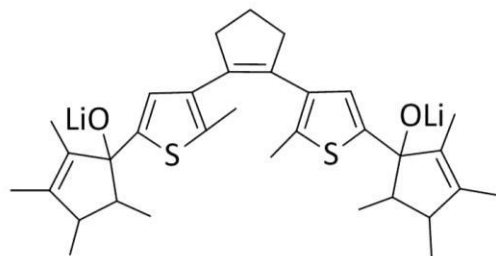
18



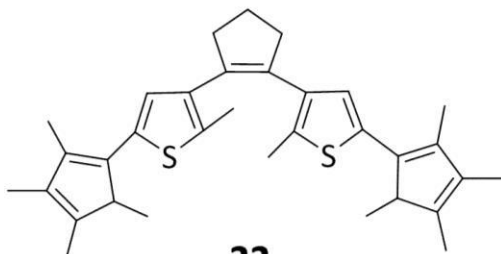
19



20



21



22

1. Introduction

Konrad Zuse is unanimously accepted as the creator of the first digital computer, feat which was accomplished in Berlin in the middle of the 20th century.^[1] Almost immediately after, a group of scientist developed in London the *Colossus*,^[2] which was employed to decipher the messages sent by the German army during the second world war. This computer was as big as a room and nowadays it would still be considered “slow”. A few years later IBM took the first steps towards the miniaturization and the first magnetic hard drive was developed in 1956, the storage memory was 5 MB and it weighed 500 kg.^[3]

Thirty-five years ago only the privileged could afford a mobile phone. They were not only expensive, but the batteries were so big that they had to be transported in a separate suitcase, so they were initially designed to be used from the car (what currently is actually prohibited without a hands-free set). It was not until 1984 that Motorola introduced onto the market the first mobile phone as we know them; it weighed 800 g, the size was 33 cm × 4.5 cm × 8.9 cm and after charging the battery for ten hours it offered 30 minutes of talk.^[4] Photo- and video cameras were in similar dimensions and only used in special occasions. Currently, almost anyone can afford a smartphone, which includes a high resolution video camera , a calculator, a diary, a contact list, a music player... not forgetting a high speed internet connection and a navigation system. Finally, can anyone remember the diskettes? At present, key rings containing a USB drive exist with more capacity than dozens of them (together!).

So far, magnetic materials had been the key in this process.^[5] However, the technological needs demand still higher data density and smaller devices. In order to overcome the existing physical barrier, new materials fulfilling these needs are required. The solution might lie in the molecular magnetic materials.

Molecular switches could also contribute on the way to further miniaturization.^[6] This type of compounds has been part of the daily life long before getting to know its properties; e.g. enabling our eyes to see.^[7] Currently, the wide variety of compounds belonging to this family and the different possible stimuli used to induce the change between the different states makes them to be found everywhere: from eyeglasses^[8] to anaesthetics,^[9,10]

1. Introduction

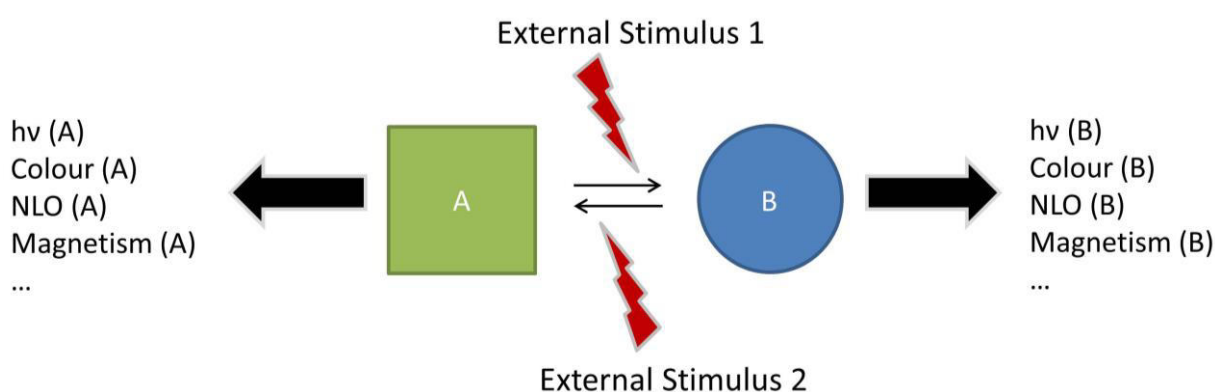
throughout pigments, ^[11] agents to immobilize microorganisms ^[12] or new “green”-inks; ^[13] even in umbrellas whose colour changes when they become wet!

The combination of molecular switches with molecular magnetic materials opens a field of infinite possibilities. Not only a higher grade of miniaturization could be achieved, but also the operator would be able to reversibly influence the environment through the application of an external stimulus. Looking into the future, it could be the beginning of a new numeral system extending the binary system to several (meta-)stable states of the molecular switch core.

2. Theoretical Background

2.1. Molecular Switches

Molecular switches are molecules which are capable to convert reversibly between two or more different (meta-)stable states due to the application of an external stimuli. The applied external stimuli can be of a different nature, like a change in the temperature, in the pH value, a redox reaction, the presence of certain ligands or solvents, etc. These (meta-)stable states have different physical and chemical properties (Scheme 1).^[14]



Scheme 1: Molecular Switches.

Classical molecular switches are pH indicators. Depending on the pH value of the solution, its colour will change due to a variation in the proton configuration. This occurs because the organic molecule (the indicator) can be found in different states, each correspondent to a different pH range.

A prominent example is phenolphthalein (4',4''-dihydroxydiphenylphthalide), a typical organic pH indicator which can be found in five different states (Figure 1).^[15]

In highly acid solutions ($\text{pH} < 0$), phenolphthalein can be found as a red carbocation (Figure 1, **1a**). In a pH range from 0 to 8.2, Phenolphthalein is a colourless lactone (Figure 1, **1b**). By adding a base the lactone ring opens (Figure 1, **1c**), a water molecule splits and a quinone ring is formed. This is increasing the size of the conjugated π -system (Figure 1, **1d**) and a pink colour is presented. For this state two mesomeric isomers describe the bonding situation. In high alkaline mediums phenolphthalein will form a colourless trianion (Figure 1, **1e**). This special case where the protonated form and the conjugated base present different colours is called "acidichromism".^[16]

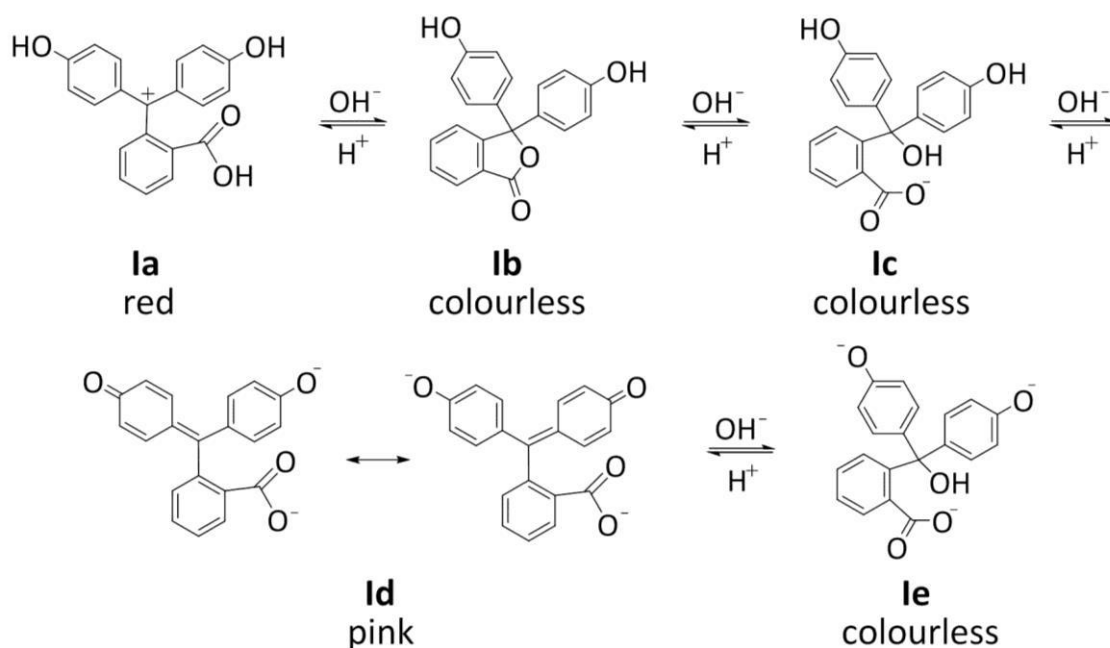


Figure 1: Possible states of phenolphthalein, depending on the pH-value.

The change among the different states is reversible, the yield of every step is almost 100 % and it barely decomposes during the process. For these reasons this indicator was commonly used in laboratories in acid-base titrations until it was classified as a carcinogenic substance.^[17]

Another example of the possible applications of this type of molecules was developed by Sheng *et al.*^[13] in 2014. They prepared different oxazolidines (Figure 2) which offer different colours depending on the amount of water in the system. They were employed as “ecological” ink.

The ring-closed form (Figure 2, **IIC**) is colourless and consist on four rings. One of these rings includes a nitrogen and a oxygen atoms and it is opened in the presence of water. The new structure, which is blue (Figure 2, **IIC**), will be stabilized due to the dipole nature of the water and its ability to form hydrogen-bonds. When the water is removed (e. g. by heating), the initial form is obtained again.

2. Theoretical Background

reversibly depending on the presence or absence of certain metal cations. The free ligands have not the optimal shape to act as hosts, while the metal-complexes do. These systems act like nano “tweezers”, binding and releasing the guest, depending on their conformation (Figure 4).

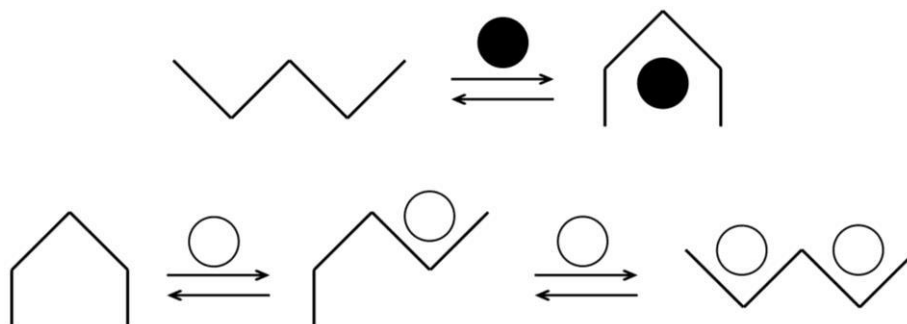


Figure 4: Schematic representation of the substrate binding and releasing process induced by the presence of metal-ions.^[20]

The first group of ligands (Figure 4, above) presented a W-conformation. When zinc(II) cations were added, the new complex presented an U-conformation. The second group of ligands (Figure 4, low) were found in a U-conformation. By adding an equivalent of copper(I) cations, the conformation changed to an S-conformation. After the addition of the second equivalent, this conformation changed to a W-conformation.

As the ability to form supramolecular adducts with different substrates depends on the conformation of the host, the molecular “tweezers” could be controlled by adding or removing metal cations to the solution.

Another possible activator for a switching reaction is a redox reaction. This phenomenon is called “electrochromism” and it describes the reversible change between two (meta)-stable states which show different absorption spectra, within an electrochemical reaction.^[21]

An example of this are the zirconocene complexes synthesized by Chirik and coworkers^[22] which were able to switch the hapticity from zirconium within a redox reaction (Figure 5).

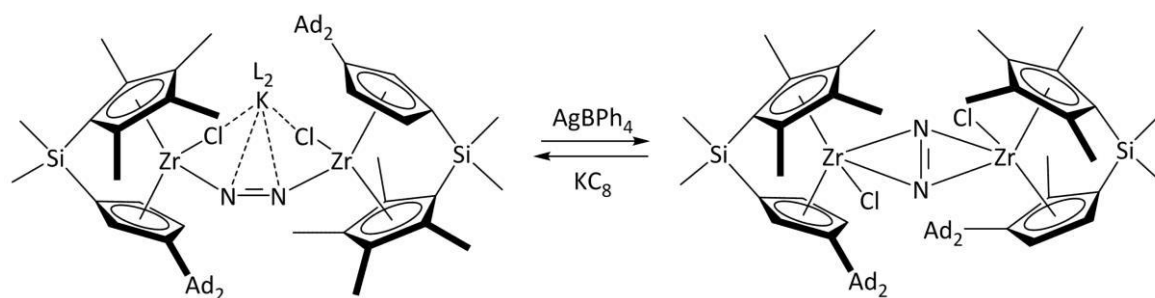


Figure 5: Hapticity-switching reaction. ^[22]

The initial state (Figure 5, left) was a zirconocene complex with an end-on dinitrogen ligand. When oxidized with silver(I), the structure of the complex changed and both zirconium centers were η^2 coordinated to the dinitrogen ligand (Figure 5, right).

The hapticity-switching was reversible; the initial state could be obtained by means of reduction. Unfortunately, after a few cycles a great amount of product had decomposed.

Quantum yield

The quantum yield of a photoreaction correlates the number of absorbed photons with the number of molecules which undergo the desired reaction (Equation 1). ^[23]

$$\Phi = \frac{\text{molecules reacted}}{\text{absorbed photons}} \quad \text{Equation 1}$$

Fatigue

Switching reactions are always accompanied by other undesirable side reactions which limit the possible number of cycles of the switching process. The term “fatigue” refers to this chemical degradation of a material, which results in the loss of performance over time. ^[16,24]

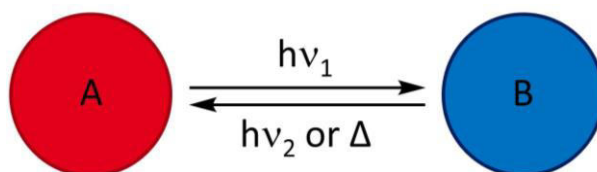
It is intrinsically linked to the term “repeteable cycle number”, which is defined as the number of switching cycles certain molecular switch can undergo without decomposing. ^[24]

During the switching cycle the terms “switch on” and “switch off” are used. ^[25]

Therefore, the more side reactions occur or the better these side reactions work, the higher will be the fatigue of the photochromic system, and the smaller will be the repeatable cycle number.

2.1.1. Photochromic molecular switches

Photochromism is the ability of a chemical species to change reversibly between two different forms within electromagnetic irradiation, in one or both directions, having different absorption spectra, accompanied by different physical and chemical properties such as oxidation/reduction potential and geometrical structure. This phenomenon is not only constricted to coloured substances, but it is also applied in systems which absorb in UV or IR region; and in cases where the back reaction takes place thermally (Scheme 2).^[24,25]



Scheme 2: Switching cycle.

In the following, a brief review of the history of photochromic molecular switches in the last century will be given. The different types, according with their properties, will be defined and the most important groups of photochromic molecular switches will be described. In the last place, we will focus on the group of photochromic molecular switches which was employed in this project: the 1,2-diarylethene “family”. How they work, their development and properties will be presented and discussed.

Beginnings of the photochromic switches

The first observed examples of photochromism were substances which changed their colour between day and night. Fritzsche^[26] reported in 1867 the bleaching of an orange tetracene solution in contact with the sunlight and the return of the orange colour during the night. Nine years later, ter Meer^[27] published the colour change of a solid potassium salt of dinitroethane from yellow (in the darkness) to red (exposed to sunlight) and Phipson^[28] reported in 1899 about certain black fence posts which became white in the night, probably caused by a zinc pigment.

However, it was not until the 1940s and the 1950s that mechanistic and synthetic studies were finally executed, particularly by the research groups of Hirshberg and Fischer^[29] in Israel. In 1950 Hirshberg established the term “photochromism” (from the Greek: *phos* = Light and *chroma* = colour).

Classification of photochromic molecular switches

Photochromic molecular switches can be classified depending on the thermal stability of the meta-stable state. If the back reaction can be thermally induced we speak about T-Type Photochromism. Alternatively, if the meta-stable state is thermally stable and the back reaction can only be photochemically induced, this is P-Type photochromism. The P-Type systems are normally preferred to be employed as molecular switches,^[16] since thermally stable states will offer materials able to maintain their properties under different conditions. The T-Type photochromic systems are referred to as “thermochromic”. This term defines the process where a thermally induced reversible colour change is involved.^[25]

Normally, the initial state is colourless or pale yellow and the obtained isomer is coloured (e.g. blue or red). This is called “positive photochromism”. The maximum in the UV-vis spectrum of the obtained isomer is displaced towards longer wavelengths in respect of the spectrum of the initial state (Figure 6). Generally, unimolecular systems show this type of photochromism.

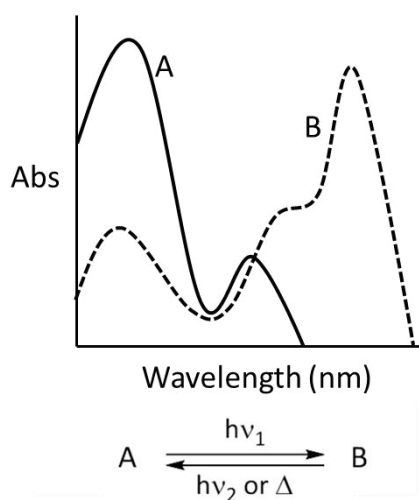


Figure 6: Positive photochromism.^[25]

On the contrary, the initial state of bimolecular systems is commonly coloured and the photochemically obtained state is not. “Negative” or “inverse photochromism” is the process where the maximum in the UV-vis spectrum of the obtained isomer is displaced to shorter wavelengths in respect of the spectrum of the initial state.^[25]

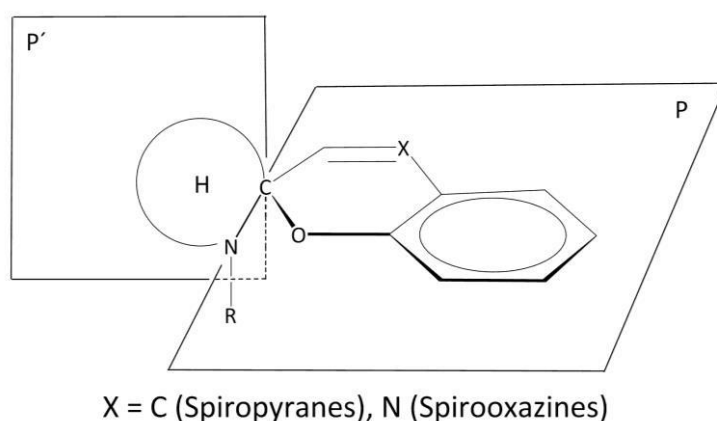
Families of photochromic molecular switches

In the last years, four different “families” of photochromic molecular switches have drawn the attention of the researchers. The reason is their excellent properties and possibilities of modification. ^[14]

2.1.1.1. Spiropyrane and Spirooxazine

Spiropyrane and spirooxazine form a very important group of thermal reversible photochromic molecular switches which has been thoroughly investigated. ^[30,31–34] The reasons for this are their excellent characteristics such as high fatigue resistance and good quantum yields, ^[35] the synthetic accessibility and the wide possibilities for structural variation and functionalization. ^[36]

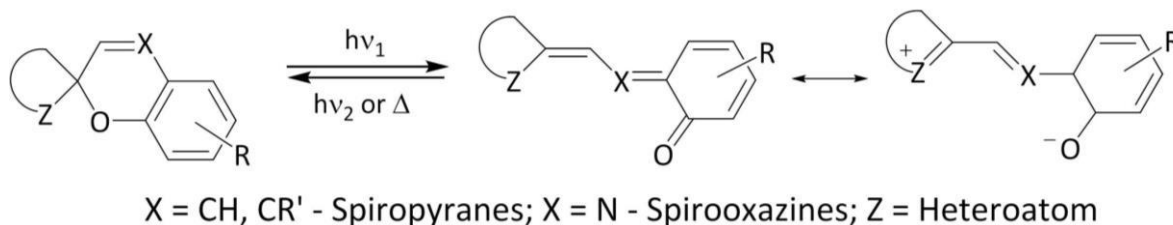
The first spiropyrane derivative was reported by Decker *et al.* ^[37] at the beginning of the last century and their thermochromic properties were discovered in 1926. ^[38] In 1952, Hirshberg and Fischer ^[39] described the first reversible photochromic reaction and the spiropyrane derivatives formed another family of molecular switches. Nine years later the first photochromic spirooxazine was reported, ^[40] and this sub-group became a part of the molecular switches family. However, it was not until the 1980s that these compounds were applied in the eyewear industry as materials for self-colouring sunglasses ^[25] and so attracted the interest of the scientific community.



Scheme 3: Two orthogonal parts of the molecule in planes P and P'. The left part is represented as H (Heterocyclic). ^[41]

The spiropyranes and spirooxazines are formed by two heterocyclic parts linked by a tetrahedral sp^3 carbon atom (Scheme 3). ^[41]

Generally, spiropyrane (SP) and spirooxazine (SO) exist, in the absence of light, in the closed colourless form (Scheme 4, right). This state is the thermodynamically most stable. By irradiating this closed form in solution with UV light, it undergoes a heterolytic C-O ring cleavage and the open coloured form can be induced (Scheme 4, left).



Scheme 4: Switching reaction of spiropyranes and spirooxazines. ^[35]

The closed form exists as neutral quinoid in nonpolar solvents while the zwitterionic merocyanine (MC) form is predominant in polar solvents. The merocyanine form has a dipolar planar structure with delocalized π -electrons and can photochemically (by irradiation with visible light) or thermally convert back to the spiropyran or spirooxazine form.

In figure 7 two examples of reversible switching reactions are shown. When the colourless spiropyran **IIIc** ^[39,41] is irradiated with UV light it turns coloured and the merocyanine isomer **IIIo** is obtained. When heating or irradiating the sample with visible light, the quinoid form is obtained again.

The spirooxazine **IV** presents the same photochromic behaviour. The colourless open isomer (**IVo**) turns blue upon irradiation with UV light, but when it is heated or irradiated with visible light, it becomes colourless again.

The chemical and physical properties change with each possible state. In spite of the potential application of these systems, their use is limited by the fact that the merocyanine form is thermally unstable. ^[34] However, recently, several approaches to improve the stability of the merocyanine form have been attempted. ^[31–33,41–43]

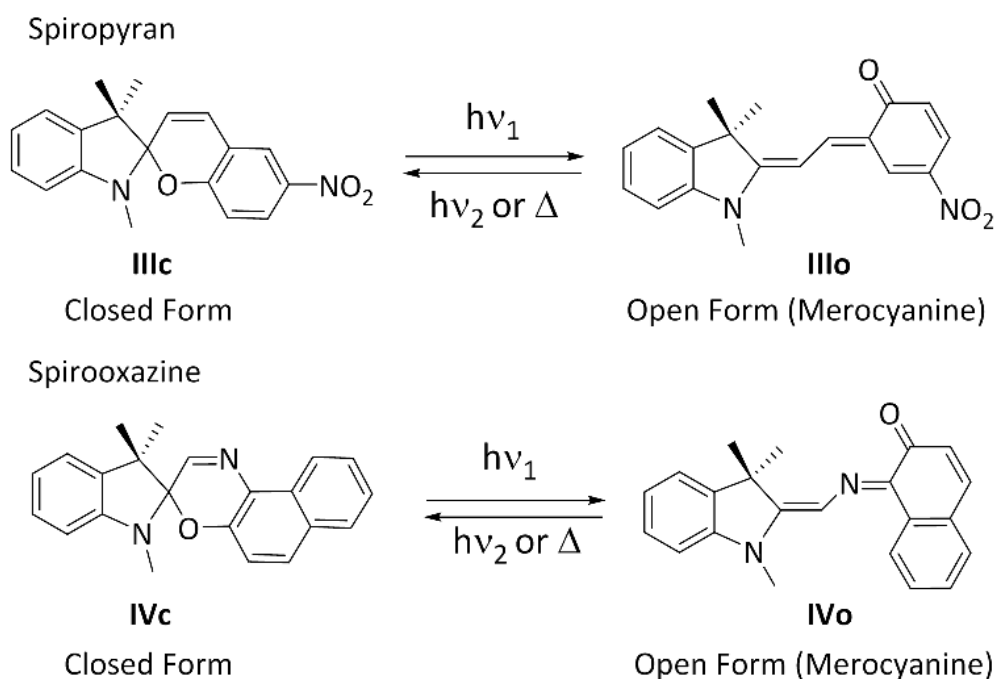
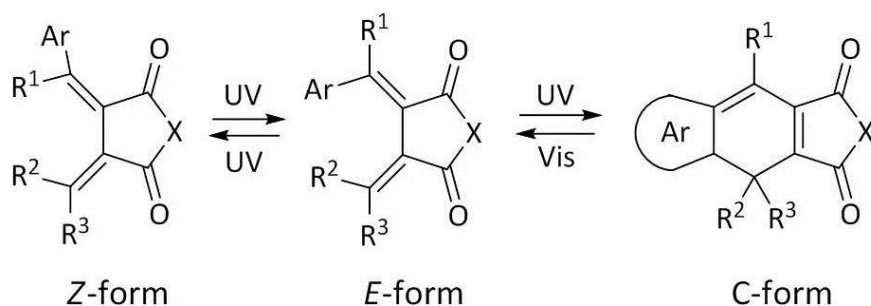


Figure 7: Reversible switching reactions of a spiropyran-^[39,41] (compound III) and a spirooxazine-derivative (compound IV).^[44] ($h\nu_1 > h\nu_2$)

2.1.1.2. Fulgides

Fulgides are organic systems which contain a basic skeleton of bismethylsuccinic anhydride (or bismethylen succinimid, known as “fulgimide”) and one or more aromatic rings connected to the *exo*-methylene carbon atom (Scheme 5), so they form a 1,3,5-hexatriene structure which will be able to undergo 6π -electrocyclization.^[45,46]



Scheme 5: Switching reaction of fulgides ($X = O$) and fulgimides ($X = NR$).

The first fulgides were synthesized and published by Stobbe^[47] at the beginning of the last century. He established the term “fulgide” (from the Latin: *fulgere* = to glisten), because the first compounds were isolated as shining crystals.^[25] These photochromic compounds were thermochromic, so the closed isomer (Scheme 5, C-form) was not thermally stable.

The photochromic reaction (Scheme 5) occurs between a colourless or pale yellow isomer (open isomer) and the coloured (from yellow to green) closed isomer. The open isomer can be found as *Z*- or *E*-isomer depending of the configuration of the double bond which connects the aromatic ring and the acid anhydride. Only the *E*-isomer is able to undergo the cyclization, but normally the geometrical photoisomerization between *E* and *Z* isomer takes place easily. However, it is an energy-consuming process which complicates the photochromic process.^[46]

During the twentieth century, the researchers have tried to understand the photochromic process of the fulgides: the *Z-E* isomerization reaction and the thermal instability of the closed isomer. In 1968, the work of Becker and coworkers^[48] helped to lighten the mechanism of the photochromic process, and the research group of Heller^[49,50] published a series of publications with the title "Overcrowded Molecules", where the chemistry of fulgides, closely related compounds and the thermal side reactions of the coloured isomers (hydrogen rearrangements and/or dehydrogenative aromatization) were dealt with.^[50,51,52]

In 1981, Heller and coworkers^[52,53] reported the first P-Type fulgide photochromic system, which shows neither thermal back reaction nor side reactions (Figure 8, left). Furthermore, the conversion from the *E*-form to the C-form (Figure 8, left) is close to 100 %, because the absorption of the *E*-form is large where the C-form does not absorb, so the back reaction by irradiation with UV light is insignificant (Figure 8, right). When irradiated with white light, the C-form turns again into the *E*-form.

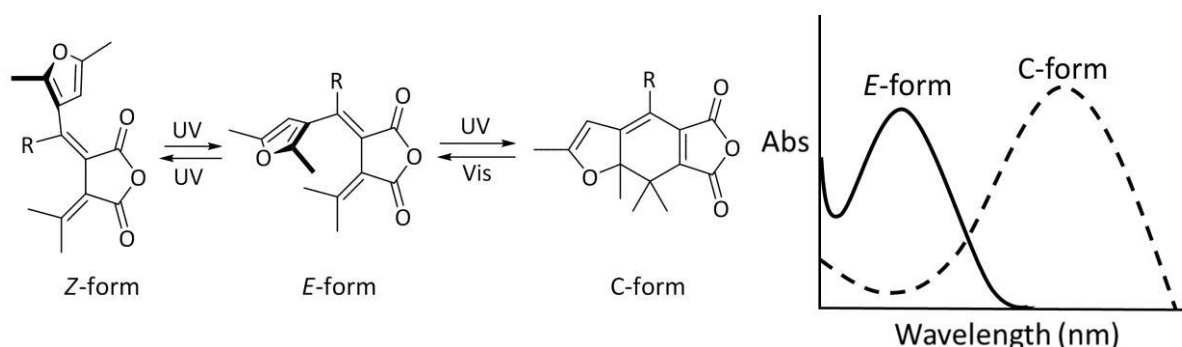


Figure 8: Fulgide molecular switch reported by Heller and coworkers^[52,53] and qualitative UV-vis spectra.

In 1988, Yokoya *et al.*^[54] investigated the effect of the R substituents (Figure 8) in the *E-Z* isomerization. They reported it was greatly suppressed when the alkyl group R became

sterically more demanding. By optimizing this *E-Z* isomerization reaction, the photocyclization was improved and accelerated.

This series of compounds laid the foundation for the generations of thermally irreversible fulgide photochromic switches. Throughout the 1980s and the 1990s, the scientific community was committed to improve the properties of this “new” fulgide. Since the early 1990s the tendency has moved on to the development of fulgide derivatives with different aromatic rings and substituents.^[46]

2.1.1.3. Azo-derivatives

The azo molecular switch is one of the smallest photo-switches since it only contains two nitrogen atoms connected with a double bond, each of them carrying a non-bonding pair of electrons.^[55]

The first azo-dye was synthesized by Martius in 1863 and only one year later Griess reported the coupling reaction of diazonium compounds. This important discovery opened the way to the development to the azo-dyes, the most important and versatile group of coloured organic compounds used as dyes and pigments.^[11]

Krollpfeiffer *et al.*^[56] reported in 1934 what could be the first elucidated photochemical reaction of an azobenzene derivative, isolating the fading products of an *o*-aminoazo compound. Following that, Hartley^[57] observed in 1937, for the first time, the reversible photochemical *E-Z* isomerization (Figure 9) of azobenzene by irradiating a solution of the *E* isomer with sunlight. Furthermore he was able to isolate and identify the *Z* isomer.

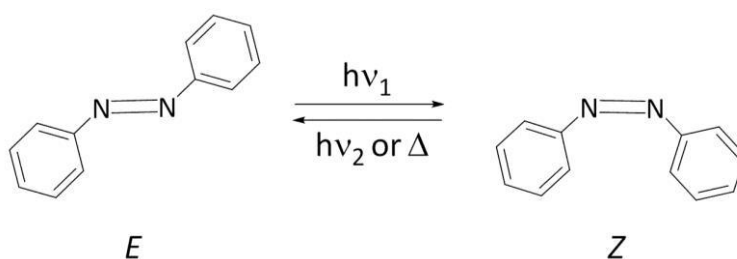


Figure 9: Reversible switching reaction of azobenzene.

In the following years, the azo-compounds have been intensely studied due to their potential applications, among others, as a molecular switch.^[58,59,59]

The organic azo-derivatives can be divided in three different types, according to the relative energetic position of the ($n-\pi^*$)- and the ($\pi-\pi^*$)-transitions: the azobenzene type, the

aminoazobenzene type, in which azobenzene is substituted by *o*- or *p*-amino groups, and the pseudo stilbenes (characterized by a low-lying (π - π^*)-transition).^[8]

Although the *E*-*Z* isomerization mechanism for each type varies, in this work only the general process, which coincide for all types, will be explained.

The *E* isomer is thermodynamically more stable than the *Z* form. However, the *Z* isomer is kinetically stabilized by an activation energy of isomerization. The *E*-*Z* isomerization can be initiated by UV-light stimulating a π -to- π^* or a n -to- π^* transition. The *Z*-*E* isomerization can be affected by means of visible light or by heat.

The geometry of the *E* isomer is more elongated while the *Z* isomer is a bent molecule and hence, more compact. This leads to different physical and chemical properties.

An example of the varied application of azo-molecular switches is the work of Shinkai *et al.*^[60] They reversibly modified the cavity of a crown ether by switching between the *E* and *Z* configuration (Figure 10).

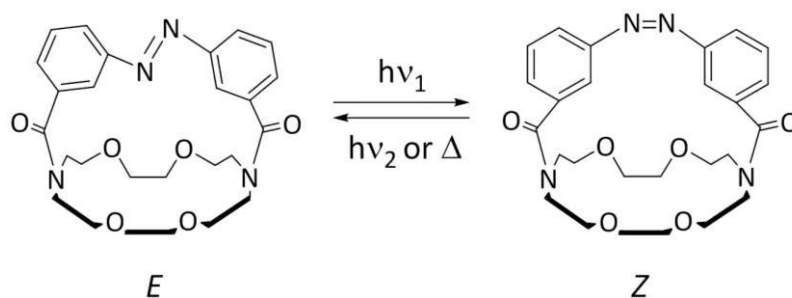


Figure 10: Shinkai's supramolecular switching system.^[60]

Different solutions of alkali metal salts of methyl orange were extracted with the azobenzene crown ether (Figure 10). It was found that depending on the configuration of the azo group, the size of the cavity varied (being bigger in the case of the *Z*-isomer). The large alkali metal ions such as rubidium(I) and caesium(I) were hardly extracted by the *E*-isomer and good extracted by the *Z*-isomer. The opposite was true for the smaller cations like sodium(I). Finally, lithium(I) cation was only extracted by the *E*-isomer.

Kurihara *et al.*^[61] studied azoferrocene, where two ferrocenes are linked by an azo bridge (Figure 11, left). The *E*-*Z* isomerization is induced by UV light through π - π^* transition of the azo group, and the back reaction occurs by irradiating the sample with visible light, through a metal-to-ligand charge transfer (MLCT) transition. This reaction leads to a change of the intrinsic properties of both isomers. In cyclic voltammetry measurements two reversible one-electron redox waves were found for the *E* form (Figure 11, right, (a)), indicating a stable

2. Theoretical Background

mixed valence cationic complex and therefore a strong coupling between the ferrocene units. After irradiation with UV light, an additional two-electron redox wave was found for the *Z* compound, indicating that in this isomer no electronic communication exist between the iron centers (Figure 11, right, (b)). In the photostationary state three different redox waves were found because both isomers were present.

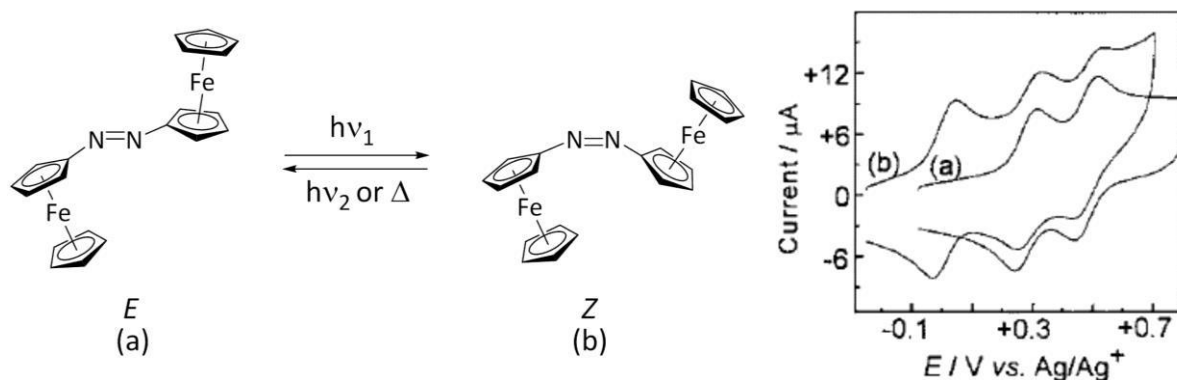


Figure 11: Azoferrocene switching reaction (left); cyclic voltammograms of *E*-azoferrocene (a) and *Z*-azoferrocene (b) obtained by irradiation with UV light of the *E*-isomer. (Solvent = benzonitrile; electrolyte = $[\text{Bu}_4\text{N}][\text{ClO}_4]$) (right).^[61]

In 2012 Stein *et al.*^[10] reported the modification of Propofol, the most widely used intravenous anaesthetic.^[62] They designed an azobenzene derivative of the famous drug (Figure 12) and observed that the substitution of the azobenzene unit with electron-donating substituents greatly decreased the thermal stability of the *Z* isomer, so it reverted to the *E* form in the dark. They took advantage of this fact and used it to control the anaesthetic effect within light irradiation. Given that both isomers react differently with certain receptors, it played an important role in the anaesthetic process.

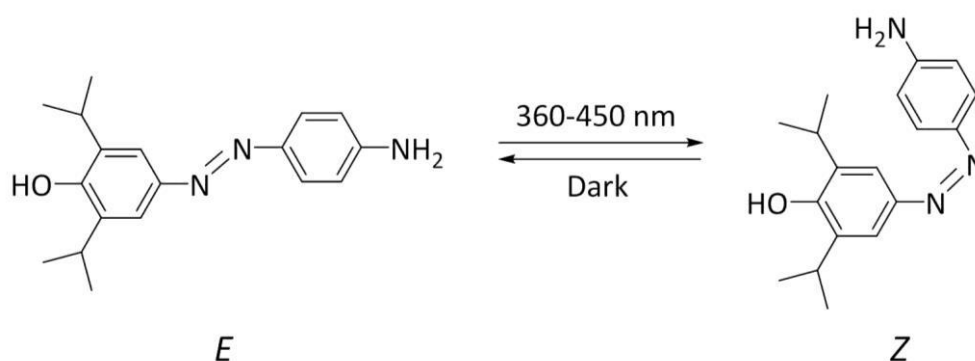


Figure 12: Reversible switching cycle of Propofol.^[10]

2.1.1.4. 1,2-Diarylethylenes

Stilbene is the simplest representative of this class of compounds. The first step of the reaction is the *E-Z* isomerization of stilbene due UV light irradiation. It occurs from both the singlet and the triplet state of the molecules. By irradiating the *Z* isomer with UV light, a cyclization *via a* conrotatory process and from the first excited singlet state ^[63] takes place and the 4a,4b-dihydrophenanthrene (DHP) is formed. ^[64] This compound can thermally or photochemically evolve to stilbene (exclusively in the *Z*-isomer). A following reaction to phenanthrene by dehydrogenation with oxygen is also possible (Figure 13). ^[24,65]

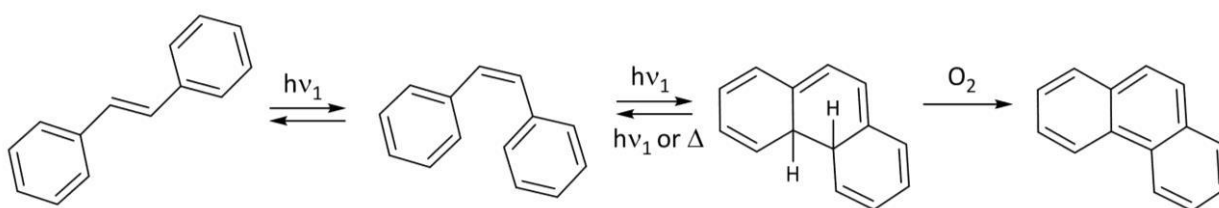


Figure 13: Photocyclization and dehydrogenation of stilbene. ^[65]

When the positions 2 and 6 of the phenyl rings and the positions 1 and 2 of the connecting double bond were substituted with methyl groups (Figure 14), the hydrogen-elimination was avoided and the DHP underwent only the back photochromic reaction, even in the presence of oxygen. However, the lifetime of the closed isomer was three minutes in the dark at 30 °C, so the system was not suitable as molecular switch. ^[66]

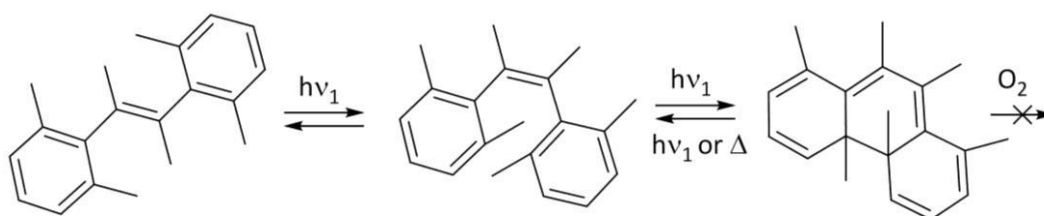


Figure 14: Photoreaction of a methyl-substituted stilbene. ^[66]

This photocyclization-dehydrogenation process can be used in the synthesis of condensed aromatic ring systems. ^[24] It was in one of this synthesis when Kellogg *et al.* ^[67] observed the lifetime of the dihydro-type intermediates were longer when, instead of the phenyl rings of the stilbene, thiophene rings were used.

In an attempt to improve the stability of the dihydro-form and based on the work of Kellogg, ^[67] Mohri ^[66] replaced the phenyl rings by other aromatic rings, i.e. thiophene and furane, and the lifetime of the dihydro-form was much longer than in the case of stilbene

2. Theoretical Background

derivatives. In addition, in the presence of oxygen, said dihydro-intermediates did not undergo to condensed rings.

In order to shift the absorption maxima of the coloured compounds to longer wavelengths, the cyano and maleic anhydride derivatives were synthesized (Figure 15). The maleic anhydride derivative also avoided the *E-Z* isomerization of the double bond, which competes with the cyclization reaction.

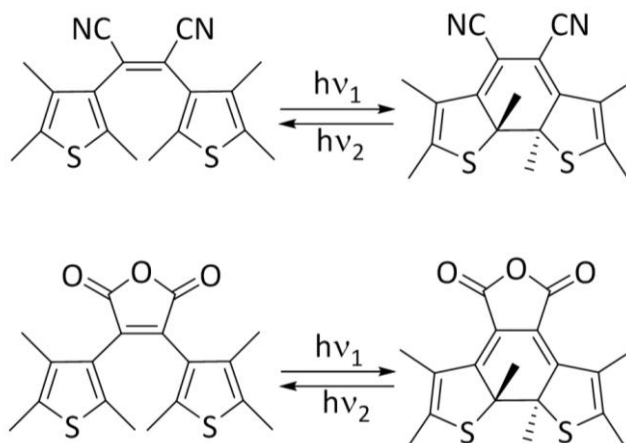


Figure 15: Cyano (top) and maleic anhydride (bottom) derivatives.

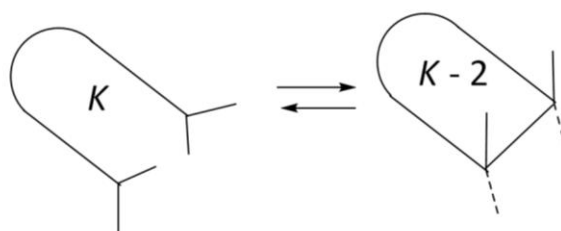
The open isomers reacted under UV light irradiation to the meta-stable closed isomers. The photogenerated isomers did not react back in the dark during three months, nor at 80 °C a thermochromic reaction was observed. Otherwise, when they were irradiated with visible light, the open isomers were obtained again.

The difference with respect to the stilbene is the aromaticity of the rings. The lower the aromatic stabilization energy, the more stable is the closed isomer, because the ring-closure process requires the loss of the aromatic character of the before mentioned rings. More than 100 colouring and bleaching cycles were carried out showing an increased resistance to fatigue.

These are the first examples of thermally irreversible diarylethene photochromic molecular switches.^[24] They laid the foundation for this important group of molecular switches, whose characteristics, thermal stability and high resistance to fatigue, make it superior to the others.

Electrocyclic reactions. Woodward-Hoffmann rules

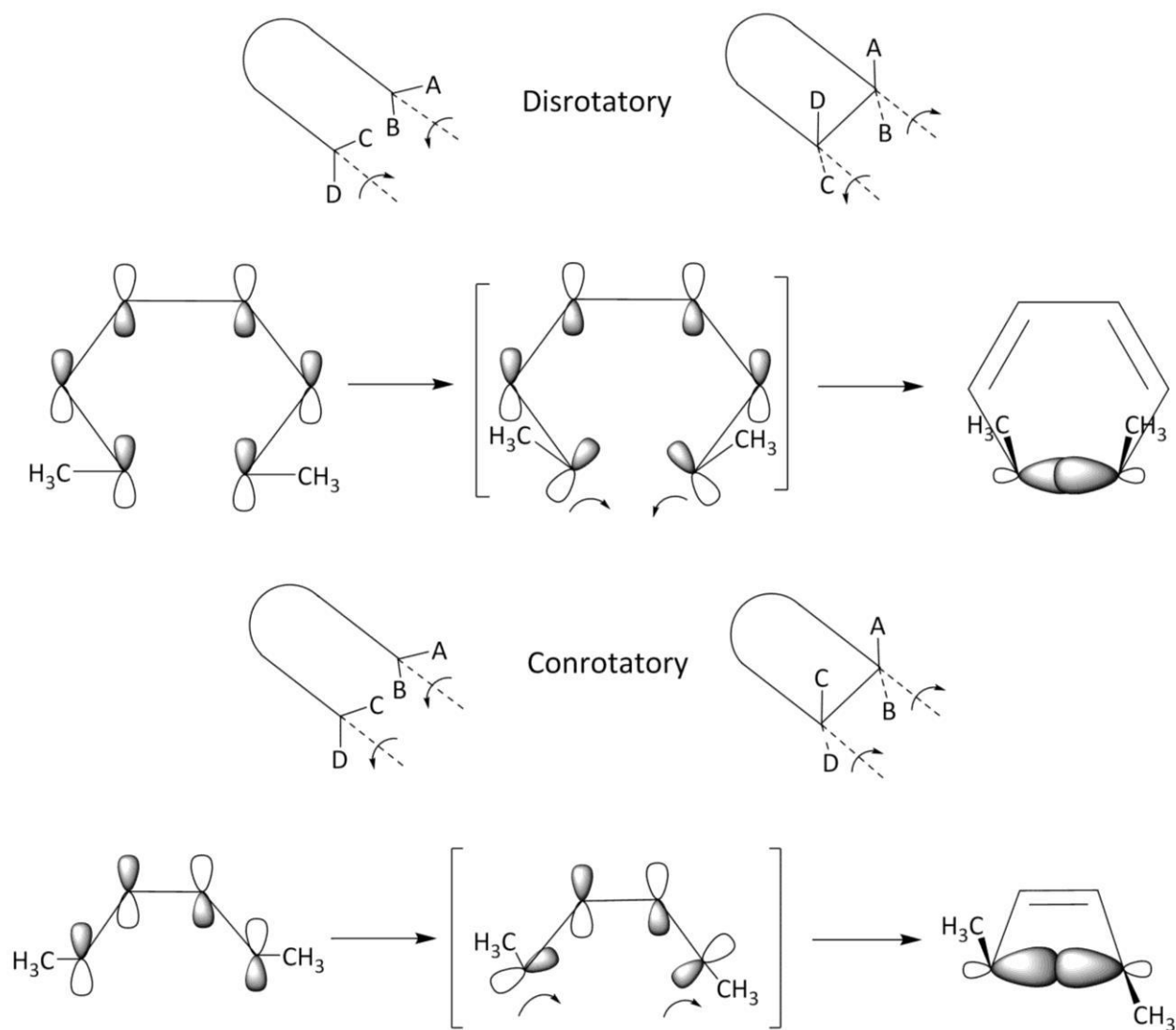
Electrocyclic reactions are those where a new single bond between the termini of a linear system containing $K \pi$ electrons is formed, and the converse process (Scheme 6).^[68]



Scheme 6: Electrocyclic reaction.

In 1965, R. B. Woodward and R. Hoffmann established the Woodward-Hoffmann rules for pericyclic reactions (concerted reactions where the first-order changes in bonding go through a transition state with cyclic geometry), including the electrocyclic reactions.^[68,69] In this type of reactions, the rigid tetrahedral isomerism of the formed cyclic structure is related to the geometrical isomerism of the initial open chain. *A priori*, this relationship could be disrotatory or conrotatory. In practice, these reactions proceed in a stereospecific manner. These rules, based on the symmetry of the HOMO of the open chain partner, will predict which transformation mode certain system will undergo, depending on the π -electrons it contains and how the reaction is induced: thermal- or photochemically.

Both possible modes differ in the rotation at each end of the molecule. In conrotatory mode, the atomic bonds of the end-groups turn in the same direction. In disrotatory mode, the contrary is true and those orbitals turn in opposite directions (Scheme 7).



Scheme 7: Possible modes to electrocyclic reactions.^[68]

In the case of systems containing $4n$ π -electrons, the symmetry of the highest occupied ground state orbital permits only a bonding interaction between both end-groups which involves an overlap between orbital envelopes on opposite faces of the system. This can only be done in a conrotatory process. On the other hand, in initial open systems with $4n+2$ π -electrons, terminal bonding interaction within ground state molecules requires overlap of orbital envelopes on the same face of the system, which can only take place in a disrotatory mode.

In the case of photochemical reactions, an electron will be promoted to the first excited state. This promotion will lead to a reversal relationship of terminal symmetry in the orbitals participating in bond redistribution. As a consequence, a process which would undergo a

conrotatory transformation when thermally induced, will follow a disrotatory course when irradiated light and *vice versa* (Table 1).^[68,69]

Table 1: Woodward-Hoffmann Rules.^[68,69]

System	Thermal	Photochemical
4n π-electrons	Conrotatory	Disrotatory
4n+2 π-electrons	Disrotatory	Conrotatory

According to these rules, for 1,3,5-hexatriene the photochemical cyclization reaction will be conrotatory, but when the same reaction is induced by heat, it will occur disrotatory. The product, cyclohexadiene, will be the same for both reaction modes. In the case of dithienylethene molecular switches the only structural consequence derived from the reaction mode will be the position of the methyl groups attached to the carbon atoms which undergo the cyclization reaction. The ring opening reaction (cycloreversion) is allowed in the conrotatory mode when it is induced by light irradiation, and in the disrotatory mode in the case of a thermal reaction.^[70]

2.1.1.5. 1,2-Diarylethenes

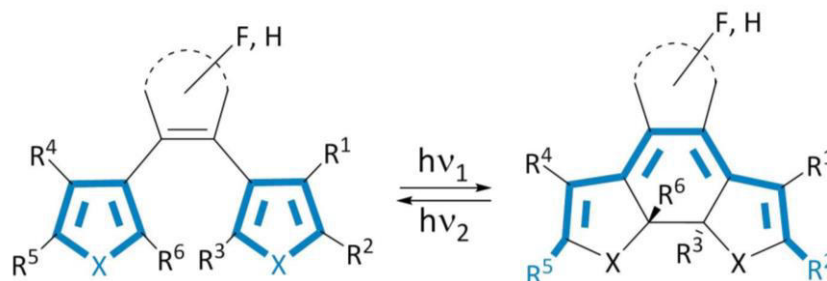
The most commonly used dithienylethene derivatives are the dithienylcyclopentenes and dithienylperfluorocyclopentenes.^[71] The interest for these molecular switches has increased in the last decade, due to its potential use in photonic devices.^[72–74]

In the literature hundreds of derivatives from those photochromism systems exist. For example, symmetrical^[72–74] and nonsymmetrical^[75] substituted, with different aromatic rings,^[76] different cycloalkene sizes^[71,77] and different organic and organometallic substituents.^[78] However, all of them have the same basic pattern in common.

Two aromatic rings (generally thiophene rings) are connected by means of a cycloalkene ring (Scheme 8, left). The cycloalkene is used instead of a simple substituted double bond in order to impede the *E-Z* isomerization, which would compete with the photochromic cyclization, thereby improving the resistance to fatigue.^[71] This is the open or “switch-off” form. The π -conjugation is predominantly restricted to both aromatic rings. The photocyclization is activated by UV light forming a new bond between the carbon atoms of the aromatic ring, which fixes the entire molecule in a plane. This arrangement provides an

2. Theoretical Background

excellent π -conjugation, which extends over eight carbon atoms and ties the functional groups R^2 and R^5 (Scheme 8, right). This rigid structure forces these groups to diverge away from each other.^[79] This is the closed or “switch-on” form. The reverse reaction occurs by irradiation with visible light.^[24]



Scheme 8: General pattern of diarylethene molecular switches.

In order to optimize the photochromic reaction, Hanazawa *et al.*^[71] synthesized the following series of molecular switches (Figure 16), which only differ in the size of the connecting cycloalkene ring.

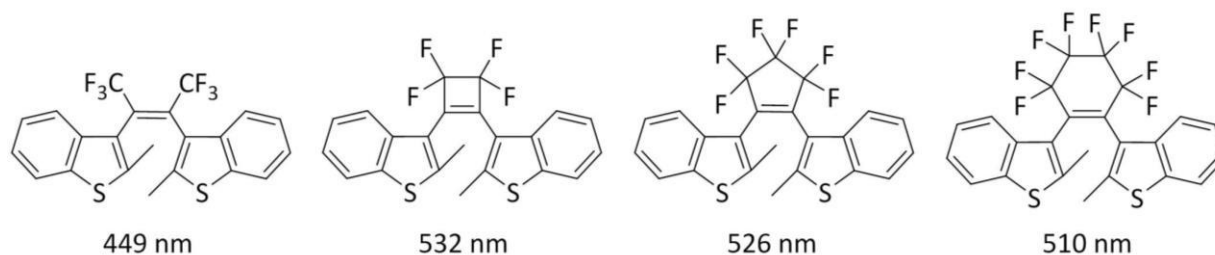


Figure 16: Diarylethene derivatives with different groups connecting the aromatic rings and their maxima in UV-vis spectroscopy after the irradiation with UV light.

It was shown, that the size of the cycloalkene influences not only the absorption spectra of the closed isomers,^[71] but also the quantum yield of the cyclization.^[77]

The ring size controls the planarity of the closed isomer and its π -conjugation. Small rings are fixing the cyclohexadiene molecular framework in a rigid structure which shows hardly deviation from planarity, maintaining the π -conjugation. Without this restriction, the dihedral angle between both aromatic rings becomes larger and the π -conjugation is vanishing, which leads to a hypsochromic shift. This is confirmed by the absorption spectra of the closed isomers of the compounds prepared by Hanazawa *et al.*^[71] (Figure 16).

The ring-closed form of the compound with no ring structure connecting the thiophene rings (Figure 16) presents a maximum absorption at 449 nm. In the case of the compounds which contain a cycloalkene, the expected shift of the absorption maxima of the closed isomers to longer wavelengths by decreasing the ring size was observed (Figure 16).^[71]

The work of Hohlneicher^[77] in 1988 showed that among different stilbene derivatives, with cycloalkenes of different sizes connecting the phenyl rings, the highest quantum yield was obtained for the six-membered ring derivative.

For the applications of photochromic switches for use in optical memory, media compounds which absorb in the wavelength region of 650-830 nm^[24] and with good quantum yields are desired. A compromise between these properties is reached in the derivatives with a cyclopentene ring connecting both aromatic rings, which have been intensely investigated in the last thirty years.^[24]

Not only the size of the cycloalkene ring exerts influence in the absorption spectrum of the molecular switches, but also the state of the molecular switch and the substituents attached to the aromatic rings.

Normally, the open isomers of diarylethene molecular switches show absorption bands at shorter wavelengths (UV region), which represent the $\pi\text{-}\pi^*$ transition. When they are irradiated with UV light and the cyclization takes place, new absorption bands are found at longer wavelengths. In figure 17 it can be seen that the absorption shift of the closed isomers depends deeply on the substituents attached to the aromatic rings.

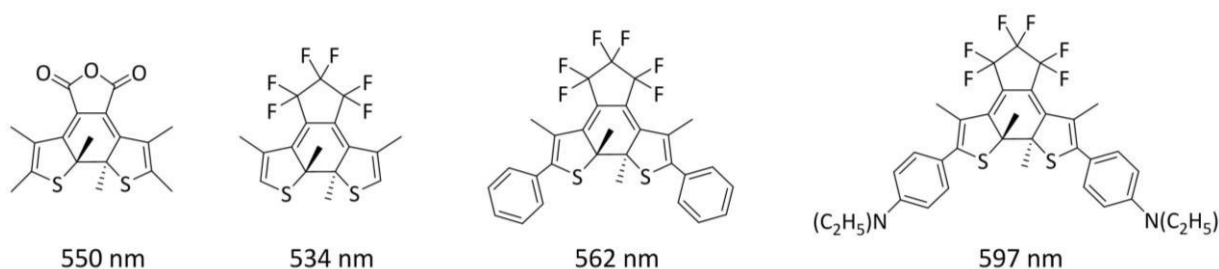


Figure 17: Diarylethene closed isomers with different substituents at the positions 5 and 5' of the thiophene rings and their corresponding maxima in UV-vis spectroscopy.

The maleic anhydride derivative presented in figure 17 became red after being irradiated with UV light and presented a new maximum at 550 nm.^[66] The closed isomer of the perfluorocyclopentene derivative with no substituents at the position 5 and 5' of the thiophene rings absorbed by 534 nm (Figure 17).^[80] When phenyl rings were substituted at these positions, the solution turned blue upon irradiation, presenting a maximum at 562 nm.^[80] Finally, the absorption maximum was further bathochromically shifted by adding electro-donating diethylamino groups at the positions 4 and 4' of the phenyl groups.^[80]

2. Theoretical Background

A compound with one of the longest absorption bands (at 828 nm) ever reported is shown in figure 18. ^[81,82] It was achieved by introducing a strong electron donating CH=benzodithiole substituent at position 5 of the thiophene ring, and a strong electron-withdrawing dicyanoethylene substituent at position 5' of the other thiophene ring. Unfortunately, the closed isomer was thermally unstable.

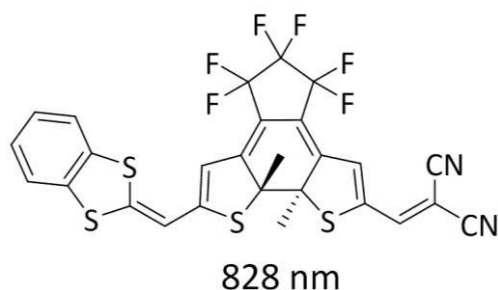


Figure 18: Diarylethene derivative after Gilat *et al.* ^[81,82]

Quantum yield in 1,2-dithienylethene molecular switches

Diarylethene molecular switches with a cycloalkene ring connecting both aromatic rings can be found in two possible conformations: one with both thiophene rings in mirror symmetry (parallel conformation) or in C_2 symmetry (antiparallel conformation), which exist in dynamic equilibrium. Only the later one can undergo the photocyclization (Figure 19). ^[70]

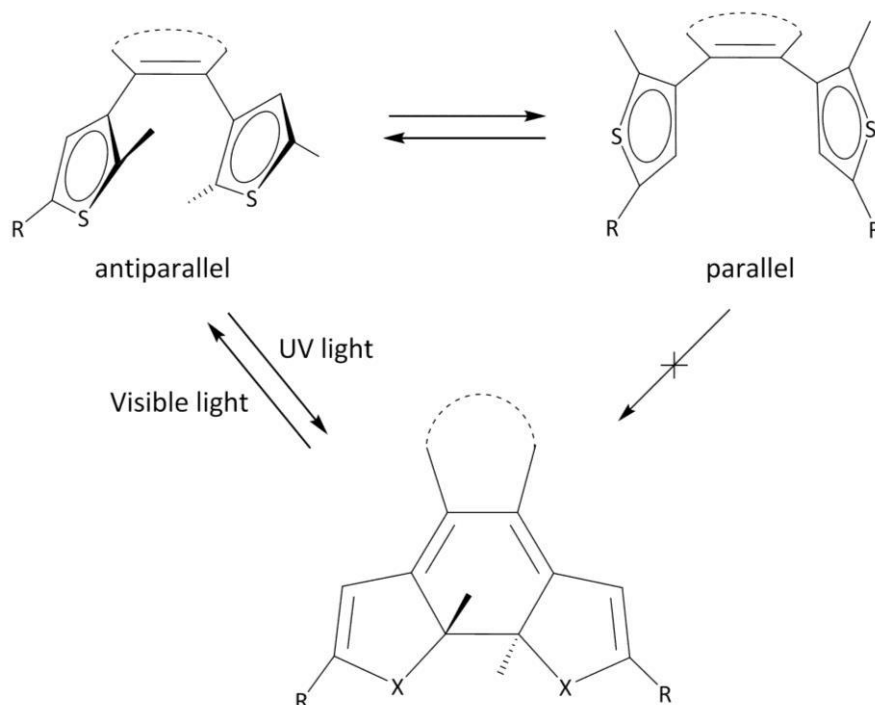


Figure 19: Possible conformations of the open isomer of a diarylethene derivative and switching reaction.

Generally, the population ratio of both conformations is 1:1. As a result, the quantum yield cannot exceed 0.5. Therefore, when the ratio is 1:1 and the quantum yield 0.5, almost all the photoexcited molecules in the antiparallel conformation undergo the cyclization. ^[24]

In order to improve the quantum yield, different methods of increasing the ratio of the antiparallel conformation have been developed.

Irie and coworkers ^[83] started in 1997 by adding β - and γ -cyclodextrins to the dissolved dithienylethenes. In the first attempt, the quantum yield was 1.5 times larger than in the reaction without cyclodextrins. The cavity of the afore-mentioned cyclodextrins was big enough to host the antiparallel conformers and the inclusion complex could be formed, but not the parallel one (Figure 20). As a consequence, the population ratio increased, improving the quantum yield of the photochromic reaction.

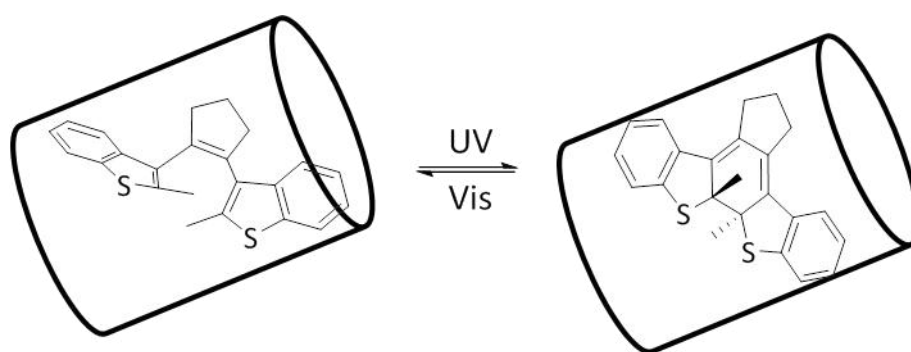


Figure 20: Switching reaction in presence of cyclodextrins.

Another approach was also attempted by Irie and coworkers ^[84] in 1999. They replaced the methyl groups at the positions 2 and 2' of the benzothiophene rings of a dithienylethene molecular switch with steric demanding isopropyl substituents (Figure 21). As a result, the antiparallel conformation ratio increased from 0.65 to 0.94, culminating in an increase of the quantum yield from 0.35 to 0.52.

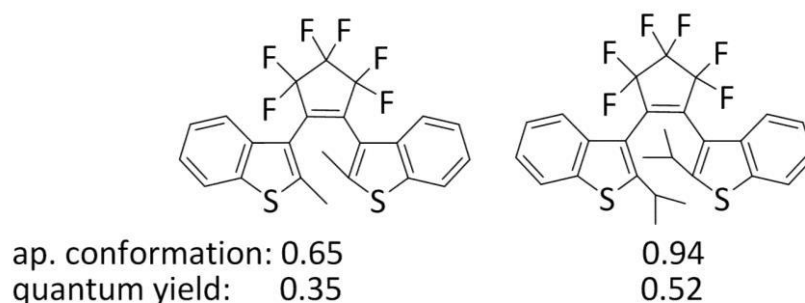


Figure 21: Increase of the antiparallel conformation and consequent quantum yield by replacing the methyl groups at the positions 2 and 2' of the thiophene with isopropyl groups.

2. Theoretical Background

Also in 1999, Stellace^[85] incorporated the dithienylethene molecules into a polymer backbone (Figure 22). Surprisingly, not only the thermal stability was higher than the one of the monomer, but also the quantum yield of the cyclization was 0.86, the highest hitherto reported for this family of molecular switches.

The reason of this astonishing quantum yield is the nearly unique existence of the antiparallel conformation of the open isomer, and the phenomenon of collective conrotatory motions, which explains why all the monomers are rotating in the same direction.

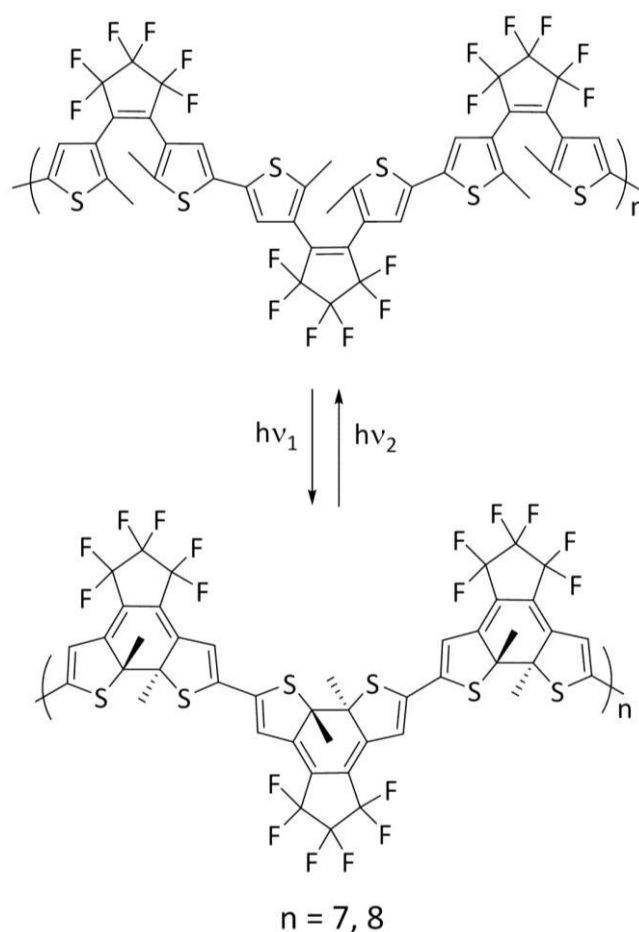


Figure 22: Diarylethene molecules incorporated in a polymer backbone.

Another strategy is to fix the aryl rings in an antiparallel conformation. Yamato and coworkers^[86] achieved it by bridging the thiophene rings at the 2- and 4-positions and avoiding the free rotation of the bonds. The obtained thiophenophan-1-ene (Figure 23) showed a quantum yield of 0.67, while for the analogous non-cyclophane dithienylethene compound, 0.40 was reported.^[87]

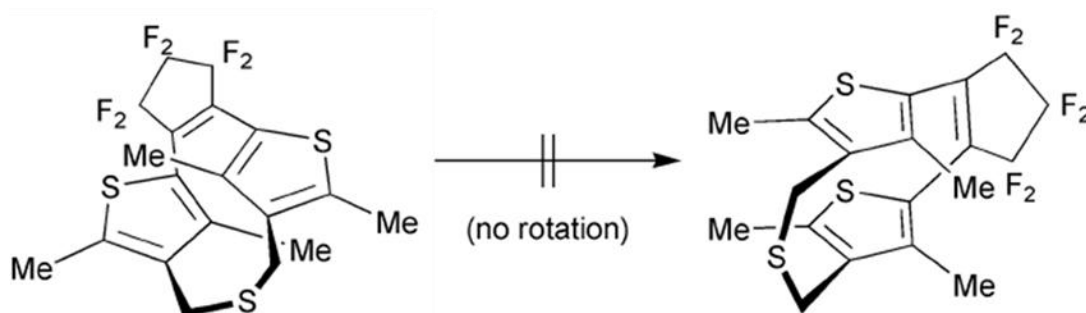


Figure 23: Cyclophane diarylethene derivative.

Hossain *et al.*^[88] designed a dithienylethene bridged by a benzene ring. It was observed that the quantum yield depended on the substitution of this benzene ring. In the case of the *meta*- and *para*- isomer, no improvement of the quantum yield was achieved, it was even worse. However, when the benzene ring was *ortho*-substituted (Figure 24), the quantum yield improved 1.3 times.

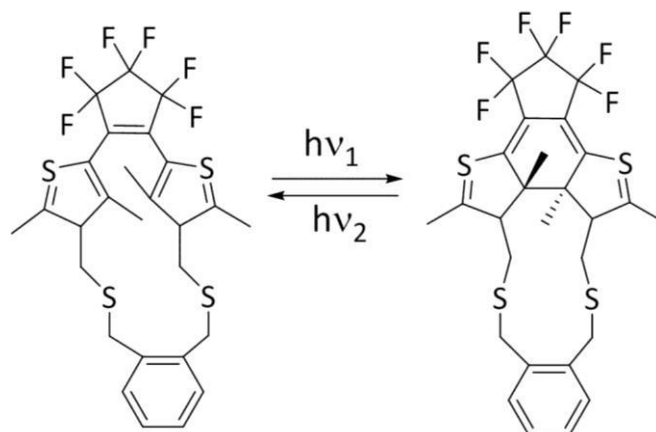


Figure 24: Diarylethene cyclophane compound after Hossein.^[88]

Hecht and coworkers^[89] decided to introduce methyl groups at the 2- and 4-positions of the cyclopentene bridge moiety (Figure 25). The quantum yield of the cyclization was 0.83, almost as high as that of the “diarylethene polymer backbone”.^[85]

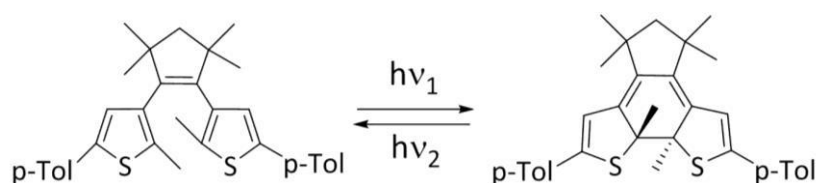


Figure 25: Diarylethene derivative synthesized by Hecht in 2012.^[89]

Fatigue in 1,2-dithienylethene molecular switches

Photochromic reactions are non-destructive chemical bonds rearrangements, but unfortunately, they are always accompanied by other undesirable side reactions (Figure 26). The most important side reactions which produce the decomposition of the photochromes are oxidation reactions.

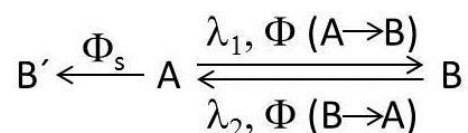


Figure 26: Quantum yield of the photochromic and side reactions.

For this group of molecular switches the repeatable cycle number (RCN) is defined as the number of photochromic cycles (whitening-colouring) under determinate conditions at which the absorbance of one of the isomers (white or coloured) decreases to 80 % in relation to the first cycle. ^[24]

The RCN varies greatly among different members of this group of molecular switches. Also, for a certain compound, the repeatable cycle number can vary widely depending on the physical state (in solution or in crystal state) and on the atmosphere where the experiments are carried out (under air, inert atmosphere or vacuum).

In figure 27 three different perfluorodiarylethene derivatives are shown. The RCN varies greatly depending of the substituents attached to the thiophene rings (Table 2).

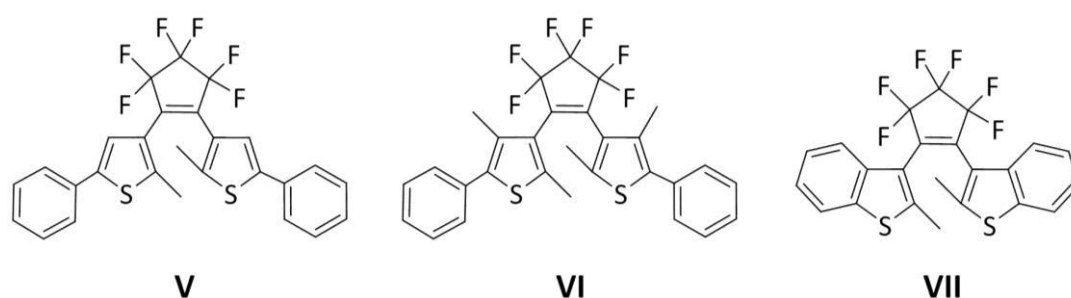


Figure 27: Diarylethene derivatives.

Table 2: Repeatable cycle number (RCN) under different conditions (Figure 27).

Compound	RCN (in air)	RCN (vacuum, sol.)	RCN (vacuum, crystal)
V ^[90]	80	200	< 10 ⁴
VI ^[80]	200	< 850	-
VII ^[71]	< 1.3*10 ⁴	-	-

In the case of compounds **V** and **VI** (with thiophene rings), the product decomposes much faster by carrying out the reaction in the air. The reason for this is the oxidation to endoperoxides. Another undesired side reaction is the formation of a six-membered condensed ring structure formed from the closed isomer during the irradiation with UV light. Such by-product formation (Figure 28) is the main fatigue process of dithienylethenes in the absence of oxygen, when the thiophene rings are not substituted at the 4- and 4'-positions with methyl groups.^[90]

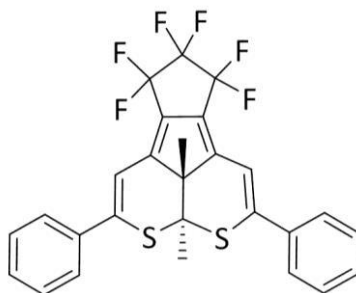


Figure 28: Side product of the photocyclization reaction.

These methyl groups at the 4- and 4'-positions of the thiophene rings avoid their rearrangement and the undesired product cannot be formed, improving greatly the RCN.

By replacing the thiophene rings with benzothiophene rings, the repeatable cycle number increased considerably. Benzothiophene is not as reactive as thiophene to oxygen, and the already mentioned by-product cannot be formed.^[24]

Compound **VII** is even able to undergo photochromism in the crystalline phase. The repeatable cycle number is huge; after 10000 cycles the six-membered condensed ring product was not detected.

In a further investigation, bis(5-pyridyl-2-methyl-thien-3-yl)perfluorocyclopentene, which has no methyl groups at the 4- and 4'-positions, was introduced in a copolymer film and its resistance to fatigue was studied.^[91] The degradation started after 15000 cycles. Thus the side reactions were partially suppressed.

Photochromism in the solid state

Although it is rare to find thermally stable photochromic reactivity in the single-crystalline phase,^[92] some diarylethene molecular switches undergo thermally stable and fatigue resistant photochromic reactions.^[72,75,93]

From both possible conformations, the antiparallel one (the only one which is able to undergo the cyclization)^[70] is dominant in the single crystal state. Therefore, in crystalline state, almost all diarylethene derivatives should show photochromic behaviour. However, in practice it does not always occur.^[94,95] The investigation of Kobatake *et al.*^[95] in 2002 demonstrated that the single-crystalline behaviour depended on the distance between the methylated carbon atoms rather than on polar and steric substituted effects. After testing different dithienylethene derivatives, it was established that when this distance is larger than 0.42 nm, the photocyclization cannot take place.

As expected, the structural changes during the irradiation are small. Only the reactive carbon and sulphur atoms change their position. This phenomenon allows the photochromic reaction to be possible in the crystal lattice.^[24]

The fatigue in crystal state is usually very low. The reason is that in the crystals the rearrangements are prohibited and the oxidation is suppressed because the oxygen can only react with the surface of the solid.

2.1.2. Metal complexes containing diarylethene molecular switches

Although the concept of organometallic complexes containing a diarylethene motif is relatively recent,^[96] a long list of coordination compounds and their properties have already been studied.^[43,96–99,100,101–103] By introducing a metal center into the switching unit it is possible not only to vary the switching reaction (allowing to modify the switching properties systematically), but also to combine it with the photophysical,^[104] electrochemical,^[99,101,104,105] optical^[98] and magnetic^[96,99,106] characteristics of the coordination compounds.^[96] In addition, combining transition metals with molecular switches can change their excited state reactivity^[98] and spectroscopic properties.^[98,99] Ideally, the metal center will be able to “feel” the geometrical and electronic structural changes of the molecular switch, and the desired function will be triggered at the metal center.

In this chapter different examples of organometallic complexes with one (or more) photochromic units will be presented and their properties discussed. In this way the advantages and possible applications of this new type of complexes will be illustrated.

In 1998 Lehn ^[107] reported two tungsten photochromic complexes (Figure 29) which exhibited light-triggered fluorescence on excitation of absorption bands that have only minimal influence on the switching reaction. The shown fluorescence came as result from the interaction of the thiophene ring with the metal center through the pyridine ring in the closed form of the molecular switch. ^[108]

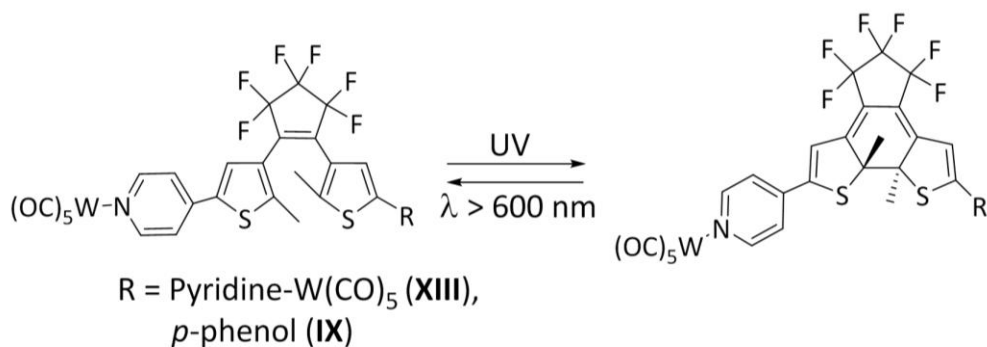


Figure 29: Tungsten photochromic complexes by Lehn. ^[107]

Adamo *et al.* ^[97] prepared in 2003 a dinuclear ruthenium complex (Figure 30) which contained a perfluorocyclopentene switching unit. The efficiency of the photochemical ring-closure was very high (96% for the photostationary state PSS) and the quantum yield was 0.93. The impressive high value for the PSS could be explained by a clear separation of the absorption bands in UV-vis spectroscopy. The excellent quantum yield of the closing process could be given by the sterically demanding substituents at the 5- and 5'-positions of the thiophene rings. An increase of steric hindrance of the substituents at these positions benefits the antiparallel conformation, ^[84] the only able to undergo the switching reaction. ^[70] Emission spectra of this complex were measured too. A large discrimination in the fluorescence, depending of the state of the switch, was observed. This phenomenon indicates a strong influence on the energy level of the switching in both possible states. However, the most interesting observation was the possibility of inducing the photochemical ring enclosure not only with UV light, but also with visible light (450 nm), by triplet sensitization of the ruthenium complex by irradiation into the MLCT band and subsequent energy transfer from the metal center to the switching unit.

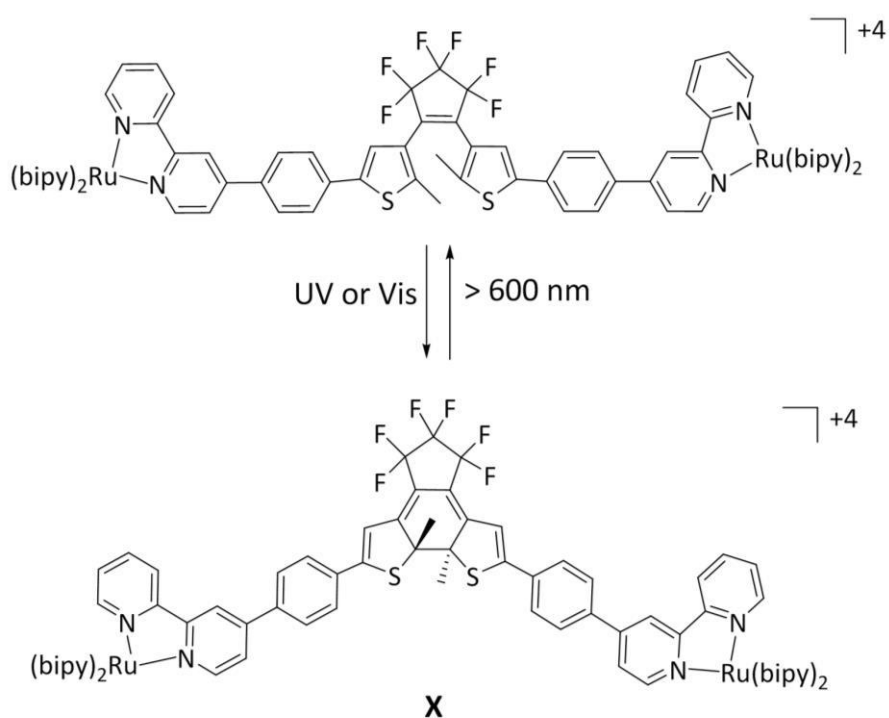


Figure 30: Dinuclear ruthenium complex containing a perfluorocyclopentene molecular switch. ^[97]

A rhenium containing dithienylethene system reported by Lee in 2007 ^[109] was demonstrated to exhibit NIR photochromic behavior (Figure 31, bottom). In the uncoordinated ligand (Figure 31, top), the heterocyclic rings were twisted with respect to each other and were not coplanar when the molecular switch was in the open form. By coordinating the rhenium(I) metal center the 2,2'-linked pyridyl and imidazolyl rings were forced into coplanarity, and a consequent increase in the extent of the π -conjugation was observed. When the closed isomer of the metal complex was obtained, the π -conjugation became further enhanced. Finally, upon excitation of the complex (open state) at $\lambda < 450 \text{ nm}$ into either the IL or MLCT bands, new absorption bands were generated. They were assigned as metal-perturbed IL transitions of the closed form with mixing of MLCT transitions.

By excitation into the MLCT absorption band at 410 nm the photocyclization took place also. Therefore, the ring closure can be triggered by irradiation with visible light via MLCT excited state photosensitization.

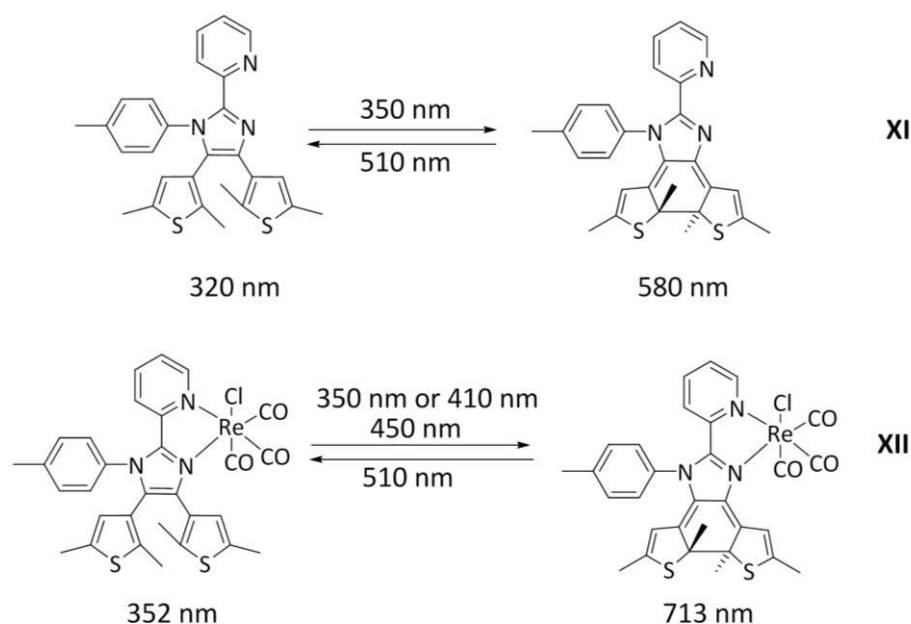


Figure 31: Organic dithienylethene molecular switch (top), rhenium(I) complex (bottom) and their absorption bands in UV-vis spectroscopy (at the longest wavelength).

The working group of Guirado ^[78] reported in 2007 the synthesis and the photochromic, spectroscopic and electrochemical behaviour of the bis(ethynylferrocene) complexes shown in figure 32.

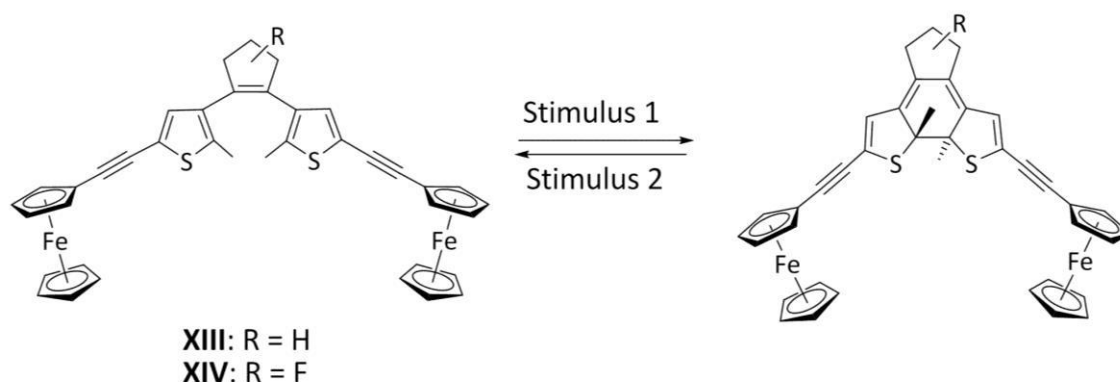


Figure 32: Bis(ethynylferrocene) - DTE complexes synthesized by Guirado *et al.* ^[78]

Ferrocene, a mild donor, was chosen as metal containing moiety because within one electron oxidation, it converts with no bond modification into ferrocenium, which acts as acceptor. This “D-to-A” redox switch has been previously employed to trigger nonlinear optical (NLO) properties. ^[110]

Both perfluoro- und perhydrocyclopentene-bis(ethynylferrocene) complexes undergo photochemical ring-closure by irradiation with UV light and ring-opening when irradiating with visible light.

2. Theoretical Background

These complexes were investigated also by means of cyclic voltammetry. Both open isomers showed only one two-electron wave for the oxidation of the ferrocene moieties, what indicates it does not exist electronic communication between the metal centers.

The closed isomers underwent chemical transformations after the oxidation reactions, but they were different for both complexes.

In the case of the perfluorocyclopentene derivative **XIVc**, only a two-electron redox reaction was observed, thus, both ferrocene units were oxidized simultaneously (like in the case of the open isomer). Additionally, a second but irreversible oxidation was found at higher potential, which was believed to correspond to the oxidation of the photochromic core ($\text{Fc}^+(\text{PCF}_{\text{closed}})^+-\text{Fc}^+ / \text{Fc}^+-\text{PCF}_{\text{closed}}-\text{Fc}^+$ couple). However, the peak intensity relative to the ferrocene wave was smaller as expected. It is known in the literature that electron-withdrawing substituents, such as ferrocenium, destabilize the closed isomer of the molecular switch and facilitate the ring-opening reaction.^[111] Under this experimental conditions, the formed tricationic radical species $\text{Fc}^+(\text{PCF}_{\text{closed}})^+-\text{Fc}^+$ underwent a rapid ring-opening reaction. The resulting $\text{Fc}^+(\text{PCF}_{\text{open}})^+-\text{Fc}^+$ species is a strong oxidizing agent and oxidized a neighbouring molecule of $\text{Fc}^+-\text{PCF}_{\text{closed}}-\text{Fc}^+$, restoring the $\text{Fc}^+-\text{PCF}_{\text{open}}-\text{Fc}^+$ molecule. This electron exchange leads to the depletion of the $\text{Fc}^+-\text{PCF}_{\text{closed}}-\text{Fc}^+$ species near the electrode decreasing the peak intensity.

The closed perhydrocyclopentene complex **XIIIc** presented only one two-electron wave for the oxidation of ferrocene and another one at higher potential. It was attempted to generate the $\text{Fc}^+-\text{PCH}_{\text{closed}}-\text{Fc}^+$ species, but it could not be found. Spectroelectrochemical experiments confirmed that the transformation to the $\text{Fc}^+-\text{PCH}_{\text{open}}-\text{Fc}^+$ form was so fast that it could not be detected in cyclic voltammetry. Comparing with the PCF-derivative, the reopening process was much faster. The difference could lie on the charge delocalization. While in the perfluorocyclopentene derivative a partial charge transfer destabilized the neutral closed photochromic core, in the perhydrocyclopentene complex a more important delocalization could be operating, therefore the weight of the $(\text{PCH}_{\text{closed}})^+$ charge localized transient would have greater influence.

In the same year, Uchida *et al.* reported the synthesis of the compounds presented in figure 33, where two ruthenium sandwich complexes are directly attached to the molecular switch core. This complex was able to undergo the switching cycle up to ten times without decomposing, despite the electron-withdrawing character of the sandwich units.^[112] However, it should be mentioned that due to the presence of the methyl groups of the Cp*-ligands and the tropilium ligands, the electron-acceptor character of these ruthenium sandwich units is weaker as in the case of ferrocenium (Figure 32).

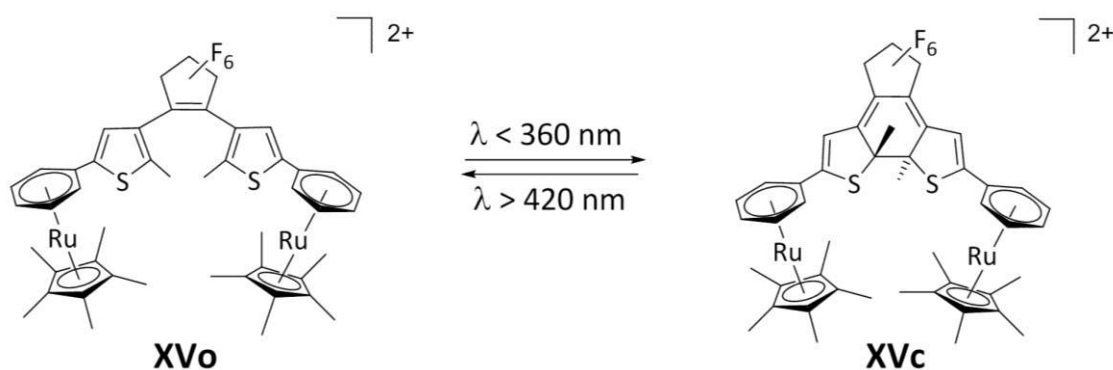


Figure 33: Ruthenium(II)-complexes after Uchida *et al.*^[112]

J.-P. Launay,^[113] in 2000, synthesized a Ru(bipy)₂(phenylpyridyl) derivative linked by an acetylene unit with the intention of measuring the metal centers communication (Figure 34). This complex reversibly underwent the switching reaction and in the photostationary state the closed isomer was found for 75 %.

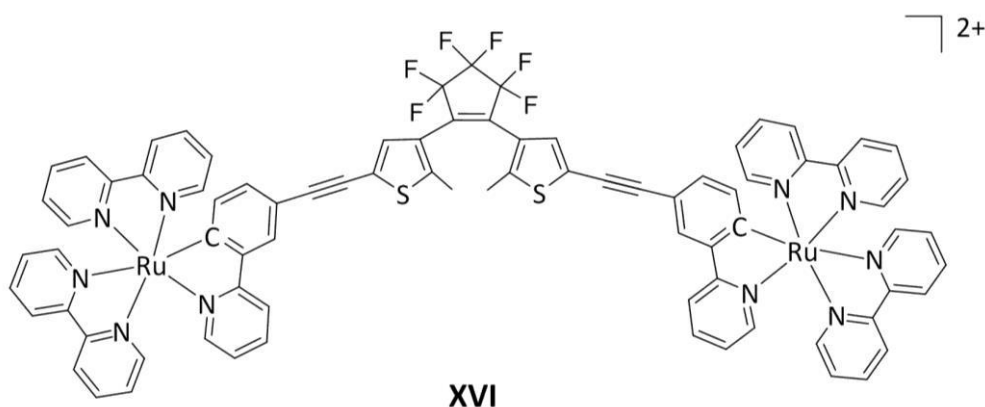


Figure 34: Ru(bipy)₂(phenylpyridyl) complex in its open form.

In order to measure the interaction between both metal centers, two different values were investigated: the first was the switching factor (SF) (Equation 3) which is defined as the quotient between the comproportionation constants K_c (Equation 2) of each state of the molecular switch. It can reach values up to a magnitude of 10^3 .^[101] The K_c , used as a

2. Theoretical Background

measure for the performance of molecular wires, is an equilibrium constant which represents the thermodynamic stability of the mixed valence monocationic species against the neutral and dicationic ones (the non-mixed valence species). It indicates the extension of the charge delocalization ^[114,115] and it is obtained within electrochemical methods.

$$Kc = \exp\left(\frac{\Delta E^*F}{R^*T}\right) \quad \text{Equation 2}$$

ΔE = potential difference between the two redox complexes

F = Faraday constant

R = Ideal gas constant

T = Temperature

$$SF = \frac{Kc(open)}{Kc(closed)} \quad \text{Equation 3}$$

The second value was the electronic coupling term (V_{ab}), ^[113] which defines the efficiency of the bridge at mediating electron transfer between the distant redox sites and it is obtained by means of IR spectroscopy.

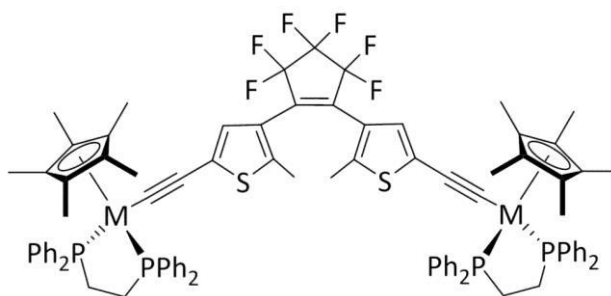
The ruthenium complex **XVI** showed switching of the communication between the metal centers, but the difference on the Kc values was insignificant. The chain of twenty carbon atoms which connected both metal centers was too long.

They could characterize the communication performance between two iron centers through the photochromic bridge and studied the photo- and electrochromic behaviour of the corresponding ruthenium complex. Moreover, depending on the oxidation state of the ruthenium atoms, it was possible to stabilize the closed isomer, which normally would undergo the photocycloreversion by irradiation of visible light, locking the switching process. This stabilization of the closed isomer by coordinating a metal center to the molecular switch has been repeatedly in the literature. ^[101,116]

Akita and coworkers, ^[101,114,115] with the motivation of creating complexes with better interaction of the metal centers, synthesized a series of organometallic compounds with a shorter carbon atoms bridge and with more electrodonating metal centers connected to the photochromic core.

In a first attempt, the iron complex **XVII** ^[114,115] and the ruthenium complex **XVIII** ^[115] (Figure 35), where the metal centers were connected by a chain of twelve carbon atoms, were synthesized. The iron complex **XVII** underwent the photochromic reaction, but the conversion was slow and the content of the closed isomer at the PSS was not large. On the

other hand, the switching factor, with a value of 39, confirmed a weak M-M interaction switching behaviour.



XVII: M = Fe

XVIII: M = Ru

Figure 35: Iron and ruthenium complexes after Akita^[114,115] in the open form of the molecular switch.

The related ruthenium complex **XVIII** showed a much faster photochromic conversion, a more efficient ring opening reaction and better quantum yields, but the SF was only 4.2.

While the iron complex did not present electrochromic properties, the ruthenium analogous complex did. Moreover, depending on the oxidation state of the ruthenium atoms, it was possible to stabilize the closed isomer, locking the switching process.

Considering the improvement in the wire performance by shortening the chain of carbon atoms, again the working group of Akita^[101] removed the acetylene linkers providing eight carbon atoms bridged complexes, where the metal centers were directly connected to the photochromic core through M-C σ -bonds (Figure 36). These complexes demonstrated not only photochromic, but also electrochromic reversible behaviour.

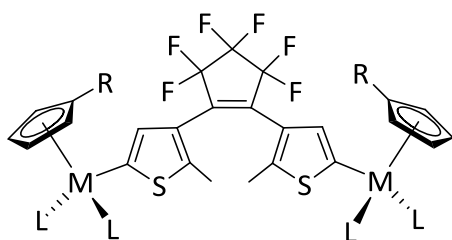


Figure 36: First M-C direct σ -bond complexes.

Table 3: Complexes XIX-XXIII.

	M	R	L ₂
XIX	Fe	H	(CO) ₂
XX	Ru	H	(CO) ₂
XXI	Fe	H	(CO)(PPh ₃)
XXII	Ru	H	(CO)(PPh ₃)
XXIII	Fe	H	dppe

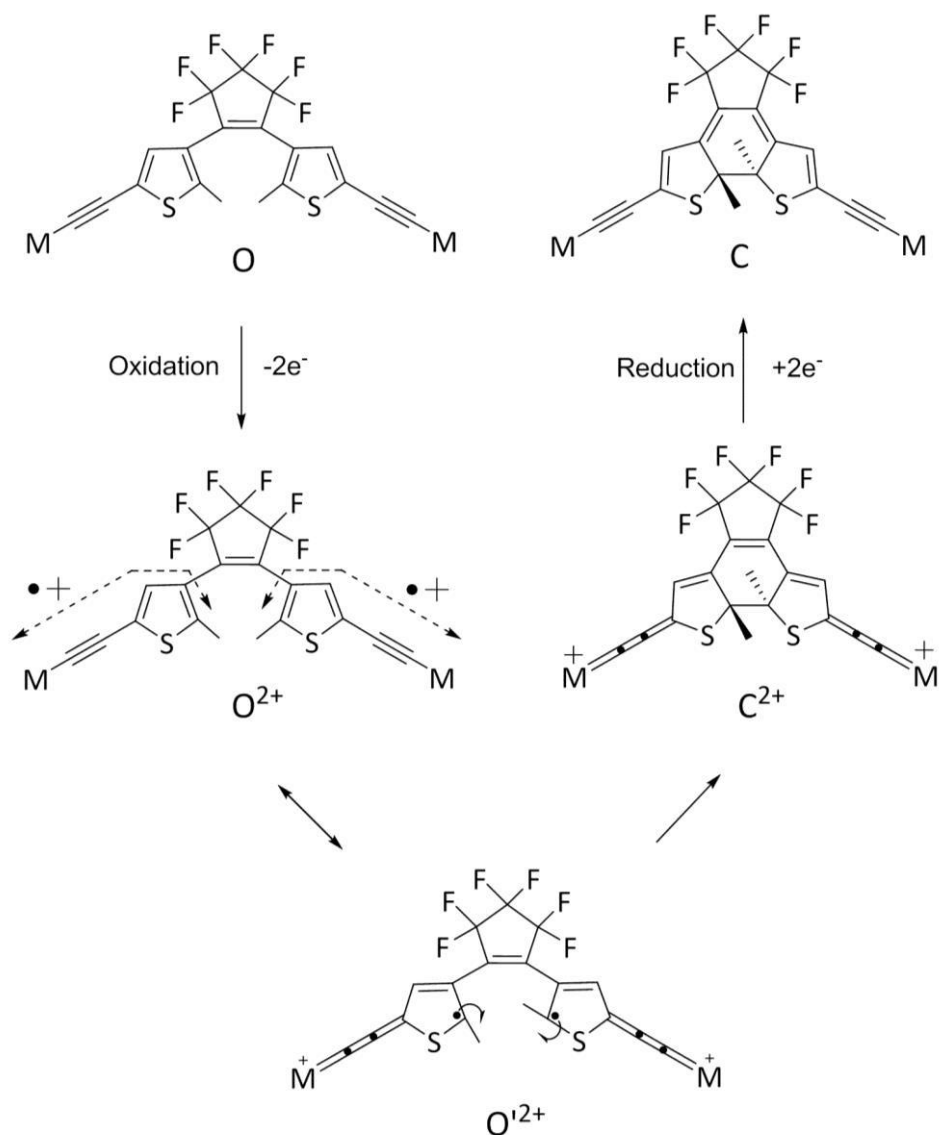
The photochromic behaviour was observed to be dependent on the metal center and on the other ligands coordinated to the metal center. The ruthenium complexes underwent the cyclization reaction in a more efficient way. Respect to the ancillary ligands, the introduction of phosphine ligands decelerated the ring closure reaction, and the iron complex with a dppe

2. Theoretical Background

ligand did not undergo the photochromic reaction at all. However, this former complex exhibited a very good electrochromic cyclization.

These complexes exhibited also remarkable switching performance. The K_c values were larger than 10000 while $K_c(O)$ remained small. As a result, the SF values were huge. In the case of the complex **XXII** it was exhibit a value as large as 5400.

Complexes **XVIII-XXIII** showed electrochromic behaviour. The mechanism is depicted in scheme 9. ^[115,117]



Scheme 9: Mechanism of the electrochromic reaction.

The open state (O) suffered a two-electron oxidation of the DTE core and the diradical species (O'^{2+}), where the radical centers were delocalized over the thienylethynyl-metal linkages with substantial spin populations on the thiophene carbon atoms adjacent to the

methyl groups (O'^{2+}). In a very fast coupling of the radical centers the closed carbene species was obtained (C^{2+}) and upon two-electron reduction, the neutral closed form was achieved. The oxidation-induced ring-closing is also known for pure organic derivatives,^[118] but the oxidized intermediates are not stable because electron donation to the electron-deficient radical species is insufficient. Metal centers, especially electron-donating ones, stabilize the radical species O^{2+} .

The electrochromic process can also lead to locking the neutral closed form.^[117]

Abruña and coworkers^[102] prepared in 2009 a series of organometallic compounds, among which the complexes depicted in figure 37 were found. These compounds do not follow the habitual structure M-DTE-M, but the metal center is found between two photochromic units.

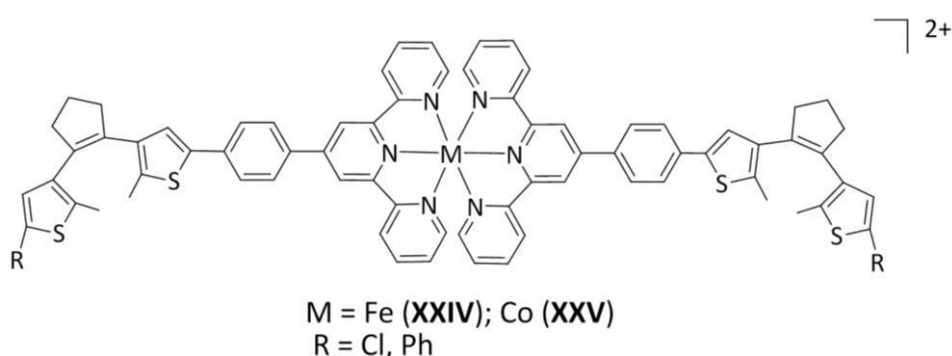


Figure 37: DTE-M-DTE complexes by Abruña *et al.*^[102]

Two different metals were employed, iron and cobalt, and two different substituents R attached to the 5-position of the thiophene ring (chloro and phenyl substituents). Both paramagnetic cobalt complexes showed photochromic behaviour, being superior the complex with the phenyl substituents. This former complex presented electrochromic behaviour.

The iron complexes demonstrated worse photochromic behaviour. The complex with the chloro substituents did not undergo the photocyclization at all, and the other iron complex showed to be photochromic but the reaction was very slow. The electrochromic reactivity of this iron complex was the best of the four complexes.

The introduction of metal centers in the photochromic system not always entails an improvement of the switching process or an increase on determinate useful properties. This case was illustrated by the cobalt complexes reported by Harvey in 2014.^[119]

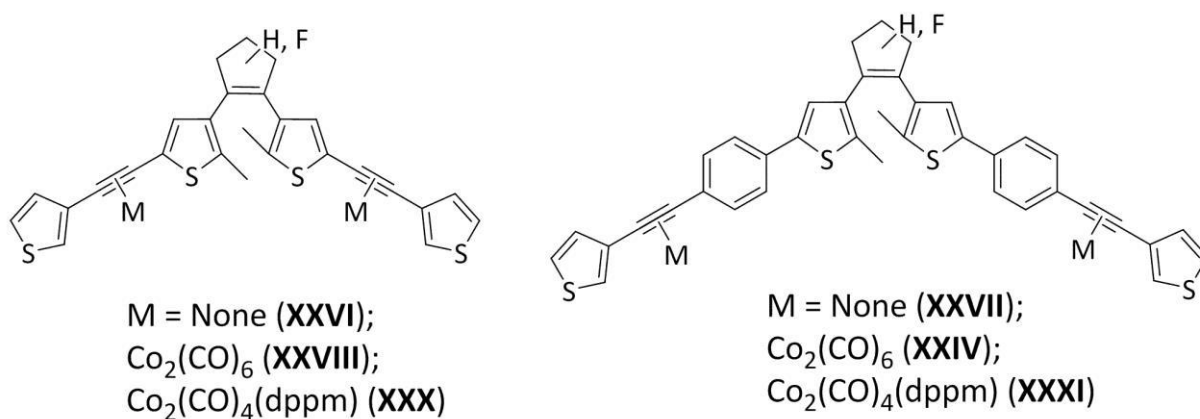


Figure 38: Organic ligands and cobalt complexes prepared by Harvey in 2014. ^[119]

Initially, the organic photochromic compounds (**XXVI** and **XXVII**, Figure 38), both with hydrogen and fluorine atoms in the cyclopentene core, were synthesized and their photochromic properties investigated. It was concluded that the perfluoropentene ring and the extension of the π -conjugation improved the ring-closure and -opening, the fatigue resistance and the thermal stability.

Afterwards, different cobalt carbonyl complexes were introduced in the switching unit (**XXVIII** - **XXXI**, Figure 38). It was observed the presence of the metal centers reduced the efficiency, the reversibility of the reaction and the resistance to fatigue. In some cases, the photochromic reaction was totally impeded and/or the complexes degraded fast.

2.2. Magnetism

Magnetism is a physical phenomenon by which an object exerts attraction or repulsion forces on other object or objects. Some materials can generate measurable magnetic fields spontaneously, but all materials will be affected by the presence of an external homogeneous magnetic field, inducing a magnetic moment μ . This effect can be transferred to the molecular level, where the electrons will generate this magnetic moment.

When an external magnetic field H is applied to a sample, the magnetic moment of the electrons of the sample will interact with the magnetic field and the substance will become magnetized.

The magnetic susceptibility χ is defined as the quotient of the magnetization M and the magnetic field H and it is an indication of the response level of the material to the applied magnetic field.

$$\chi_v = \frac{M_v}{H} \quad \text{Equation 4}$$

The volume magnetic susceptibility χ_v is a non-dimensional proportionality constant. The magnetic mole susceptibility χ_m (cm^3/mol) is used more often and it can be measured with a Gouy balance.^[120]

Most of the researchers involved in the field of magnetism and quite all the available literature employ the cgs emu system instead the SI. Therefore, the mole magnetic susceptibility χ_m will be expressed in:^[121]

$$[\chi_m] = \frac{\text{emu}}{O_e \times \text{mol}} \quad \text{Equation 5}$$

2.2.1. Diamagnetism

Diamagnetism is a ubiquitous property of matter, present and quantifiable in all materials. Diamagnetic behaviour is mostly observed when the material contains only paired electrons. When an external magnetic field is applied, the motion of those electrons in their orbit is perturbed, and as a consequence a magnetic field is induced in the direction opposite to the externally applied magnetic field. As a consequence, these materials are repelled by the magnetic field. Due to this opposition to the magnetic field and consequent weakening, the

2. Theoretical Background

susceptibility of diamagnetic materials χ^D is negative. It is also independent of the temperature and the strength of the applied field.

χ^D is additive and can be roughly calculated from the atomic susceptibilities and constitutive corrections, or from group susceptibilities (whole molecules, fragments of molecules or individual atoms, ions or bonds) which can be found in the literature, known as Pascal's constants. [3]

Although the value of χ^D is almost negligible, much lower than the susceptibility of paramagnetic materials χ^P (materials containing unpaired electrons; see section 2.2.2), it is still needed to properly calculate the experimental susceptibility χ^{Exp} :

$$\chi_m^{Exp} = \chi_m^D + \chi_m^P \quad \text{Equation 6}$$

The susceptibility of diamagnetic materials χ^D plays an important role, especially at high temperatures, and often cannot be neglected. [121,122]

From this moment, and for the sake of simplicity, the paramagnetic susceptibility will be expressed as χ_m .

2.2.2. Paramagnetism

Paramagnetic materials are those which have unpaired electrons, presenting nonzero spin or orbital angular momentum. [3] In the absence of an external magnetic field, the resulting magnetic moments in a solid interface are arranged in a disordered fashion and as a consequence no magnetization can be detected. When an external magnetic field H is applied, the single magnetic moments in the molecule or atom orbital reorder themselves in parallel with the applied magnetic field, generating an energetically favourable situation. For this reason, this type of materials are attracted to the external magnetic field.

This induced parallel arrangement is countered by the thermal motion of the atoms and their respective spins. Therefore, the lower the temperature, the stronger the described phenomenon will be. The Curie Law describes the relation of the magnetic susceptibility χ_m with the temperature:

$$\chi_m = \frac{C}{T} \quad \text{Equation 7}$$

Being C the Curie-constant.

The Curie-Law is only valid for atoms and ions (isolated magnetic moments), weak magnetic fields and non-extreme low temperatures. For molecules and crystals the Curie-Weiss-Law should be applied instead:

$$\chi_m = \frac{C}{T - \theta} \quad \text{Equation 8}$$

This law considers the interaction between the magnetic moments; parallel and antiparallel interactions result in a negative or positive Weiss-constant θ (see 2.2.3).

In a χ^{-1} -over- T plot, a straight line is observed. In case of Curie Law, the line goes through the axis origin (0,0), but in the Curie-Weiss Law, it does not. The line intercepts the T -axis exactly in the θ value (Figure 39).^[122]

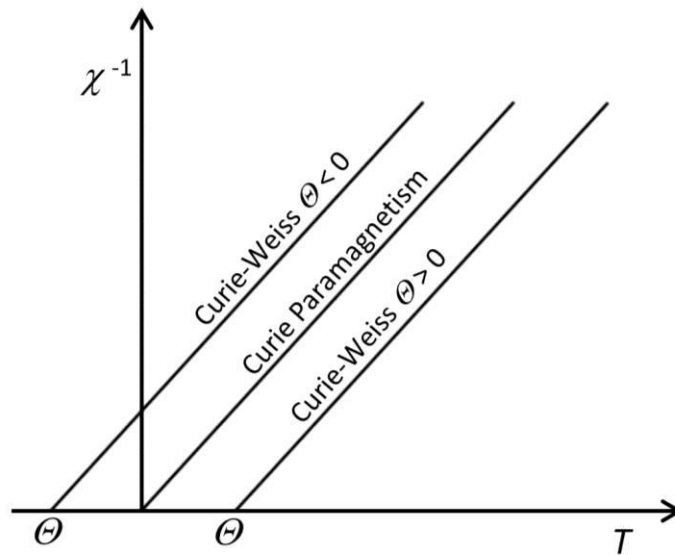


Figure 39: Curie and Curie-Weiss paramagnetic behaviour.

The θ value can provide valuable information about the collective phenomena (section 2.2.3.) taking place in a magnetic material. However, it should not be forgotten that these collective interactions are not present in all paramagnetic materials, independently of the value of θ . It is possible that the deviation from the Curie Law could have other reasons than intermolecular interactions.^[121–123]

2.2.3. Collective Phenomena

The magnetic moments of a substance cannot be considered as separate and independent particles, but they interact with each other. At lower temperatures, when the thermal motion is slow, this interaction can lead to a coupling between single electron spins. As a consequence, a spontaneous arrangement of these spins can be observed.

These collective phenomena can be classified in three categories: ferromagnetism, antiferromagnetism and ferrimagnetism (Figure 40).^[120,122]

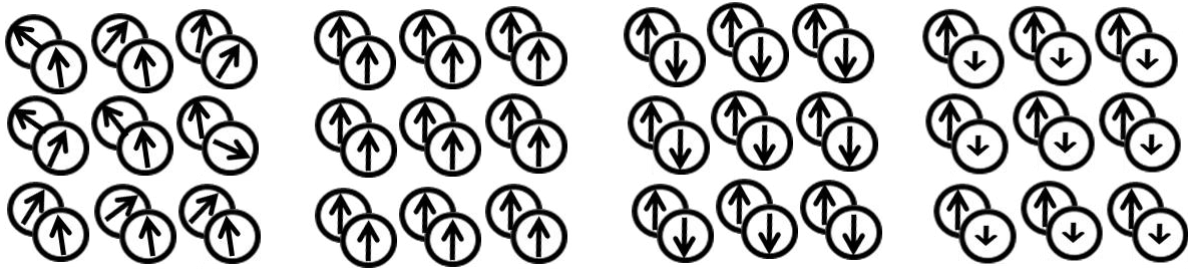


Figure 40: Spin orientation in paramagnetic (left), ferromagnetic (centered left), antiferromagnetic (centered right) and ferrimagnetic (right) materials.

The simplest case of cooperative interaction is the coupling between two nuclei, each with an unpaired electron. Both centers have a spin $S_A = S_B = \frac{1}{2}$, and they can couple in parallel ($S = 1$); or in antiparallel ($S = 0$) way. These two different spin states differ in their energy ($E_{(S=0)}$ and $E_{(S=1)}$). Between them exists an energy difference of $2J$. The exchange interaction J is the isotropic coupling constant that can be calculated as:

$$J = \frac{E_{(S=0)} - E_{(S=1)}}{2} \quad \text{Equation 9}$$

2.2.3.1. Ferromagnetism

Ferromagnetic materials (Figure 40, centered left) are those in which the unpaired electrons show a spontaneous parallel configuration by means of the cooperative interaction. These materials do not show a spontaneous magnetic moment due to the existence of ferromagnetic regions known as Weiss-domains. These domains exist in the solid state and show different orientations, which leads to a weakening of the magnetic moment. As a result, the material behaves diamagnetically. However, this situation can be changed by applying an external magnetic field. The Weiss-domains, and with them the unpaired electrons, will reorder themselves in the same direction as the external magnetic field. The material undergoes thus a magnetization and a spontaneous magnetic moment is observed.

This magnetization will endure when the external magnetic field is not longer applied. As a consequence, in field-dependent measurements, a remanent magnetization (or remanence) will be observed, hence a hysteresis loop will also occur. ^[120,122]

The magnetization M increases with the applied magnetic field H (initial magnetic curve, Figure 41), until all unpaired electrons are oriented in the same direction as H and the magnetic saturation M_S is reached. When the external magnetic field intensity decreases, the magnetization also decreases and a hysteresis loop is observed. When the external magnetic field is zero, the magnetization does not disappear, but a residual magnetization (remanence, M_R) remains. To obtain again a magnetization equal to zero it is necessary to apply a coercive field $-H_C$. This is also a measure of the resistance of the material to becoming demagnetized. When the external magnetic field decreases again, a magnetic saturation $-M_S$ is reached, and when the field increases afterwards, the hysteresis loop passes through $-M_R$, H_C and M_S . ^[120]

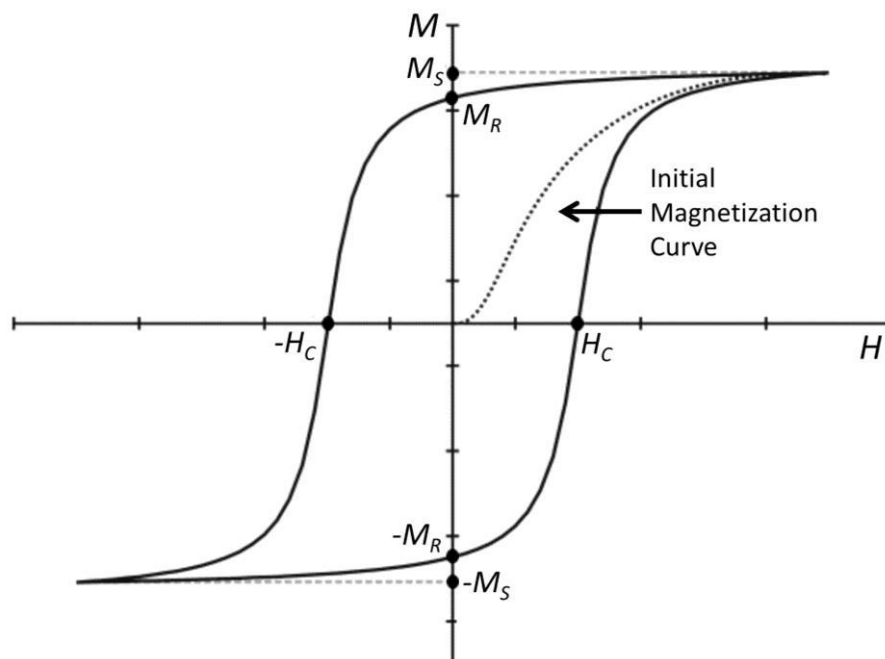


Figure 41: Hysteresis loop of a ferromagnetic compound. H_C is the coercive field, M_S the magnetic remanence and M_R the magnetic saturation.

The Weiss-domains can only be observed under a determined temperature, known as Curie Temperature T_C . Above this temperature the thermal motion destroys the parallel spin orientation and the material behaves as a paramagnet. ^[122]

Other characteristics of this type of magnetic materials are a positive Weiss-constant Θ and a positive J value. ^[123]

2.2.3.2. Antiferromagnetism

Contrary to ferromagnetic materials, antiferromagnetic materials (Figure 40, centered right) are characterized by a spontaneous antiparallel orientation of the unpaired electrons. This phenomenon can only be observed below the Néel Temperature T_N . Above this temperature the thermal motion disturbs the spontaneous orientation and the material behaves as a paramagnet. When an external magnetic field is applied, half of the unpaired electrons orient themselves in the opposite direction of the magnetic field. At low temperatures all unpaired electrons show the expected antiparallel orientation and the susceptibility is zero. At higher temperatures the susceptibility increases. When the energy of the thermal motion is higher than the energy of the coupling (T_N), the unpaired electrons do not show the antiparallel orientation anymore and the susceptibility decreases with increasing temperatures. These materials are characterized by a negative J value and a negative Weiss-constant Θ . ^[120,122,123]

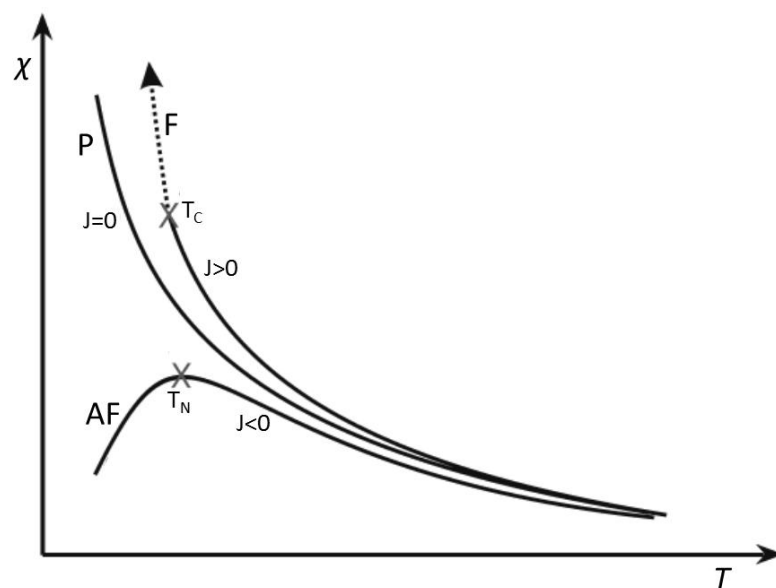


Figure 42: Susceptibility χ vs. Temperature T for paramagnetic (P), ferromagnetic (F), and antiferromagnetic (AF) materials.

2.2.3.3. Ferrimagnetism

Ferrimagnetism (Figure 40, right) is a special case of antiferromagnetic coupling. The unpaired electrons are oriented in an antiparallel way below a certain temperature T_C . The difference with antiferromagnetic materials is that the value of the spins is not identical,

hence the magnetic moments are not completely cancelled, and as a result a permanent magnetic moment can be measured. ^[122]

2.2.3.4. Mechanisms of Spin Coupling

Spin density ρ is the term which defines the “fraction” of unpaired electron present at each point of the molecule, as in a paramagnetic system the unpaired electron is not localized in a single point but delocalized on the entire molecule. ^[124] This spin interaction can take place “through-bond” or “through-space”.

The “through-bond” interaction can take place by different pathways. One mechanism of spin interaction is the spin polarization (polarization of the paired electrons in the MO due to the presence of an unpaired electron) ^[124] over a σ -bond-system (Figure 43). An unpaired electron in an orbital polarizes the neighbour electron. The coupling will induce a parallel-oriented according to the Hund-rule. The second electron of the bond, according to the Pauli-Principle, will be antiparallel-oriented and will also polarize the next neighbour electron, etc... Therefore, depending on the number of bonds, the final coupling will be parallel or antiparallel. ^[125]

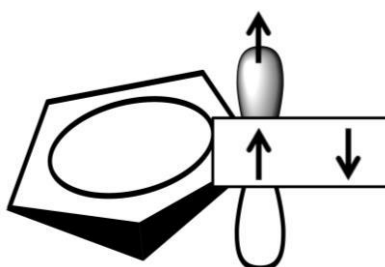


Figure 43: Spin polarization of the C-H bonding electrons in the orbital 2p of the carbon atom.

Another magnetic interaction is the “Super Exchange”, which occurs when the paramagnetic units are bound with other ions or atoms which do not present a permanent magnetic moment, e.g. a diamagnetic ligand. In this case a spin polarization is induced to the fully occupied orbital of the diamagnetic ligand, which allows the coupling between both unpaired electrons. This indirect interaction induces an antiferromagnetic coupling (Figure 44). ^[120]

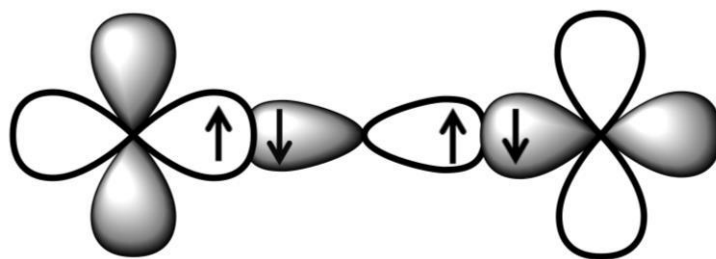


Figure 44: „Super Exchange“ spin interaction.

“Double Exchange” (Figure 45) occurs between mixed-valence metal centers. An exchange with a charge transfer is observed, inducing a ferromagnetic coupling.

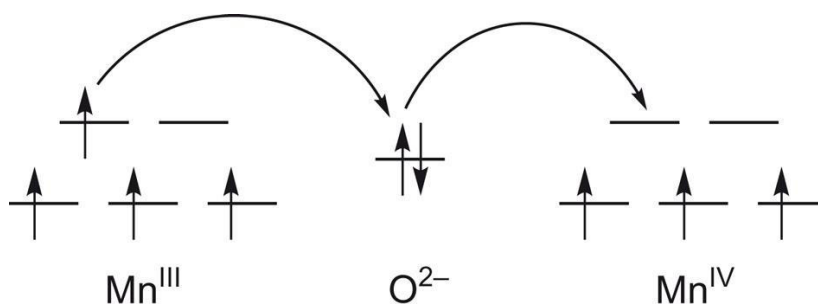


Figure 45: „Double Exchange“ spin interaction. ^[126]

Finally, when direct overlaps of the orbitals exist where the unpaired electrons are found, it is known as “Direct Interaction” (Figure 46).

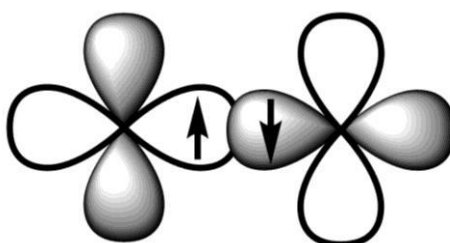


Figure 46: Direct spin interaction.

The “through-space” or “dipole-dipole” exchange, which does not involve the overlap of orbitals or spin density, is also possible. However, this type of interaction is normally weak and it depends on the distance between the paramagnetic centers (r^{-3}). At low temperatures this type of coupling should not be neglected. ^[125,127]

2.3. Cobaltocene

The synthesis ^[128] and following characterization ^[129,130] of the crystallographic structure of ferrocene between 1951 and 1952 fired the starting signal for the study of similar structures with other transition metals. G. Wilkinson reported in 1952 ^[131] the synthesis of the first cobaltocenium salts and in 1953 E. O. Fischer ^[132] presented and characterized a cobaltocene molecule. In the last sixty years different research groups have continued with the investigation of cobaltocene, and now its synthesis and derivatization, ^[133] crystallographic structure ^[130] as well as redox, ^[134,135] electronic ^[136,137,138,139] and magnetic ^[138,140] properties no longer remain unknown to us.

The cobaltocene structure ^[130] is the one expected for a metallocene ($d_{C-C} = 1.43 \text{ \AA}$, $d_{C-M} = 2.21 \text{ \AA}$) and it lies between ferrocene ^[141] and nickelocene ^[130]/ruthenocene structures. ^[142]

Cobaltocene contains 19 valence electrons and is easily oxidized to the 18 valence electron cobaltocenium-cation, which is air stable and isoelectronic to ferrocene. In cyclic voltammetry measurements cobaltocene displays two different redox waves: the reduction to bis(cyclopentadienyl)cobaltat-anion (Co(I)) and the oxidation to cobaltocenium-cation (Co(III)). ^[143]

Cobaltocene has a degenerated E_{1g} ground state and the unpaired electron resides in an e_{1g} antibonding molecular orbital, which shows a large covalency effect with a 40 % ligand contribution. ^[144]

Among others, Ammeter contributed to explain the electronic configuration of cobaltocene. ^[136,139,144,145] ESR-spectroscopic experiments in different matrices were carried out. Since the ground state is degenerate, it presents a dynamic Jahn-Teller effect, and thus a g -factor (1.6 – 1.7) largely depends on the matrix used. Moreover, the signals are measurable only at very low temperatures, due to the short spin relaxation times. ^[146]

König *et al.* ^[140] carried out an extensive study about the magnetic properties of the cobaltocene molecule in 1978. He observed that between 300 K and 12 K, the μ_{eff} was a slowly decreasing function of the temperature. However, between 12 K and 3 K the μ_{eff} values were almost constant. From 3 K to 1 K, the μ_{eff} values decreased dramatically, which is a normal behaviour in paramagnetic materials. Considering the $(\chi_m^{corr})^{-1}$ -Temperature

2. Theoretical Background

dependence, the Curie-Weiss behaviour is found between 300 K and 25 K ($\Theta = -13 \pm 3$ K). Within this temperature range the Curie Law is obeyed. The reason for the deviation of $(\chi_m^{corr})^{-1}$ from the Curie Law above 25 K is that at least one excited level is thermally occupied.

The paramagnetic behaviour of the cobaltocene molecule also becomes evident in the large chemical shifts observed in NMR-spectroscopy^[146] (Figure 47). F. H. Köhler published a series of papers about the spectroscopic properties of paramagnetic metallocenes, including cobaltocene.^[146,147,148–151]

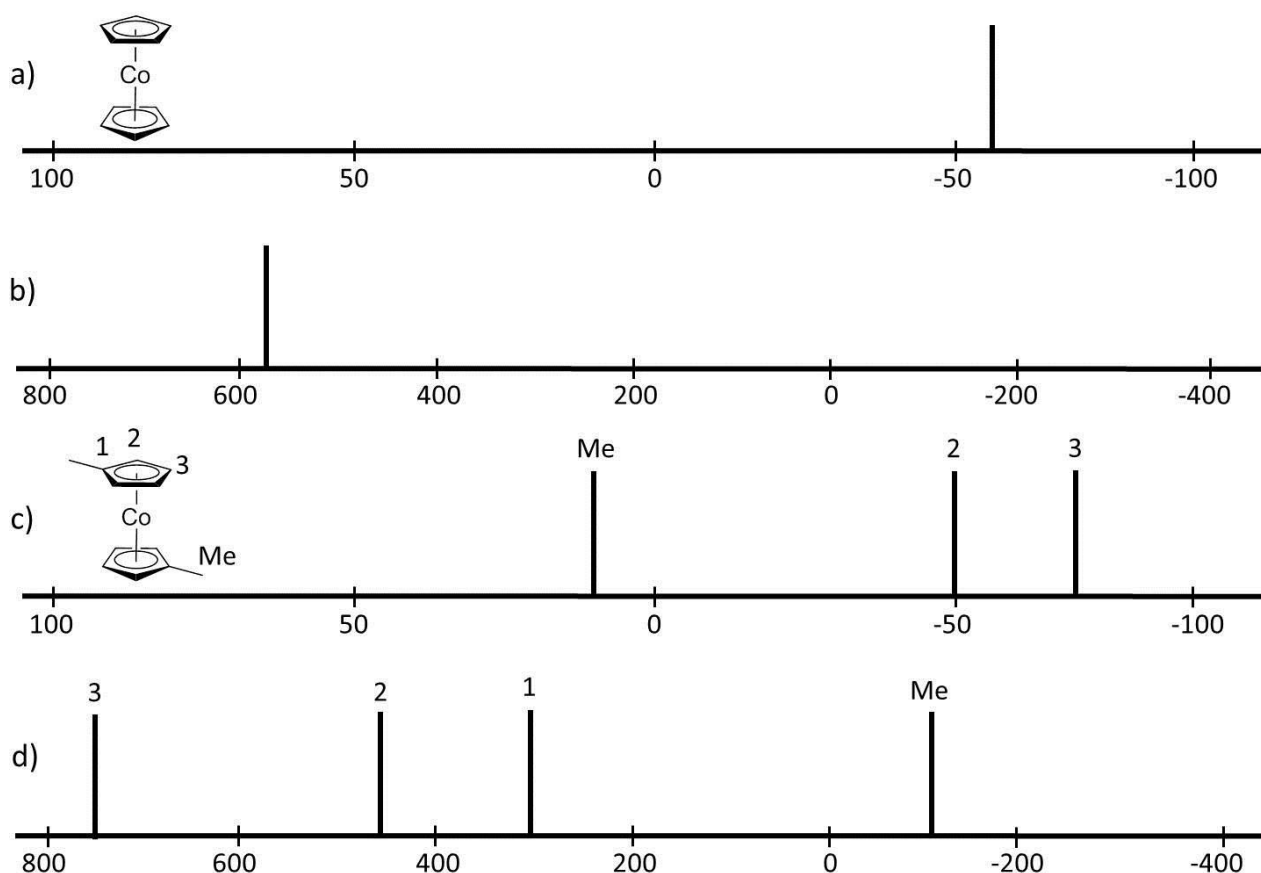


Figure 47: (a) ¹H-NMR and (b) ¹³C-NMR chemical shift of cobaltocene (ppm). (c) ¹H-NMR and (d) ¹³C-NMR chemical shift of 1,1'-dimethylcobaltocene.

The chemical shift of paramagnetic organometallic complexes is influenced by the interaction of the unpaired electrons of the metal center with the correspondent nucleus of the ligands. This interaction can be divided in two types: dipolar (or pseudo-contact), and through-bond (or Fermi-contact). The latter prevails in the case of cobaltocene.^[149]

Cobaltocene cannot be considered as the classic rigid sandwich complex.^[148] Two different structures (A and B, Figure 48), which differ in the interaction of the five-membered ring of carbon atoms with the cobalt center, exist in dynamic equilibrium. They have the same energy and at room temperature the exchange is so fast that only one signal for each position can be observed. In VT-NMR, the chemical shift of these signals follows the Curie Law.^[149]

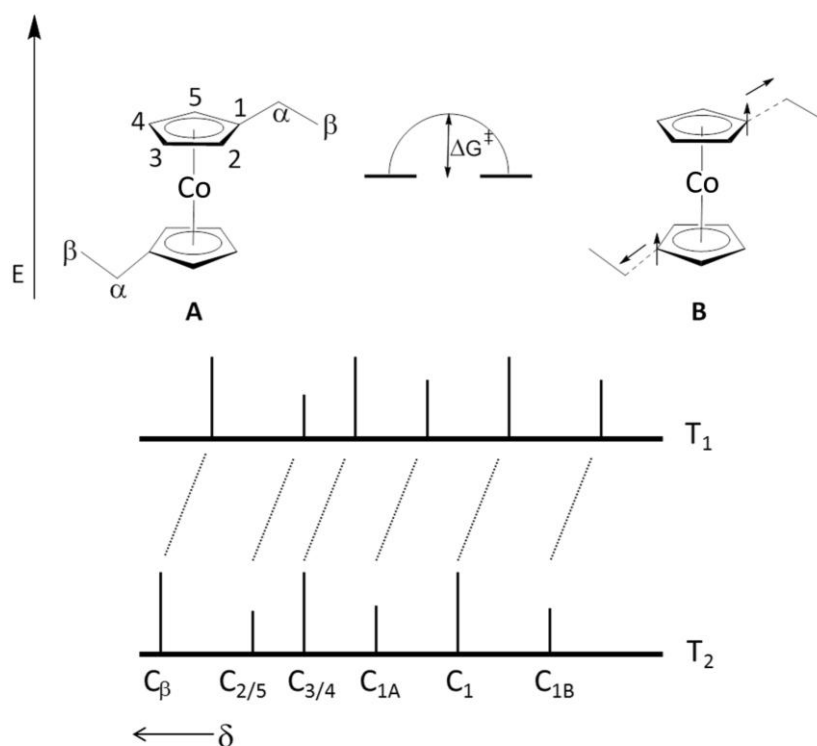


Figure 48: ^{13}C -NMR chemical shifts of paramagnetic metallocenes (except for substituted cobaltocenes) at different temperatures, having A and B the same energy (C_α is omitted). In this case the Curie Law is obeyed in the measured temperature range.

In the case of substituted cobaltocenes (Figure 49), A and B do not have the same energy because between C_1 , C_β and H_α a hyperconjugation^[151] exists and an electron spin transfer from C_1 to C_β and H_α (nuclei which are found at “two bounds” distance) takes place. The A/B ratio depends on the energy difference between both structures (ΔG°) and on the temperature of the measurement. In VT-NMR the intensity and the chemical shifts of the carbon atoms affected by the hyperconjugation will depend on the mentioned A/B ratio. In a chemical shift (δ) vs. the inverse of the temperature (T^{-1}) plot, these signals will not offer a straight line but a curve (see 2.2.2). ΔG° depends on the substituents of each carbon atom and the “Cobaltocene Anomaly” will be observed when this ΔG° is high enough. In the case

2. Theoretical Background

of hydrogen atoms as substituents ΔG° is very small and for this reason this phenomenon is not found in pure cobaltocene. ^[148,149]

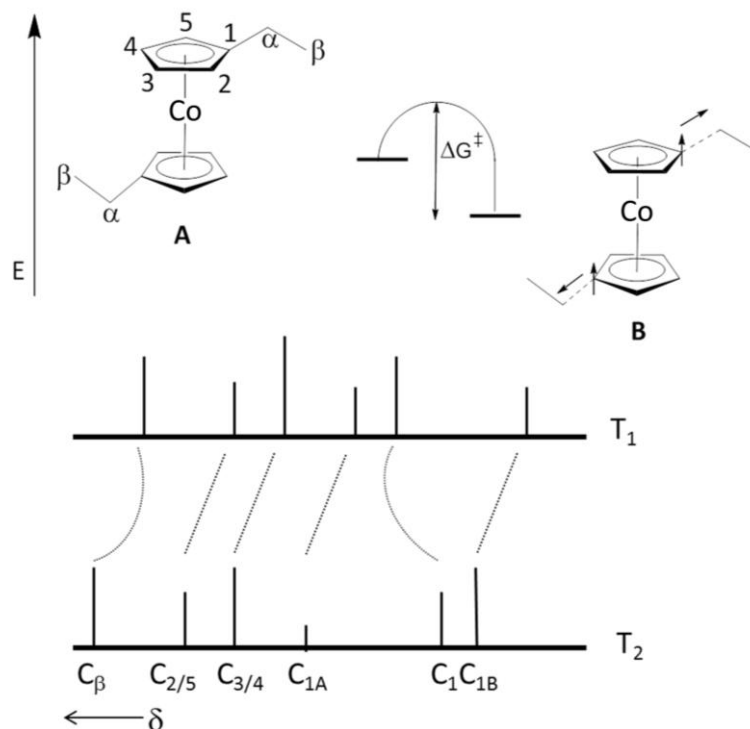


Figure 49: Influence of the non-rigid structure of cobaltocene on the ^{13}C -NMR chemical shifts at different temperatures, having A and B different energies. (C_α omitted).

In the last sixty years numerous cobaltocene derivatives have been synthesized and characterized, such as the reducing agent decamethylcobaltocene, ^[152–154] other alkyl derivatives which vary in the number and position of the substituents, ^[146,148,155] or 1,1'-dicyanocobaltocene. ^[150]

The magnetic behaviour of these cobaltocene derivatives was also investigated. Decamethylcobaltocene, ^[152–154] as expected, presents an analogous behaviour to cobaltocene. Other alkyl derivatives like 1,1'-dimethylcobaltocene ^[156] and 1,1',2,2'-tetramethylcobaltocene ^[156,157] show paramagnetic behaviour and follow the Curie Law. The paramagnetic character of these derivatives at also very low temperatures indicates an intermolecular coupling among the cobalt centers. The Co-Co distances are about 600 pm, therefore these couplings are very weak. ^[158]

1,1'-dicyanocobaltocene, ^[150] however, shows a deviation from the described character. It is not as air-sensitive as the parent cobaltocene and its magnetic behaviour is also different. The $\chi_m T$ value is higher than expected and decreases more and more rapidly until it reaches

a minimal value at a temperature of 2 K. In a $\chi_m T$ vs. T plot an antiferromagnetic interaction ($J = -30.4 \text{ cm}^{-1}$) can be observed. According to the NMR spectroscopic experiments, this interaction is intermolecular. This result confirms the influence of the organization of the molecules in the crystalline material.

Another type of cobaltocene derivatives which have been deeply investigated in the last years, being also very interesting for this work, are the complexes which contain two cobaltocene moieties connected by means of an organic bridge. These complexes present new properties when compared to pure cobaltocene.

In 1992 Köhler and coworkers,^[159] continuing with the work of McManis,^[160] published the synthesis of decamethylbiscobaltocene (Figure 50, left), where two cobalt centers are connected by means of a fulvalene unit. Between 1998^[161] and 1999^[162] the ferromagnetic magnetic behaviour of this complex, which is still not completely clarified, was discussed.

In 1995 Manriquez *et al.*^[163] published a series of bismetallocenes with pentalene (Figure 50, centered) and indacene (Figure 50, right) as bridging ligands, including the cobaltocene derivatives. Cyclic voltammetry measurements showed that the cobalt centers are electronically communicated in these complexes. The magnetic measurements displayed an antiferromagnetic coupling and a diamagnetic character at room temperature.

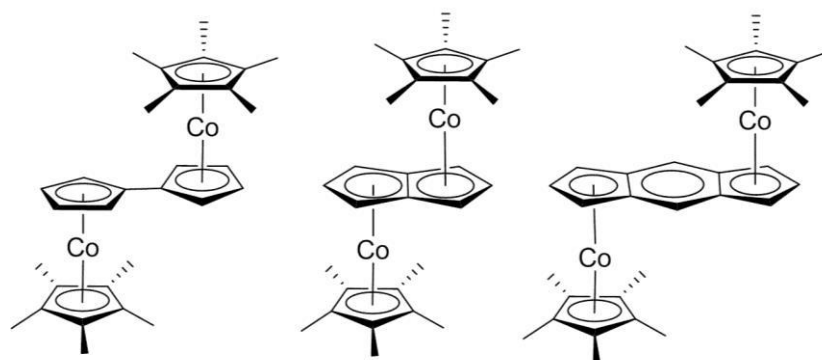


Figure 50: Biscobaltocenes with a (left) fulvalene-, (centered) pentalene-, and (right) indacene-bridging ligand.

Phenyl connecting synthesized biscobaltocene complexes do not reveal electronic communication between the metal centers in cyclic voltammetry experiments, as only one two-electrons wave is observed for both isomers.^[164] Regarding to the magnetic properties, both isomers exhibited high magnetic moments at room temperature, but they were even larger in the case of *meta*-substitution. Therefore it was shown that the positional

2. Theoretical Background

substitution of the benzene ring plays a role in the interaction between the cobalt centers. *Para*-substituted (Figure 51, left) and *meta*-substituted (Figure 51, right) complexes presented antiferromagnetic ground states.

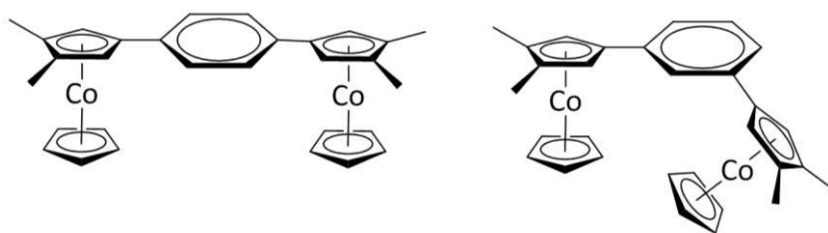


Figure 51: Bis(cobaltocenyl)benzene complexes.

In the 80's, Rosenblum^[165] developed the concept of “stacked metallocenes”. Those “stacked metallocenes” were connected by means of a naphthalene clamp and arranged head-to-head to each other. On the basis of this concept, Pagels^[166] dedicated his Ph.D. thesis to the synthesis, characterization and comparison of the two bis(cobaltocenyl)naphthalene complexes depicted in figure 52.

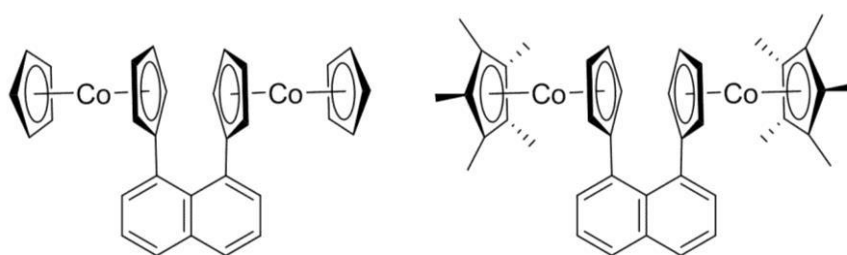


Figure 52: Bis(cobaltocenyl)naphthalene complexes after Pagels.^[166]

Cyclic voltammetry experiments revealed an electronic communication between the cobalt centers, and the magnetic studies discovered a weak intramolecular antiferromagnetic coupling between the unpaired electrons through the π - π interaction of the two stacked cobaltocene units. The exchange coupling constant was $J = -28.1 \text{ cm}^{-1}$ for the non-methylated derivative and $J = -5.9 \text{ cm}^{-1}$ for the decamethylated complex. The difference in the J values is due to the different geometries of the biscobaltocenyl moieties. In the decamethylated complex their position is less face-to-face than in the other complex, which exerts an influence in the “through-space” coupling.

2.4. Analytical methods

2.4.1. Cyclic Voltammetry

Cyclic voltammetry (CV) is an electrochemical analytical method which offers information about the redox behaviour of a chemical species. With this method it is not only possible to measure the electrochemical potentials, but also to understand the kinetic and thermodynamic aspects, as well as the mechanisms of these redox reactions. ^[143]

Cyclic voltammetry is also a widely used tool in the study of the metal-metal interaction in organometallic systems. The advantages of this method compared to other analytical techniques are numerous: it is applicable to any chemical species in solution, it is not necessary to isolate the substance of interest but we can use the most stable member of a redox series, and the needed equipment and measurements are simple, which greatly facilitates the work under inert-atmosphere. ^[167]

The measurement cell contains the solution of the analyte in contact with three different electrodes: the reference electrode, the working electrode and the counter electrode.

The applied potential in the working electrode will vary linearly from an initial potential E_i to a final potential E_λ at a constant scan rate ν . Once the final potential is reached, the potential ramp of the electrode will be inverted maintaining the same scan rate as the initial potential is reached again. ^[143]

The scan rate ($\nu = \frac{\partial E}{\partial t}$ [V s⁻¹]) varies normally between 20 – 500 mV s⁻¹ and it is a very important variable in cyclic voltammetry.

In the literature the SCE (Saturated Calomel Electrode), ferrocene or decamethylferrocene are normally used as reference. ^[143]

In order to secure the conductivity in the solution despite the concentration gradient that is produced when the redox reaction takes place, an electrolyte should be added to the solution, e.g. Tetra-*n*-butylammoniumhexafluoridophosphate, which is soluble even in aprotic solvents and it is stable at the applied voltage range. ^[168]

2. Theoretical Background

During the measurement a triangular voltage is applied between the working and the counter electrodes, and the generated current is plotted versus the applied voltage to obtain the cyclic voltammogram trace. When the starting potential value is more positive than the standard potential E° shown by the electrochemical-active species, and the measure proceeds at a scan rate toward values more negative than E° , then a Faraday current flows and the characteristic redox-waves are observed in the cyclic voltammogram (Figure 53).^[143]

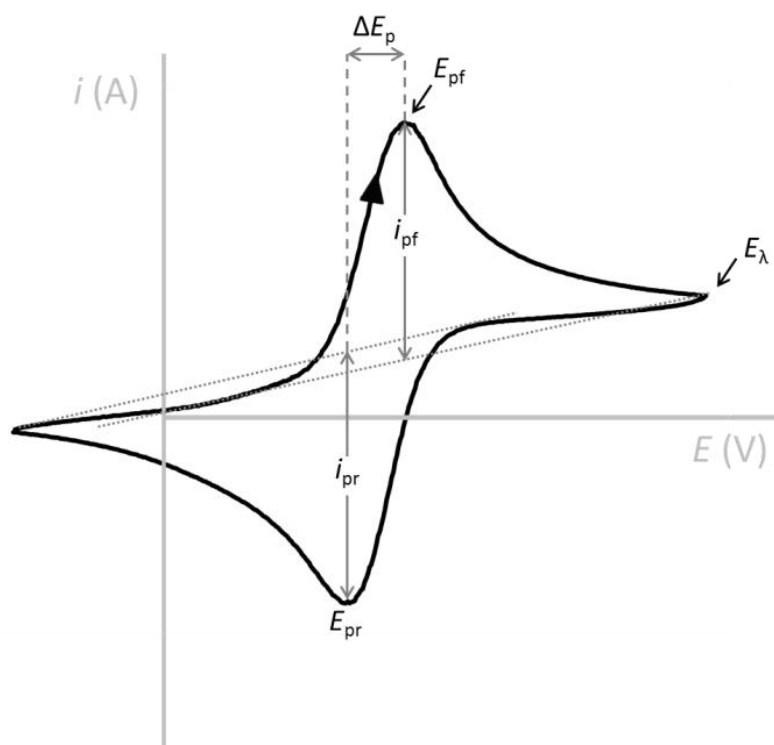
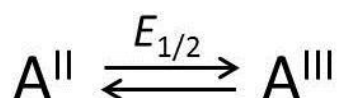


Figure 53: Cyclic voltammogram of a reversible process with basic parameters: E_{pf} = potential of the forward peak; E_{pr} = potential of the return peak; E_λ = potential value at the inversion of the scan direction; i_{pf} = current of the forward peak with respect to its baseline; i_{pr} = current of the return peak regarding its baseline; ΔE_p = peak-to-peak separation.

The redox reactions occur through electron-transfer at the working electrode interface. Depending on the voltage, the analyte will be reduced or oxidized. Two different processes play an important role in the experiment: the heterogeneous charge transfer at the electrode interface and the mass transport produced by the diffusion current.



Scheme 10: Oxidation and reduction reactions.

In the redox reaction represented in scheme 10, when the potential $E(t)$ increases and reaches an appropriate value for the oxidation of A(II), the concentration of A(II) decreases at the electrode surface while the concentration of A(III) does the contrary. This phenomenon produces a concentration gradient and a current begins to flow. When the concentration of A(II) is almost zero, the current reaches a maximum value (i_{pc}). After this point, the gradient cannot increase further, it no longer depends on the potential, and as a consequence the current drops. When the scan direction is reversed and the reduction of A(III) to A(II) occurs, analogous phenomena are observed. It leads to a negative current, which reaches a minimum (i_{pa}). These two processes together provide the characteristic redox-waves of the cyclic voltammograms (Figure 53).

The half step potential ($E_{1/2}$) is an important information. It is the potential between the anodic and cathodic peaks.

$$E_{1/2} = \frac{(E_{pf} + E_{pr})}{2} \quad \text{Equation 10}$$

The peak separation is defined as the difference between the anodic and cathodic peaks:

$$\Delta E_p = |E_{pf} - E_{pr}| \quad \text{Equation 11}$$

The experiment can start at any voltage and proceed in any direction. The adequate conditions should be adjusted depending on the solvent and on the electroactive substance. In figure 53 the measure goes first (forward peak, pf) to the positive potential and the substance is oxidized. Afterwards (reverse peak, pr) the oxidized species is reduced again.

The redox processes in cyclic voltammetry can be divided in three different types: reversible, quasireversible and irreversible processes.

In figure 53 a reversible process is presented. In this case the rate of electron transfer is higher than the mass transport, which allows for the thermodynamic equilibrium to be reached at the electrode interface. The reaction at the electrode responds to the Nerst equation (Equation 12):

$$E = E^\circ + \frac{RT}{nF} \ln \frac{c_{ox}}{c_{rd}} \quad \text{Equation 12}$$

2. Theoretical Background

This type of process can be recognized by some characteristics: E_{pf} and E_{pr} are not scan rate dependent. The ratio between the current of the reverse peak and the current of the forward peak (i_{pr}/i_{pf}) is equal to 1; which indicates that the current, as the number of transferred electrons, is identical in both semi-processes. The peak-to-peak separation is $59/n$ mV (being n the number of electrons involved in the electrochemical reaction) at 25 °C. This value can be calculated using the next expression:

$$\Delta E_p = 2.3 \frac{RT}{nF} \quad \text{Equation 13}$$

Finally, the currents i_{pf} and i_{pr} are proportional to the square root of the scan rate \sqrt{v} .

In a reversible mechanism, no molecule reorganizations accompany the redox reaction.

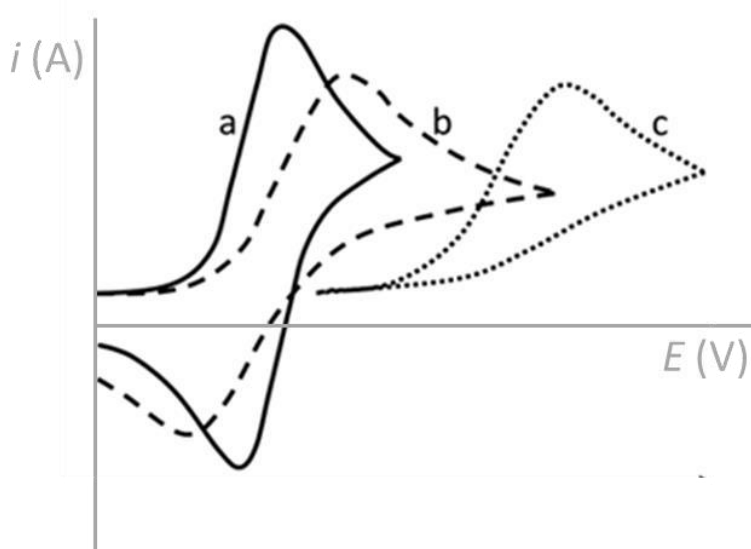


Figure 54: Cyclic voltammogram of a a) reversible process, b) a quasireversible process and a c) irreversible process. ^[143]

In case of a quasireversible processes (Figure 54, b) the shape of the cyclic voltammogram changes with the scan rate v . At low scan rates it shows a reversible behaviour, but at high scan rates, it does not. It occurs when the rate of the electron-transfer and the mass transport share the same order of magnitude.

Although i_{pf} increases with \sqrt{v} , it does it non-linearly, so the value of E_{pf} shifts with the scan rate v . The same occurs with the values defined by the reverse peak. The ratio i_{pr}/i_{pf} is, nevertheless, almost 1.

But not only the peak shape varies with respect to the reversible processes. The peak separation increases at high scan rates, although at low scan rates approaches the theoretical value of 59 mV/ n , expected for electrochemically reversible processes.

It must be emphasized that quasireversibility is an electrochemical criterion which defines a situation where some important reorganization takes place at the redox reaction, but the active species does not suffer fragmentation. It certainly does not mean “partial chemical reversibility”.

The last possible mechanism is the irreversible mechanism (Figure 54, c), which is characterized by an electron transfer rate much lower than the mass transport, so only the anodic or the cathodic processes can alternatively be detected. As a consequence, no thermodynamic equilibrium can be reached at the electrode interface. The expression $i_{pf} * (\sqrt{v})^{-1}$ stays constant, but E_{pf} will shift with the scan rate v .

The activation barrier to the electron transfer of this type of process is so high that normally the original frame undergoes fragmentation and several new species are formed.^[143]

An interesting application of the cyclic voltammetry method is the study of organometallic complexes with more than one metal center and the electronic communication between them.

The Robin-Day Classification^[169] explains the nature of mixed valence compounds, which contain ions of the same element in two different oxidation states.^[170] The classification is based on the degree of electronic delocalization between the metal centers, which is directly related to the electronic communication between them.

The metal complexes of Class I (Figure 55, above) are those in which the charge is localized in only one of the metal centers, and also where an electronic communication between them does not exist. In cyclic voltammetry only one redox-wave will be observed for each redox process, and that is because the metal centers will undergo the redox reaction exactly at the same potential.

In the metal complexes of Class II (Figure 55, middle) the charge is slightly delocalized among the redox centers. An electronic communication between the metal centers exists, but its

intensity is not very high. In cyclic voltammetry two different redox-waves will be identified for each redox processes, but the peak separation will be minimal.

Finally, Class III (Figure 55, bottom) includes the metal complexes where the charge is completely delocalized among the metal centers. In these complexes a high electronic communication between the redox centers exists. Two well defined and separated redox-waves will be observed in the cyclic voltamgram for each redox processes. ^[143]

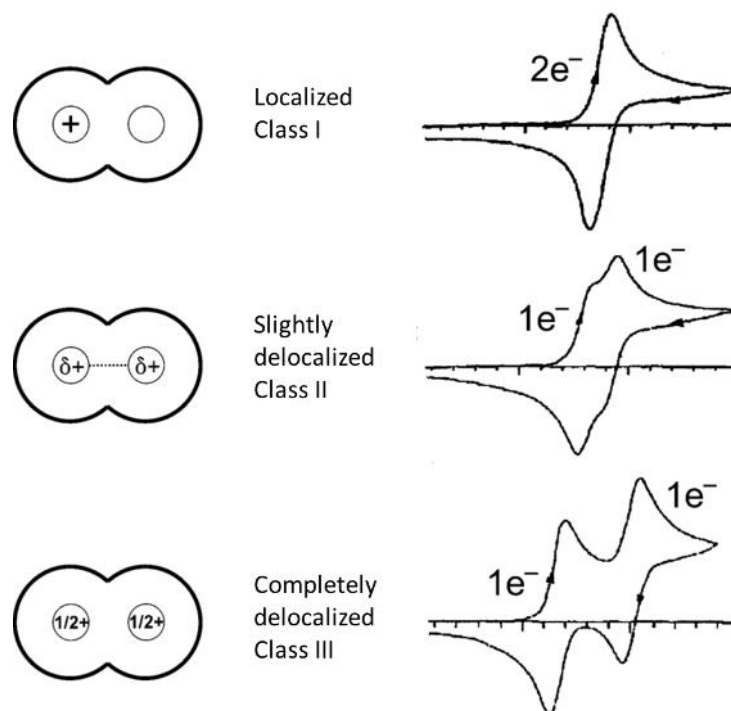


Figure 55: Schematic representation of the electronic effects in mixed valence species according to the Robin-Day classification (the charge assumed as positive) (left); and different cyclic voltammograms expected from biferrocene-complexes, depending on the reach of the electronic communication. ^[143]

2.4.2. NMR-Spectroscopy

Diamagnetic and paramagnetic substances can be investigated by means of NMR-Spectroscopy. However, the spectra of diamagnetic and paramagnetic species present some differences. The cause of those differences is the interaction of the unpaired electrons in paramagnetic substances with the applied magnetic field. ^[171]

The signal shifts are much larger than those of diamagnetic complexes. E.g. cobaltocene displays a signal at -56.2 ppm in ¹H-NMR spectra ^[146] while the diamagnetic cobaltocenium-cation reveals one signal at 5.97 ppm.

The signal width normally is larger and varies strongly. The possibility of detecting a determined signal is proportional to the spin and nuclear relaxation rate, which are normally large. As a consequence, the ^1H - ^1H -couplings cannot usually be detected.

The NMR shift of a paramagnetic compound is the sum of three different contributions, and it is dependent on the temperature (Equation 14):

$$\delta_T^{exp} = \delta_T^{con} + \delta_T^{dia} + \delta_T^{dip} \quad \text{Equation 14}$$

δ_T^{con} is the contact shift (or Fermi-contact shift) and describes the hyperfine coupling of the nuclei with the unpaired electrons through bonds. It can be calculated using the next expression (Equation 15):

$$\delta_T^{con}(N) = A_N \frac{g_{av} \mu_B S(S+1)}{3\gamma_N kT} \quad \text{Equation 15}$$

where A_N is the hyperfine coupling constant of the measured nucleus, g refers to the isotropic g -factor of the molecule, μ_B is the Bohr magneton, S is the electron spin quantum number, γ_N the nuclear gyromagnetic ratio, k the Boltzmann constant and T the temperature.

The δ_T^{dia} is the shift that the signal would have if the molecules were diamagnetic, and it is not temperature dependent. Often this term can be taken from the literature from a diamagnetic compound showing an identical structure. It can be eliminated by referencing each signal to the corresponding diamagnetic compound.

Finally, the last term of the expression is the δ_T^{dip} shift or pseudocontact shift. It defines the distance-dependent coupling through the space. It depends on the symmetry of the orbital where the unpaired electron is localized. For an axially symmetric species δ_T^{dip} can be calculated by (Equation 16):

$$\delta_T^{dip}(N) = \frac{\mu_0 \mu_B^2 S(S+1)}{4\pi 9kT} \frac{(3 \cos^2 \theta - 1)}{r^3} (g_{\parallel}^2 - g_{\perp}^2) f(g, D) \quad \text{Equation 16}$$

The last term of the equation is a function of the g -factor and the zero-field splitting D . It is S dependent and equal to 1 when $S = \frac{1}{2}$. The former term takes in account the anisotropy of the g -factor, where g_{\parallel} and g_{\perp} are, respectively, the g -factors parallel and perpendicular to

the magnetic axis. The more spherical the symmetry is, the smaller this term will be. The third term is the geometric factor and it relates the spatial arrangement of the nucleus with the spin-bearing orbital; r is the vector relating the spin center and the investigated nucleus and θ is the angle between r and the magnetic axis.

In case of measurements in solution, the needed variables for the geometric term (r , θ) can be taken from the crystal structures or from the theoretical calculations. When r is large (> 560 pm) or when the angle θ is close to 54.7°, this term can be neglected.

After eliminating δ_T^{dia} , the signal shift is only dependent on the paramagnetism of the studied compound (Equation 17).

$$\delta_T^{para} = \delta_T^{con} + \delta_T^{dip} \quad \text{Equation 17}$$

2.4.2.1. VT-¹H-NMR-Spectroscopy

Despite the limitations of this spectroscopic method when measuring paramagnetic compounds (broad signals, lack of ¹H-¹H coupling, no reliable signal integration...), a very important piece of information about the magnetic behavior can be obtained due to the temperature dependence of the signal from paramagnetic substances.

To this end, spectra are recorded at different temperatures. Then, a δ_T^{exp} -over- T^{-1} plot is represented. In case of a linear function, the compound behaves as a paramagnet in the measured temperature range, then it obeys the Curie Law (see 2.2.2). From the slope of the plot it is possible to calculate the hyperfine coupling constant A_N , and as a consequence obtain information about the spin density.

When the plot does not represent a straight line, several spin states can be thermally populated and it is possible to calculate the energy difference between them. The change in the chemical shift compared to the chemical shift of the analogous diamagnetic substance can offer information about the coupling mechanism in the molecule.

The chemical shift corresponds to the spin density at the measured nucleus. According to the convention, positive spin density appears at down field and negative spin density at high field.

2.4.3. UV-vis Spectroscopy

When a continuous radiation radiographes a material, a portion of this radiation can be absorbed by this material. If the non-absorbed radiation is forced to pass through a prism, an absorption spectrum can be recorded. During this process, the absorbing molecules are getting excited to an excited state (higher energy).

According to the Bohr theory, the energy changes produced by light absorption can occur only in multiples of an amount of energy whose measure unit is known as quantum. A quantum is characteristic of each species.

The Bohr-conditions allow us to calculate the relation between the energy changes in the molecule and the frequency of the absorbed light:

$$h\nu = E_i - E_f \quad \text{Equation 18}$$

h is the Planck's constant, ν the frequency and E_f and E_i are the energies of a single molecule in its final and initial states. In case of light absorption, the E_i value is larger than E_f value. In the opposite case, the light is not absorbed but emitted.

The electronic absorption spectrum, which includes changes in the rotational and vibrational states, arises from transitions between electronic states. The $(E_i - E_f)$ values are large, hence absorption takes place at large frequencies or short wavelengths (ultraviolet (10-400 nm) and visible (400-800 nm) regions).

In figure 56 the energy states of a diatomic molecule are depicted. The line H represents the ground state and G the first excited state (Figure 56, left). These two levels represent the two states assuming that the nuclei do not rotate or vibrate. In the center of figure 56, the vibrational states associated with each electronic state can be observed (assuming not rotations are taking into account). At the left of the figure 56, the broken lines show the rotational levels associated with the two electronic states and the various vibrational levels in each state. The vertical lines correspond to different transitions: A-B demonstrates a transition in the pure rotation spectrum and C-D displays a vibration-rotation spectrum. It represents a greater energy change; consequently, absorption of light at shorter wavelength is needed. The last transition E-F corresponds to a transition in the electronic spectrum, therefore it requires absorption of light at even shorter wavelength.

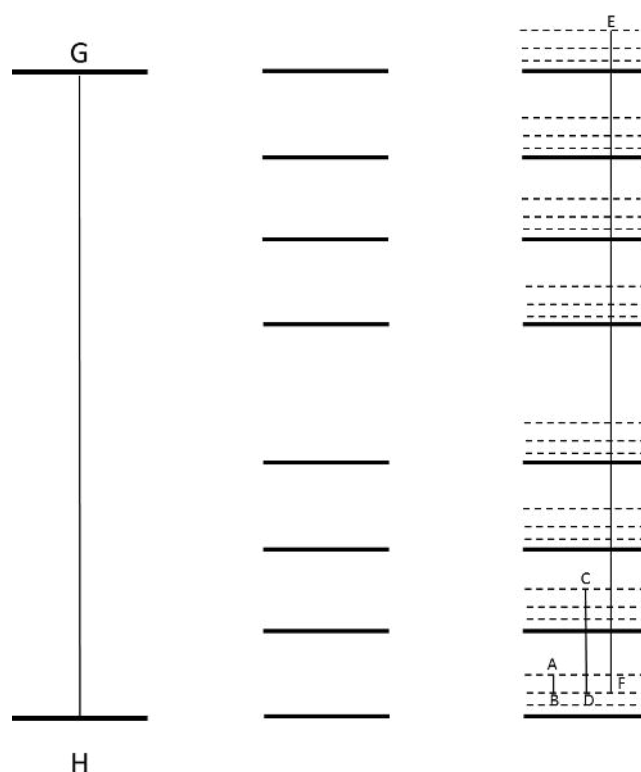


Figure 56: Energy levels of a diatomic molecule in electronic (left), vibrational (center) and rotational (right) states.^[172]

The electronic states are associated with a very large number of vibrational and rotational states. Therefore, a transition between two electronic states results in a large number of vibrational/rotational transitions in which no single spectral line is observed, but a relatively broad absorption band.

The first law of light absorption was established by Bouger in 1729 and confirmed by Lambert in 1760. It states that the light absorbed by a transparent medium is not dependent of the intensity of the incident light and that each successive layer of the medium absorbs an equal fraction of the radiated light.

$$I = I_0 \times e^{-\alpha b} \quad \text{or} \quad I = I_0 \times 10^{-k\alpha} \quad \text{Equation 19}$$

Where I is the intensity of light transmitted, I_0 is the intensity of the incident light, b is the thickness of the layer in centimetres, and α , k are absorption coefficients (characterized by the medium). These coefficients did not contain the concentration factor and were applicable only to pure materials.

In 1852 Beer^[173] took into account the concentration factor. He postulated that a photon can be absorbed only if collides with a molecule. The probability of photon-molecule

collision is directly proportional to the number of absorbing molecules in the light path and with it, the amount of absorbed light. In the case of a solution, the concentration will be proportional to its absorption when the solvent is transparent. The Lambert-Beer Law establishes:

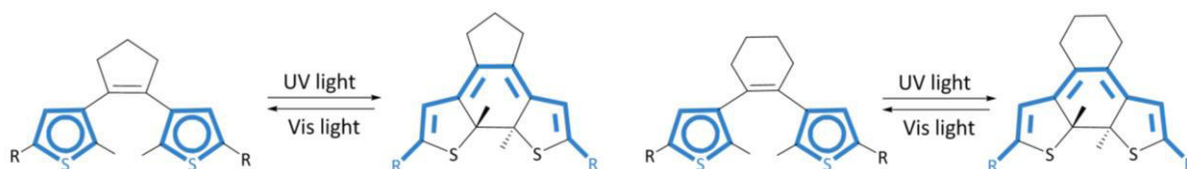
$$\log \frac{I_0}{I} = A = \varepsilon \times d \times c \quad \text{Equation 20}$$

A is called absorption and it is non-dimensional, d is the thickness of the light path and is usually expressed in centimetres. Finally, ε is the coefficient of the molar absorptivity and it is characteristic for each material at a determined wavelength. ^[172,174]

The limitation of this law is that at higher absorbance that 1, deviations from linearity are observed. ^[175]

3. Motivation and Task-settings

In the last thirty years a considerable amount of research has been dedicated to dithienylethene switches with a cyclopentene connecting both thiophene rings.^[176] Derivatives of those molecules were synthesized with organic-^[73,177] and with metal-containing substituents.^[78,102,103,178] There are only few other molecular switches which have been studied so thoroughly, except for the related dithienylperfluorocyclopentene switch.^[73] However, so far only little attention has been paid to dithienylethene switches with a cyclohexene connecting both thiophene rings, although they display also the reversible switching reaction^[71,179] and offer an important advantage over the analogous cyclopentene derivatives. That is the possibility of chiral functionalization of the cyclohexene core, which can be easily done, for example within a Diels-Alder reaction.^[180] A comparable chiral modification of the cyclopentene derivative in the hydrocarbon backbone would be more difficult and time-consuming.^[89] In addition, it was observed that the quantum yield of the photocyclization in stilbene depended on the size of the cycloalkene, and the highest value was found for the six-membered derivative.^[77] It was assumed that this phenomenon could be extrapolated to the systems under study (Scheme 11).



Scheme 11: Molecular switches under study.

Therefore, the first target of this work was the synthesis and characterization of organic dithienylethene-derivatives with a cyclohexene ring connecting both thiophene rings, in order to compare their switching properties with the classical cyclopentene-derivatives.

Furthermore, in the last years metal complexes containing a dithienylethene unit have been investigated. Some of these complexes were formed by two metallocene units connected by a molecular switch,^[78,112] and they displayed the expected reversible photoswitching reaction. In addition, it was observed that by shortening of the carbon atom chain between the metal centers the interaction between them gets stronger^[112] (see section 2.1.2.).

In our working group different coordination compounds where metallocenes (ferrocene, nickelocene, cobaltocene) were connected by an organic bridge have been synthesized and characterized.^[181-183] The behaviour of these complexes varied with the oxidation state of the metal centers. Among the numerous properties of these complexes the electronic interaction and the magnetic coupling between the metal centers were investigated. Accordingly, the second goal of this project was to combine the general knowledge of our working group with that what has been described in the literature about metal complexes containing molecular switches. Desired was the synthesis of complexes where the metallocene units are directly attached to the 5- and 5'- positions of the thiophene rings of a dithienylthene molecular switch; minimizing as far as possible the connecting chain of carbon atoms in order to obtain complexes with strong metal-metal interaction. These complexes would offer an additional advantage with respect to the other metallocene complexes reported by our working group:^[181-183] the ability of switching the aforementioned interaction by means of light irradiation. The electronic interaction and, in case of paramagnetic metallocenes, the magnetic coupling, would depend on the state of the molecular switch core. In addition, the influence of the metal centers in the switching reaction should be also investigated.

To this aim two different paramagnetic metallocenes were chosen: cobaltocene and ferrocenium-cation. Using the cyclopentene- and the cyclohexene-backbone as organic bridges the corresponding complexes (and the analogous diamagnetic complexes) should be synthesized, characterized and their spectroscopic, redox and photochromic behaviour, investigated. After optimization of the switching reactions the magnetic coupling between the paramagnetic units should be studied. When the molecular switch is found in the open state no magnetic coupling is expected. Nevertheless, when the ring closure reaction takes place and the metal centers are connected by means of a π -conjugated system, the unpaired electrons can present a ferromagnetic or an antiferromagnetic coupling (Figure 57).

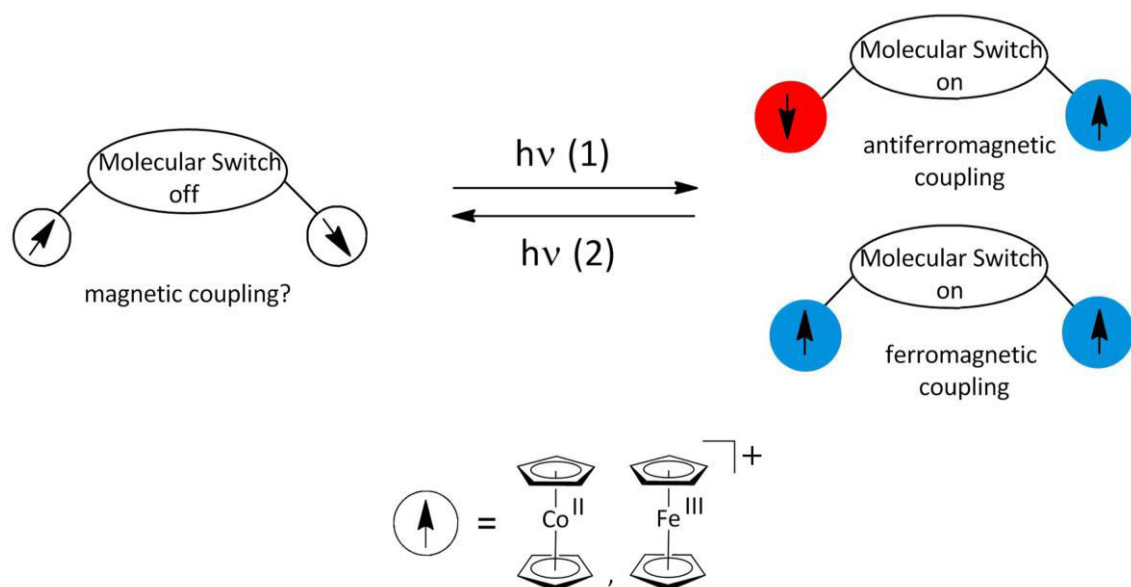


Figure 57: Switching reaction and possible magnetic coupling between the paramagnetic metal centers. Below, the employed paramagnetic sandwich complexes.

This concept, the photoswitching of the intramolecular magnetic interactions using molecular switches, is not unknown in the literature. Matsuda *et al.* ^[184] connected two nitronyl nitroxide radicals by means of a dithienylethene molecular switch and studied the magnetic coupling in the open and closed states of the molecular switch (Figure 58). Otherwise, using a metallocene as paramagnetic unit was still no attempted.

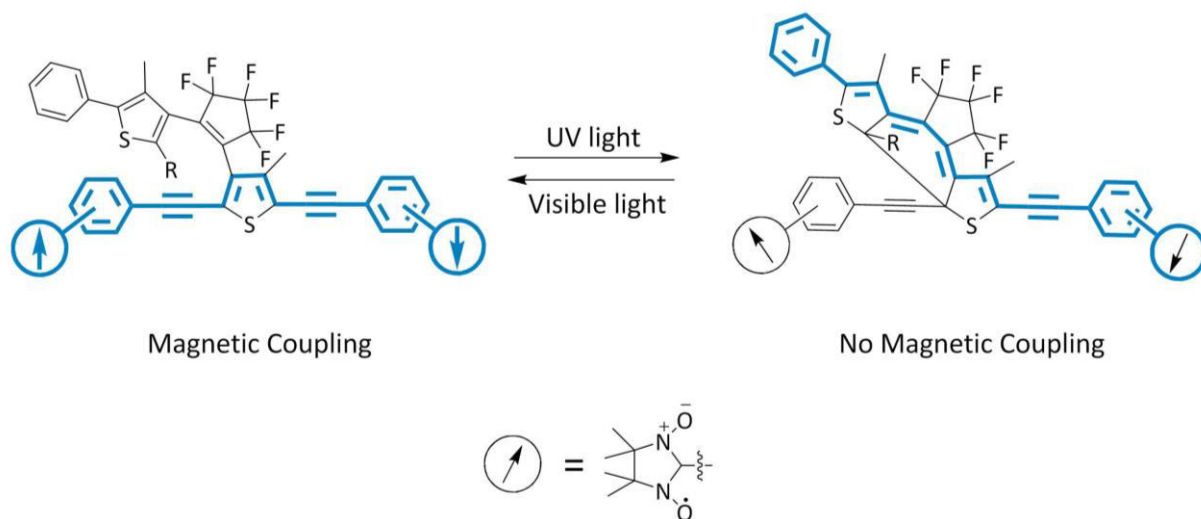


Figure 58: Nitronyl nitroxide radical units connected by a dithienylethene backbone and corresponding magnetic coupling presented by each possible state of the molecular switch.

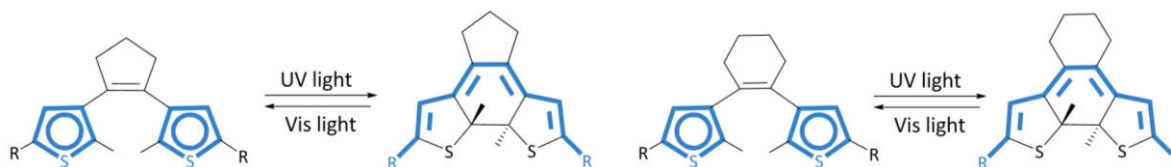
Finally, the experimental data should be contrasted with the theoretical calculations carried out by Torben Steenbock, member of the working group of Prof. Herrmann (Universität Hamburg), who collaborated with us during this project.

4. Results and Discussion

4.1. Synthesis

4.1.1. Synthesis of the organic molecular switches

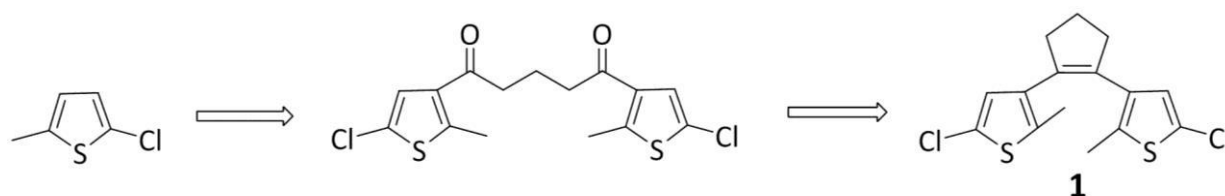
For this work two different molecular switches, both belonging to the dithienylethene molecular switches class, were synthesized and employed (Scheme 12).



Scheme 12: Molecular switches employed in this work.

4.1.1.1. Synthesis of the organic cyclopentene-derivatives **1** and **2**

The cyclopentene-derivative has been largely known in the literature and numerous researchers have focussed their efforts to synthesize organic derivatives following its framework. For this work, the chloro-derivative **1** was synthesized following the instructions of Feringa and coworkers,^[73] starting from 2-chloro-5-methylthiophene, which underwent a Friedel-Craft acylation in order to obtain the correspondent diketone, and following McMurry reaction with TiCl_4 as titanium source (Scheme 13).

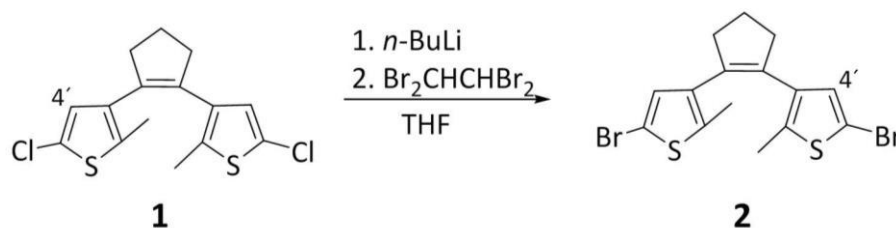


Scheme 13: Retrosynthetic scheme for the molecular switch **1**.

In order to facilitate future derivatizations, the bromo-derivative **2** (which contains a better leaving group than chlorine) was synthesized. To that end, the chloro-derivative **1** was lithiated with *n*-butyllithium in THF at room temperature (lithium-chlorine exchange) and then treated with dry 1,1,2,2-tetrabromoethane (Scheme 14). The obtained material was purified by column chromatography and subsequent sublimation. The direct synthesis of the bromo-derivative was not possible, according to Feringa *et al.*^[73] It was found that during the synthesis of the diketone, the bromo substituent shifted from the 2- to the 3-position. As a consequence, the Friedel-Craft acylation took place at the more reactive position 2. This

4. Results and Discussion

phenomenon, known as “halogen dance” has been observed before for bromothiophenes.^[185]



Scheme 14: Synthesis of **2**.

After having carried out this synthesis, Branda *et al.*^[186] published in 2012 another synthesis path, but instead of 1,1,2,2-tetrabromoethane, elemental bromine was employed. The synthesis designed by Branda presented higher yields.

The compound **2** was characterized, among other methods, by means of ¹H-NMR-spectroscopy and the results were compared with the chloro- (**1**) and iodo- (**3**) derivatives^[111]. It was observed that the higher the electronegativity of the halogen-atom at the 5'-position was, the lower was the chemical shift of the proton at the 4'-position (Table 4). It agrees with the literature values^[187] but it contradicts the general idea of a correlation between the chemical shift and the electron density of the corresponding atom. Abraham *et al.*^[188] explained this phenomenon considering the anisotropy of the C-X bond, the steric and the electric field effects.

Table 4: Chemical shift (ppm) of the protons at the position 4' (Scheme 14) in chloroform-d₃, depending on the thiophene substitution at the 5'-position.

X	Cl ^{a)}	Br ^{a)}	I ^{b)}
Chemical Shift (ppm)	6.58	6.71	6.89

^{a)} 200 MHz, ^{b)} 400 MHz

4.1.1.2. Synthesis of the organic cyclohexene-derivatives **5** and **6**

The cyclohexene-derivative **5** was synthesized through a McMurry reaction (Scheme 15) from the corresponding diketone **4**, which was prepared according to Branda *et al.*^[189] Good quality crystals (**4**) were obtained from recrystallization in hexane and the characterization by X-ray diffraction was possible (Figure 59).

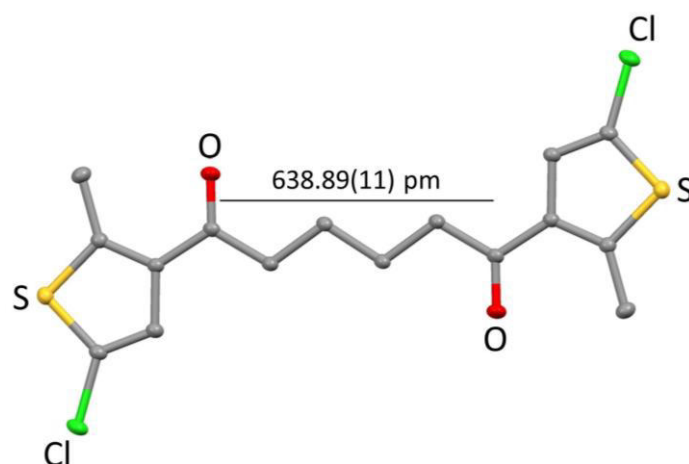


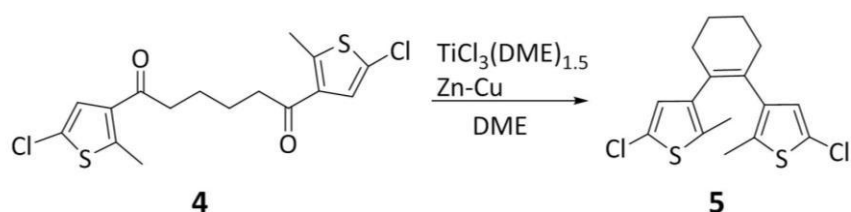
Figure 59: Molecular structure of **4**. $P2_1/c$, $R = 2.55\%$, $Z = 1$.

In a first attempt, titanium(IV)-chloride was used as Ti-precursor, zinc as reducing agent and THF as solvent, in close analogy to the reaction conditions used by Feringa *et al.* [73] in order to synthesize the analogous cyclopentene compound.

Though the product was found, the yield was below 2 %, while Feringa *et al.* [73] reported 44 %. The same yield (below 2 %) was reported when $\text{TiCl}_3(\text{THF})_3$ instead of TiCl_4 was employed, although different reaction times and temperatures were tested.

Probably, the distance between both ketone groups in **4** (638.89(11) pm) is too large (Figure 59) for the intramolecular reductive coupling, and the intermolecular coupling is statistically more favorable.

McMurry *et al.* [190] investigated different titanium sources, reducing agents and optimal solvents for this type of reaction. They reported the best titanium source was $\text{TiCl}_3(\text{DME})_{1.5}$, possibly because the titanium atom coordinates with both oxygen atoms of the dimethoxyethane ligand, and each titanium atom shares a dimethoxyethane ligand with another titanium atom. When the titanium atoms are reduced during the reaction, they are stabilized by this dinuclear chelating structure. With regard to the reducing agent, the Zink-Copper couple was reported to offer the best results; probably due to the more electronegative character of the alloy comparing with pure zinc. When these reagents were used in a great excess and dried DME as solvent, yields of up to 60 % were obtained (Scheme 15).



Scheme 15: Synthesis of 5.

On the basis of the work of Guirado,^[111] the molecular switch **5** was lithiated with *n*-butyllithium in THF at room temperature and then treated with iodine. The impure 1,2-bis(5-iodo-2-methylthien-3-yl)cyclohexene **6** was purified by column chromatography, crystallized in petroleum ether and light yellow crystals were obtained, which became bright yellow at contact with light.

By the characterization with ¹H-NMR-spectroscopy, the same trend as in the analogous cyclopentene-derivatives **1** and **3** was observed.

4.1.2. Synthesis of the organometallic complexes

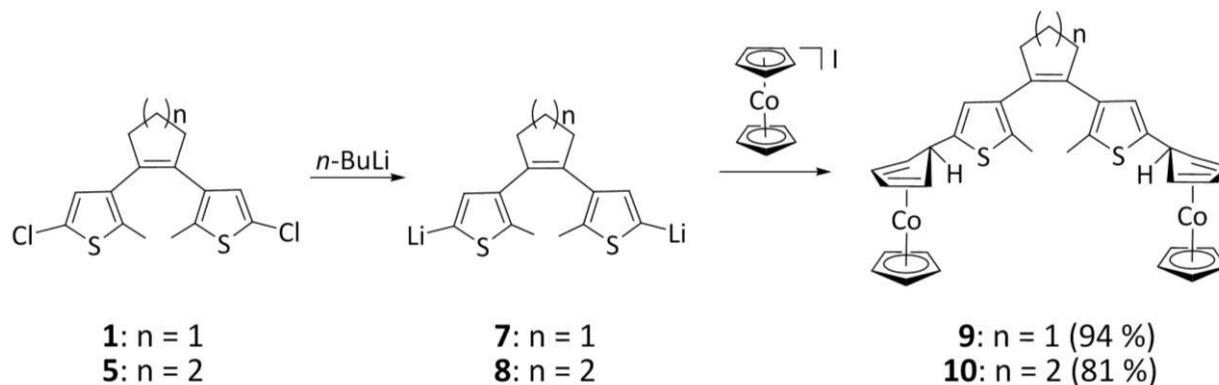
4.1.2.1. Synthesis of the cobalt complexes 9-14 and 16

Two different series of cobalt complexes were synthesized, using both molecular switches (cyclopentene- and cyclohexene-diarylethene backbones) as a bridge between two sandwich moieties.

For this work a synthetic approximation based on the work of Pagels *et al.*^[182] was employed. Unlike ferrocene, the direct electrophilic substitution on cobaltocenium-cation is not possible.^[135] For this reason the first step was the transformation of the molecular switches **1** and **5** in THF into the dilithiated intermediates **7** and **8** with *n*-butyllithium at low temperature, which were subjected to a double nucleophilic addition with two equivalents of cobaltocenium iodide (Scheme 16). Although a light excess of *n*-butyllithium was added, the formation of cobaltocene, formed by the reaction of the Co(I)-complex with the lithiumorganyl,^[191] was not observed.

The resulting neutral red complexes (which agrees with the literature^[191]) **9** and **10** were obtained in good yield and both were air- and water-stable. Although they contain 18 valence electrons and their stability should not be surprising, the bond between the cyclopentadiene ring and the molecular switch was expected to be weak and easy to break.^[191] On the contrary, these complexes displayed a high water and oxygen stability. In

the case of complex **10**, a fast work up was needed in order to improve the yield. The reason for that is that during the reaction an unknown side product, which was oxidized at the presence of air, was obtained. As the reaction was quenched with water, the formation of cobaltocene could be excluded.



Scheme 16: Synthesis of the Co(I)-complexes **9** and **10**.

The cobalt(I) atoms are only η^4 -coordinated to the cyclopentadiene rings which connect the sandwich complexes to the molecular switch. It is known that for this type of complexes the *exo*-isomer is formed,^[192] although exceptions to this rule can be found in the literature.^[193] The formation of the *exo*-isomer of complexes **9** and **10** was confirmed by X-ray analysis (section 4.3.2).

The next step was the elimination of the two hydrogen atoms bound to the sp^3 -carbon atoms of the substituted cyclopentadiene ligands as hydride ions, in order to restore the aromaticity of the cyclopentadiene ligands.

Although it is possible to perform the oxidative elimination by means of an electrochemical oxidation, the yield for this method is very poor (~10 %).^[135] Therefore the hydride ions were eliminated by addition of tritylium-cation^[135] (Scheme 17). The diamagnetic 18 valence electrons complexes **11** and **12** are air- and water-stable and present the expected bright yellow colour.

In order to achieve the target of obtaining two paramagnetic units connected by means of a molecular switch, both cobalt(III) centers had to be reduced to cobalt(II). In a first attempt, following the instructions of Pagels *et al.*^[181] sodium amalgam (1.1 %) was used as reducing agent in the reaction with the complex **9**. It is fast to synthesize, but it is difficult to prepare the alloy with the exact concentration of sodium. The reaction was carried out in THF and the expected color change, from yellow to dark violet, was observed. However, after the

4. Results and Discussion

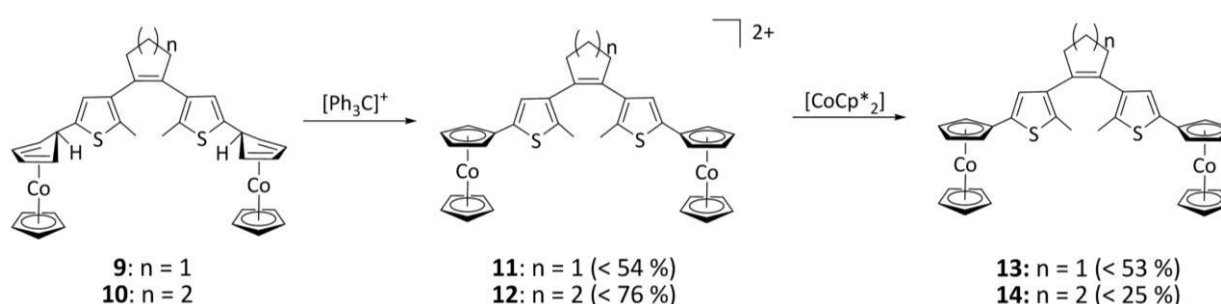
corresponding work up, the paramagnetic complex was not found in $^1\text{H-NMR}$ -spectroscopy. As the relaxation times of paramagnetic substances are very short, the NMR signals are broad.^[171] Thus, the concentration of the NMR sample must be very high or the signals will disappear in the noise. Attending to the violet colour, it is possible that the paramagnetic complex was synthesized, but other side products were present in the sample and the real complex concentration was not high enough.

In a second attempt, the reduction was carried out employing decamethylcobaltocene as reducing agent (Scheme 17). Even though it is tedious to synthesize^[153] and expensive, it has certain advantages comparing to sodium amalgam. It is easy to use the exact quantity of reducing agent and the reduction potential is not too negative, but sufficient to reduce the cobaltocenium complexes **11** and **12** (Table 5).^[194] The reduction potentials of these complexes were obtained by means of cyclic voltammetry (see section 4.4).

Table 5: Formal Potentials (V vs. FcH/FcH⁺).^[194]

Reducing Agent	Na/Hg	[Cp* ₂ Co]	11	12
E° (V)	-2.36	-1.94	-1.27	-1.18
Solvent	Nonaqueous	DCM	Acetonitrile	THF

Complexes **13** and **14** were obtained in moderate yields (**13**: < 53 %, **14**: < 25 %) in form of an extremely air-unstable black powder, which became violet when solved in nonpolar organic solvents.



Scheme 17: Hydride abstraction and subsequent reduction.

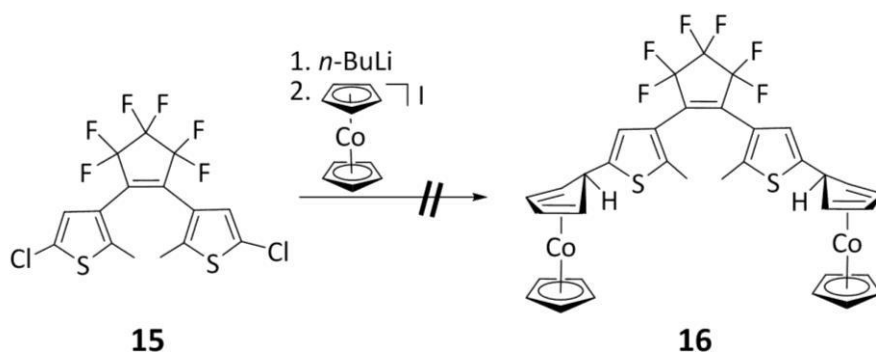
Both complexes **13** and **14** were characterized by NMR-Spectroscopy ($^1\text{H-NMR}$ for **13**, ^1H - and $^{13}\text{C-NMR}$ for **14**). The results for these measurements will be discussed in section 4.2.

When ESI-mass-spectra of these complexes (**13** and **14**) were recorded, the expected molecule peaks were not found. According to the work of Bildstein,^[195] an aliquot of each

complex was dissolved in a THF-degassed water mixture (1/1 v/v) and stirred for 30 min. Afterwards, the Schlenk-flask was opened and the solutions were allowed to be in contact with air. The yellow cobaltocenium complexes were extracted with chloroform and the corresponding [M/z] peaks could be found in the ESI-Mass-spectra.

Attempt to the synthesis of 1,2-bis{2'-methyl-5'-[(η^5 -cyclopentadienyl)](η^4 -1'',3''-cyclopentadien-5''-yl)cobalt(I)-thiophen-3'-yl}perfluorocyclopent-1-en (16)

As another important member of the dithienylethene molecular switches "family", the 1,2-bis(5-chloro-2-methylthien-3-yl)hexafluorocyclopentene **15** has been deeply investigated. It was attempted to use it to connect two cobalt sandwich complexes applying the same reaction conditions as for the synthesis of complex **9** (Scheme 18). The colourless molecular switch **15** was lithiated with *n*-butyllithium in THF at low temperature and the solution immediately turned green. Afterwards, cobaltocenium iodide was added and the solution became yellow. After stirring it overnight and evaporating the solvent, a red oil was obtained. The red colour is an indication of the formation of a Co(I)-complex, but when $^1\text{H-NMR}$ and EI-mass spectra were recorded, the desired complex could not be identified. Initially it was thought that the red oil was 1-[(η^5 -cyclopentadienyl)](*n*-butyl- η^4 -cyclopentadien-1'-yl)cobalt(I)], a complex which is found when an excess of *n*-butyllithium is added.^[196] However, this product was neither found in the $^1\text{H-NMR}$ or EI-mass spectra.



Scheme 18: Proposed synthesis of **16**.

The synthesis of this complex was not attempted again due to the lack of time.

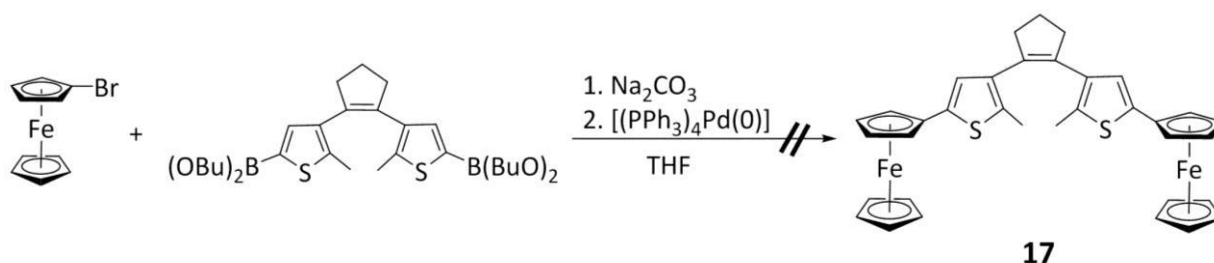
4.1.2.2. Synthesis of the iron complexes 17-19

Cobaltocene was not the only paramagnetic metallocene used in this project. Ferrocenium is paramagnetic as well and has some advantages over cobaltocene. First of all, it is big far not as air-sensitive as cobaltocene, facilitating the synthesis, characterization and subsequent

4. Results and Discussion

application as molecular switch. In addition, the toxicity of iron compounds is much lower than of the cobalt derivatives. Therefore, it was tried to synthesize a complex where two ferrocenium moieties were connected through a diarylethene molecular switch unit.

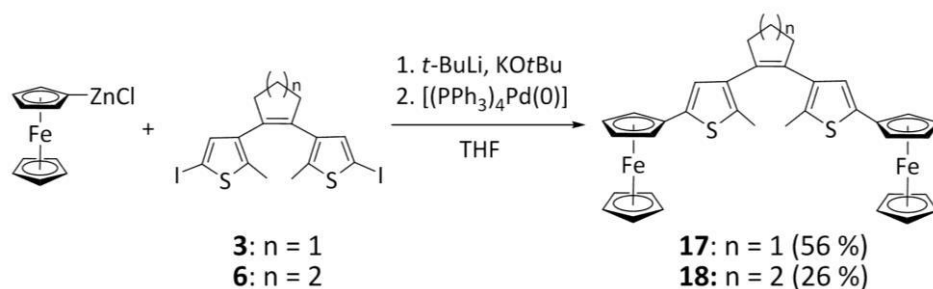
In order to synthesize the bisferrocene complex **17** different synthesis protocols were applied. In the first place a protocol of Suzuki cross-coupling reaction according to Feringa and coworkers^[73] was applied. Since the low reactivity of the chloro-thienyl bond of the molecular switch impedes the reaction, the molecular switch **1** was converted into a boronic acid in accordance with Lehn and coworkers.^[197] This boronic acid was used without further purification in a reaction with 1-bromoferrocene. THF and several drops of ethylene glycol were used as solvent, Pd(PPh₃)₄ as catalyst and Na₂CO₃ as base. Unfortunately, this reaction did not lead to the desired product but the starting materials were found back (Scheme 19).



Scheme 19: Unsuccessful Suzuki cross-coupling reaction.

In a second attempt, a Negishi cross-coupling reaction based on Hildebrandt's^[198] work was carried out. Ferrocene was lithiated with *tert*-butyllithium in the presence of KO*t*Bu.^[199] The lithiated ferrocene was transformed to the ZnCl-compound, which was allowed to react with the molecular switch 1,2-bis(5-chloro-2-methylthien-3-yl)cyclopentene (**1**) in the presence of Pd(PPh₃)₄. However, the low reactivity of the chlorine substituents impeded the reaction.

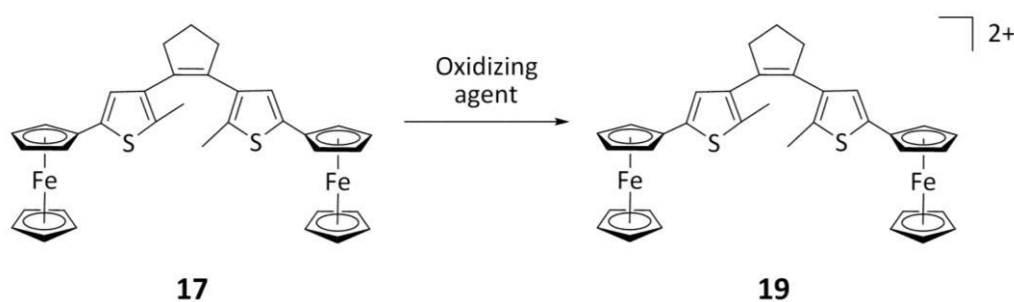
When the same reaction conditions were applied with the bromo-derivative 1,2-bis(5-bromo-2-methylthien-3-yl)cyclopentene (**2**), the desired ferrocene complex was obtained (at least 14 %). By using the iodo derivative **3**, the compound with the best leaving group, the yield considerably improved to 56 % (Scheme 20).



Scheme 20: Synthesis of the ferrocene complexes **17** and **18**.

The analogous complex **18**, with a cyclohexene connecting the thiophene rings, was synthesized using the same reaction conditions.

Once the ferrocene complexes had been synthesized, there was only one step left to obtain the paramagnetic ferrocenium complexes: the oxidation of the iron(II) centers. This reaction was only carried out with the complex **17**, and different oxidizing agents were tested for it. In a first attempt silver(I) was employed.^[200] This method was chosen because after the reaction it should be possible to separate the silver(0) from the reaction mixture only by filtration. As expected, the solution turned from orange to brown and a silver mirror was visible at the bottom of the Schlenk-flask. Unfortunately, after washing the eventual side products with hexane, there was no product left to continue with the characterization. This fact contradicts the formation of the dicationic complex **19**.



Scheme 21: Oxidation of the iron(II) centers of complex **17** to iron(III) (complex **19**).

In a second attempt iodine was employed as oxidizing agent.^[201] After suspending the starting products in dried hexane, the mixture was refluxed for one hour before the dark suspension was filtered. The pink mother liquor was separated from the navy blue solid, which was washed with pentane until the filtrate did not become pink. The navy blue residue (a typical colour for ferrocenium complexes) was almost insoluble in all the common solvents and when ¹H-NMR measurements were carried out, no signals in paramagnetic range were visible, probably due to the low concentration of the sample.

Afterwards, the synthesis of the ferrocenium complex **19** was carried out with nitrosyl tetrafluoroborate as oxidizing agent.^[202] It presents the advantage that the nitrosyl cation will be transformed to nitrogen(II)-oxide gas, which will evolve during the reaction facilitating the work up. In addition, in contact with oxygen it reacts to nitrogen(IV)-oxide,^[122] an orange gas which could be taken as indication of the success of the reaction. As in the other cases, the orange diferrocenyl-complex solution in dichloromethane turned dark in contact with the oxidizing agent and, moreover, the development of a gas could be observed. The suspension was filtered and both the dark blue mother liqueur and the solid were investigated. ¹H-NMR and EI-Mass spectroscopic measurements were carried out and the target complex was only found in the mother liquor. In the EI-Mass spectrum the product peak (**19**) and the peak correspondent to the neutral diferrocenyl-complex **17** were visible. The possibility that a part of the diferrocenium complex **17** had been reduced during the measurement exists, but as these both peaks are visible too when measuring the pure neutral complex **17**, this method offers no confirmation of the synthesis of the goal complex **19**.

The synthesis of the complex was confirmed by means of X-ray structure analysis although the quality of the crystals was not sufficient for discussion (R = 17.15 %).

When ¹H-measurements were carried out in dichloromethane-d₂ different signals in the paramagnetic range could be observed, although in the diamagnetic range not signals could be identified (Figure 60).

The signal at 40.57 ppm represents the protons at the α and β positions of the substituted Cp-ligands, although it does not integrate for eight hydrogen atoms. For substituted ferrocenium complexes it is not unexpected that the signals for these two positions have the same chemical shift, as it was observed for 1,1'-dimethylferrocenium-cation.^[203] The signal at 28.55 ppm could correspond to the non-substituted Cp-ligands, and the signal at 33.13 ppm coincides with the chemical shift of ferrocenium in dichloromethane,^[203] which could be a side product of the decomposition of the complex. At 23.76 ppm the protons of the methyl groups and at -25.42 ppm the aromatic protons of the thiophene rings are found. The last two signals coincide with the analogous signals of the cobaltocene complexes **13** and **14** (see section 4.2.1.1).

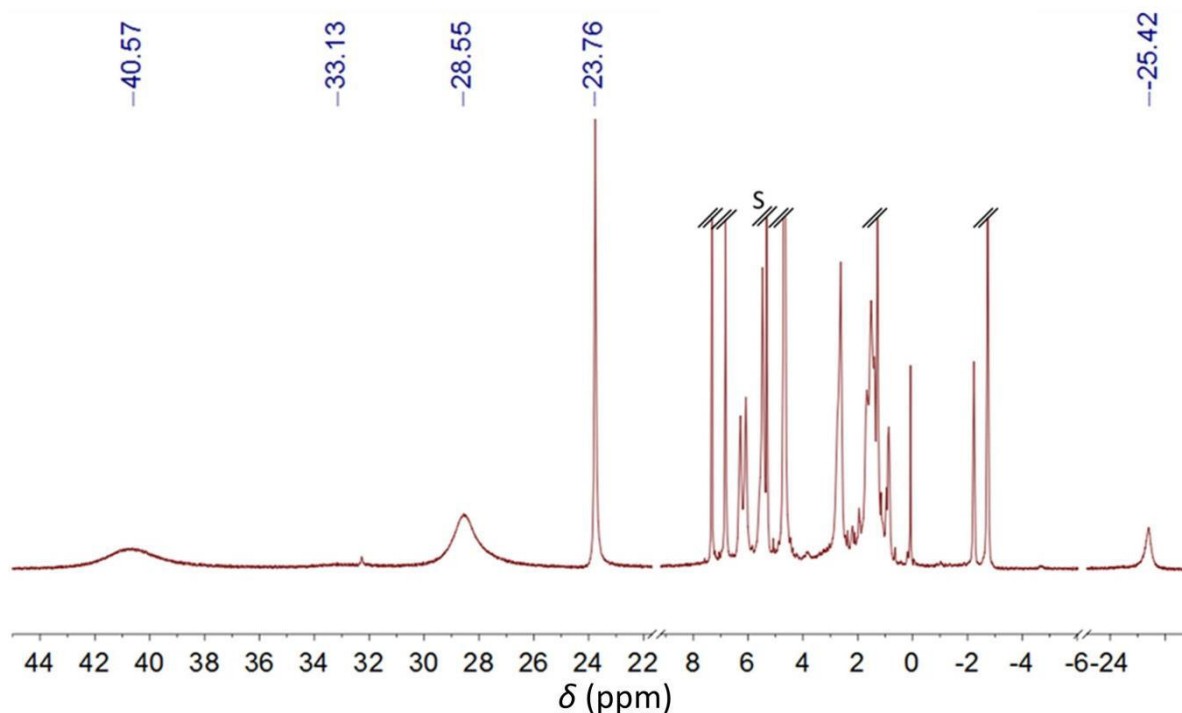


Figure 60: ¹H-NMR Spectrum in dichloromethane-d₂ of the supposed diferrocenium complex **19** (400 MHz, S = Solvent)).

In a last attempt to optimize the reaction, iron(III)-chloride was employed. In accordance to Neuse *et al.* ^[204] ferrocene can be oxidized by the former oxidizing agent in the presence of an acid. As the dithienylethene reagent did not show stability at acidic pH, the reaction was carried out without adding any acid. Like in the other cases, the solution turned dark and an almost insoluble solid was obtained. When ¹H-NMR measurements in acetonitrile were carried out, no paramagnetic signals were found.

4.1.2.3. Alternative synthesis path

In 1988 Bunel *et al.* ^[205] developed a general strategy for the synthesis of bridged biferrocenes. Instead of fixing two complete ferrocene moieties to an organic bridge as in the last synthesis protocol (Scheme 20), only two cyclopentadiene rings are linked to the bridge. In order to “complete” the ferrocene moieties, the corresponding Cp-metal halfsandwich precursor was added, e.g. (η⁵-C₅Me₅)Fe(acac).

The advantage of this method is that after preparing successfully the organic bridge, which in this case would be a dithienylethene derivative, not only ferrocene complexes could be prepared, but also dicobaltocene complexes, only by changing the metal-precursor.

In order to prepare the organic bridge, a stepwise addition of dry 2,3,4,5-tetramethylcyclopent-2-en-1-one to the molecular switch in Et₂O was done.

4. Results and Discussion

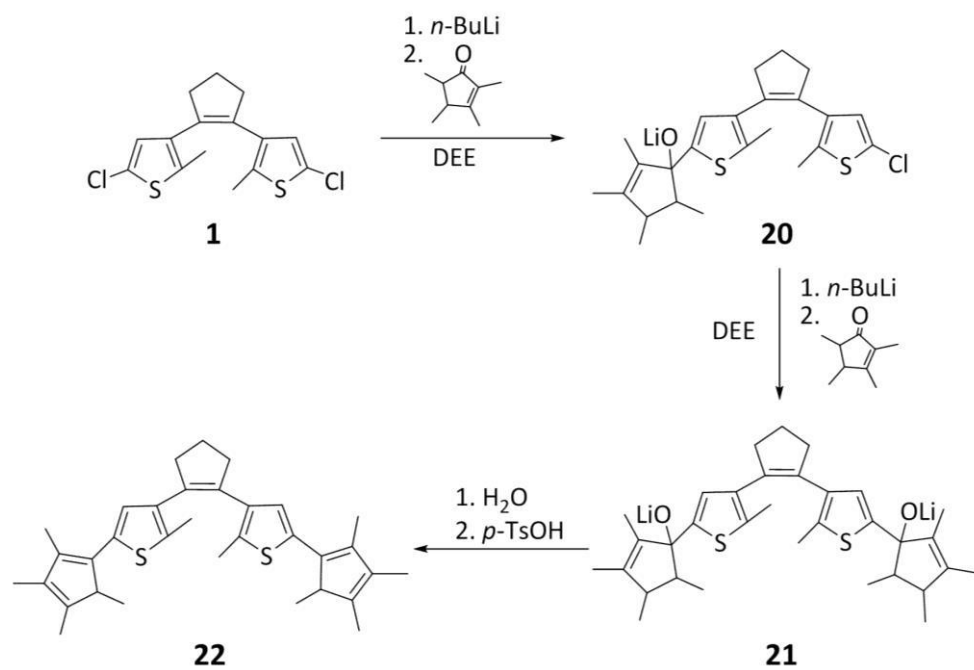
Afterwards the lithium salt **21** was quenched with aqueous ammonium chloride and *p*-sulfonic acid was added, which produced the deoxygenation of the product (Scheme 22).

After column chromatography and following recrystallization, it was tried to characterize the product *via* ¹H-NMR spectroscopy. The peaks correspondent to the dithienylethene backbone could be identified, contrary to the peaks which represent the other methyl groups. The reason for this complicated spectrum could be the large number of isomers, which differ from another in the position of the double bonds in the cyclopentene rings.

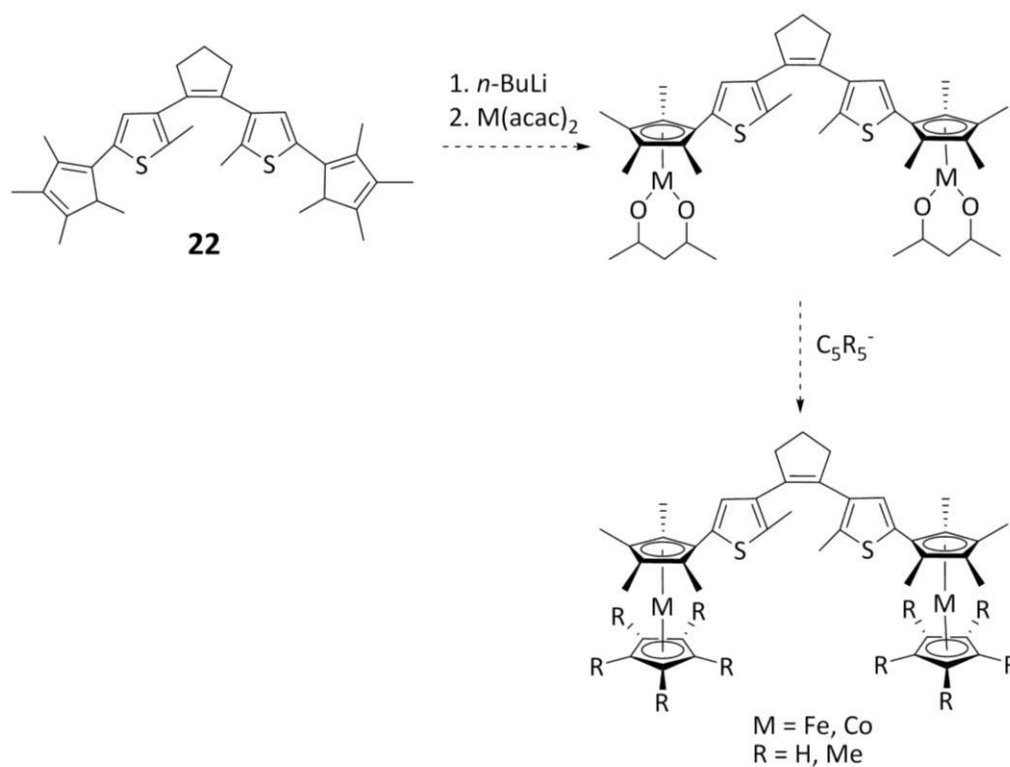
Although it could not be isolated, the synthesis of the molecule was confirmed by ESI-Mass-spectroscopy. A peak at 501.0819 represents [M+H]⁺ (calculated 501.26) and several fragments could be also identified.

After having obtained the pure product **22**, the next step would have been the metallation of the organic linker (Scheme 23), for which an iron or cobalt precursor would have been employed. However, due to the difficulties in the purification of the organic ligand and the success of the other proposed synthesis paths, the work in this direction was not continued.

This synthesis protocol was already employed by Akita and coworkers^[112] in 2007, when a series of ruthenium complexes was prepared. However, instead of the stepwise addition of dry 2,3,4,5-tetramethylcyclopent-2-en-1-one to the molecular switch, the cyclopentenone was added to 2,4-dibromo-5-methylthiophene at the position 2. Afterwards, the obtained compound was lithiated in the presence of 1,2,3,3,4,4,5,5-octafluorocyclopentene and the analogous to compound **20** perfluorocyclopentene derivative was obtained.



Scheme 22: Synthesis of the organic compound **22**.



Scheme 23: Proposed metalation of **22**. This reaction was not carried out.

4.2. NMR-spectroscopic experiments of the paramagnetic complexes

4.2.1. NMR-spectroscopic experiments of the paramagnetic cobaltocene complexes **13** and **14**

^1H -NMR experiments with both paramagnetic Co(II)-complexes (**13** and **14**) and ^{13}C -NMR, HSQC and HMBC experiments with complex **14** were carried out. In this work, chemical shifts with a negative sign indicate a shift at low frequency or high field, and in turn a negative spin density.

The signal shifts found for both complexes probates an indication about their nature. The unpaired electrons interact with the applied magnetic field producing such a large chemical shift. ^[171] In figures 61 and 62 the ^1H -NMR spectra of complexes **13** and **14**, respectively, are presented. In figure 63 the ^{13}C -NMR spectrum of complex **14** can be found.

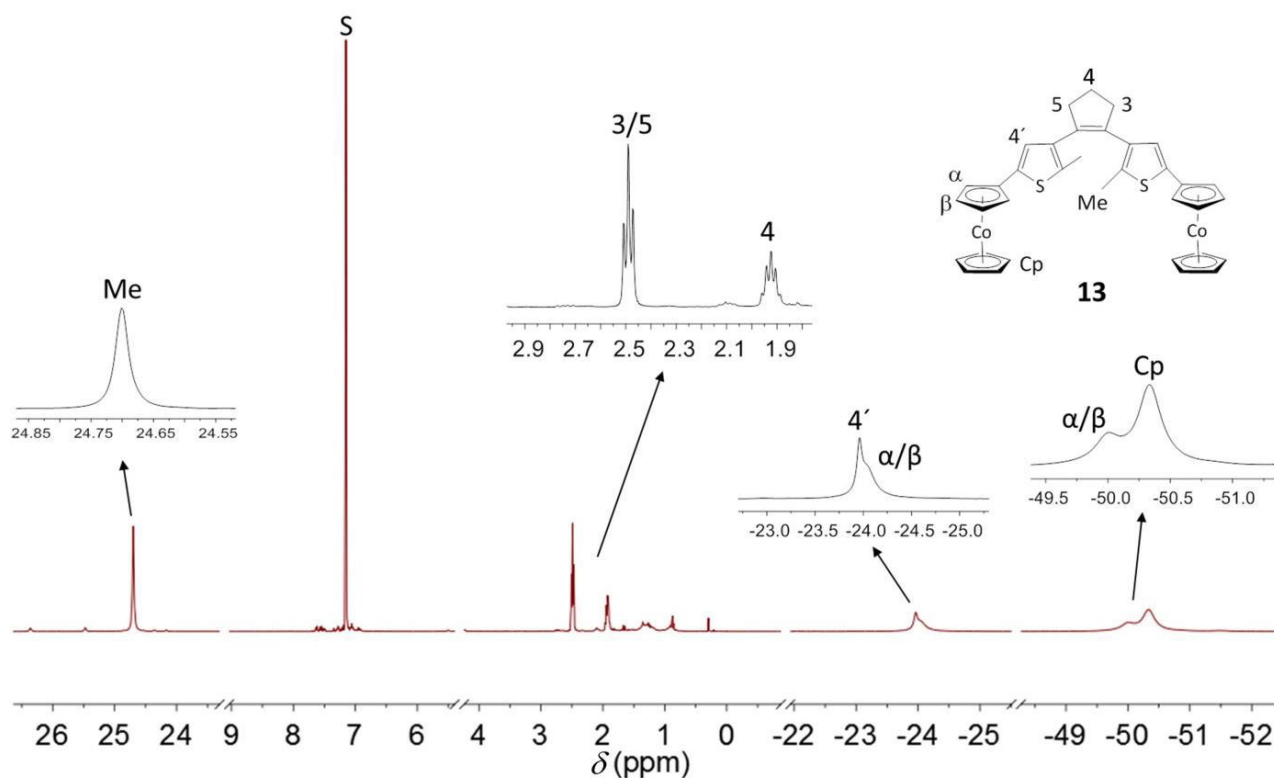


Figure 61: ^1H -NMR-spectrum of complex **13** in benzene- d_6 at room temperature (400 MHz, S = Solvent).

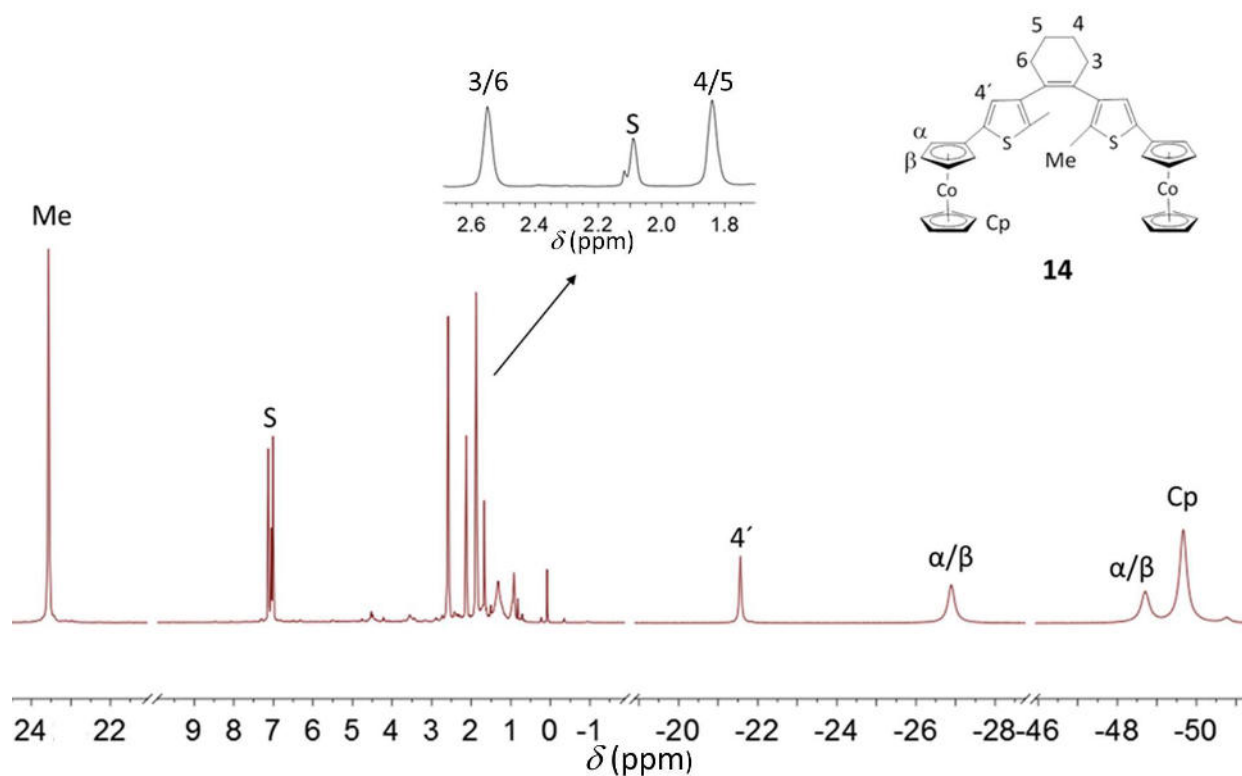


Figure 62: ^1H -NMR-spectrum of complex **14** in toluene- d_8 at room temperature. (400 MHz, S = Solvent).

The ^1H -NMR signal shifts are very similar for both cobalt(II) complexes (Table 6), as it was expected for such resembling complexes. The signal assignment was done by comparing these complexes with the cobaltocene complexes synthesized by Pagels *et al.* [206] and with the help of the C-H correlation NMR-experiments (HMQC, HSBC. See section 10) carried out for complex **14**. In the case of the ^{13}C -NMR signal shifts, only seven from the twelve signals could be securely identified.

Table 6: ^1H -NMR signal shifts for complexes **13** and **14** in toluene- d_8 (400 MHz).

δ_{293}^{exp} (ppm)	Me	3/5 (3/6)	4 (4/5)	4'	α/β	α/β	Cp
13	24.38	2.50	1.93	-23.95	-24.06	-50.00	-50.33
14	23.53	(2.55)	(1.84)	-21.60	-26.93	-48.73	-49.70

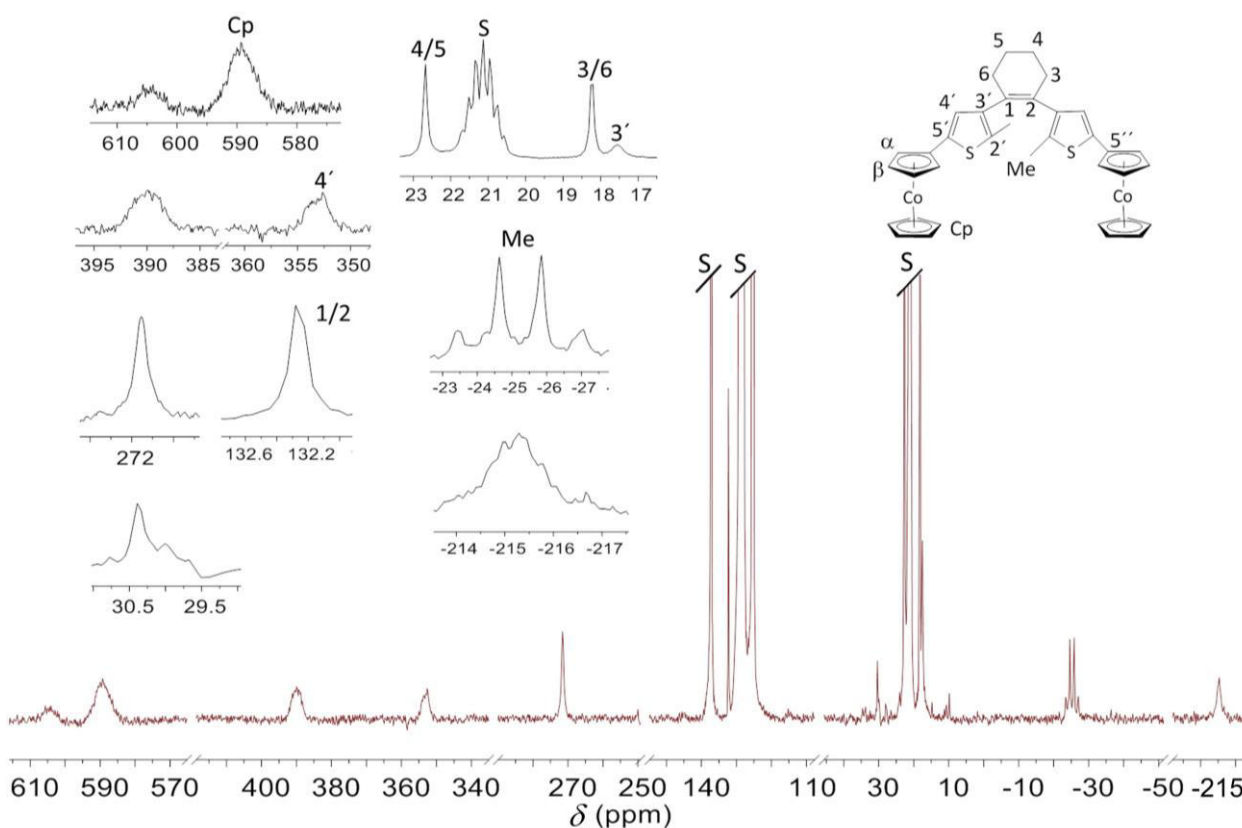


Figure 63: $^{13}\text{C}\{\text{H}\}$ -NMR-spectrum of complex **14** in toluene- d_8 at room temperature. (400 MHz, S = Solvent)

In a paramagnetic system the unpaired electron is not localized in a single point but on the entire molecule delocalized (see section 2.2.3.4). The “fraction” of unpaired electron present at each point of the system is called spin density ρ .^[124] It is known that for sandwich complexes having more than six d electrons (the case of cobaltocene), positive spin density is transferred from the metal to the ligand based on two different spin transfer mechanisms: direct spin delocalization, where the spin sign remains unchanged, and a σ -bond polarization, which induces a sign inversion of the spin.^[158] It corresponds with the observed chemical shifts in the ^{13}C -NMR-spectrum of complex **14** (Figure 63): the signals belonging to the carbon atoms of the Cp-ligands appeared down field, indicating a positive spin density. Probably, the signals at 390 ppm and 272 ppm represent the carbon atoms at α and β positions of the substituted Cp-ligands, and the unsubstituted Cp-ligands appear at 590 ppm. The sign inversion within C-H bond polarization becomes evident in the ^1H -NMR signal shifts at high field of the corresponding protons (Figures 61 and 62), which indicates a negative spin density.

Spin density can be transferred to various nuclei of substituents bound to the π -ligands of paramagnetic complexes (see section 2.2.3.4). In this case, the switching core is attached to

the Cp-ligands of the metal complexes. How the spin density is transferred depends on the spin delocalization and on the distance of the observed nucleus to the spin-carrying π orbital (spin polarization). This distance will be measured in “number of σ -bonds”. Normally, the convention α , β , γ ... is used to denominate the nuclei which are separated by one, two or three “ σ -bonds” from the unpaired electron, respectively.^[158] It should not be confused with the numbering given in the NMR-spectra in figures 61-63, where α and β were used to define the carbon atoms of the substituted Cp-ligands.

The carbon atom at position 5'' (Figure 63) is probably represented by the signal at 610 ppm. It agrees with the positive spin density which was expected, and the area is smaller than in the other two no assigned signals, which are allocated to the carbon atoms in α and β positions of the substituted Cp-ligands.

The spin density at the atom found at a “ σ -bond distance” to the π -ligand normally reveals a sign inversion of the spin through spin polarization.^[158] Therefore, the carbon atom at position 5' in complexes under study is expected to have a negative spin density and be represented by the signal at -215.5 ppm.

The spin density at the atom found at two “ σ -bonds distance” (position 4' in complexes **13** and **14**) could be induced by different mechanisms. It is possible that, as in the former case, a sign inversion takes place due to spin polarization. The sign would be the same as for the carbon atoms of the π -ligand and opposite to the spin sign for the carbon atom at the 5'-position. Nevertheless, this carbon atom is part of the π -bond, therefore a hyperconjugation could lead to selective spin transfer: less spin density would be transferred from the position 5'' to 5' and much to 4'. Although normally hyperconjugation dominates, spin polarization cannot be neglected.^[158]

The carbon atom at position 4' presents a signal down field (positive spin density) and the corresponding hydrogen-atoms, which are expected to support a negative spin density, appear high field (Figure 62). This observations agree with the work of Köhler *et al.*^[158,207] where it is postulated that in case of cobaltocene, the spin density in this position (position 4' in complexes **13** and **14**) is positive. In this type of complexes it has been observed that the dihedral angle (Figure 64) exerts a great influence in the hyperconjugation.^[158]

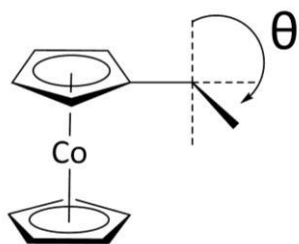


Figure 64: Dihedral angle.

The resonance signal of the carbon atom 3' appears at 17.5 ppm. Comparing this chemical shift with the chemical shift of the same atom in the corresponding diamagnetic complex **12** (132.98 ppm), a shift towards negative spin density can be observed (spin polarization). A sign inversion with respect to the carbon atom at the 4'-position was not observed, probably because spin delocalization is also taking place.

The signals corresponding to the connecting cycloalkene are found in the diamagnetic shift range (similar chemical shift as in the corresponding diamagnetic complexes **11** and **12**). Therefore, it can be supposed that there is no significant spin transfer from the metal atoms to these carbon atoms due to the large separation (in number of σ -bonds) between the nuclei and the unpaired electron.

The carbon atom 2' is expected to support a negative spin density, due to the hyperconjugation mechanism between the members of a π -bond. However, spin polarization cannot be neglected. Taking into account the chemical shifts of the carbon atom at position 3' and the carbon atom of the methyl groups (see below), it is probably that the signal at 30.5 ppm represents the carbon atom at position 2'.

Finally, the carbon atoms of the methyl groups present a negative spin density shown by the chemical shift to high field. This signal is easy to be recognized due to the quartet formed by the C-H coupling. Although a proton-decoupled spectrum was recorded, the measured range is so large that it was not possible to suppress the C-H coupling in the whole spectrum. On the contrary, the corresponding protons support a positive spin density, represented by a positive chemical shift (24.1 ppm, Figure 62).

One day later and with the same sample, another four ^{13}C -NMR spectra were recorded. Each measurement lasted twelve hours and the sample remained all time in the sampler, so it was not exposed to sun or artificial light. The only difference was the adjusted decoupling frequency, which only exerts an influence in the C-H coupling of the methyl groups.

The results were surprising. The first measurement presented exactly the same signal shifts as the spectrum taken the day before (Figures 63, 65 and 66), but later it was observed that the molecule underwent a slow change over time in its structure. In spectrum 2 (Figures 65

and 66) are two different species present while in spectra 3 and 4 (Figures 65 and 66) only one species is present and it is not the same as in the first measurement.

The chemical shift of these new signals indicates that the complex was not oxidized. At first was thought that the switching reaction had taken place. Different researchers have achieved to identify both states, open and closed, in $^1\text{H-NMR}$.^[112,208,209] However, in the NMR-equipment the solution was not in contact with any light source. In addition, the variation in the chemical shifts is not as big as expected. The carbon atoms at position 2' present a sp^2 -hybridization in the open state of the molecular switch and a sp^3 -hybridization in the closed state. Had the switching reaction taken place, the variation in the chemical shift would have been dramatic. Nevertheless, the signal at 30.5 ppm did not shift. It would also be expected that the chemical shift of the carbon atoms of the methyl groups (which in the different states of the molecular switch are bound to carbon atoms with different hybridizations) undergo an important change, but it does not.

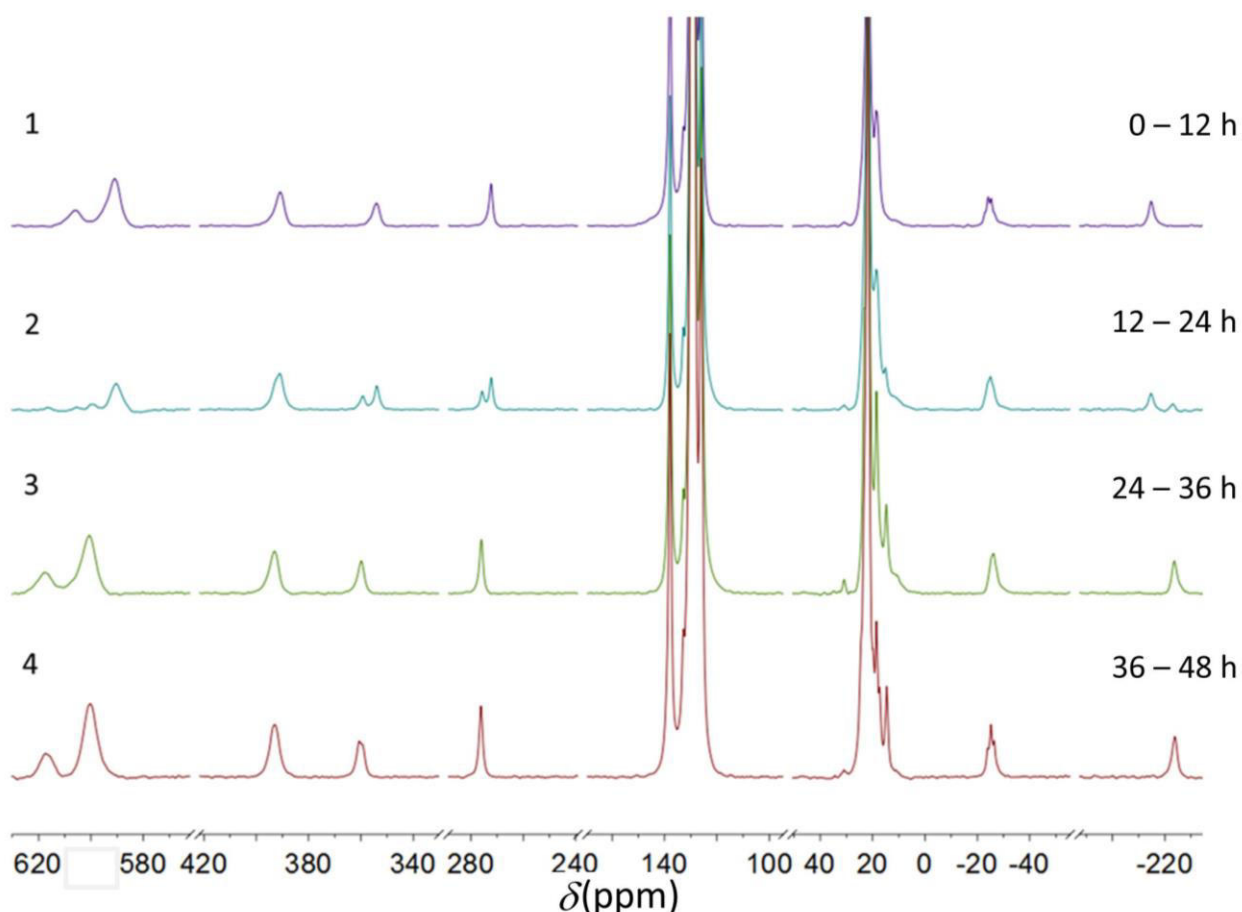


Figure 65: Over-time structural change (complex **14**) observed within $^{13}\text{C-NMR}$ spectroscopy in toluene- d_8 .

4. Results and Discussion

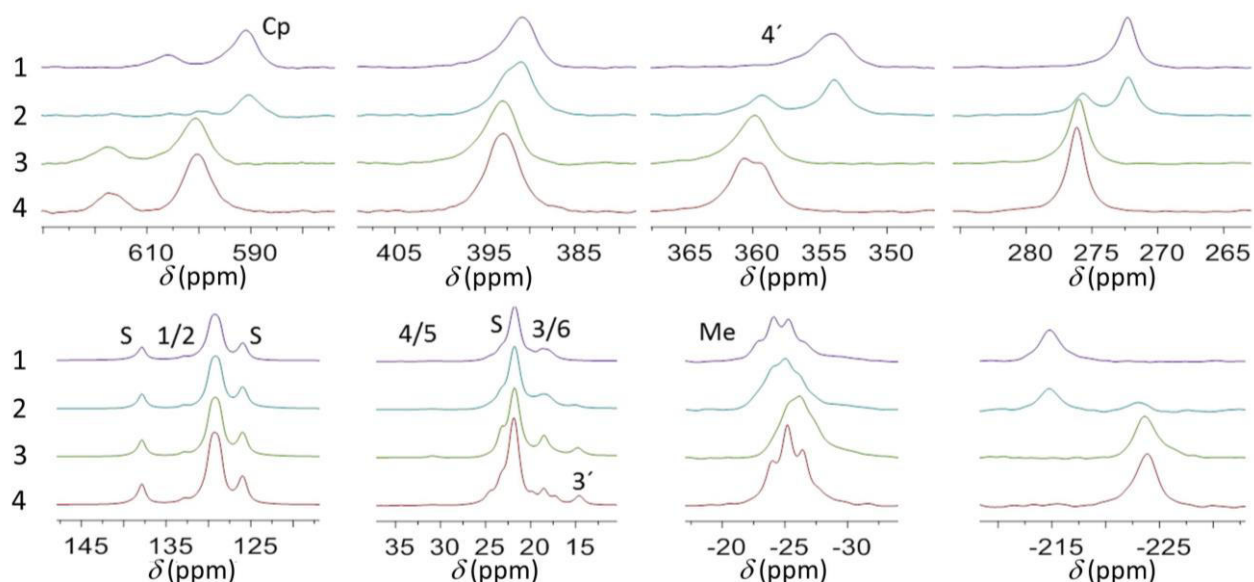


Figure 66: Several cuts from the ^{13}C -NMR spectra where the over the time structural change underwent by complex **14** is observed (toluene- d_8).

After dropping the switching reaction, the possible conformers present in this type of complexes, parallel and antiparallel, were considered (Figure 67). In diarylethene derivatives with small substituents at the position 5', the conformers' ratio is normally 1:1. ^[24,210] When these substituents are sterically more demanding, as in the case of complex **14**, the antiparallel conformer is favoured. ^[24] Several researchers ^[208,209] investigated the existence of these conformers by means of NMR-Spectroscopy at room temperature. However, this equilibrium is normally so fast, that only the averaged signal shifts are to see. Nevertheless, in some cases it is possible, even at room temperature, to identify both conformers by the two differentiated signals for the methyl groups in ^1H -NMR, one for each conformer. ^[210] In the case of complex **14** the observed chemical shift variation for the methyl carbon atoms is not significant (Figures 65 and 66). Furthermore, no examples of spontaneous displacement of the dynamic equilibrium over the time towards one conformer or the other are known in the literature.

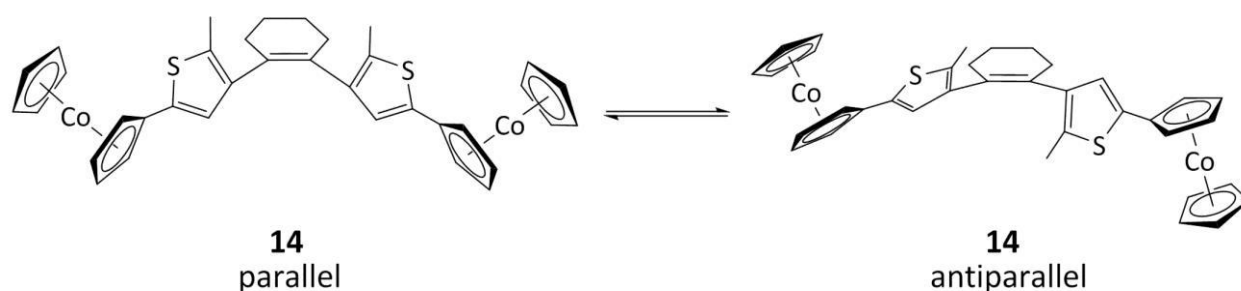


Figure 67: Possible conformations.

In a last attempt to observe the conversion of one conformer to the other and with the intention of obtaining the most thermodynamically stable conformer, the diamagnetic ferrocenyl-complexes **17** and **18** were solved in toluene- d_8 and the solutions were heated for 45 h (80 °C-100 °C). Unfortunately, no new signals were observed in ^1H - and ^{13}C -NMR-spectroscopy. Therefore, the idea of a thermodynamically more stable conformer could be dismissed.

Another possibility could be to focus on the cyclohexene connecting the thiophene rings. In the obtained crystal structures of the diamagnetic Co(III)-complexes **11** and **12**, the cyclohexene ring was found in a half-chair conformation. In solution exists a dynamic equilibrium between different conformations (Figure 68) which could explain the presumably conformational change suffered by compound **14** over time.^[211,212] However, the half-chair conformation is the most stable and the proportion of the boat form is normally far too small to be detected in NMR-spectroscopy.^[211] Nevertheless, in the spectra presented in figures 65 and 66, the signals which represent the carbon atoms of the cyclohexene ring are not precisely those which evolve over time.

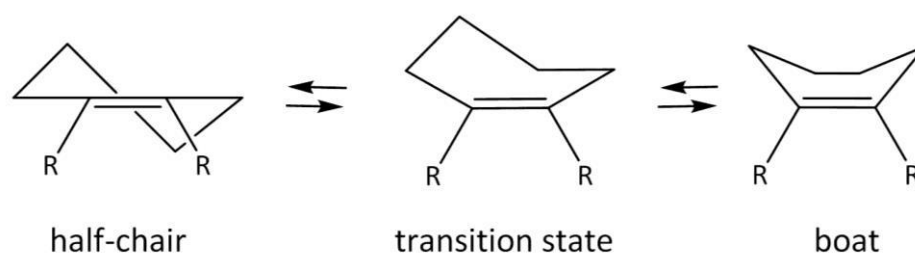


Figure 68: Different conformations for the cyclohexene ring.

Another fact which contradicts the last three explanations to the observed phenomenon is the lack of one species at a time. Thus, at the initial situation there is only one of both species to see and at the time the fourth spectrum was measured, this species had completely disappeared (or it was present in a low concentration so it could not be detected NMR-spectroscopically) and only the second species was present. Therefore, the idea of two species in equilibrium can be dismissed. Regarding to the switching reaction it does not seem feasible that it presents a yield of almost 100 %, and the same occurs for the parallel/antiparallel and cyclohexene conformation ratios. Normally both conformations can be found in dynamic equilibrium and at room temperature only one signal for each atom is visible.

Finally, the last factor which could produce a change in the environment of the metal complex was the employed solvent: toluene. Toluene is a π -rich solvent ^[213] which could interact with the other π -systems present in the cobalt complex, e.g. thiophene rings. It is not unthinkable that over the time a π -interaction, weak and highly dynamic, is formed between both aromatic rings and the new structure presents NMR signals shifts slightly different as from the starting complex. The work of Collins *et al.* ^[213] demonstrated that this type of interaction can exert a great influence in the geometry of certain compounds, even in solution.

In the literature two different arrangements of aromatic rings are known: face-to-face and edge-to-face (C-H $\cdots\pi$). ^[214] In the former the aromatic rings adopt a sandwich structure where a direct π - π interaction exists (π - π Stacking) while in the latter exist an interaction between the electron-poor protons of one aromatic ring and the π -rich system of the other ring, forming a T-shaped structure. Thiophene systems which contribute to form this type of systems are not unknown in the literature. ^[215]

After having discussed the possible explanations for the structural change seen in the ¹³C-NMR-spectra over the time, it is not possible to confirm what actually happened and, as a consequence, if this change is or is not reversible. If only a displacement of the dynamic equilibrium has taken place, the initial situation will be restored after an undetermined amount of time. Taking into account that before the ¹³C-NMR spectra were recorded, the solution was kept five days under nitrogen atmosphere, heated (353 K) and cooled down to 193 K and afterwards the “new signals” were not visible in the first ¹³C-NMR spectrum but in the spectra taken hours later, the idea of a reversible reaction might be conceivably.

Alternatively, if the observed change has occurred as a consequence of the interaction with the solvent, the new situation will remain. What it can be ensured is that the geometrical change suffered by the cobalt complex has not modified its nature.

4.2.1.1. VT-¹H-NMR Measurements from complexes **13** and **14**

As it was explained in section 2.4.2.1, VT-NMR measurements offer important information about the magnetic behaviour of paramagnetic compounds. VT-¹H-NMR measurements of both paramagnetic complexes (**13** and **14**) were carried out in toluene-d₈.

The results of the measurement of complex **13** are shown in the figure 69 and plotted as chemical shift δ vs. $1/T$ in figure 70. The graphical presentation displays linear behavior of the shift of the proton signals with the reciprocal temperature, which probes that the magnetic behavior in solution obeys the Curie Law in the measured temperature range, except for the protons at α or β position (Figures 70 and 71). The linearity of the chemical shifts δ vs. $1/T$ is common to cobaltocene itself, but not to cobaltocene derivatives, due to the “Anomaly of Cobaltocene” (see section 2.3.).^[146,148] The so-called anomaly was only found for the hydrogen atoms in α or β position of the substituted Cp-rings. In figure 69 it can be seen that the signals of the protons at position 4' and of protons at α or β position are crossing, as the protons of the non-substituted Cp-rings and of the α or β position do.

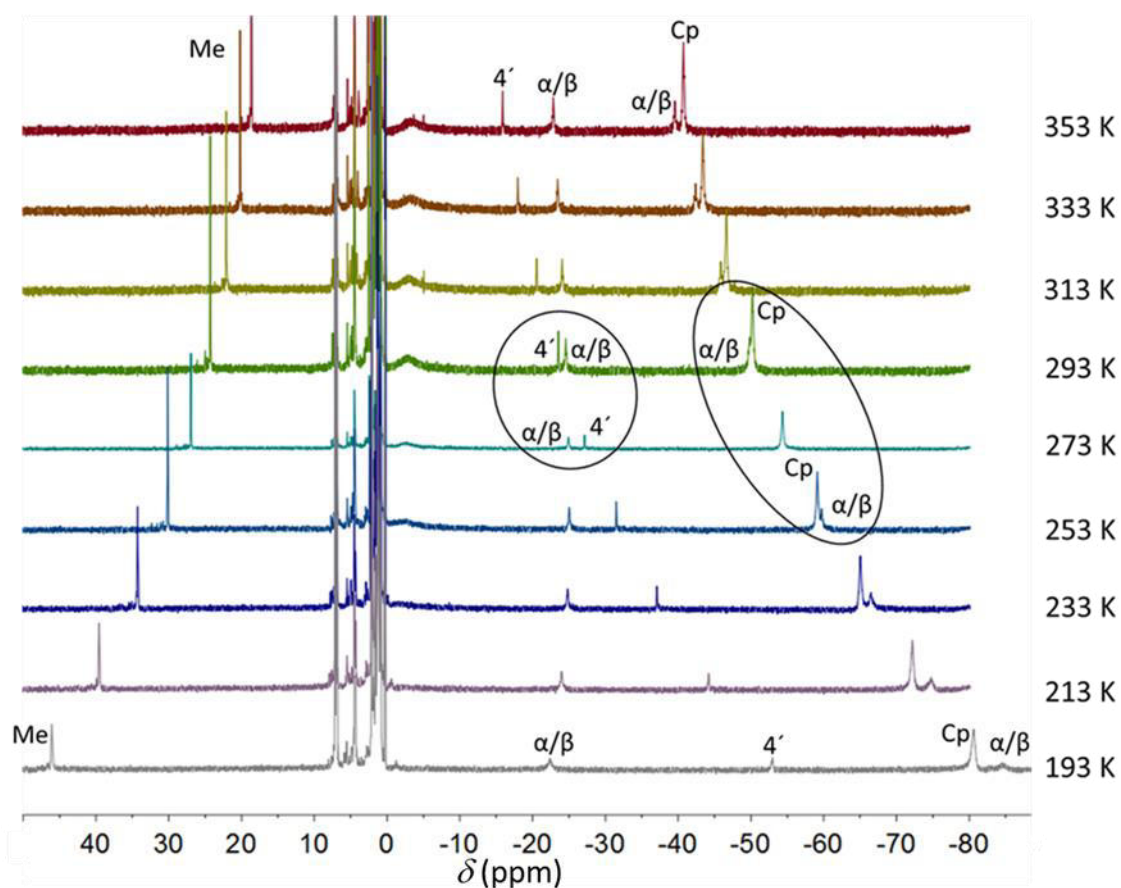


Figure 69: VT-¹H-NMR of the cobalt complex **13** in toluene-d₈.

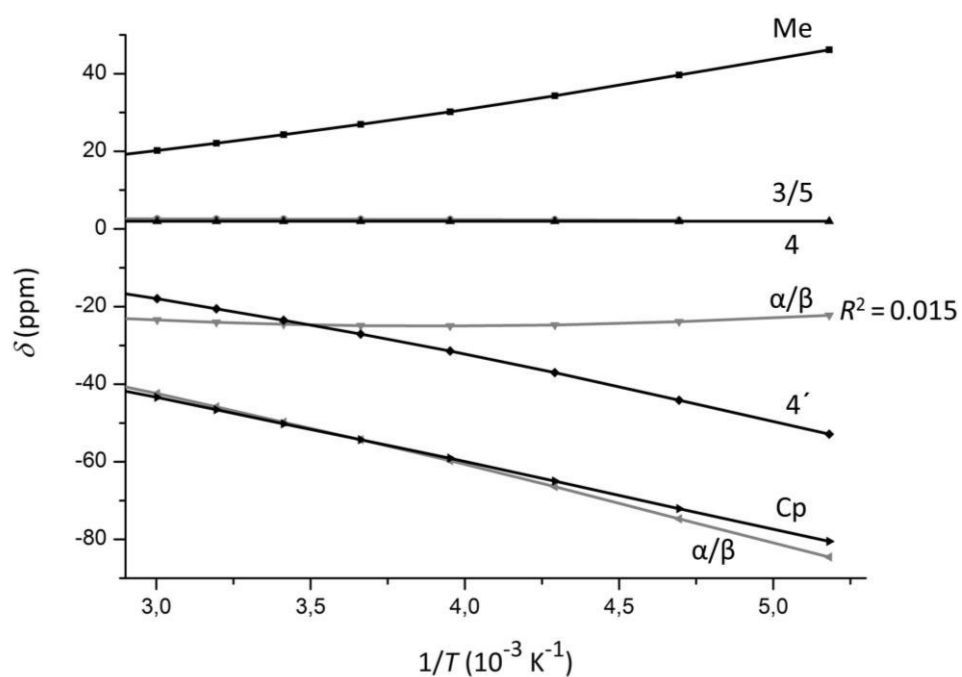


Figure 70: Temperature dependence of the proton signals (complex **13**). When no indicated $R^2 \sim 1$.

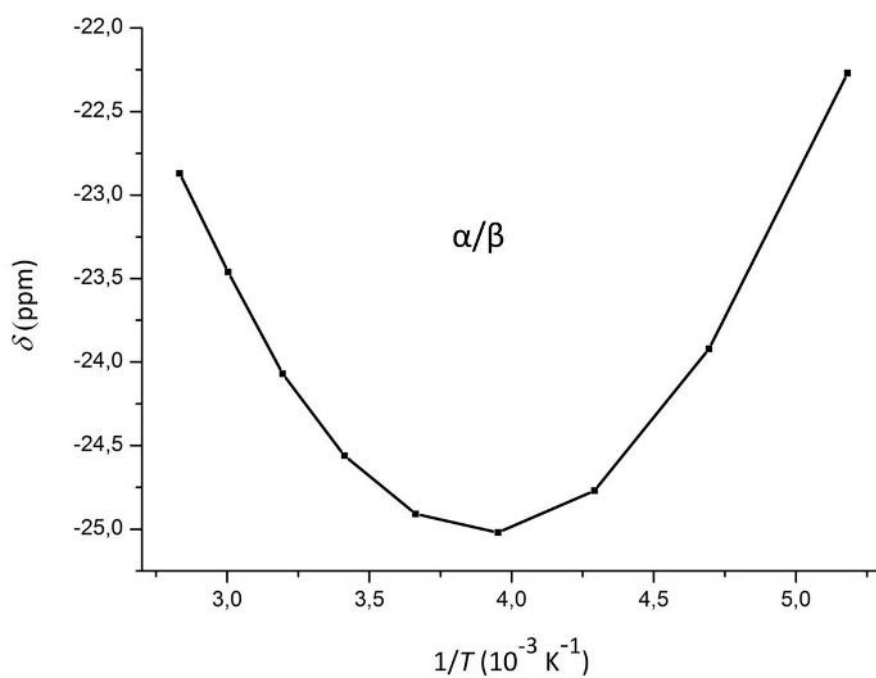
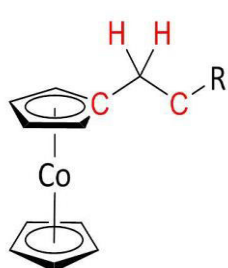


Figure 71: Temperature dependence of the protons signals at position α/β (complex **13**).



Köhler^[148] described this phenomenon in cobaltocenes with alkyl substituents for the in red indicated nuclei in figure 72. He postulated that the energy differences in the other positions of the Cp-rings in the different structures in equilibrium are too small to be detected.

Figure 72: Alkyl-cobaltocene complex. Red: Nuclei where the “Cobaltocene Anomaly” was found.

Rettig and Drago^[216] observed also a deviation from the linearity in VT-NMR measurements of 1,1'-dimethylcobaltocene, but this time the anomaly was found in the α position of the substituted Cp-ring and in the non-substituted Cp-ring. The proton at the β position did display a straight line in the δ -over- $1/T$ plot.

The behavior of complex **14** differs from that which was observed in complex **13**. In a first place, below 203 K it is possible to see that the signal which represents the hydrogen atoms at the α or β positions of the substituted Cp-rings splits in two (or even more) signals (Figure 73). Altmannshoffer *et al.*^[150] observed also the splitting of the signal regarding to the proton in β position of the substituted Cp-ring in 1,1'-dicyanocobaltocene; however, not in solution but in the solid state. Although the origin of the splitting could not be explained, they attributed it to intermolecular interactions.

Contrary to the complex **13**, in the δ -over- $1/T$ plot (Figure 74) two different signals established deviation from the linearity: the protons at the α and β positions of the substituted Cp-rings. One of those signals shows also the splitting at low temperatures and both new signals illustrate the mentioned anomaly (Figure 75). On the other hand, the protons at the other position, α or β , obey the Curie Law only above 223 K. Below this temperature a deviation from the linearity can be observed.

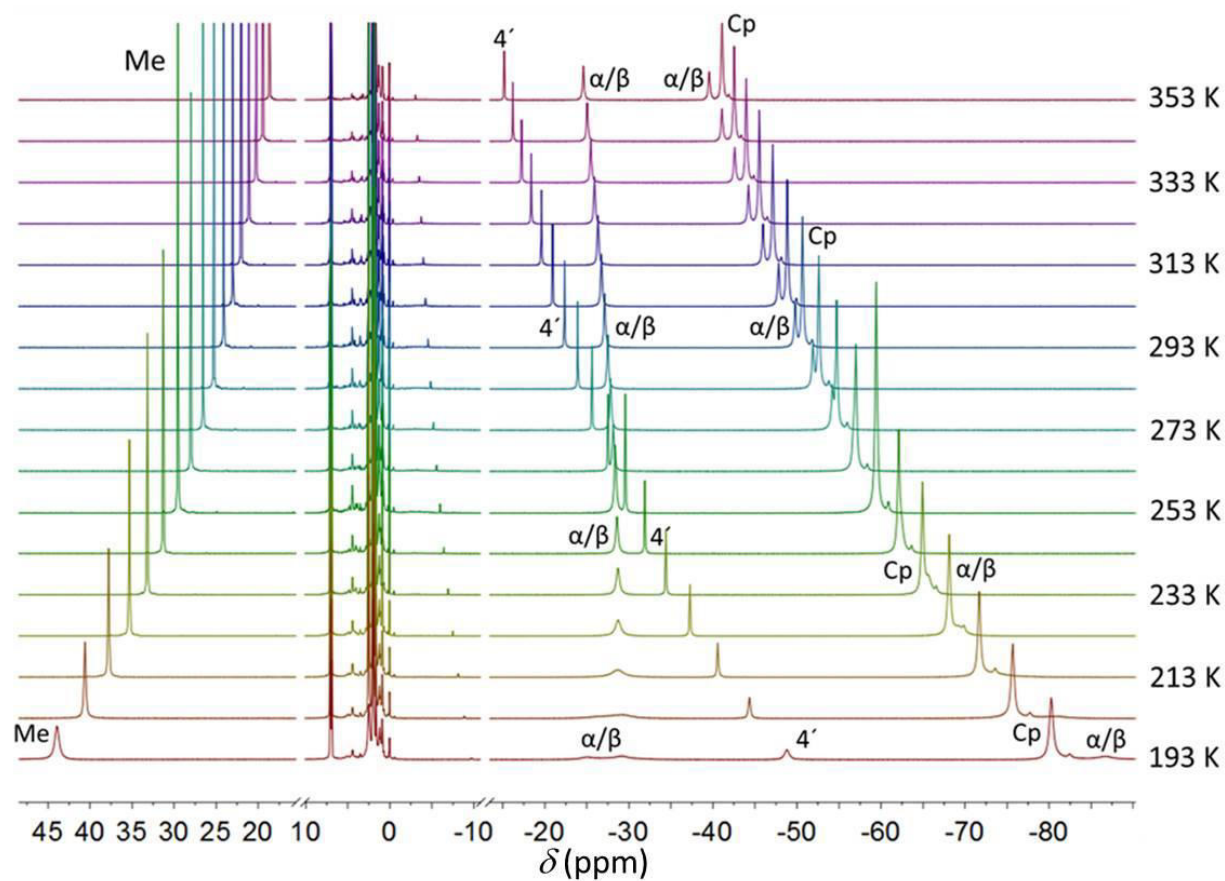


Figure 73: VT-¹H-NMR of the cobalt(II) complex **14** in toluene-d₈.

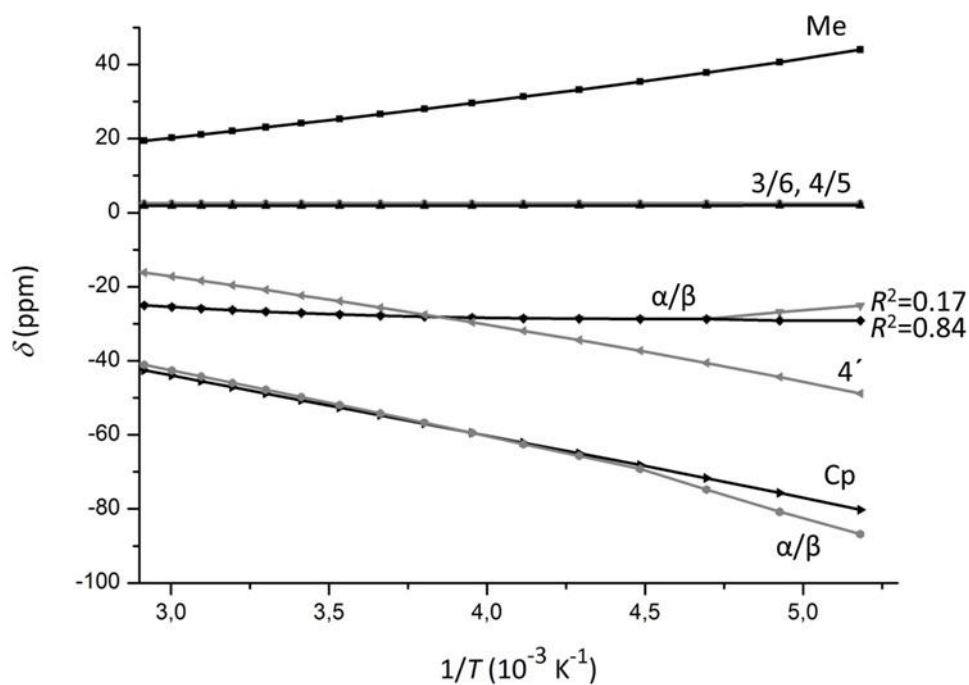


Figure 74: Temperature dependence of the proton signals (complex **14**). When no indicated $R^2 \sim 1$.

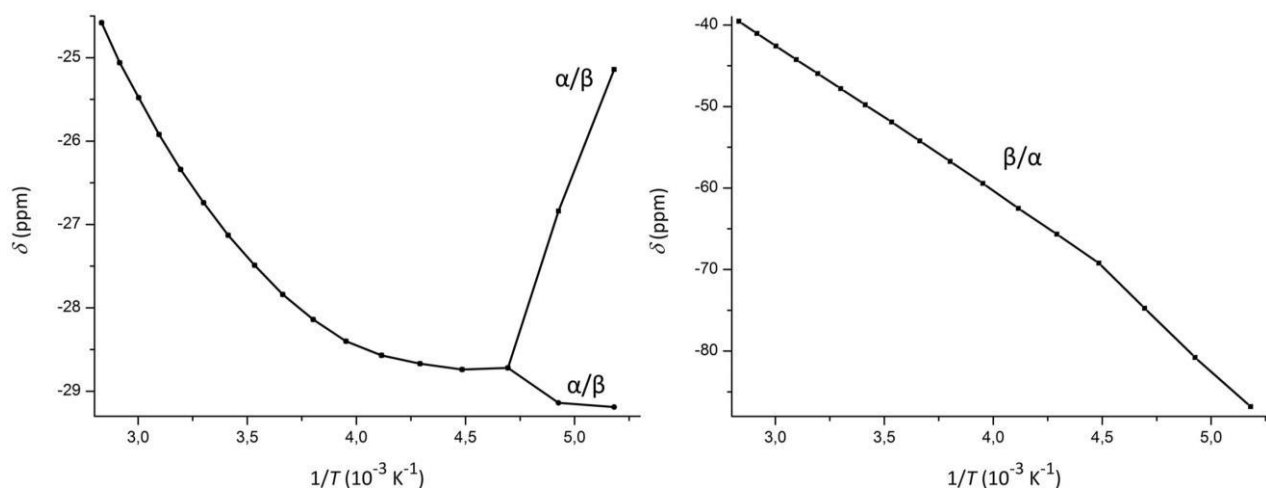


Figure 75: Temperature dependence of the proton signals at positions α and β (complex **14**).

4.2.2. NMR-spectroscopic experiments of the ferrocenium-complex **19**

In section 4.1.2.2 the ^1H -NMR spectrum of the complex **19** was shown (Figure 60) and described. By comparing the chemical shifts of the hydrogen atoms of the Cp-ligands in the cobaltocene (**13**, **14**) and the ferrocenium (**19**) complexes, a distinct difference between both metallocene radicals becomes obvious (Table 7). In the cobaltocene complexes the signals regarding to the substituted and non-substituted Cp-ligands appeared high field, indicating a negative spin density. However, in the case of the ferrocenium complex, the same signals are found down field, which is indicative for a positive spin density for these hydrogen atoms. The reason for it is that in sandwich complexes with less than six d electrons, metal-ligand bond polarization dominates.^[217] A successive polarization step of the C-H bonds explains the observed positive spin density for the hydrogen atoms (Table 7).

Table 7: ^1H -NMR signal shifts for complexes **13**, **14** and **19** (400 MHz).

δ_{293}^{exp} (ppm)	α/β (1)	α/β (2)	Cp
13 ^{a)}	-24.60	-49.99	-50.38
14 ^{a)}	-26.93	-48.74	-49.70
19 ^{b)}	40.57	40.57	28.55

a) Toluene- d_8 , b) Dichlormethane- d_2

4.3. Molecular Structures

The molecular structures of the molecular switch derivatives in the crystalline phase were analysed by means of X-ray structure determination. They offer significant information, not only about the structure itself, but also about the switching reaction. It allows us to know in which of the both possible conformations each molecular switch is found. Since only the antiparallel conformation is able to undergo the photocyclization reaction,^[70] it is possible to predict whether a certain compound will be able to behave as a molecular switch in the solid state.

The distance between the methylated carbon atoms is a determining factor for the switching reaction, especially in the crystalline state. To be able to undergo such cyclization reaction it is not enough to have the appropriate conformation (antiparallel), but the afore mentioned distance needs to be shorter than 420 pm.^[95] In solution a dynamic equilibrium exists between both conformations and this distance, which is so important in the crystal state, changes continuously.

In this work, the molecular structure of the organic cyclohexene-derivative **6** was obtained, making the comparison between 1,2-diarylethene-derivatives with a cyclopentene and with a cyclohexene connecting both thiophene rings possible. In addition, the molecular structures of the Co(I)- (**9,10**), Co(III)- (**11,12**) and Fe(II)- (**13,14**) complexes were also investigated. These molecular structures are an important tool to achieve one of the targets of this project, the comparison of the switching properties of the classical cyclopentene- with the cyclohexene-backbone.

Torben Steenbock, from the research group of Prof. Dr. Herrmann (University of Hamburg), carried out some theoretical calculations. Structure optimizations were performed and compared with the experimental results.

4.3.1. Molecular crystal structures of the organic molecular switches

The molecular structure of 1,2-bis(5-chloro-2-methylthien-3-yl)cyclopentene (**1**) was published in 2006 by Wissler *et al.*^[218] As it was not possible to obtain crystals with the quality required to X-ray analysis of the analogous 1,2-bis(5-chloro-2-methylthien-3-yl)cyclohexene (**5**), the iodo-derivative **6** was used instead for the comparison.

The molecular switch **1** crystallizes only in the antiparallel conformation, while for the cyclohexene-derivative **6** both conformers were found in a single crystal (Figure 76), which is unusual for this type of complexes. One molecule in the antiparallel conformation (AP) and half a molecule in the parallel conformation (P) were found in the formula unit, therefore the parallel conformer represents one third of the crystal packing (Figure 76, P). The ratio of both conformers in solution depends on the substituents at the 5- and 5'-positions of the thiophene rings. In this case, since iodine is a relative non-steric demanding substituent and it does not have an influence in the conformation, this ratio is probably 1:1. ^[84]

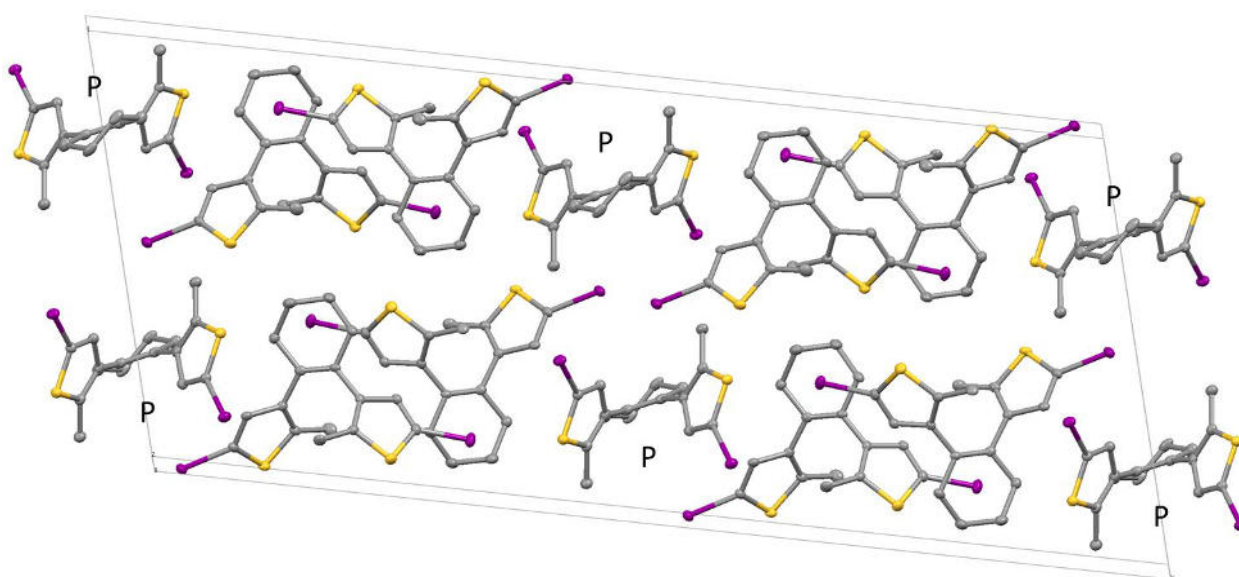


Figure 76: Crystal packing of **6**. (P = parallel conformer).

In the antiparallel conformation (AP) (Figure 77, left) the distance between the methylated carbon atoms is 345.79(53) pm, about 160 pm shorter than the corresponding distance in the parallel conformation (P) (508.32(49) pm; Figure 77, right). This extreme difference between both configurations helps us to understand why the parallel conformation is not able to undergo the photocyclization. The distance between the iodine atoms is with 330 ppm dramatically shorter in the parallel conformation than in the antiparallel conformation. Finally, the torsion angles (C12-C11-C21-C22; Figure 77, left) are 84.81(29)° for the so-called antiparallel conformer and 12.37(40)° (C42-C41-C51-C54, Figure 77, right) for the analogous parallel conformer.

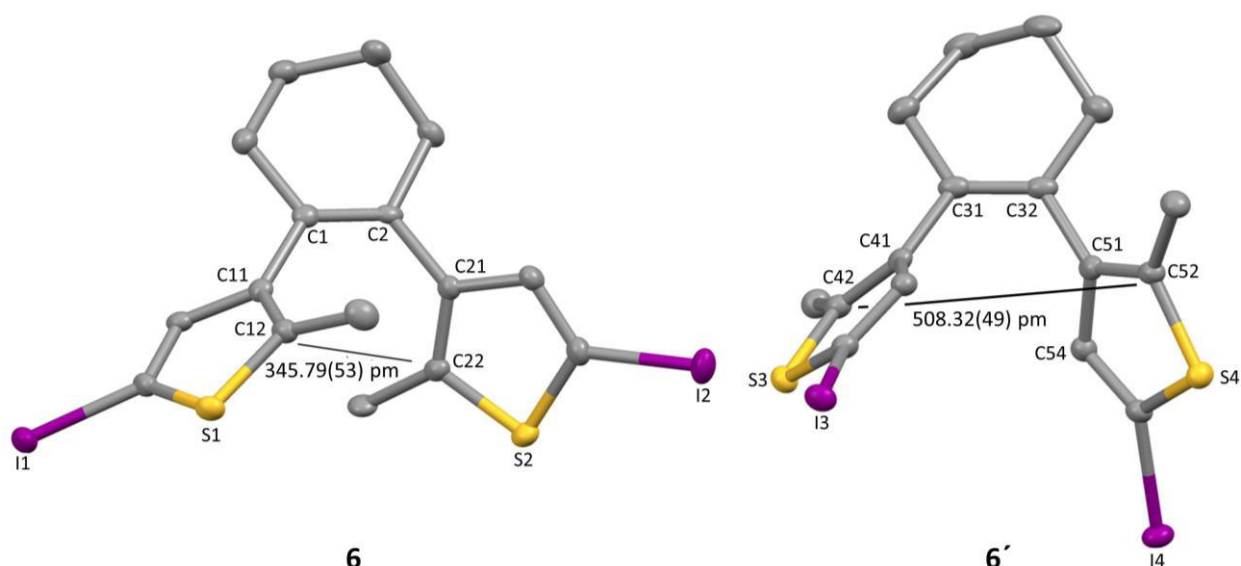


Figure 77: Molecular structures from X-ray structure determination of **6**, displaying two different conformers in the unit cell. Left: (**6**) antiparallel conformation (C1-C2: 133.5(6) pm; I1-I2: 1062.42(5) pm; torsion angle (C12-C11-C21-C22): 84.81(29) °) Right: (**6'**) parallel conformation (C31-C32: 133.8(8) pm; I3-I4: 731.10(5) pm; torsion angle (C42-C41-C51-C54): 12.37(40) ° (C2/c, Z = 6, R = 3.56 %). The hydrogen atoms were omitted for clarity.

Comparing the antiparallel conformers of the cyclopentene- (**1**) and cyclohexene-(**6**) derivatives, the distance between the methylated carbon atoms is very similar, being only about 5 pm longer in the case of **1** and in both cases shorter than 420 pm. Therefore, according to Kobatake *et al.* ^[95] **1** and **6** should be able to undergo the switching reaction in the crystal state. The torsion angle is 12 ° shorter in **1** (Tables 8 and 9).

Another difference between both structures lies in the central cycloalkene: while the cyclopentene ring in **1** presents an almost planar envelope conformation, the cyclohexene ring in **6** shows a half-chair conformation.

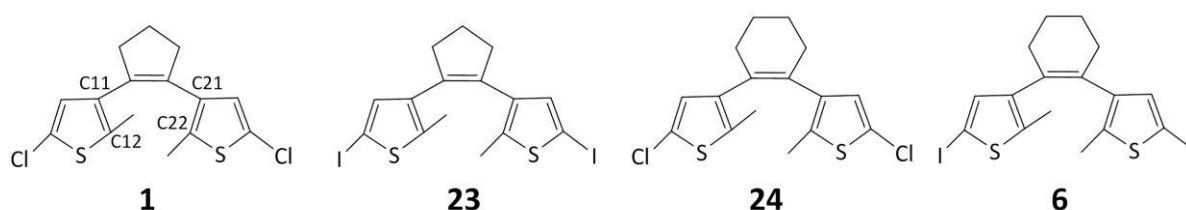
Torben Steenbock carried out structure optimizations with BP86 and B3LYP with and without including the second generation of the dispersion correction of Grimme ^[219] to see if dispersion plays a role, especially in the open form isomer. ^[220]

Table 8: Distances between the methylated carbon atoms (C12 – C22, Figure 78) using different density functionals (D=dispersion correction of Grimme). Basis set: def-TZVP.

C12 - C22				
Method	1	23	24	6 (AP)
Exp.	350.9(2)	--	--	345.79(53)
BP86	362.9	362.9	363.0	362.8
BP86-D	336.5	336.3	325.3	324.9
B3LYP	367.4	367.1	367.4	373.1
B3LYP-D	340.9	339.9	331.2	331.3

Table 9: Torsion angle (C12-C11-C21-C22, Figure 78) using different density functionals (D=dispersion correction of Grimme). Basis set: def-TZVP.

Torsion angles (C12-C11-C21-C22)				
Method	1	23	24	6
Exp.	77.5(1)	--	--	84.81(29)
BP86	74.3	80.7	92.5	92.2
BP86-D	73.6	73.9	79.3	79.9
B3LYP	75.2	82.7	82.7	94.3
B3LYP-D	74.6	74.8	80.9	81.2

**Figure 78:** Molecular switch derivatives whose experimental and calculated molecular structures are shown in tables 8 and 9.

In tables 8 and 9 the results for experimental and optimized data, for not only the molecular switches **1** and **6**, but also for the cyclopentene-iodo derivative **23** and the cyclohexene-chloro derivative **24**, are shown. By comparing the experimental data with the optimized structures it can be observed that the BP86 and the B3LYP functional offered shorter C12 - C22 distances and torsional angles. When including Grimme's dispersion correction, the opposite happened. However, the B3LYP-D functional in both cases was in best agreement with the experimental data. The halogen substituents exert no influence in the interatomic distances and the torsional angles. For both substituents, dispersion-corrected functionals revealed shorter distances between the methylated carbon atoms for the cyclohexene- than for the cyclopentene- structures. Without this correction, the opposite was true. The torsional angles are always larger in the case of the cyclohexene- compounds.

4.3.2. Molecular crystal structures of the cobalt complexes 9-12

The red cobalt(I) complexes (**9**, **10**) crystallize in the monoclinic space groups Pc (**9**) and $P2_1/n$ (**10**). In both cases, the diarylethene units are bound in *exo*-position relative to the sandwich complexes, which was expected for these complexes. ^[193] The connecting sp^3 carbon atoms are not located in the same plane as the other four carbon atoms of the cyclopentadiene ring, and they present a tetrahedral geometry. The cobalt centers are bound to the other four sp^2 carbon atoms of the ring and η^5 to the carbon atoms of the unsubstituted cyclopentadienyl ring. The molecules are not planar and they contain a C_2 axis (Figures 79 and 80)

Complex **9** crystallizes in two different structures (**9** and **9'**) (Figure 79). Both present the antiparallel conformation but some little differences exist between them. The interatomic distance between the methylated carbon atoms is a bit shorter in **9**, while the torsional angle (C12-C11-C31-C32) is larger. Thus, while the cycloalkene ring is almost planar in complex **9**, in the complex **9'** is not, presenting the typical envelope conformation (Table 10). Finally, in both structures the sandwich complex moieties are pointing away from the switch, each one in a different direction.

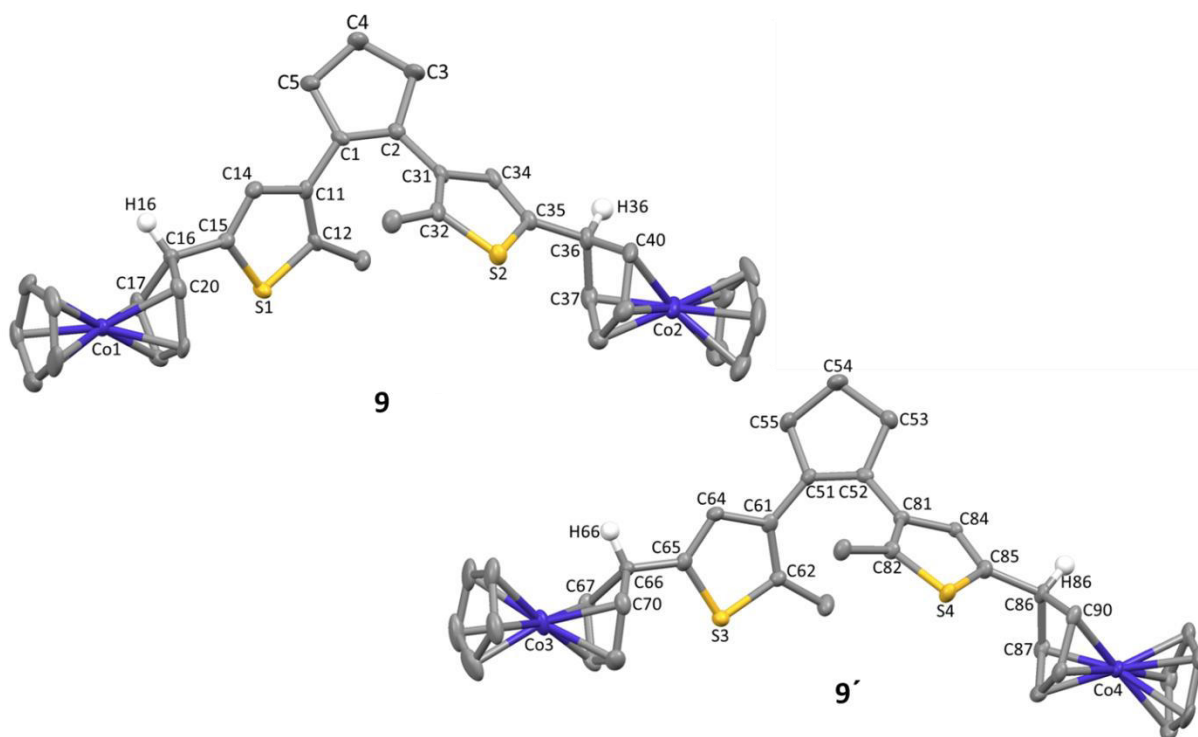


Figure 79: Molecular structures of complex **9** (Pc , $R = 3.86\%$, $Z = 4$). The hydrogen atoms and the diethylether molecules were omitted for clarity.

The crystalline structure of complex **10** presents an excess of electronic density in one of the cyclopentadiene rings which connects the cobalt center to the thiophene ring; it is possible to see a second ring (coordinated to Co2). However, as the molecule presents a C_2 symmetry axis, the data were collected from the other half of the molecule.

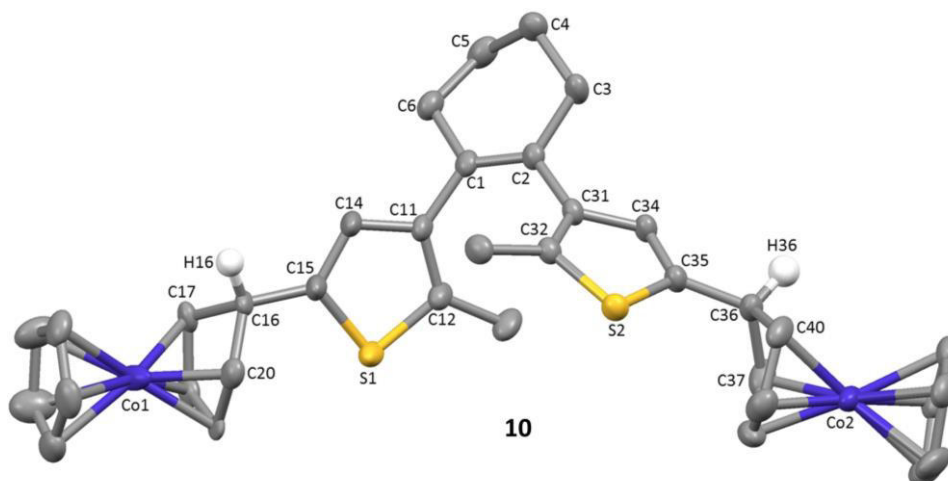


Figure 80: Molecular structure of **10**. ($P 2_1/n$, $R = 4.29\%$, $Z = 4$). The hydrogen atoms and the excess of electronic density were omitted for clarity.

4. Results and Discussion

The central cyclohexene ring presents a half chair conformation. The distance between the methylated carbon atoms is slightly shorter than in complex **9** (and **9'**) while the torsional angle (C12-C11-C31-C32) is larger (Figure 80).

Table 10: Selected distances (pm) and torsional angles (°) in complexes **9**, **9'** and **10**.

	9	9'	10
C1 – C2	132.97(7)		134.9(3)
C51 – C52		136.4(7)	
C12 – C32	344.94(63)		330.6(4)
C62 – C82		347.04(60)	
Co1 – Co2	1380.25(15)		1344.56(7)
Co2 – Co3		1396.89(15)	
Torsional angle C11 – C1 – C2 – C32	74.89(34)		76.65(21)
Torsional angle C62 – C81 – C82 – C62		71.94(32)	

The yellow crystals of the diamagnetic complexes **11** and **12** were also suitable for X-ray analysis (Figure 81). Complex **11** crystallizes in the monoclinic space group $P2_1/c$ and the complex **12** in the orthorhombic space group Fdd . The diarylethene units are directly bound to the cyclopentene rings, which are η^5 coordinated to the cobalt centers. The structures are not planar and display a C_2 -axis.

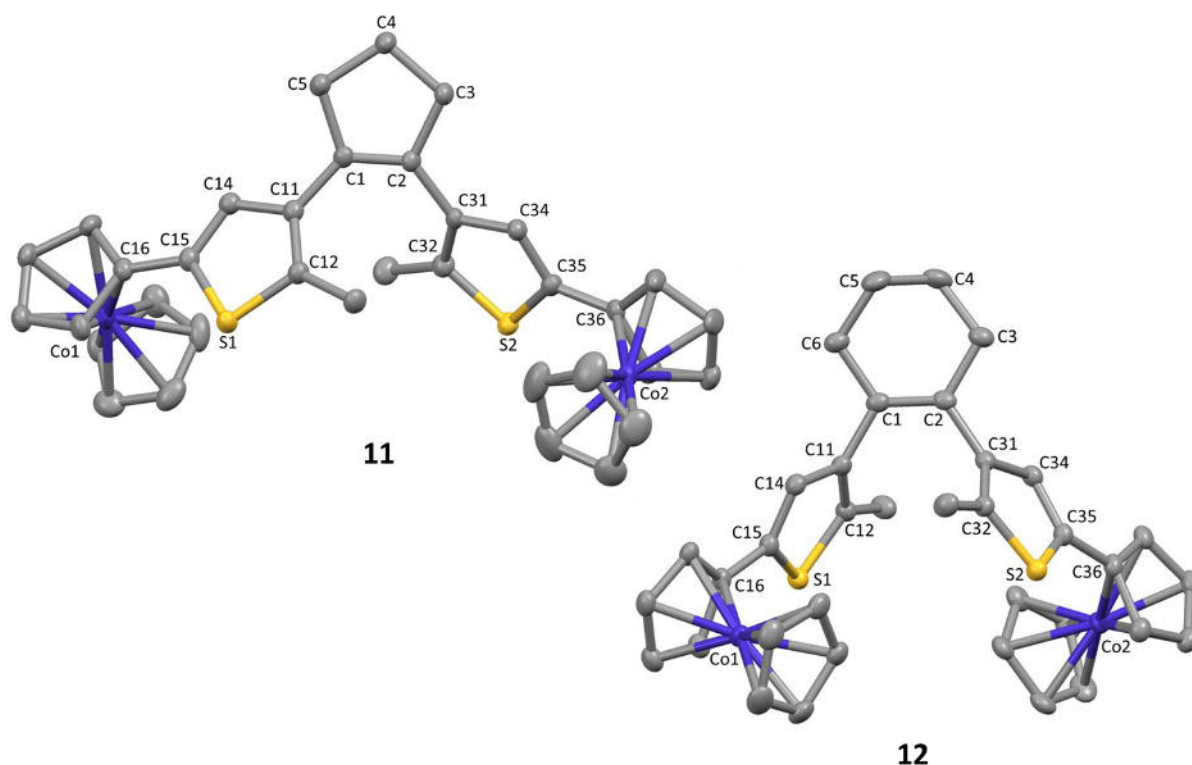


Figure 81: Molecular structures of the dicationic complexes **11** (left, $P2_1/c$, $R = 6.08\%$, $Z = 4$) and **12** (right, $Fdd2$, $R = 2.64\%$, $Z = 4$). Hydrogen atoms and counter ions were omitted for clarity.

The interatomic distance between the methylated carbon atoms is almost the same in both complexes (and similar to the same distance in complex **9**); however, the torsional angle in complex **11** is 20° smaller than in complex **12**. The cobaltocenium moieties are located in both structures towards the switch, in opposite directions respecting to the plane defined by C11-C1-C2-C31, one upwards and the other downwards. The distance between the cobalt centers is 1145.88(8) pm in complex **11**, but due to the big torsional angle, this distance is only 983.41(5) pm in complex **12** (Table 11).

The cyclopentene ring of complex **11** is almost planar (envelope configuration) while the cyclohexene ring of complex **12** presents a half chair conformation.

Table 11: Selected distances (pm) and torsional angles ($^\circ$) in complexes **11** and **12**.

	11	12
C1 – C2	134.3(5)	135.9(4)
C12 – C32	349.36(63)	349.25(31)
Co1 – Co2	1145.88(8)	983.41(5)
Torsional angle (C12 – C11 – C31 – C32)	74.977(323)	94.743(170)

4.3.3. Molecular crystal structures of the iron complexes 17-19

The compounds **17** and **18** were crystallized from dichloromethane solutions and the obtained orange crystals had sufficient quality for X-ray structure determination (Figure 82). Complex **17** crystallizes in the orthorhombic space group $P2_12_12$ and the complex **18** in the monoclinic space group $P2_1/c$. The non-bonding distance between the methylated carbon atoms is 361.48(43) pm in the cyclopentene-complex **17**, more than 17 pm longer than the corresponding distance in complex **18** (344.421(26) pm). The torsion angle in complex **17** is 81.209(269)°, which is almost identical to the torsion angle in the complex **18** (82.844(153)°) (Table 12).

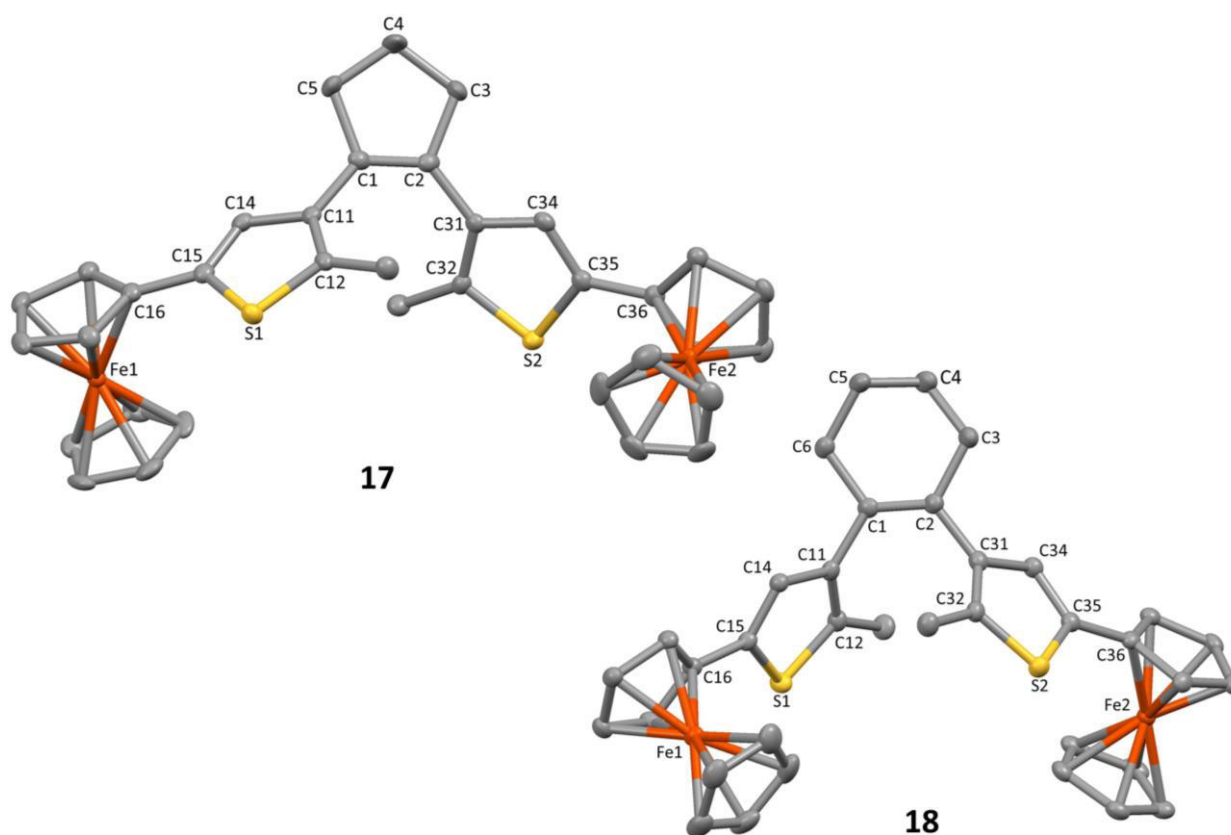


Figure 82: Molecular structures of the neutral complexes **17** (left, $P2_12_12$, $R = 4.32\%$, $Z = 2$) and **18** (right, $P2_1/c$, $R = 3.13\%$, $Z = 1$). The hydrogen atoms were omitted for clarity.

These torsional angles are larger than in the former cobalt complexes, except for the complex **12**, which shows the largest torsion angle of all the synthesized complexes. The cyclohexene ring in complex **18** presents a half chair conformation while the cyclopentene in complex **17** is almost planar. Nevertheless, the size of the corresponding ellipsoid (Figures 82 and 83) indicates that it possibly presents an envelope configuration, but what we see is the

middle point of two different conformations, in which C4 is displaced of the plane in different directions.

In figure 83 both iron complexes **17** and **18** are represented from a new perspective. The ferrocene moieties are pointing in different directions respecting to the plane defined by C11-C1-C2-C31 and they display a 90 ° angle respecting with each other.

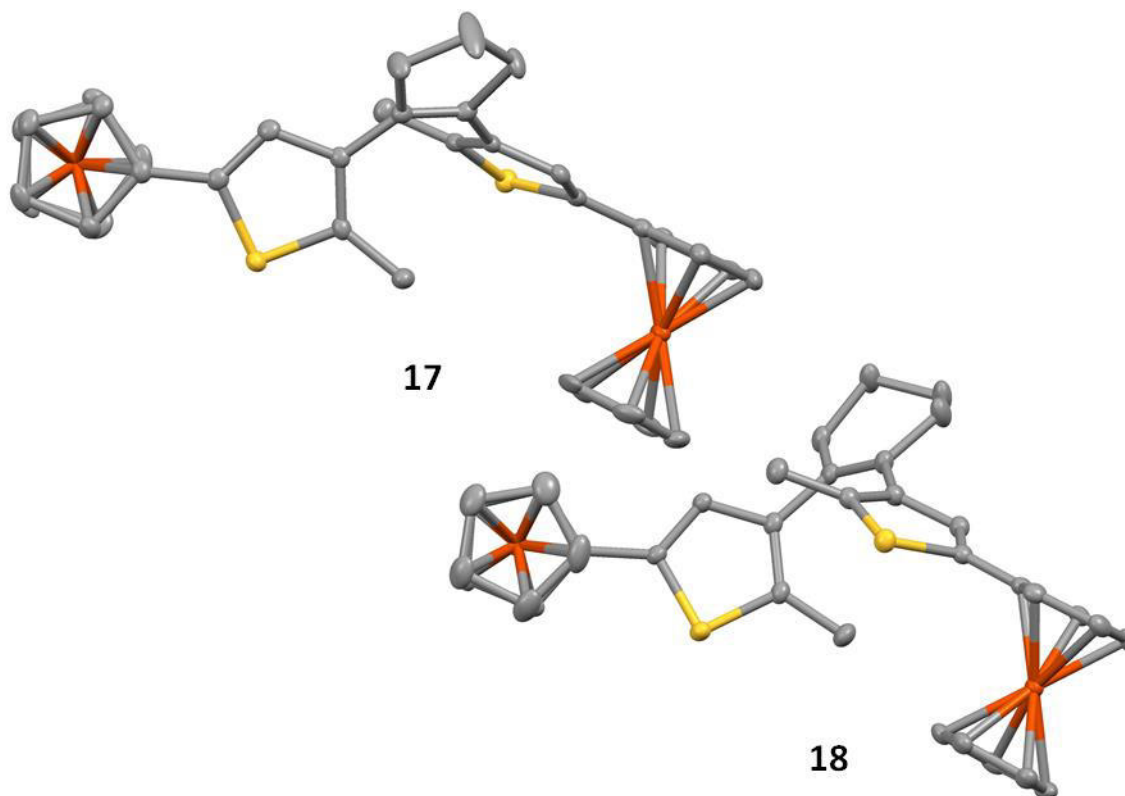


Figure 83: Molecular structures of complexes **17** and **18**. The hydrogen atoms were omitted for clarity.

Some structure optimizations with BP86 were carried out. Two different structures, depending on the position of the ferrocene moieties, were proposed: the “in” and “out” isomers (Figure 84). In the “out” isomer, the metallocene units are pointing away the molecular switch unit. In the “in” isomer the ferrocene moieties are pointing towards the molecular switch core but in opposite directions respecting to the plane defined by C11-C1-C-C31, one upwards and the other downwards.

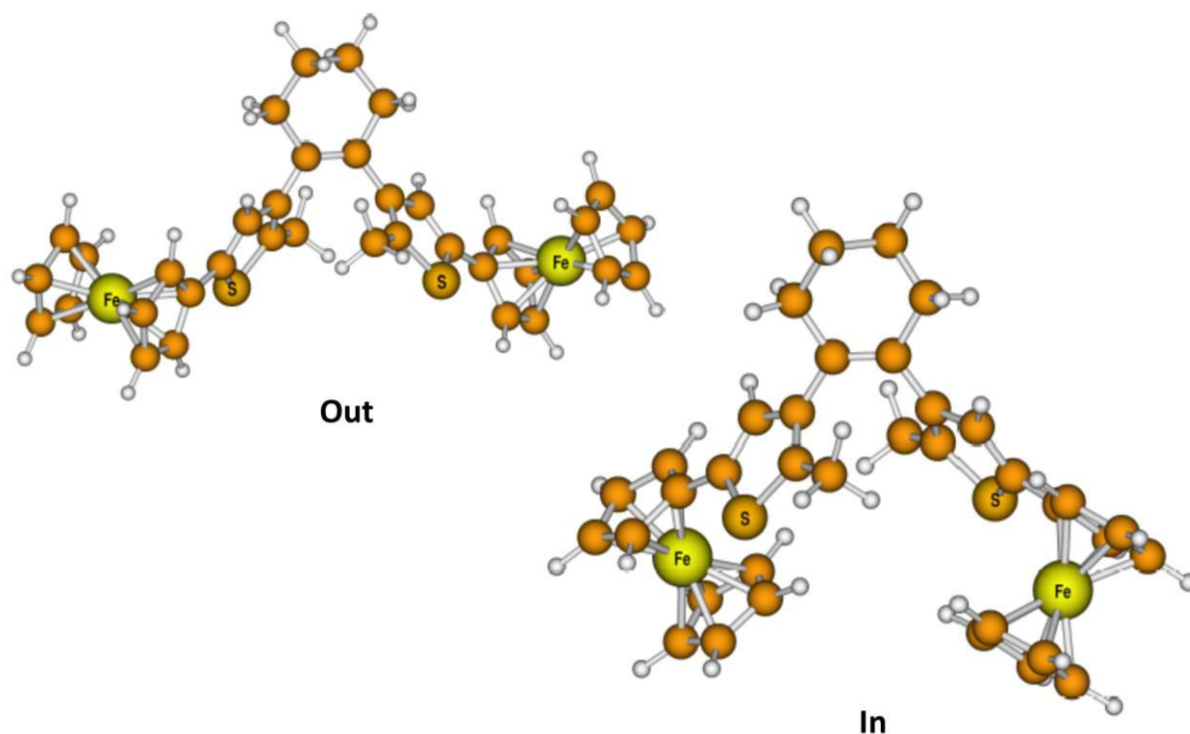


Figure 84: “In” and “out” isomers of complex **18**.

Table 12: Selected distances (pm) and torsion angles (°) in complexes **17** and **18**. The structure optimizations were carried out with the BP86 functional. Basis set: def-TZVP.

17				
Method	C1 – C2	C12 – C32	Fe1-Fe2	Torsion angle (C12 – C11 – C31 – C32)
Exp.	134.62(43)	361.48(43)	1165.42(6)	81.209(269)
BP86 (out)	136.20	362.82	1356.23	81.881
BP86 (in)	136.35	360.59	1199.83	77.112
18				
Exp.	134.02(26)	344.21(26)	1073.81(4)	82.844(153)
BP86 (out)	135.99	367.39	1286.07	96.209
BP86 (in)	135.91	365.88	1039.47	94.748

In table 12 the experimental and the theoretical data are compared. Although the “in” isomer coincides better to the obtained structures, for complex **17** the torsional angle agrees

more with the calculated for the “out” isomer. In the case of complex **18**, the calculated torsional angles for both isomers (“in” and “out”) differ in more than 10 ° with the reality.

Finally, also the paramagnetic complex **19** was investigated by means of X-ray analysis (Figure 85). The crystals were obtained by slowly diffusion of *n*-pentane in a concentrated DCM solution. Unfortunately, the quality of the crystals was not not as good as desired ($R = 17.5\%$) and the bond distances and the angles cannot be discussed. However, the obtained molecular structure offers some important information. The molecular switch is found in the antiparallel conformer, so it is possible that the switching reaction takes place even in the solid state.

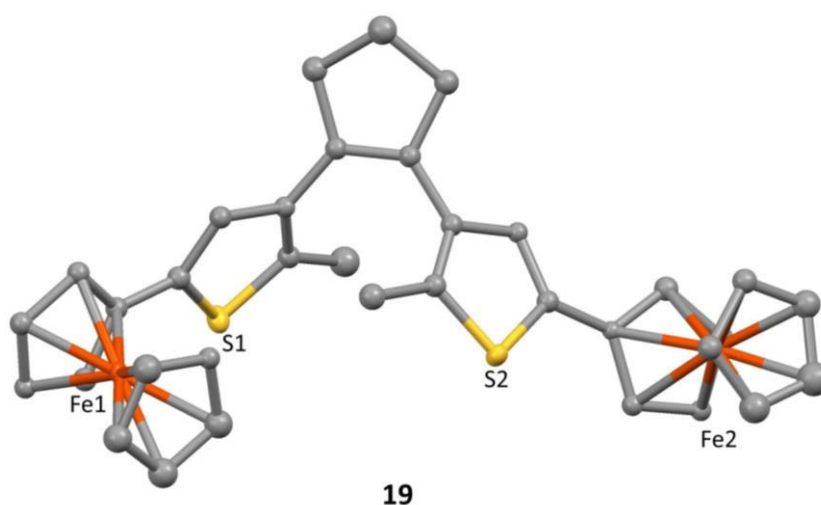


Figure 85: Molecular structure of the dicationic complex **19** ($P-1$, $R = 17.15\%$, $Z = 1$). Hydrogen atoms and counter ions were omitted for clarity.

4.3.4. Conclusions (I)

1,2-Bis(5-iodo-2-methylthien-3-yl)cyclohexene (**6**) crystallizes in two different conformations (parallel and antiparallel), offering a particular crystal packing not reported yet in the literature. The antiparallel conformer structure fulfills the structural prerequisite established by Kobatake *et al.* [95] to undergo the photocyclization in the solid state. The parallel conformer is not photoactive. [70]

All investigated metal complexes were found only in the antiparallel conformation and, except for the ferrocenium complex **19** (the obtained interatomic distance is not reliable due to the poor quality of the crystals), the distance between the methylated carbon atoms was shorter than 420 nm. Therefore, these metallocene complexes should be able to undergo the switching reaction even in the crystal state. [95]

4.4. Redox behaviour and irradiation experiments monitored *via* CV

The redox behaviour of the synthesized metal complexes in the open state of the molecular switch was investigated *via* cyclic voltammetry (CV), using a Potentiostat PGSTAT 101 (Metrohm) and three platinum electrodes. As reference ferrocene (F_cH/F_cH⁺) was employed. In addition, the dissolved complexes were irradiated with UV light and the switching reaction was monitored using the same technique. Other analytical methods, as UV-vis and NMR-spectroscopy were employed to follow these reactions, but these experiments are described in section 4.5.2.

4.4.1. Redox behavior of the cobaltocenium complexes **11** and **12**

The redox behavior of the cobaltocenium complexes, cyclopentene-derivative **11** and cyclohexene-derivative **12**, was investigated. Complex **11**, dissolved in acetonitrile, displays a single reversible (Co(III)/Co(II)) at -1.27 V and a quasireversible (Co(II)/Co(I)) at -2.19 V redox waves. The analogous complex **12**, solved in THF, displays also two redox waves, but in this case, both are reversible processes (Table 13, Figure 86). Probably the difference lies on the solvent. According to Stojanovic *et al.*,^[221] the Co(II)/Co(I) redox reaction depends deeply on its nature. Two different solvents were employed for these measurements due to experimental requirements.

Unsubstituted cobaltocenium-cation shows two separate and reversible redox processes,^[143,221] therefore the cobaltocenium moieties of complexes **11** and **12** behave as single and independent units and there is no indication for an electronic coupling between the cobalt centers.

Although the measurements were carried out in different organic solvents, what could make the comparison doubtful, the data presented in table 13 shows that both complexes have (in the open state of the molecular switch) a similar redox behavior, which is comparable with cobaltocenium itself.

Table 13: Cyclic voltammetric data (scan rate = 100 mV s⁻¹) at room temperature (vs. F_cH/F_cH⁺).

	$E_{1/2}(\text{Co(III)/Co(II)})$ (V)	$E_{1/2}(\text{Co(II)/Co(I)})$ (V)	Solvent
[Cp ₂ Co] ⁺	-1.35	-2.30	Acetonitrile
11	-1.27	-2.17	Acetonitrile
12	-1.18	-2.17	THF

$$E_{1/2} = \frac{1}{2}(E_{\text{pf}} + E_{\text{pr}})$$

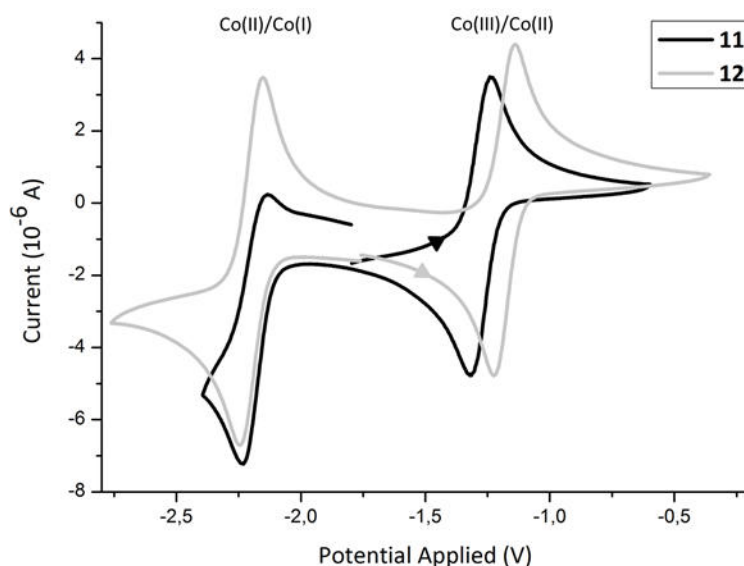


Figure 86: Cyclic voltammogram of complex **11** (black) solved in acetonitrile and complex **12** (grey) solved in THF vs. FcH/FcH⁺. [Bu₄N][PF₆] was used as electrolyte. Each cobalt center is independent of each other.

4.4.1.1. Irradiation experiments monitored by means of CV with complex **12**

The cyclohexene-complex **12** was irradiated with UV light employing THF as solvent and a Rayonet lamp (366 nm, 16 W, r.t.). The redox behaviour was investigated before and after the UV light irradiation and the results were compared (Figure 87, Table 14).

Table 14: Cyclic voltammetric data (**12**), before and after the irradiation with UV light in THF. (Scan rate = 200 mV s⁻¹)

	Before Irradiation	After Irradiation
$E_{1/2}(\text{Co(III)/Co(II)})$ (V)	-1.19	-1.28
$(\Delta E_p)_{\text{Co(III)/Co(II)}}$ (mV)	88	83
$(i_{pr}/i_{pf})_{\text{Co(III)/Co(II)}}$	0.97	0.97
$E_{1/2}(\text{Co(II)/Co(I)})$ (V)	-2.16	-2.31
$(\Delta E_p)_{\text{Co(II)/Co(I)}}$ (mV)	90	90
$(i_{pr}/i_{pf})_{\text{Co(II)/Co(I)}}$	1.10	1.14

(vs. FcH/FcH⁺; $(\Delta E_p)_{\text{Fe(III)/Fe(II)}} = 120$ mV, $(i_{pr}/i_{pf})_{\text{Fe(III)/Fe(II)}} = 1,10$)

When comparing the redox behavior before and after the UV light irradiation, the first thing which can be observed is that the redox potentials have slightly changed (Table 14). These potential values should be carefully interpreted. Not only the standard ferrocene was added after the irradiation experiments, but during the irradiation processes the measurement cell was opened several times and an indefinite volume of the solvent was evaporated. If this is added to the fact that the temperature of the solution did not remain constant, it is

impossible to assign small alterations in the redox potentials to the switching reaction. Therefore, in the following, the small variations in the potential electrode will not be discussed.

The peak-to-peak separation and the i_{pr}/i_{pf} ratio are criteria to identify the nature of a redox process in a cyclic voltammetry experiment. In ideal case and at 25 °C, the peak-to-peak separation for a reversible process is mean to be $59/n$ mV, being n the number of exchanged electrons.^[143] However, the peak-to-peak separation of the one-electron redox process of the standard ferrocene is 120 mV. This discrepancy is attributable to uncompensated solution resistance.^[221] Therefore, it is reasonable to assume that the peak-to-peak separation of the redox waves of the cobalt centers will also differ from the ideal case.

Before the UV light irradiation, the peak-to-peak separation (200 mV s^{-1}) was 88 mV for the Co(III)/Co(II) process and 90 mV for the Co(II)/Co(I) process. Even considering the expected peak-to-peak separation $120/n$ mV instead of the literature value $59/n$ mV (for the investigated complex $n = 2$, one electron for each cobalt center), the observed peak-to-peak separations are still too big. An explanation could be to consider the idea that a minimal electronic communication between both metal centers exists, but it is too small to offer two separate one-electron redox waves. It would be the case of a multiple electron transfer mechanism (EE-mechanism) with a $\Delta E_p < 150$ mV.^[222] Therefore, the observed redox waves present a shape which does not correspond to the typical one-electron process, so when using the maxima to determinate the peak-to-peak separation, the obtained value is not the real one. Levanda *et al.*^[223] already observed this behaviour in biferrocenyl-complexes. Only a redox wave was shown but the peak-to-peak separation was 140 mV (instead of 30 mV; $n = 2$). This phenomenon is known as “superimposed one-electron waves”.^[224]

After the UV irradiation the peak-to-peak separation values were similar to the observed ones before the irradiation: 83 mV for the Co(III)/Co(II) process and 90 mV for the Co(II)/Co(I) process.

Although in case of reversible processes the peak-to-peak separation would not vary with the scan rate,^[143] in the performed measurements, it does. The values increase with the scan rate by up to 25 %. Although it could be an indication of a quasireversible process, in the measurements performed by Stojanovic and Bond,^[221] who studied the redox behavior of cobaltocenium-cation in different solvents, the peak-to-peak separation varies also with the scan rate. Furthermore, the peak-to-peak separation values for the standard ferrocene

differ also up to 40 %. Therefore, this phenomenon will be attributed, at least partly, to experimental problems.

Finally, the i_{pr}/i_{pf} ratios before and after the irradiation with UV light were also compared (Table 14). Theoretically, for reversible processes this ratio should be equal to one. In this measurement, the i_{pr}/i_{pf} for ferrocene was 1,11. The value of this quotient remains constant with the scan rate.

Before the irradiation the $(i_{pr}/i_{pf})_{Co(III)/Co(II)}$ was 0,97 and $(i_{pr}/i_{pf})_{Co(II)/Co(I)}$ was 1,10. Both values are in the range for reversible processes considering the experimental deviation. After the irradiation, these values did practically not change: $(i_{pr}/i_{pf})_{Co(III)/Co(II)}$ was 0,97 and $(i_{pr}/i_{pf})_{Co(II)/Co(I)}$ was 1,14.

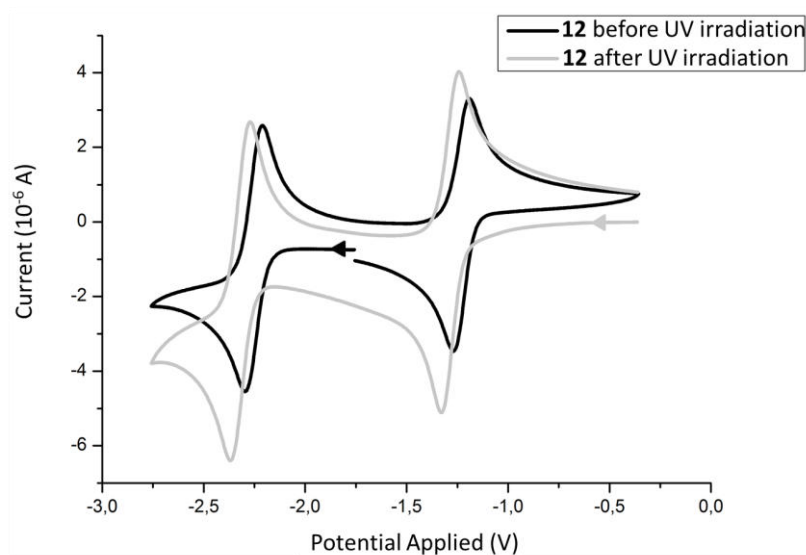


Figure 87: Cyclic voltammogram of complex **12** before (black) and after (grey) the irradiation with UV light vs. FcH/FcH^+ . $[Bu_4N][PF_6]$ was used as electrolyte and THF as solvent.

Concluding, the redox behavior before and after the irradiation with UV light is very similar. Little differences are observed, but they could not be directly attributed to the formation of the closed isomer of the molecular switch. The electronic communication between both metal centers when the molecular switch is open is insignificant; and after the irradiation, there is not evidence from the formation of the closed isomer. The increase in the absolute value of the current after the irradiation is due to the solvent evaporation (and consequent increase of the concentration) when the measurement cell was opened.

4.4.1.2. Irradiation experiments monitored by means of CV with complex 11

In a first attempt, in order to investigate the switching reaction of the cyclopentene-Co(III)-complex **11**, it was solved in acetonitrile and cyclic voltammetric measurements were performed (Table 15). Afterwards, the solution was irradiated with a mercury medium pressure lamp TQ-150 (366 nm, 25 W, 0 °C) during 4 h and 27 h with a TL-lamp (350 nm, 8 W, r.t.). Finally, the yellow solution had turned into a light brown suspension. Cyclic voltammetric measurements were carried out again (Table 15).

This time, ferrocene was added at the beginning of the experiment and not after the light irradiation, as in the case of the irradiation experiments carried out with complex **12**. The reason was to avoid carrying the measurements in different systems (with and without ferrocene) and to minimize the error caused by the evaporation of the solvent by opening the measurement cell. Before the irradiation with UV light, the peak-to-peak separation for the reference ferrocene/ferrocenium redox reaction was 68 mV, but later on, the separation was 78 mV. Taking the standard deviation of the measurements (0.05 V), 10 mV is not a significant value.

Table 15: Cyclic voltammetric data in acetonitrile (**11**), before and after the irradiation with UV light. (Scan rate = 200 mV s⁻¹).

	Before Irradiation	After Irradiation
$E_{1/2}(\text{Co(III)/Co(II)})$ (V)	-1.29	-1.37
$(\Delta E_p)_{\text{Co(III)/Co(II)}}$ (mV)	76	148
$(i_{pr}/i_{pf})_{\text{Co(III)/Co(II)}}$	1.04	1.11
$E_{1/2}(\text{Co(II)/Co(I)})$ (V)	-2.21	-2.41
$(\Delta E_p)_{\text{Co(II)/Co(I)}}$ (mV)	98	-
$(i_{pr}/i_{pf})_{\text{Co(II)/Co(I)}}$	0.92	-

(vs. FcH/FcH⁺; before the irradiation: $(\Delta E_p)_{\text{Fe(III)/Fe(II)}} = 68$ mV; $(i_{pr}/i_{pf})_{\text{Fe(III)/Fe(II)}} = 1,00$; after the irradiation: $(\Delta E_p)_{\text{Fe(III)/Fe(II)}} = 78$ mV; $(i_{pr}/i_{pf})_{\text{Fe(III)/Fe(II)}} = 1,00$).

Before the irradiation with UV light, the complex presented two two-electron redox processes. The first represents a reversible process, and the second, a quasireversible one, as the i_{pr}/i_{pf} ratios show (Table 15). After the irradiation with UV light, the redox-wave for the quasireversible redox process was almost not visible (Figure 88). Only at high scan rates it was possible to identify it. As the reversible process was still visible, it could not be concluded that the complex fully decomposed during the irradiation with UV light. Probably,

the diffusion rate was influenced by the existence of the suspended solid observed after the irradiation and it partially impeded the quasireversible process at the electrode surface.

Before the UV irradiation the peak-to-peak separation in the reversible process was 76 mV, larger than expected when considering the theoretical value ($n = 2$; 30 mV); but not as big as for complex **12**. After the irradiation, the same ΔE_p was 148 mV. This value depends dramatically on the scan rate, although it does not lead a determinate tendency. However, this dramatic change in the peak-to-peak separation could indicate an alteration in the electronic communication between the metal centers, perhaps induced by the appearance of the closed isomer of the molecular switch. This evolution of the reversible redox wave was not comparable to the same phenomenon in complex **12**.

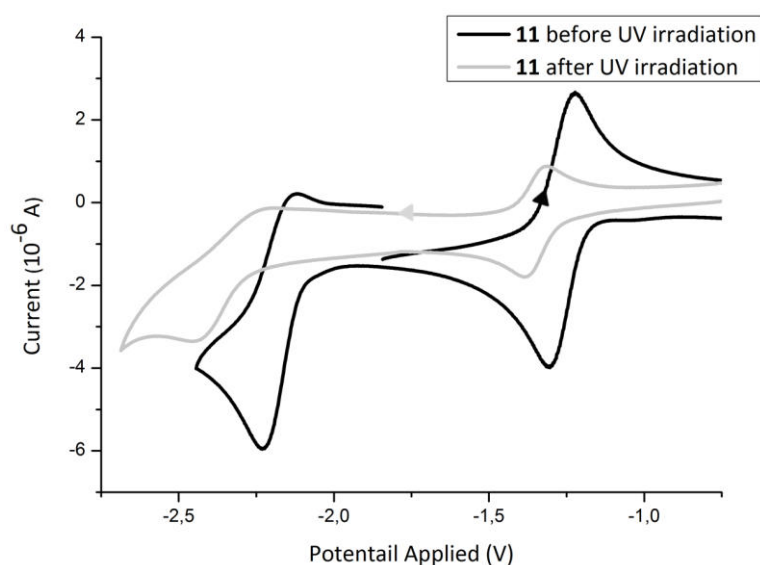


Figure 88: Cyclic voltammogram of complex **11** before (black) and after (grey) the irradiation with UV light (4 h with a mercury lamp (366 nm, 25 W, 0 °C) and 27 h with a TL-lamp (366 nm, 8 W, r.t.)) vs. FcH/FcH⁺. [Bu₄N][PF₆] was used as electrolyte and acetonitrile as solvent.

In order to avoid the partial decomposition of the complex and eventual errors in the measurements, the same experiment was carried out varying the irradiation times. This time, the sample was irradiated 2 h 45 min with a mercury medium pressure lamp TQ-150 (366 nm, 25 W, 0 °C, 1st Irradiation) and 4 d with the TL-lamp (350 nm, 8 W, r.t., 2nd Irradiation). This time no solid precipitation was observed. Ferrocene was added after the irradiation experiments (Table 16).

4. Results and Discussion

Table 16: Cyclic voltammetric data (**11**) in acetonitrile, before and after the irradiation with UV light (Scan rate = 200 mV s⁻¹).

	Before Irradiation	1st Irradiation	2nd Irradiation
$E_{1/2}(\text{Co(III)/Co(II)})$ (V)	-1.17	-1.28	-1.29
$(\Delta E_p)_{\text{Co(III)/Co(II)}}$ (mV)	98	85	83
$(i_{pr}/i_{pf})_{\text{Co(III)/Co(II)}}$	0.99	0.94	0.93
$E_{1/2}(\text{Co(II)/Co(I)})$ (V)	-2.09	-2.15	-2.19
$(\Delta E_p)_{\text{Co(II)/Co(I)}}$ (mV)	156	95	95
$(i_{pr}/i_{pf})_{\text{Co(II)/Co(I)}}$	0.57	1.13	1.12

(vs. FcH/FcH⁺; $(\Delta E_p)_{\text{Fe(III)/Fe(II)}} = 76$ mV; $(i_{pr}/i_{pf})_{\text{Fe(III)/Fe(II)}} = 0.99$)

Before the UV irradiation, the complex **11** in the open state of the molecular switch presented the expected two redox waves. The electrode potential $E_{1/2}$ varied a little from the former measurements, but these small deviations can be attributed to the little changes in the system, e.g. the absence of ferrocene in the solution; and to the standard deviation of the measurements. The reversible process presented an i_{pr}/i_{pf} ration equal to 0.99 and a peak-to-peak separation of 98 mV. After the irradiation with the mercury lamp (1st Irradiation) the peak-to-peak separation was 13 mV smaller, which coincides with the observed for complex **12**, and the i_{pr}/i_{pf} ratio equal to 0,94. The decrease in the i_{pr}/i_{pf} ratio is in the margin of error of the measurement. After the irradiation with the TL-lamp, (2nd Irradiation), these values barely changed (Table 16, Figure 89).

The quasireversible redox process presented, before the irradiation, a peak-to-peak separation of 156 mV and an i_{pr}/i_{pf} ratio equal to 0.57. These values do not agree with the former measurements carried out with the same complex in acetonitrile. After the first irradiation, the observed peak-to-peak separation was 95 mV and the i_{pr}/i_{pf} ratio was 1.13.

These results were more in agreement with the former measurement. After the second irradiation, these values remained almost constant (Table 16, Figure 89).

As in the case of the analogous complex **12**, there was not a separation of the redox-waves to see (from one two-electrons redox wave to two one-electron redox waves). The starting and the final situations present little differences, but both represent complexes which present no electronic communication between the metal centers. There is no measurable indication of the closure of the molecular switch and the formation of the π -conjugated

system which would connect both metal centers, making the electronic communication between the two cobalt atoms possible.

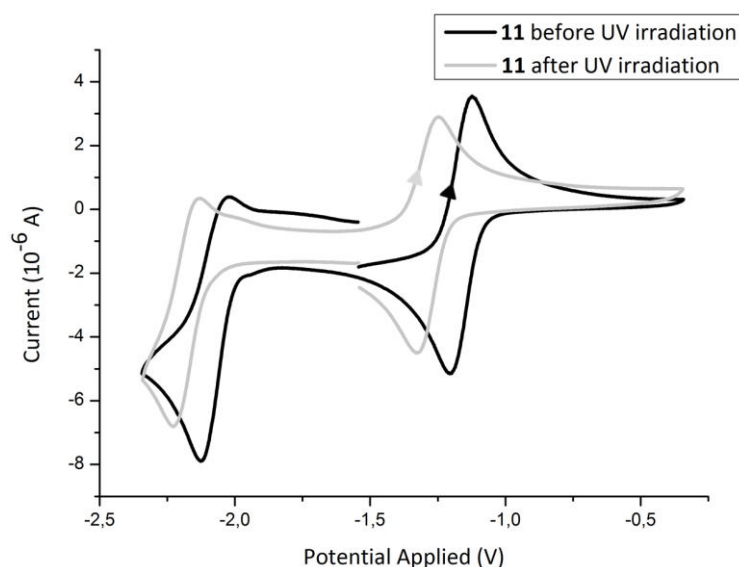


Figure 89: Cyclic voltammogram of complex **11** before (black) and after (grey) the irradiation with UV light ((2 h 45 min with a mercury lamp (366 nm, 25 W, 0 °C) and 4 d with a TL-lamp (366 nm, 8 W, r.t.) vs. FcH/FcH⁺. [Bu₄N][PF₆] was used as electrolyte and acetonitrile as solvent.

4.4.2. Redox behavior of the ferrocene complexes **17** and **18**

Cyclic voltammetry measurements were performed for complexes **17** and **18** (Figure 90). In both cases, only one redox-wave was observed. As expected, when the molecular switch is in the open state the π -conjugation between the metal centers is interrupted and the metal centers do not communicate electronically. The redox potential for both complexes is very similar (Table 17), as was expected for two so resembling complexes.

Table 17: Cyclic voltammetric data of **17** and **18** (scan rate = 200 mV s⁻¹) at room temperature (vs. FcH/FcH⁺).

	$E_{1/2}(\text{Fe(III)/Fe(II)})$ (V)	Solvent
17	-0.0319	THF
18	0.135	THF

$$E_{1/2} = \frac{1}{2}(E_{\text{pf}} + E_{\text{pr}})$$

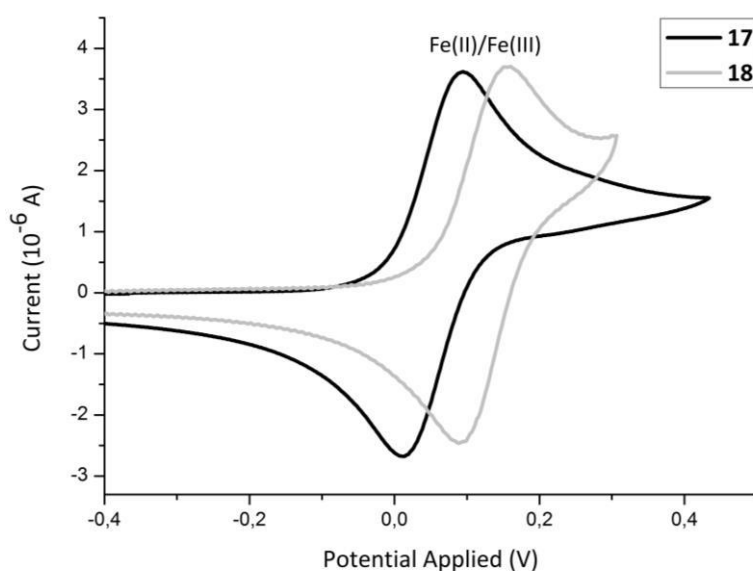


Figure 90: Cyclic voltammogram of complexes **17** (black) and **18** (grey) solved in THF vs. FcH/FcH^+ . $[\text{Bu}_4\text{N}][\text{PF}_6]$ was used as electrolyte. Each iron center is independent of each other.

4.4.2.1. Irradiation experiments monitored by means of CV with complex **17**

Complex **17** was dissolved in THF and its redox behavior was investigated. Before the irradiation with UV light measurements at 200 mV s^{-1} were carried out. Only the expected two-electrons redox wave was observed. The peak-to-peak separation was 63 mV (Table 18). This value is larger than the literature value of $59/n \text{ mV}$, but considering that the peak-to-peak separation for the reference ferrocene redox wave (161 mV), is even smaller than expected. The i_{pr}/i_{pf} ratio was equal to 1.14. Therefore, this process does not fulfill exactly the prerequisites for an electrochemically reversible process, but the deviation is within the experimental errors.

The orange solution was irradiated 36 min with an mercury lamp (366 nm, 25 W, 0 °C) and it turned clear pink. Afterwards, the solution was irradiated for another four days with a TL-lamp (350 nm, 8 W, r. t.). The salmon pink solution was subjected again to cyclic voltammetric experiments. This time, not only one redox wave was observed, but two (Figure 91).

Table 18: Cyclic voltammometric data (**17**), before and after the irradiation with UV light in THF. (Scan rate = 200 mV s⁻¹).

	Before the Irradiation	After the Irradiation
$E_{1/2}(\text{Fe(III)/Fe(II)})$ (V)	-0,07	0,02
$(\Delta E_p)_{\text{Fe(III)/Fe(II)}}$ (mV)	63	71
$(i_{\text{pr}}/i_{\text{pf}})_{\text{Fe(III)/Fe(II)}}$	1.14	1.06
$E_{1/2}$ (V)	-	-0,20
(ΔE_p) (mV)	-	51
$(i_{\text{pr}}/i_{\text{pf}})$	-	1.65

(vs. FcH/FcH⁺; $(\Delta E_p)_{\text{Fe(III)/Fe(II)}} = 161$ mV; $(i_{\text{pr}}/i_{\text{pf}})_{\text{Fe(III)/Fe(II)}} = 1.06$)

The difference in the peak-to-peak separation was 8 mV for the iron-complex redox reaction and the variation in the $i_{\text{pr}}/i_{\text{pf}}$ ratio was also insignificant.

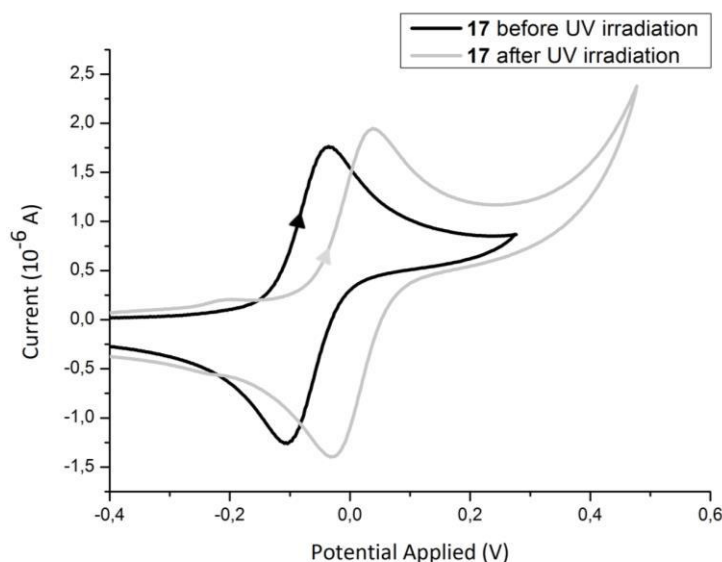


Figure 91: Cyclic voltammogram of complex **17** before (black) and after (grey) the irradiation with UV light (36 min with a mercury lamp (366 nm, 25 W, 0 °C) and 4 d with a TL-lamp (366 nm, 8 W, r.t.)) vs. FcH/FcH⁺. [Bu₄N][PF₆] was used as electrolyte and THF as solvent.

The second redox wave found at -0.20 V is not a one-electron redox process caused by the reduction/oxidation of the iron centers of the complex. When the molecular switch is found in the closed state, the iron atoms are connected by means of a π -conjugated eight carbon atoms “chain”. Therefore the iron atoms should electronically communicate and not one two-electrons redox wave, but two different one-electron redox waves for the metal centers would be expected. Nevertheless, the separation between both observed processes is too large; also it is the difference in the current. This second redox reaction might come from a side product developed during the irradiation with UV light. As no similar side reaction has

been found in the literature, and given its electrode potential (-0.20 V), it is possible that this side product is a ferrocene derivative. The i_{pr}/i_{pf} ratio (1.65) indicates an irreversible process. When the experiments were repeated, but this time employing a Rayonet lamp (366 nm, 16 W, r.t), the formation of the second redox wave was also observed (Figure 92). Furthermore, after 5 h 45 min irradiation, two additional redox waves appeared, confirming that the complex partially decomposed.

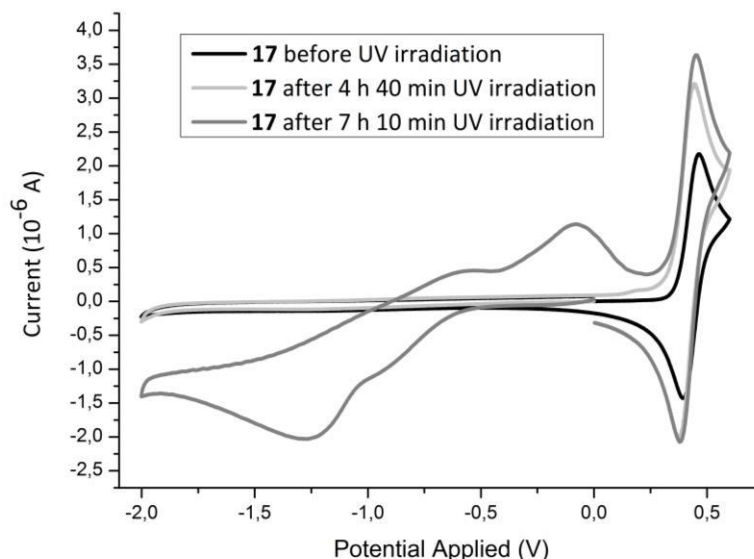


Figure 92: Cyclic voltammogram of complex **17** before (black) the UV irradiation, after 4 h 40 min UV irradiation (clear grey) and after 7 h 10 min UV irradiation (dark grey) with a Rayonet lamp (366 nm, 16 W, r.t.) vs. FcH/FcH^+ . $[\text{Bu}_4\text{N}][\text{PF}_6]$ was used as electrolyte and THF as solvent.

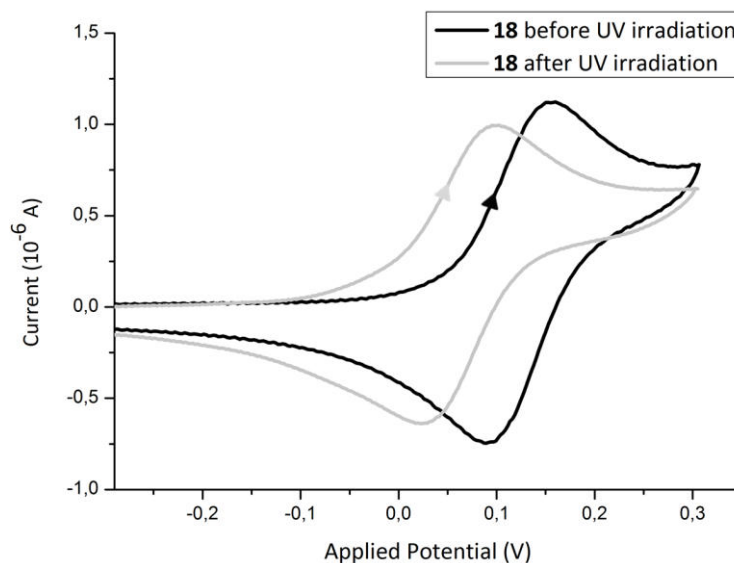
4.4.2.2. Irradiation experiments monitored by means of CV with complex **18**

Finally, the last of the diamagnetic complexes, the cyclohexene-complex **18**, was subjected to similar experiments in THF. In the open state of the molecular switch of complex **18** a unique redox wave was observed where the peak-to-peak separation was 73 mV. As the peak-to-peak separation in the redox wave of the added ferrocene was 67 mV, the former peak-to-peak separation did not seem reasonable for a reversible two-electrons redox process. The i_{pr}/i_{pf} was 1.30, while the same value for ferrocene was 1.62 (Table 19). Both presented a deviation from the ideal value. The reason could be an uncompensated solution resistance.

Table 19: Cyclic voltammetric data (**18**) in THF, before and after the irradiation with UV light. (Scan rate = 200 mV s⁻¹)

	Before the Irradiation	After the Irradiation
$E_{1/2}(\text{Fe(III)/Fe(II)})$ (V)	0.135	0.07
$(\Delta E_p)_{\text{Fe(III)/Fe(II)}}$ (mV)	73	73
$(i_{\text{pr}}/i_{\text{pf}})_{\text{Fe(III)/Fe(II)}}$	1.32	1.20

(vs. FcH/FcH⁺; $(\Delta E_p)_{\text{Fe(III)/Fe(II)}} = 67$ mV; $(i_{\text{pr}}/i_{\text{pf}})_{\text{Fe(III)/Fe(II)}} = 1.62$)

**Figure 93:** Cyclic voltammogram of complex **18** before (black) and after (grey) the irradiation with UV light (4 h with a Rayonet lamp (366 nm, 16 W, r.t.)) vs. FcH/FcH⁺. [Bu₄N][PF₆] was used as electrolyte and THF as solvent.

After 4 h UV light irradiation using a Rayonet lamp (366 nm, 16 W, r.t.), the orange solution turned pink. The second redox process, which appeared after the UV irradiation of complex **17**, was not observed this time. The peak-to-peak separation and the $i_{\text{pr}}/i_{\text{pf}}$ ratio remained almost constant (Figure 93, Table 19). As in the other cases, the variation in the electrode potential was assigned to changes in the measurement cell.

Guirado and coworkers^[78] made the same observation when they tried to carry out similar measurements with the analogous bis(ethynylferrocene) complexes. In a former publication of the same workgroup^[111] it was established that the presence of electron-withdrawing substituents (e. g. ferrocenium) destabilize the closed isomer of the molecular switch, favouring a very fast ring-opening process. It was also observed, that the photochromic core undergoes an irreversible oxidation at higher potentials, and a cation-radical is obtained. Therefore it was postulated that a ferrocene unit oxidizes first, what destabilizes the neutral closed photochromic core. The presence of the electron withdrawing ferrocenium and its

influence in the closed photochromic core allow the second ferrocene unit to oxidize at the very same potential as the first one. Afterwards the photochromic core is oxidized and the obtained cation-radical is destabilized by the ferrocenium groups. In this moment the molecular switch undergoes the ring-opening reaction. Once opened, the cation-radical acts as an oxidant and both iron centers are found in the oxidation state (III) (see section 2.1.2)

Taking the behaviour of the analogous ferrocene complexes into account, and the observation of only one redox-wave in the measured range in cyclic voltammetry after irradiating the samples with UV light, it could be assumed that the iron complexes (**17** and **18**) undergo the same process. It would explain why the same electrochemical behaviour in cyclic voltammetry was shown before and after the irradiation with UV light (Figures 91-93, Tables 18 and 19).

Regarding to the cobalt complexes, the withdrawing cobaltocenium substituents could be the reason which explains the spontaneous ring-opening process.

4.4.3. Conclusions (II)

The redox behaviour of complexes **11**, **12**, **17** and **18** was investigated by means of cyclic voltammetry. The cobaltocenium complexes (**11**, **12**) suffered from two two-electrons redox processes, indicating that no electronic communication exist between the metal centers. However, the peak-to-peak separation was larger than expected, what would suggest superimposed one-electron redox processes. The ferrocenyl-complexes **17** and **18** showed only a two-electrons reversible reaction, therefore the iron centers are neither communicating.

When the molecular switch is in the open state the π -conjugation is interrupted, therefore the metal centers are not expected to be electronically communicated. Expecting the opposite to be true when the molecular switch undergoes the cyclization and the metal centers are connected by a π -conjugated system, the dissolved complexes were irradiated with UV light and cyclic voltammetric measurements were carried out again. Unfortunately, no new one-electron processes was observed. Therefore, the switching reaction did not work or the closed isomers were unstable and the molecular switch underwent the opening reaction again.

Besides the temperature variation during the UV light irradiation, which plays a role in this type of measurements and may cause problems when reproducing them, it was observed

that the addition of the standard ferrocene to the solution after the irradiation experiments is not a good method to monitor this class of reactions. It is not only that the solvent evaporates when the CV vessel is opened (modifying the concentration), but the presence of a new compound alters the environment of the measurement.

In figure 94 the cyclic voltammograms of the standard ferrocene before and after the irradiation with UV light are showed. The $E_{1/2}$ values differ, and it confirms the lack of rigour in referencing when ferrocene is not present during the whole measurement process, but only in the end.

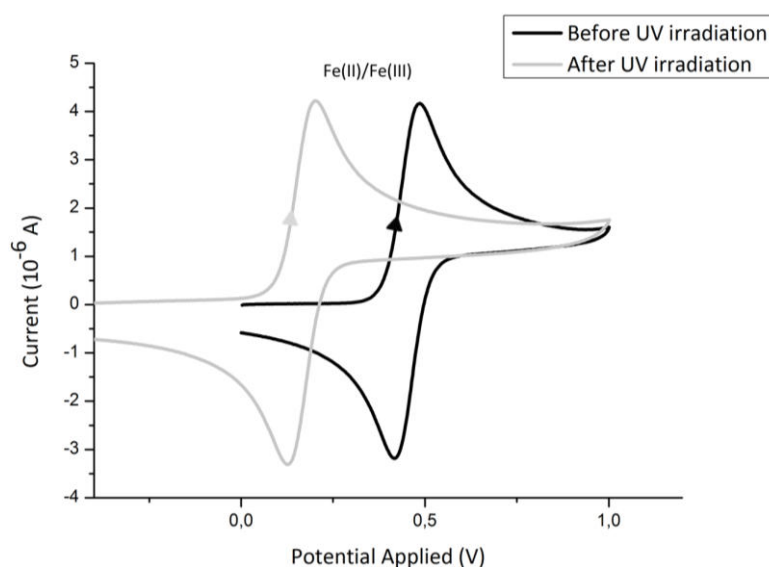


Figure 94: Cyclic voltammogram of ferrocene before (black) and after (grey) the irradiation with UV light. $[\text{Bu}_4\text{N}][\text{PF}_6]$ was used as electrolyte and acetonitrile as solvent.

In the measurements with the ferrocene complexes **17** and **18**, it would be a problem to carry out the measurements with ferrocene present in the solution, because it would overlap the redox waves of the complex. In this case decamethylferrocene or even cobaltocenium-cation could be employed as intern reference. ^[221]

Table 20: Calculated energy differences (KJ mol⁻¹) between the closed and the open isomers for the four structures under study, optimized with different density functionals (D=dispersion correction of Grimme). Basis set: def-TZVP.

Functional	$E_{(\text{closed})}-E_{(\text{open})}$	$E_{(\text{closed})}-E_{(\text{open})}$
	Cyclopentene-switch	Cyclohexene-switch
chloro-substituted derivatives		
BP86	27.1	23.7
BP86-D	15.7	11.9
B3LYP	44.1	42.0
B3LYP-D	30.1	27.0
iodo-substituted derivatives		
BP86	32.2	29.0
BP86-D	20.8	17.6
B3LYP	50.1	48.0
B3LYP-D	36.1	33.5

Irradiation Experiments Monitored *via* UV-vis Spectroscopy

Both compounds were irradiated under the same conditions: *n*-hexane was used as solvent, the concentration of the prepared solutions was very similar, the irradiation times were identical also were the light sources: a TL-lamp (366 nm, 8 W) was used for the irradiation with UV light and a work hot spot for the irradiation with visible light. Therefore, both switching reactions could be compared.

The photocyclization and subsequent ring opening reaction (Scheme 24) were monitored *via* UV-vis spectroscopy (Figure 96).

4. Results and Discussion

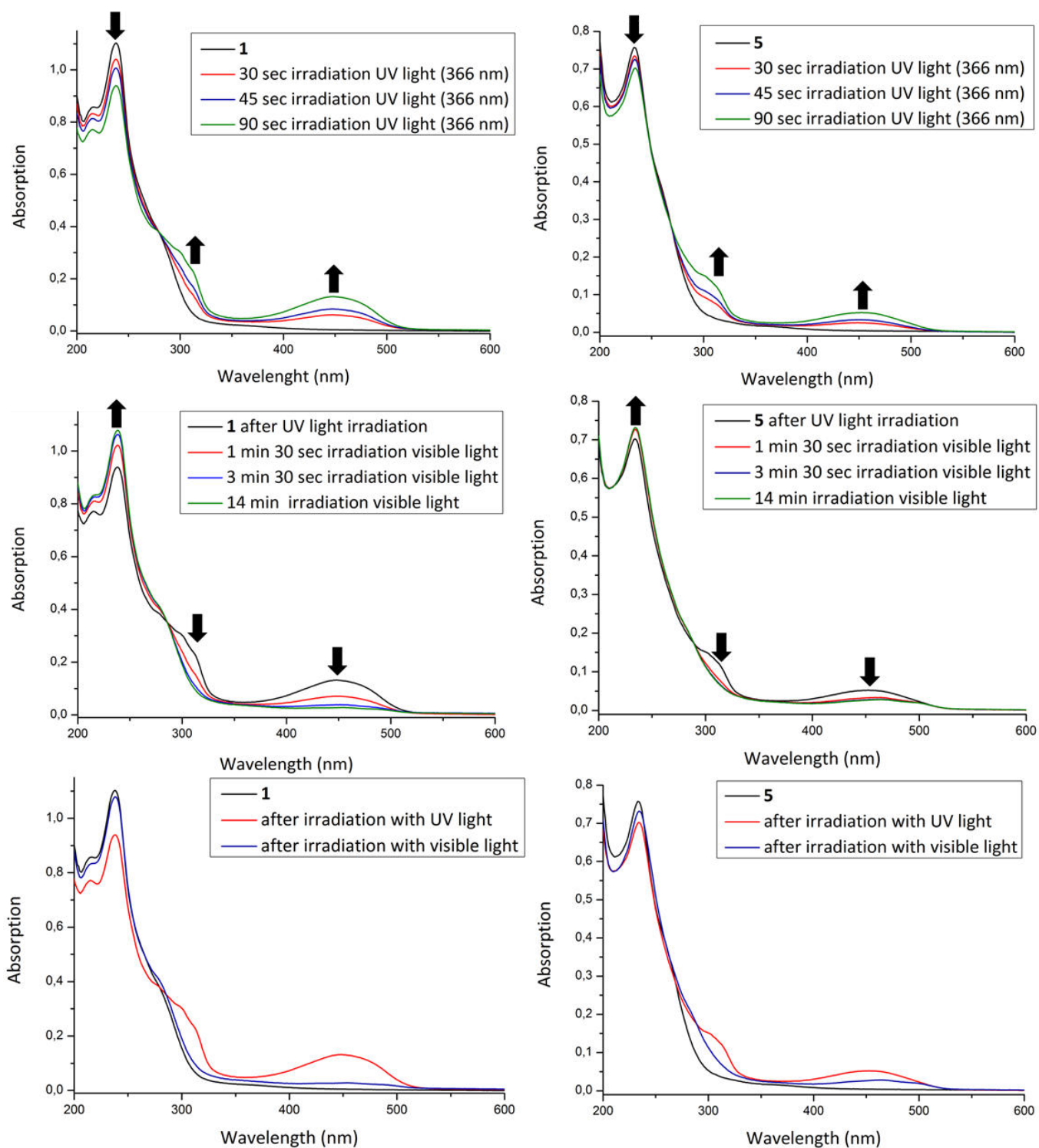


Figure 96: Irradiation experiments with compounds **1** ($4.5 \cdot 10^{-4}$ M, $d = 1$) and **5** ($4.2 \cdot 10^{-4}$ M, $d = 1$) in hexane. Upper: 90 sec UV light irradiation; middle: 14 min visible light irradiation; below: 90 sec UV light irradiation (red) and 14 min visible light irradiation (blue).

Theoretical UV-vis spectra were calculated and compared with the experimental results (Figure 97).

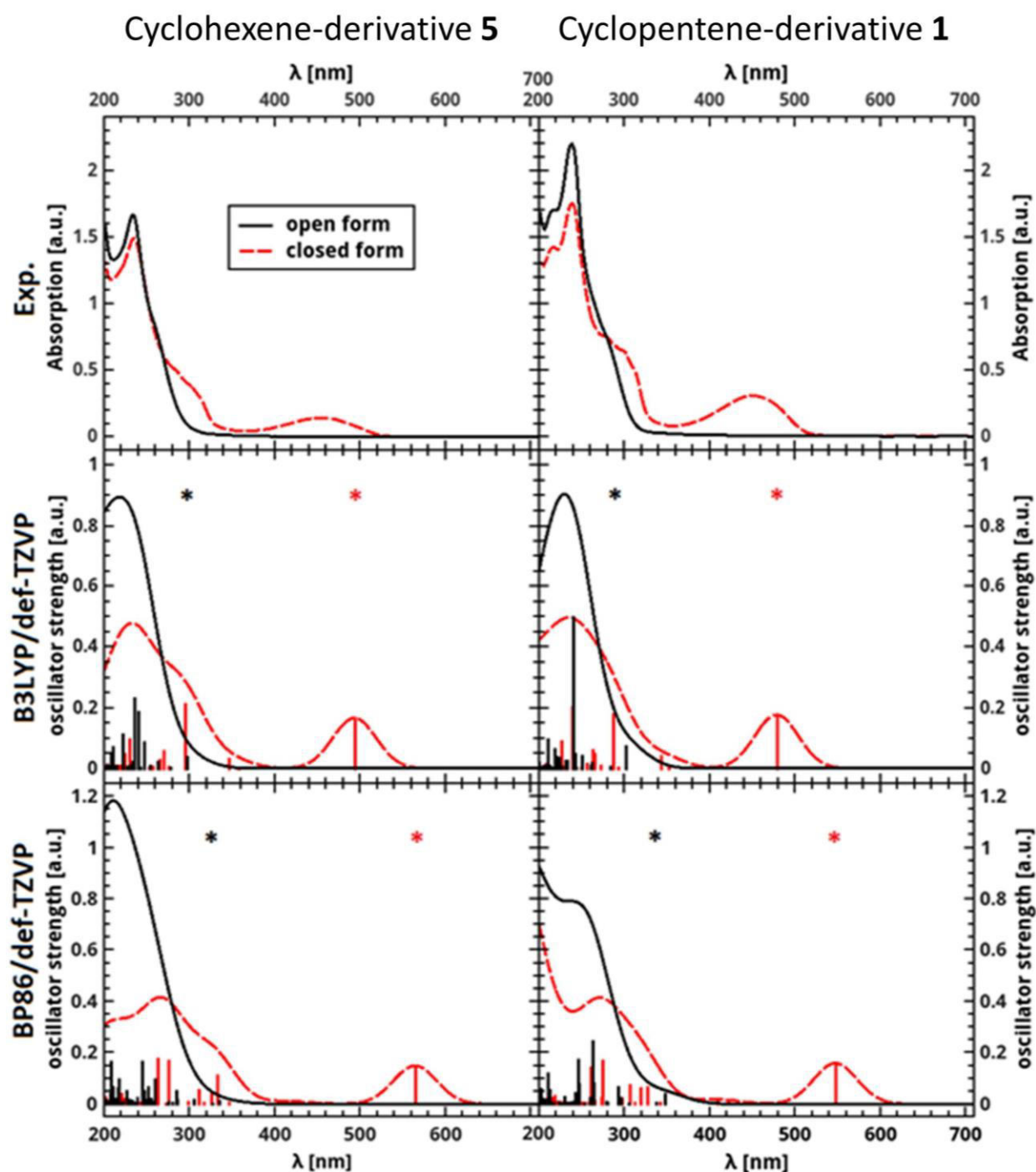


Figure 97: Calculated UV-vis spectra (Gaussian broadening with a half-width of 60 nm for the theoretical spectra) of compounds **1** and **5**. The spectra were calculated with BP86/def-TZVP and B3LYP/def-TZVP using TDDFT and the structures optimized with BP86/def-TZVP and B3LYP-D/def-TZVP (The stars denote the positions of the HOMO-LUMO transitions).^[220]

In figure 97 the experimental (upper-left for **5** and upper-right for **1**) and the calculated (with B3LYP/def-TZVP: middle-left panel for **5** and middle-right panel for **1**; with BP86/def-TZVP: lower-left panel for **5** and lower-right panel for **1**) UV-vis spectra of compounds **1** and **5** in the open form (black curve) and in the closed form (red-curve) are shown.

4. Results and Discussion

Before the irradiation, compounds **1** and **5** were colourless and they only absorbed in the UV region. Both compounds present maxima around 240 nm and a shoulder around 270 nm. There is also a clue for another band appearing below 200 nm. The spectra calculated with TDDFT give similar results: an absorption band at 230 nm for B3LYP and an absorption band at 300 nm for the BP86 functional were found.

After the irradiation with UV light the solutions became deep yellow and a new maximum appeared in visible region. In addition, the absorption bands below 200 nm and around 240 nm decreased, while the shoulders at 278 nm (**1**) and 260 nm (**5**) presented a bathochromic shift (red shift) (Figure 96, upper, Table 21). Similar results were found in the theoretically obtained UV-vis spectra, where new absorption bands appeared at 300 nm (320 nm) and at 500 nm (550 nm) for the B3LYP (BP86) functional. The absorption decrease at 240 nm was not as intense for the experimental spectra as for the calculated ones and the reason could be that under experimental conditions, not all the molecules undergo the photocyclization, so in the PSS both states are found.

Compound **1** showed one isosbestic point (279 nm) and compound **5**, two (at 248 nm and 268 nm). The isosbestic points indicate that only one product is being produced in the reaction also no decomposition is taking place.

Table 21: Experimental UV-vis absorption spectroscopic data for compounds **1** and **5** in hexane.

λ , nm (ϵ , M ⁻¹ cm ⁻¹)	
Open isomer	PSS
1 200 (2005); 215 (1916); 237 (2451); 278 (sh, 891)	200 (1738); 215 (1716); 237 (2094); 296 (sh, 713); 451 (290)
5 200 (1844); 234 (1797); 276 (sh, 899);	200 (1608); 234 (1655); 306 (sh, 331); 452 (116)

* sh = shoulder, PSS = photostationary state

When the solutions were irradiated with visible light, the yellow colour disappeared almost completely indicating the ring-opening reaction had taking place. The absorption of the maxima in UV range increased again and the maxima in the visible region almost disappeared (Figure 96, middle). In the spectra recorded during the irradiation with visible light isosbestic points were also observed (**1**: 286 nm; **5**: 289 nm).

When comparing the starting with the final state in both compounds (Figure 96, bottom) it can be concluded that the back reaction does not occur completely, the spectra before and after the switching cycle are not identical. Furthermore, there are not isosbestic points to see. These facts could indicate the formation of a side product during the irradiation cycle. It was also observed that with shorter UV irradiation times, the degradation took place in lesser extent. However, the cyclopentene derivative **1** showed a better resistance to fatigue than the cyclohexene-derivative **5**.

A difference in the switching behavior of compounds **1** and **5** was observed when, after two switching cycles, several UV-vis spectra of the solution were measured in a row. The UV-vis spectrum of the cyclopentene-derivative **1** remained invariable, while the UV-vis spectrum of compound **5** did not. The cuvette with the sample stayed in the darkness and still the absorption changed in a reversible way (Figure 98). An isosbestic point at 288 nm indicated that the product was not decomposing.

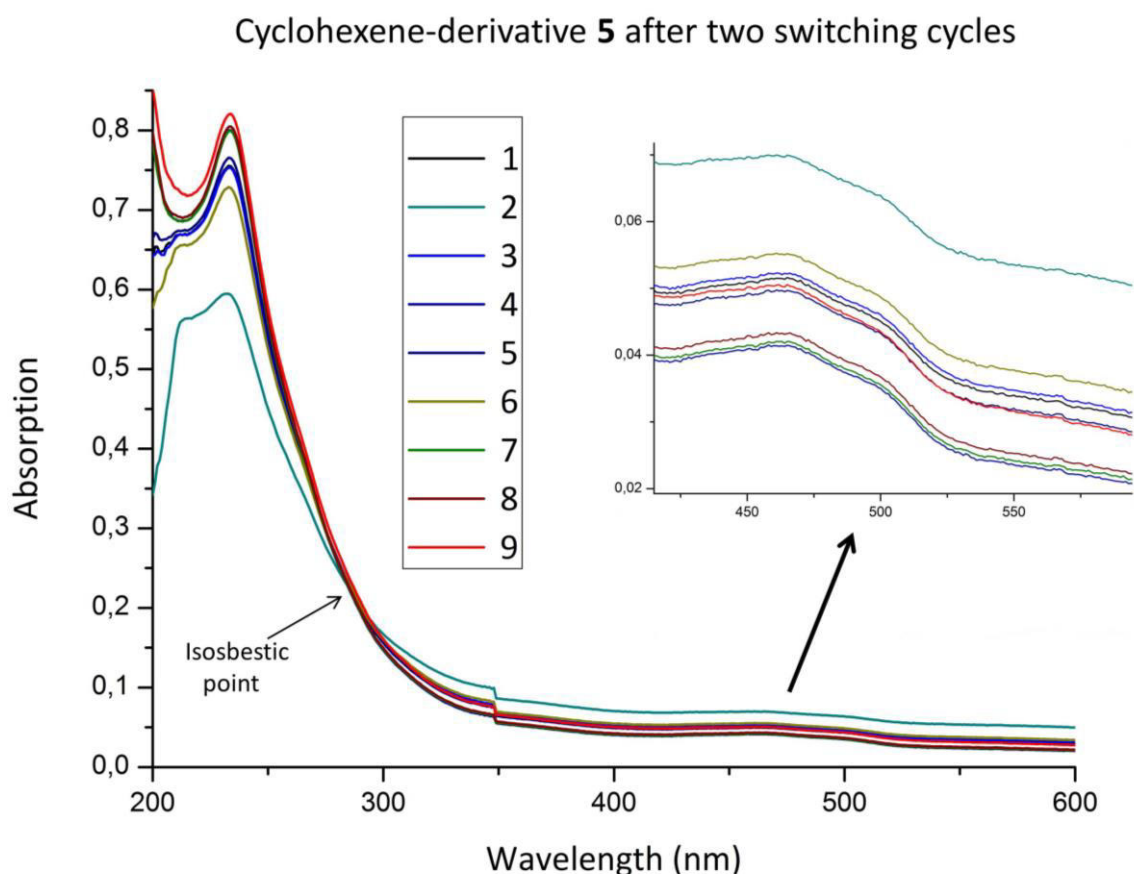


Figure 98: UV-vis spectra of compound **5** solved in hexane after two switching cycles ($4.2 \cdot 10^{-4}$ M, $d = 1$ cm).

As this behavior was not observed in the cyclopentene-compound **1**, it is presumed that the cyclohexene-backbone is responsible of it.

As the broad maximum in the visible region does not appear, indicating that the closed isomer is not being formed during this reaction, a chemical dynamic equilibrium between the open and closed isomer can be discarded.

The cyclohexene-backbone of the molecular switch core can take part in two different processes: the conversion between the possible conformations of the molecular switch (parallel/antiparallel)^[70] and the equilibrium between different conformations of the connecting cyclohexene ring.^[212,228,229] These possibilities were already discussed in section 4.2.1

To the best of my knowledge, no examples exist in the literature where the conformation of the molecular switch changes spontaneously (and reversibly) in the dark at room temperature, and that the interconversion can be followed by UV-vis spectroscopy. While it is true that the literature is focused on the cyclopentene-backbone, it exists no reason to think the cyclohexene-derivative could establish a different behaviour.

Respecting to the conformation of the cyclohexene ring, the energy barrier between the half-chair and boat conformation ist very low. Therefore, in solution and at room temperature, the equilibrium between them is too quickly to be observed.^[228] Also this second hypothesis seems also improbable.

It has been concluded that this behavior could not be explained yet. Therefore, it cannot be excluded that the observed reversible reaction influences the switching properties of the molecular switch. However, those properties have proved to be very similar for both molecular switches **1** and **5**. Finally, as the existence of an isosbestic point indicates that the compound is not decomposing, there is no reason to think that this phenomenon decreases the resistance to fatigue of the molecular switch **5**.

It is known in the literature that the molecular switches which follow this pattern and have not substituents in the position 4', apart from the oxidation in contact with oxygen, undergo a side reaction which competes with the switching process^[90] (see section 2.1.1.5). Feringa and coworkers^[73] reported in 2003 that the cyclopentene derivative **1** revealed a high grade of decomposition after short times of irradiation with UV light, higher than the analogous dithienylethene derivatives with another substituents instead of chlorine atoms. Furthermore, compound **5** is supposed to undergo the same side reaction.

Despite of the fatigue observed for both compounds, it was seen that they react reversibly and following a similar mechanism. The UV-vis spectra and their evolution during the switching cycle are very similar.

In accordance to Feringa and coworkers,^[73] the band at 240 nm represents the HOMO-LUMO transition. However, in figure 97, the absorption band which constitutes the HOMO-LUMO transition for the cyclohexene switch **5** in the open state is found at 297 nm calculated with the B3LYP functional (and for BP86 at 347 nm, not shown) as a small band with low intensity. In case of cyclopentene-derivative **1**, the same transition was found at 302 nm (347 nm) for B3LYP (BP86), which is only very slightly bathochromically shifted compared to **5**. These observations coincide with the reports of Staykov^[230] and Guillaumont,^[231] who reported low intensity HOMO-LUMO transitions for different dithienylethene derivatives. The calculated intensities are small for the HOMO-LUMO transition,^[230] what could be an indication, that the large band at 240 nm is a superimposition of the HOMO-LUMO and other transitions which are split in two different absorption bands in the calculated spectra (see below).^[232]

Although the most intense absorption bands (**1**, **5**) are located around 250 nm (Figures 96 and 97), it can be observed that the MOs of compound **5** in the open state (Figure 99), which contribute to these transitions, do not have the appropriate shape to lead to ring closure. In some cases the MOs have suitable phases on the cyclohexene carbon atoms where the double bond is located in the open form, as for example in the HOMO-1. For the HOMO-2 the important coefficients on the thiophene rings are missing. The HOMO and the LUMO are the only MOs which have coefficients and phases suitable to the ring closure, which agrees with the literature.^[232]

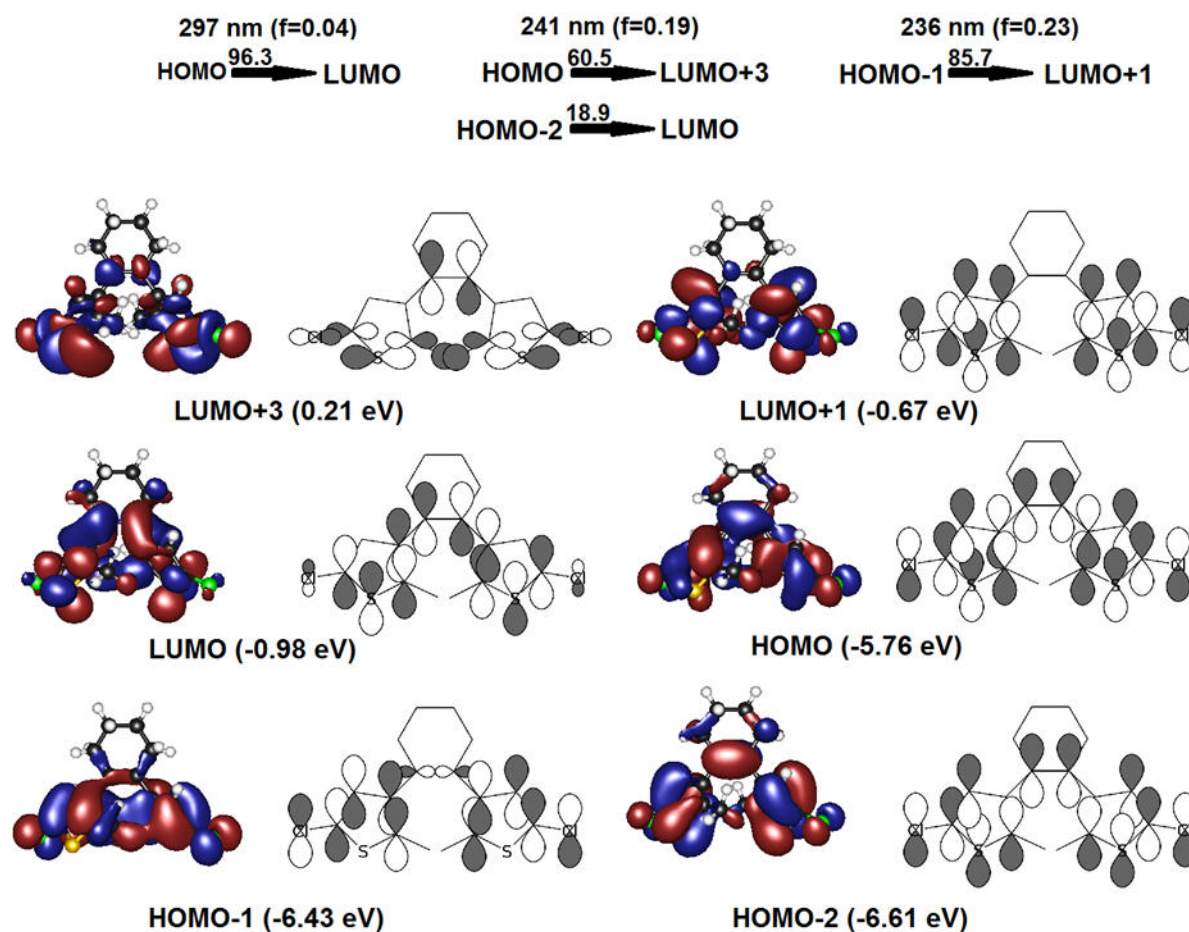


Figure 99: Molecular orbital excitations with their weights (given on the arrows), oscillator strengths f and molecular orbital energies (given in eV) corresponding to the most intense peaks in the UV-vis spectrum of the open form of **5** calculated with B3LYP-D/B3LYP/TZVP.^[220]

The molecular orbital excitations responsible for the UV-vis spectra of the closed state of the cyclohexene-derivative **5** (Figure 100) are very similar to observed in the open form (Figure 99). However, the HOMO-LUMO transition which leads to the ring-opening is more intense than the HOMO-LUMO transition in the open state and appears in the visible region. As in the open form, the high-energy excitations do not support the ring-opening reaction due to the mismatching molecular orbital coefficients.

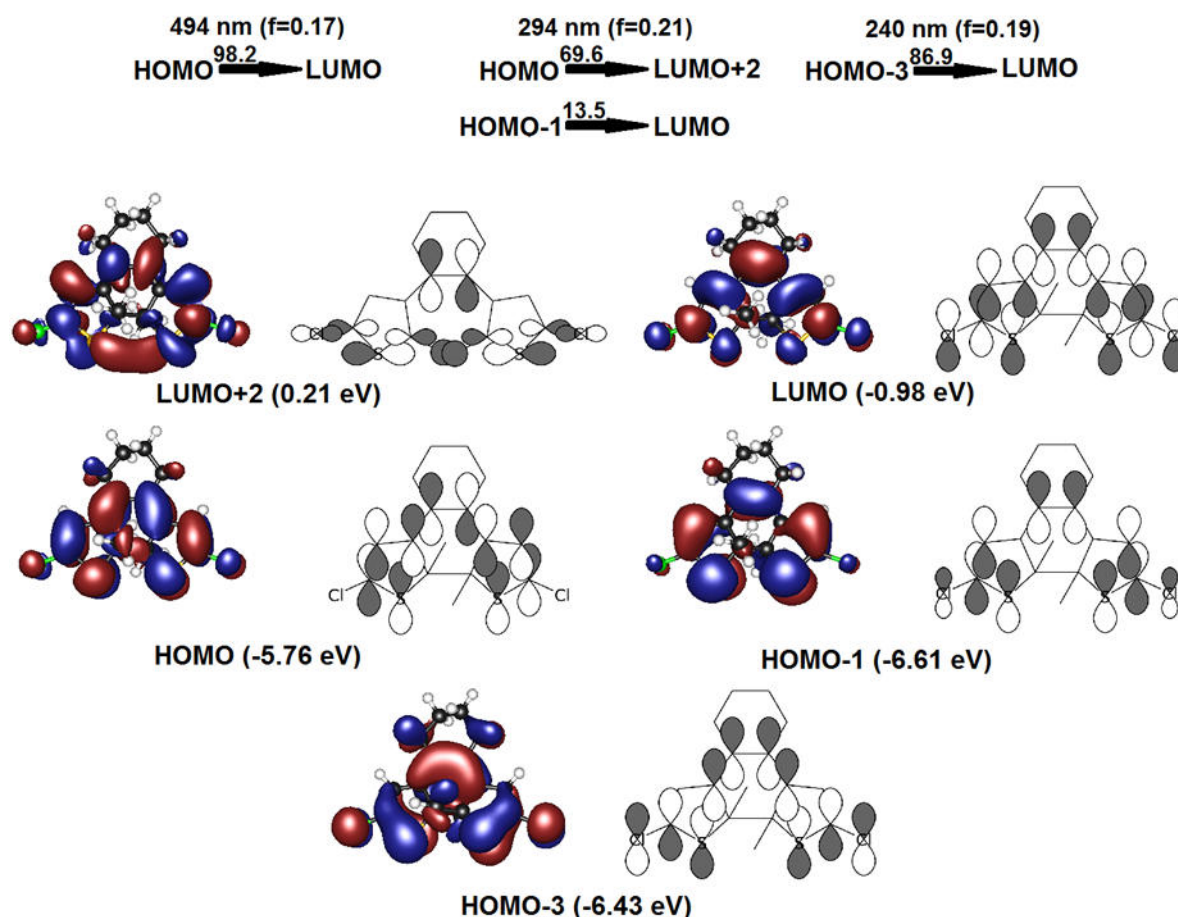


Figure 100: Molecular orbital excitations with their weights (given on the arrows), oscillator strengths f and molecular orbital energies (given in eV) corresponding to the most intense peaks in the UV-vis spectrum of the closed form of **5** calculated with B3LYP-D/B3LYP/TZVP.^[220]

Due to the importance of these molecular orbital transitions, the shapes of the HOMOs and LUMOs for all calculated structures were carefully analyzed. The MOs for the dithienylethene derivatives (**1** and **5**) in both possible states (open and closed) calculated with BP86 are presented in figure 101. The HOMO-LUMO transitions for both molecular switches are almost identical. The MOs calculated for the structures optimized with B3LYP-D (Figure 102) have the same relative coefficients on the carbon atoms participating in the cyclization and ring-opening reactions.

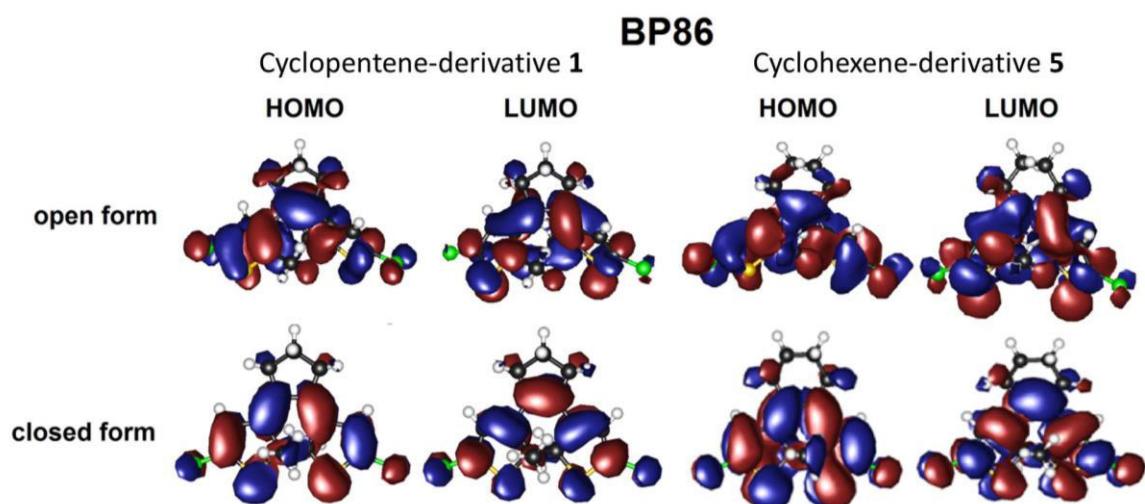


Figure 101: HOMOs and LUMOs for both switches and both isomeric forms calculated with BP86/def-TZVP. ^[220]

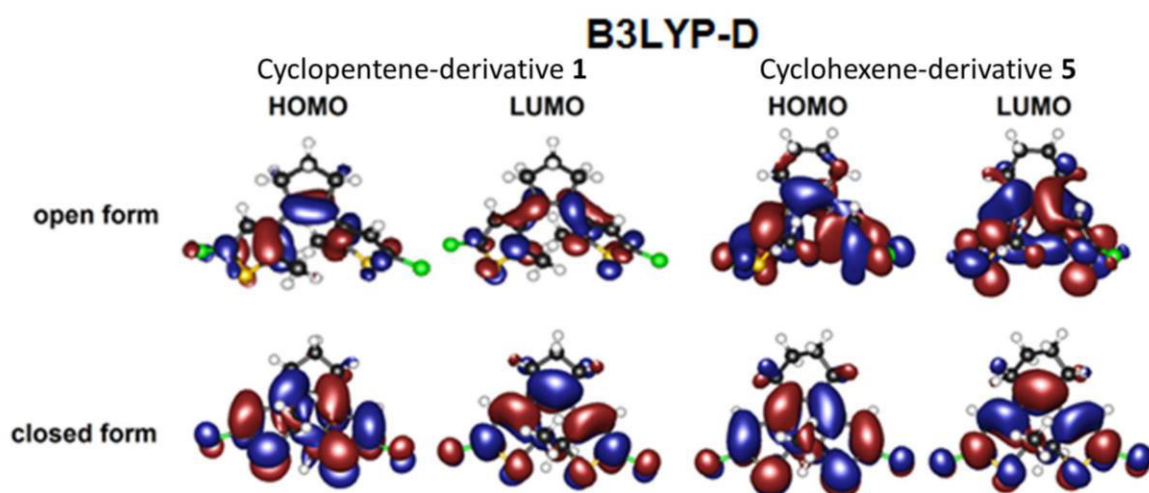


Figure 102: HOMOs and LUMOs for both switches and both isomeric forms calculated with B3LYP-D/def-TZVP. ^[220]

Not content with it, and with the aim of obtaining a better understanding of the transition probabilities, the transition dipole moments for the HOMO-LUMO transition for the cyclopentene- (**1**) and cyclohexene-dithienylethene (**5**) derivatives $d_{01,open}$ and $d_{01,closed}$ were studied (Table 22).

The square of the transition dipole moment is equal to the probability of the transition and proportional to the oscillator strengths reported in figures 99 and 100. Therefore is a characteristic quantity for the efficiency of the excitations. For both dithienylethene derivatives (**1** and **5**), the transition dipole moments of the HOMO-LUMO excitations are much larger for the closed than for the open forms, and their value is not dependent on the functional. In the case of the open state the transition probability calculated with B3LYP

(BP86) is 41% (75%) higher for the cyclopentene switch **1** than for the cyclohexene derivative **5**.

Table 22: Transition dipole moments for the HOMO-LUMO transition of the optimized structures of **1** and **5** (in both possible states). Basis set: def-TZVP.

Compound	Functional	$d_{01,open}$ (Debye)	$d_{01,closed}$ (Debye)
1	B3LYP	2.12	4.14
1	BP86	1.66	4.19
5	B3LYP	1.50	4.08
5	BP86	0.95	4.13

PES scans

In order to learn more about the reaction mechanism, the potential energy surfaces (PES) of the ground states and the first excited states, as a function of the distance between the methylated carbon atoms which will be bound in the cyclization reaction, were scanned. As the halogen substituent was not expected to exert a great influence in the switching cycle, only the chloro-compounds **1** and **5** were investigated. Since the structures calculated with B3LYP-D and BP86 offered the closer results to the experimental data, they were employed to carry on these calculations.

The transition dipole moments at the energetic minimum structures of the open and closed states offer important information about the transition. However, it is not enough to completely understand the reactivity of these molecular switches. Different types of photoreactions are possible (Figure 103).^[230,233] In the first reaction type, the adiabatic photoreaction, (Figure 103, top-left) the molecules are excited from the ground state to a higher electronic state. Afterwards they relax to the minimum of the excited state which coincides with the minimum on the PES of the ground state. For this type of photoreaction it is possible that all molecules undergo the reaction. The second type comprehends the diabatic photoreactions (Figure 103, top right and bottom left) where the minimum of the PES of the excited state nearly coincides with the transition state (TS) of the ground state PES. As a consequence, a radiationless transition from the energy minimum of the excited

states's PES to the TS of the ground state is found, from which the switch reacts to the closed state or to the reactant minimum. The exact location of the minimum on the PES of the excited state exerts a great influence on the quantum yields. When this minimum shifts to the right of the ground state (Figure 103, top-right), more molecules will undergo the cyclization. On the contrary, the back reaction will be favoured if the minimum is shifted to the left (Figure 103, bottom-left) of the TS. The last type is the Hot ground-state reaction. It is characterized by the gaining of enough energy to overcome the TS in the ground state by a radiationless relaxation from the excited state to the ground state (Figure 103, bottom right).

As it was already discussed, only the first excitation energy referring to the HOMO-LUMO excitation is important for the switching reaction (Figure 99). For this reason, an analysis of the potential energy surfaces (PES) of the ground state (S_0) and the first excited states (S_1) as a function of the distance between the methylated carbon atoms (between which a new bond will be formed during the cyclization) was done. T. Steenbock^[220] carried out structure optimizations with B3LYP-D and BP86 and the def-TZVP basis set for several points on the PES keeping the distance between the reactive carbon atoms $R(C-C)$ fixed. Furthermore, energies, transition dipole moments and molecular orbital contributions for the 30 highest singlet excitations for each optimized ground state structure with different fixed $R(C-C)$ values were calculated within TDDFT, where the same exchange-correlation functionals as used in the structure optimizations were applied (B3LYP and BP86).

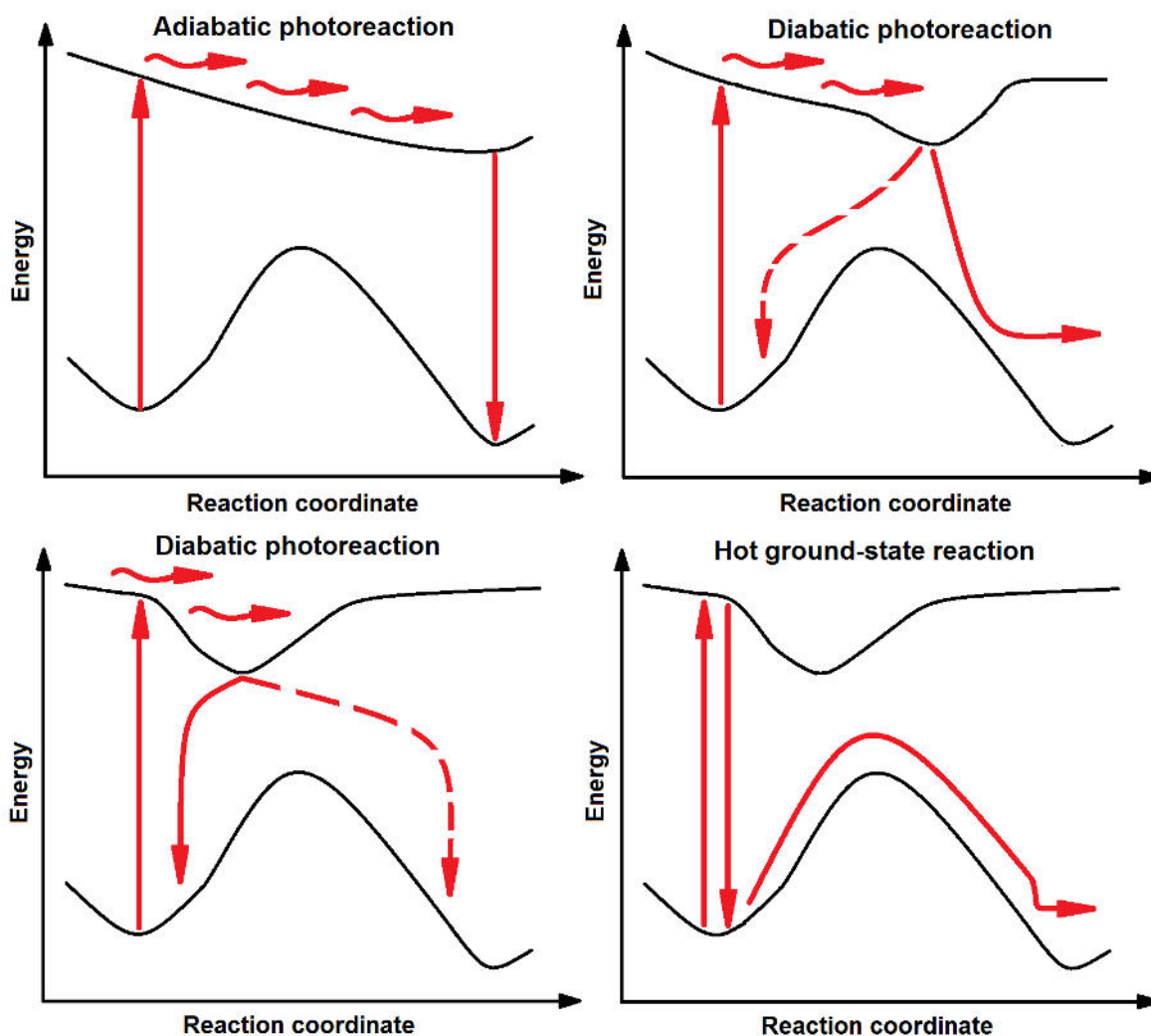


Figure 103: Different types of photoreactions. ^[230,233]

The activation barrier between the two possible states (open and closed) in the ground state for both molecular switches (and both applied exchange correlation functionals) is large. The PES of the first excited singlet state presents a global minimum which coincides with the minimum of the closed form in the ground state, and a shallow local minimum at a C-C distance of around 2.3 Å (except for **5** when calculated with BP86), which cannot be clearly distinguished from a numerical error. Nakamura^[40] found a similar shallow minimum in the PES for the first excited state of a diethienylethene molecular switch where instead a cycloalkene, an ethene-group connected both thiophene rings, when CASSCF/CASPT2 was employed.

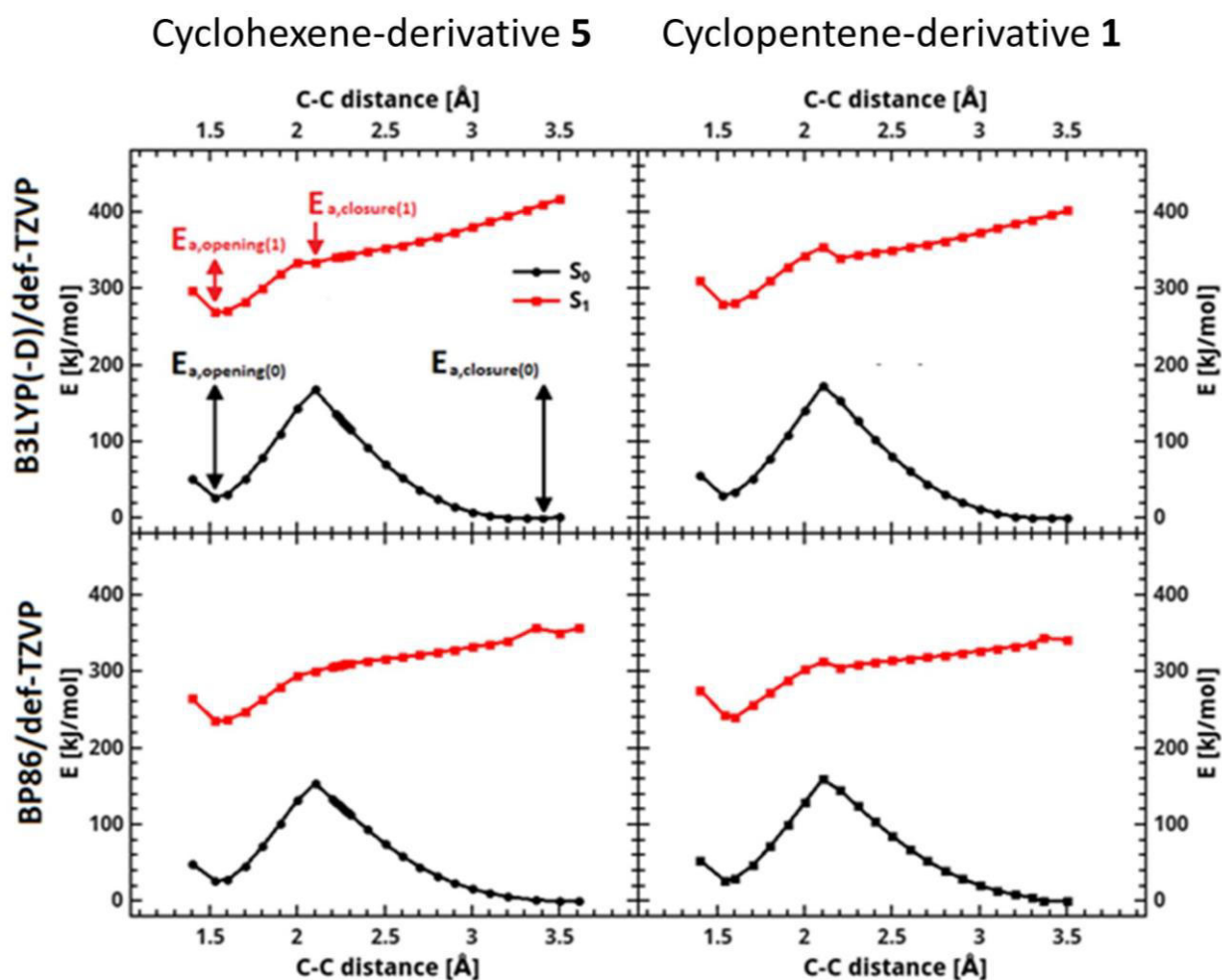


Figure 104: Potential energy surface (PES) for 1,2-bis(5-chloro-2-methylthien-3-yl)cyclohexene (**5**) (left column) and 1,2-bis(5-chloro-2-methylthien-3-yl)cyclopentene (**1**) (right column) for B3LYP(-D)/def-TZVP (upper row) and BP86/def-TZVP (lower row) of the ground state and the first excited singlet state as function of the C-C distance of the carbon atoms participating in the switching reaction.

In order to compare the PESs of **1** and **5**, the thermal activation barriers in the ground state and the first excited state were estimated (Figure 104, Table 23). The activation energy of the cyclization (ring-opening) reaction in the ground state $E_{a,closure(0)}$ ($E_{a,opening(0)}$) was calculated as the energy difference between the optimized closed state (open state) and the maximum on the ground state PES. The reaction barrier in the first excited state for the cyclization $E_{a,closure(1)}$ was calculated as the energy difference between the energetic maximum between the two minima and the energy of the shallow minimum on the PES. It was done in this way because after excitation of the closed state in the first excited state the energy decreases until the local minimum is reached and then it has only to overcome this small barrier to achieve the global minimum of S_1 . Afterwards it relaxes back to the ground state (adiabatic reaction). Staykov *et al.*^[230] reported the same phenomena for the perfluorinated analogous of **1**. The activation barrier for the ring opening reaction in the first

excited state $E_{a,opening(1)}$ was calculated as the energy difference between the local maximum and the global minimum on the first excited state PES. According to Nakamura,^[231] the molecular switch molecules relax to the ground state at the local minimum of the first excited state (diabatic reaction). The amount of energy needed to follow the first excited state's PES makes the adiabatic reaction improbable, as it constantly increases in energy as the distances between the reactive carbon atoms increase.

Table 23: Estimated activation barriers for switches **1** and **5** in the ground states and the first excited singlet states evaluated with BP86 and B3LYP. Values are given in kJ/mol. Basis set: def-TZVP.

B3LYP(-D)/def-TZVP				
Compound	$E_{a,closure(0)}$	$E_{a,opening(0)}$	$E_{a,closure(1)}$	$E_{a,opening(1)}$
1	173.4	143.3	14.5	74.4
5	168.1	141.1	0.1	64.9
BP86/def-TZVP				
1	159.1	128.8	7.5	40.9
5	153.6	126.5	-no local minimum-	-no local minimum-

The reaction barriers for both reactions in the ground state are only slightly larger for the cyclopentene-derivative **1** than for the cyclohexene-derivative **5** (for both applied exchange-correlation functionals). The obtained large values indicate symmetry-forbidden reactions; therefore for both switches thermally stable and no hot ground-state reactions are expected. Furthermore, the reaction barriers in the first excited state are much smaller than those in the ground state. There is no local minimum for the PES of the first excited state of switch **1** calculated with BP86 and the activation barrier calculated with B3LYP(-D) is only 0.1 kJ/mol. The energy barrier $E_{a,opening(1)}$ is much larger than $E_{a,closing(1)}$, and as a consequence, the quantum yield of the ring opening reaction will be lower than for the cyclization reaction, what agrees the data from the literature.^[231,234]

Irradiation Experiments monitored *via* NMR-spectroscopy

It was also tried to monitor the switching reaction within NMR-spectroscopy. This has been already done by other researchers, ^[208,209] even though the limitations of this spectroscopic method, whose limit of detection is high. The researchers describe the appearance of new signals related to the methyl groups at the position 2' of the thiophene rings, which are, in the open state, attached to a sp² carbon atom, and to a sp³ carbon atom in the closed state. The same was described for the substituents at position 4', although the carbon atom at this position does not change its hybridization during the switching reaction.

Both chloro-derivatives (**1** and **5**) were solved in benzene-d₆ and the colourless solutions were subjected to ¹H- and ¹³C-NMR experiments. The samples were irradiated with a TL-lamp (366 nm, 8 W, r.t.) a total of 20 h (with a break of 19 h in the dark after the first hour). In this time period seven NMR-spectra were carried out. After the irradiation with UV light, the cyclopentene-bridged (**1**) molecular switch solution was dark brown and the cyclohexadiene-derivative (**5**) solution had turned dark orange.

Despite the colour change, no significant alterations in the NMR-spectra were observed. For the cyclopentene-derivative **1** no new signals were observed but for the cyclohexene-derivative **5** appeared a very small peak upfield shifted to the peak correspondent to the proton at 4' position. In addition, other two signals (2.35 ppm, 2.40 ppm), which could not be assigned, appeared (Figure 105). However, it could not be confirmed that the new observed signals presented the closed isomer and no other degradation product.

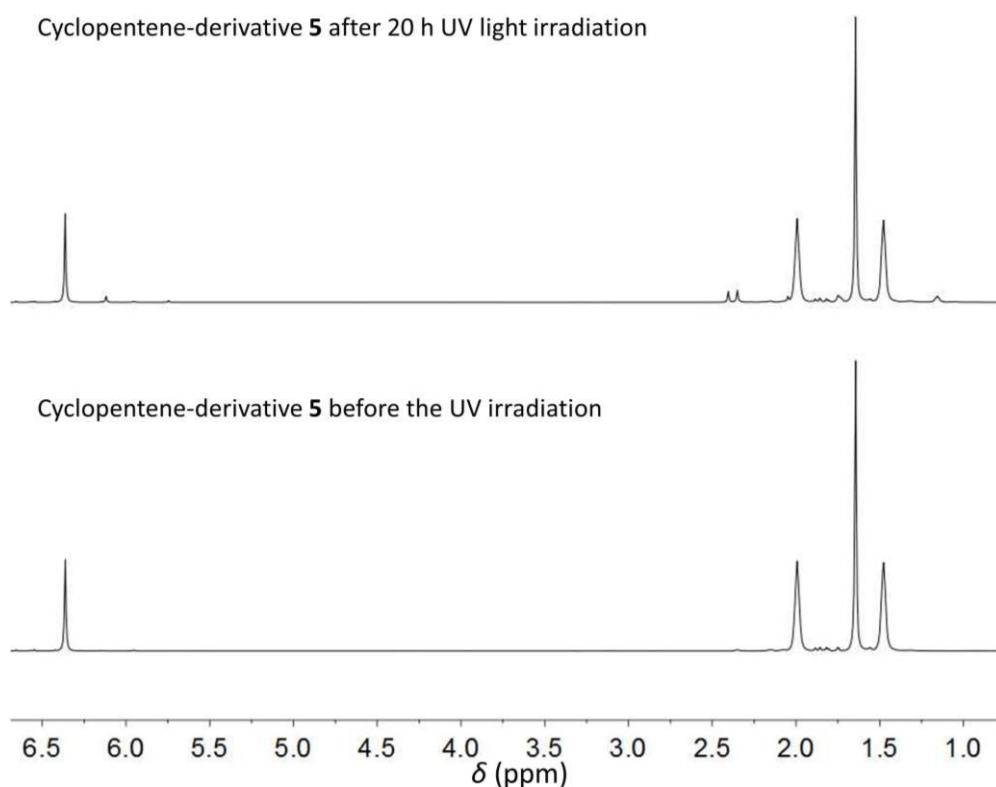


Figure 105: Irradiation experiment (**5**) monitored *via* ^1H -NMR-spectroscopy (chloroform- d_3).

When observing the ^{13}C -NMR spectra, not large differences between the starting materials and the irradiated compounds were found. The expected shift of the reactive carbon atoms which build a new bond during the photocyclization within a change of the hybridization did not occur. Only a very small new peak appeared in the ^{13}C -NMR spectrum of the cyclohexene-bridged molecular switch (**5**) at 22.83 ppm, 0.3 ppm upfield shifted from the peak corresponding to the protons at positions 4 and 5. However, it does not confirm the switching reaction.

The dramatic colour change demonstrates that a reaction takes place in both samples. Unfortunately, the concentration of the formed product is not high enough to be detected by means of NMR-spectroscopy. The observed small new peaks cannot be securely assigned to the closed isomers of the molecular switches.

4.5.1.1. Conclusions (III)

Both organic molecular switches, the cyclopentene- (**1**) and the cyclohexene- (**5**) derivatives, were subjected to irradiation experiments and the results were compared with the theoretical calculations. The theoretical spectra calculated with TDDFT for the open state of the molecular switches, using the BP86 and the B3LYP functionals, were in good agreement

with experimental data, while those for the closed isomers were not as good. The reason of these differences could be explained by assuming that in the photostationary state a mixture of both states (open and closed) is found. The calculations reveal that only the HOMO-LUMO transition (of low intensity) contributes to the cyclization reaction. The same was found for the ring-opening reaction, but the intensity of this HOMO-LUMO transition is much more intensive. The transition-dipole moments for the closed isomers are similar for both switches, while those for the open isomers are significantly larger for the cyclopentene-derivative (**1**) than for the cyclohexene-analogous (**5**). As a consequence, a higher efficiency of this excitation is found for the derivative **1**. From a scan of the potential energy surface (PES) of the ground state and the first excited singlet state it could be seen that there are no significant differences between both switches, although the thermal reaction barriers are slightly lower for **5**. In the ground state, the activation barriers for the ring-closure and ring-opening are considerably larger than in the first excited state, also both isomers are thermally stable at room temperature. In the first excited state the reaction barriers are strongly reduced and the activation barrier for the ring-opening reaction is much higher than for the ring-closure reaction. Therefore, it can be confirmed that the switching properties do not change significantly when comparing the cyclohexene- (**5**) and the cyclopentene- (**1**) derivatives.

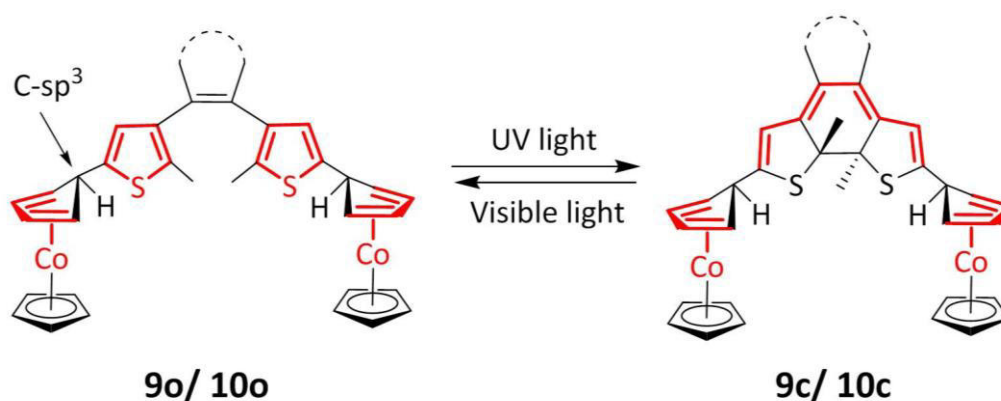
4.5.2. Irradiation experiments with the metal complexes 9-14, 17, 18

4.5.2.1. Irradiation experiments with the cobalt complexes 9-14

In the course of this work, cobalt sandwich complexes which are directly attached to the dithienylethene core were synthesized. These sandwich complexes contain cobalt atoms in different oxidation states. In order to get a deeper insight in the role of the metal centers in stimulating or hampering the formation of the carbon-carbon single bond between the thiophene units upon irradiation, the diamagnetic Co(I) and Co(III) sandwich complexes were also subjected to irradiation experiments. Additionally, it might be of interest that not only the metallocenes linked to the dithienylethene core *via* a direct interaction of the π -bonds exert a strong influence, but also the hybridization of the carbon atom connecting the sandwich unit to the molecular switch core is important to the reversible switching reaction.

Irradiation experiments with the Co(I)-complexes 9 and 10

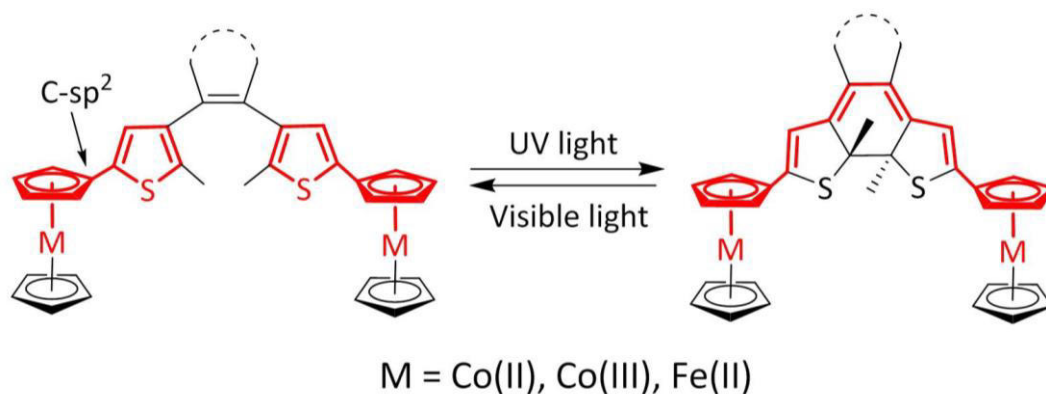
In complexes **9** and **10** the cobalt center is found in oxidation state +1, and it is only η^4 -coordinated to the Cp-ring which is bound to the molecular switch unit (Scheme 25).



Scheme 25: Switching reaction of Co(I)-complexes **9** and **10**. The π -system (red) is interrupted by a sp^3 carbon atom; the cobalt centers are not direct connected to the switching core.

This interruption of the π -conjugated system (Scheme 25), which considerably reduces the electron coupling of the cobalt centers with the switching core, is expected to play an important role in the switching reaction.

In the other metallocene complexes (Co(II), Co(III), Fe(II)) the metal centers are η^5 -coordinated to both Cp-ligands. Therefore, they are connected to the switching core by a conjugated π -system (Scheme 26) and the electron density of the metal center could exert an influence in the switching reaction.



Scheme 26: Switching reaction of the metallocene complexes. The π -system (red) is not interrupted by a sp^3 carbon atom as in the former case; the metal centers are direct connected to the switching core.

Cobalt(I)-complexes **9** and **10** were irradiated using an TL-lamp (366 nm, 8 W, r.t.) and the process was monitored by recording UV-vis spectra (Figure 106).

The visible region of the spectra was dominated by the absorption of the cobalt(I) sandwich units (red in the solid state). The highly diluted solutions used for the photoreactions were yellow coloured and after the irradiation with UV light the colour of both solutions turned red. After two minutes of irradiation the maxima around 400 nm increased and a new maximum at 468 nm for complex **9** and at 465 nm for complex **10** appeared. 90 sec later the broad maximum about 465 nm has superimposed the maximum around 400 nm. This behaviour of complexes **9** and **10** indicates that the irradiation with UV light resulted in a photocyclization.

The back reaction was induced by irradiating the solutions with visible light using a 40 W light bulb. This reaction occurred much slower than the cyclization reaction, taking from one to two hours.

The term “fatigue” is intrinsically linked to the term “cycle number”, which can be defined as the number of photochromic cycles (closing-opening) under certain conditions at which the absorbance of the one of the isomers decreases to 80 % respect to the first cycle.^[24]

Considering these prerequisites, the cyclopentene-complex **9** underwent four irradiation cycles while the cyclohexene-complex **10** underwent only two cycles. The new maximum at 465 nm did not completely disappear and after three cycles the absorption at this wavelength was more than 20 % larger than the absorption after the first cycle (**10**) (Figure 106, right bottom). Therefore, it can be concluded that the resistance to fatigue for the cyclopentene-derivative **9** is better than the resistance to fatigue of the analogous cyclohexene-derivative **10**.

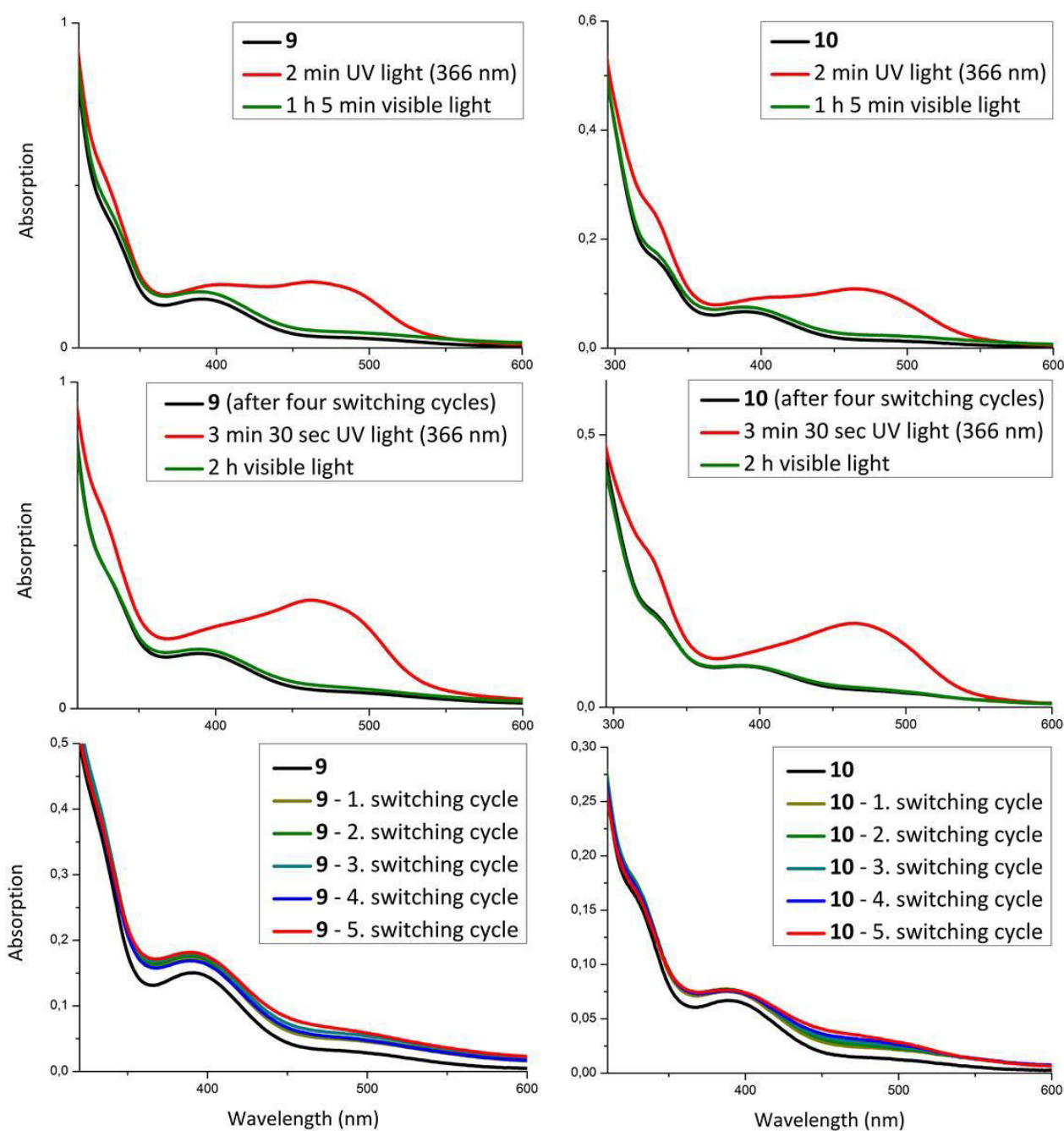


Figure 106: Irradiation experiments (366 nm, visible light) monitored *via* UV-vis spectroscopy in hexane. Left: complex **9** ($9.43 \cdot 10^{-5}$ M, $d = 1$); right: complex **10** ($8.46 \cdot 10^{-5}$ M, $d = 1$).

4. Results and Discussion

Table 24: UV-vis absorption spectroscopic data for complexes **9** and **10** in hexane.

λ , nm (ϵ , $M^{-1} \text{ cm}^{-1}$)		
	Open Isomer	PSS (2 min irradiation UV light)
9	220; 250; 334 (sh, 3477); 390 (1697)	220; 250; 329 (sh, 5302); 400 (2015); 468 (2121)
10	220; 242; 301 (sh, 4492); 332 (sh, 1891); 392 (827)	220; 245; 265; 302 (sh, 5083); 328 (sh, 2955); 403 (1111); 465 (1217);

* sh = shoulder, PSS = photostationary state

The irradiation experiments were repeated using ethanol as solvent. The reversible reaction took place but it was not as fast as in hexane, and it was observed that the fatigue was faster, especially in the case of the cyclopentene derivative **9**. Examples exist where the ability of ethanol to form hydrogen bonds with the substituents at the positions 5 and 5' of the thiophene rings has been observed to exert an influence on the switching reaction,^[235] however, this time it cannot be confirmed. In 2012 Meng *et al.*^[236] published a theoretical study confirming that the polarity of the solvent affects the electronic structures of the excited states, although it has only little influence on the ring closure reaction in the ground state. They concluded that the polar solvents contribute to the stabilization of the parallel conformer (the one which is not able to switch),^[70] hindering the ring closure reaction.

Switching reaction monitored *via* $^1\text{H-NMR}$ spectroscopy

After confirming that the Co(I)-complexes **9** and **10** undergo the switching cycle by means of UV-vis spectroscopy, it was attempted to monitor it *via* NMR-spectroscopy. Highly concentrated solutions of both complexes were prepared in pyridine- d_5 and irradiated with UV light (8 W, 366 nm, r.t.) in the NMR-tubes. Unfortunately, after more than 18 h irradiation, no colour change was observed and no new signals indicating the photocyclization reaction were visible, either in ^1H - or in ^{13}C -NMR.

Irradiation experiments with the Co(III)-complexes **11** and **12**

Complexes **11** and **12** belong to the class of complexes represented in scheme 26. The sandwich units are bound to the molecular switch within a sp^2 carbon atom. Therefore, when the molecular switch undergoes the ring closure reaction, the metal centers are both connected to each other by the conjugated π -system of the molecular switch.

The Co(III)-complexes **11** and **12** were subjected to irradiation with UV light employing different organic solvents and light sources. Different results were observed. In some cases the photocyclization did not take place or the complex decomposed after a long exposure to UV light. In other cases, only the ring closure reaction was observed.

In a first attempt, the cyclopentene-complex **11** was solved in acetonitrile and irradiated with black light (~400 nm, 75 W). A little reversible change in the UV-vis spectrum was observed but it was so small that it was taken only as an indication.

The same complex (**11**), also dissolved in acetonitrile, was irradiated with a TL-lamp (350 nm, 8 W, r.t.) and the absorption decreased through the whole range excepting for the minimum at 342 nm, where the absorption increased (Figure 107). Afterwards, the ring opening reaction was induced by irradiating the sample with a 532 nm LED lamp. The absorption increased again, almost reaching the starting absorption values. An isosbestic point was observed at 305 nm. Complex **11** underwent two switching cycles. However, the yield of the ring closure reaction was poor.

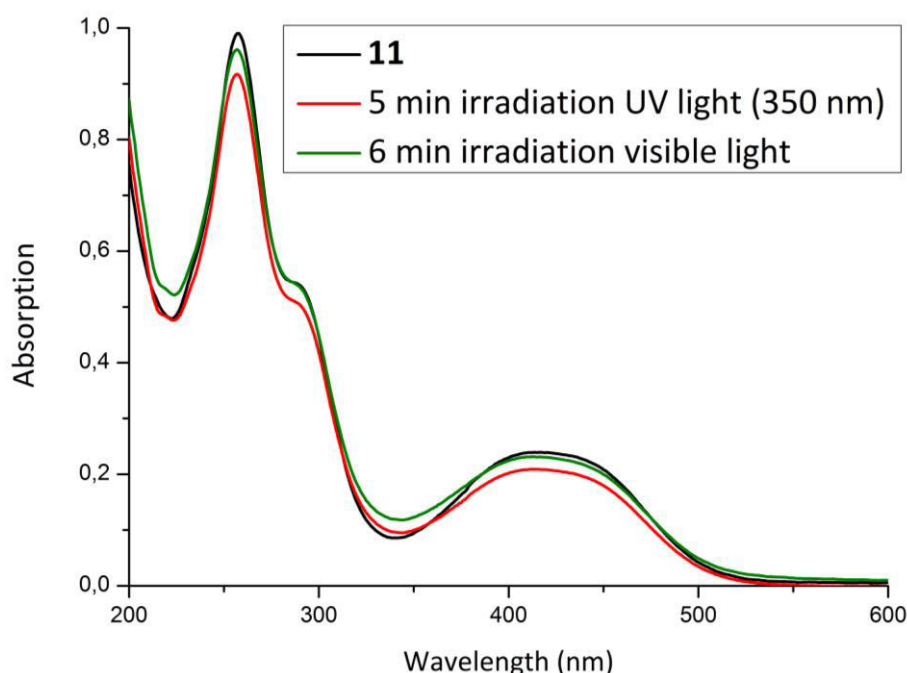


Figure 107: Irradiation experiments (350 nm, visible light) with the cyclopentene-Co(III)-complex **11** solved in acetonitrile ($d = 1$), monitored *via* UV-vis spectroscopy.

By comparing the UV-vis spectrum of this complex with the dinuclear cobaltocenium diamagnetic complexes of Pagels *et al.*^[182] it was determined that the first maximum by 260 nm corresponds to a π - π^* transition of the organic molecular switch, the shoulder at

4. Results and Discussion

297 nm, to a Cp-Co transition and the second maximum at 410 nm, to a weak d-d transition of cobaltocenium (Figure 107).

In an attempt to optimize the switching reaction, complex **11** was dissolved in acetonitrile and a LED UV lamp with a wavelength of 385 nm was employed to induce the ring closure reaction. As in the former irradiation experiment, the absorption decreased in the whole range, except for the minimum at 342 nm and an isosbestic point appeared at 305 nm. The ring opening reaction was carried out by irradiating the sample with 532 nm. This time the complex underwent two switching cycles, but the yield of the photocyclization was also poor (Figure 108).

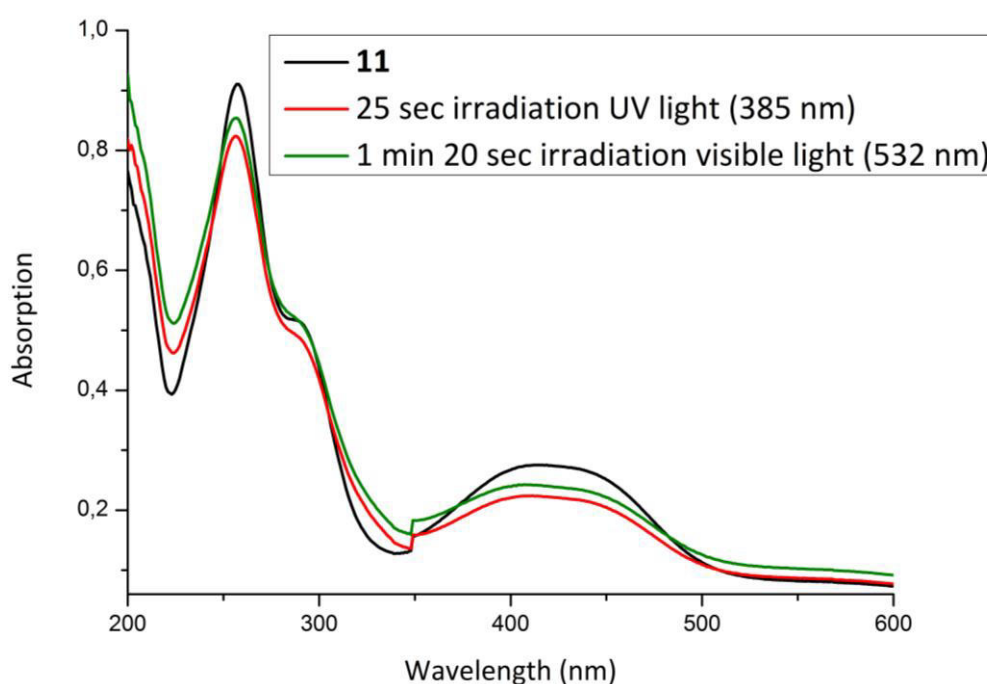


Figure 108: Irradiation experiments (385 nm, 532 nm) with the cyclopentene-Co(III)-complex **11** solved in acetonitrile, monitored *via* UV-vis spectroscopy ($3.13 \cdot 10^{-6}$ M, $d = 1$).

In the next step in the optimization of the photocyclization, ethanol was chosen as solvent and both Co(III)-complexes **11** and **12** were investigated (Figure 109).

When the cyclopentene-derivative **11** was irradiated with a TL-lamp (366 nm, 8 W, r.t.), the UV-vis spectra presented the same evolution as in the former experiments: the absorption decreased within the whole range except for the minimum at 342 nm, and not only the expected isosbestic point at 305 nm appeared, but also two new isosbestic points at 379 nm and 500 nm. In addition, the maximum found in the visible range was slightly blue shifted respect to the initial situation (Figure 109). This time the difference between the initial absorption and the absorption after the irradiation was much more pronounced, indicating

an improvement of the yield of the photocyclization. On the other hand, when the ethanol solution of **11** was irradiated with visible light using a work spot light in order to induce the ring opening reaction, the absorption did not increase again, but continued slightly decreasing.

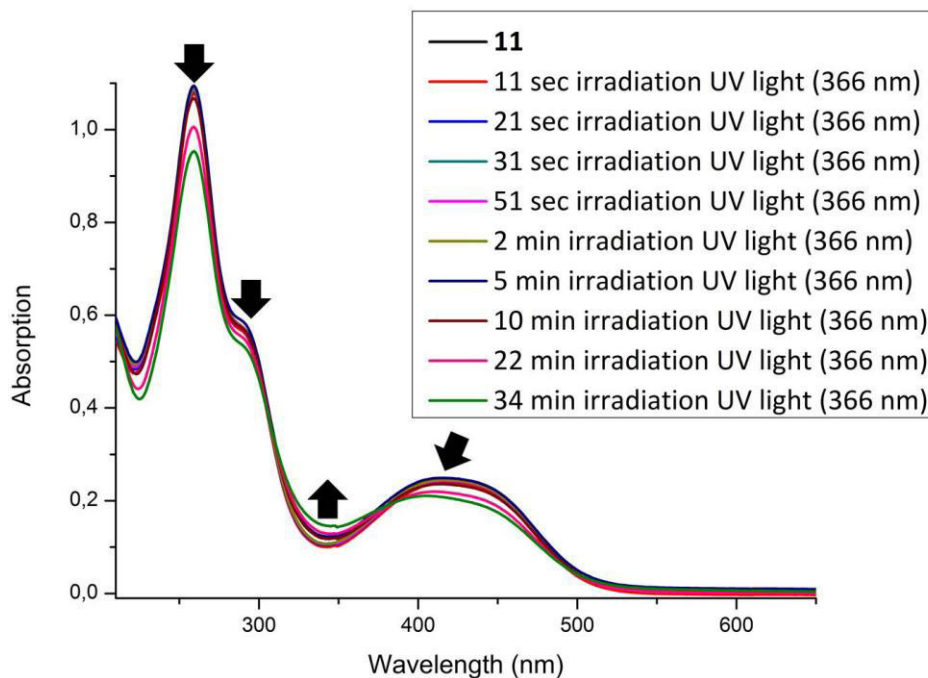


Figure 109: Irradiation experiments with UV light (366 nm) with the cyclopentene-Co(III)-complex **11** solved in ethanol, monitored *via* UV-vis spectroscopy ($1.10 \cdot 10^{-4}$ M, $d = 0.2$ cm).

The same experiments were repeated with the cyclohexene-complex **12**. Contrary to what would be expected, the presented behavior was not the same as for complex **11**. The changes in the absorption values did not follow a defined tendency and there were no isosbestic points indicating the compound was not decomposing. The ring opening reaction did not take place when the solution was irradiated with visible light.

Another difference with respect to complex **11** is the behavior of the cyclohexene-derivative **12** in the photostationary state. In the figure 110 the UV-vis spectra of the complex **12** before (black) and after (different colours) the irradiation with UV light are displayed. It should be noted that the absorption did not increase through the whole range after the irradiation, as did the absorption of complex **11**, but it decreased in the UV region and increased in the visible region. After 30 sec irradiation, six different spectra were recorded and before each measurement the solution was shaken. It could be observed that the spectra differ from each other (Figure 110). However, an isosbestic point at 307 nm which is

4. Results and Discussion

not recognized for the starting complex confirms that the complex **12** was not decomposing. The absorption changed reversibly in both directions, indicating a chemical equilibrium. This phenomenon was already observed and discussed for the organic molecular switch **5** (see section 4.5.1, p. 127).

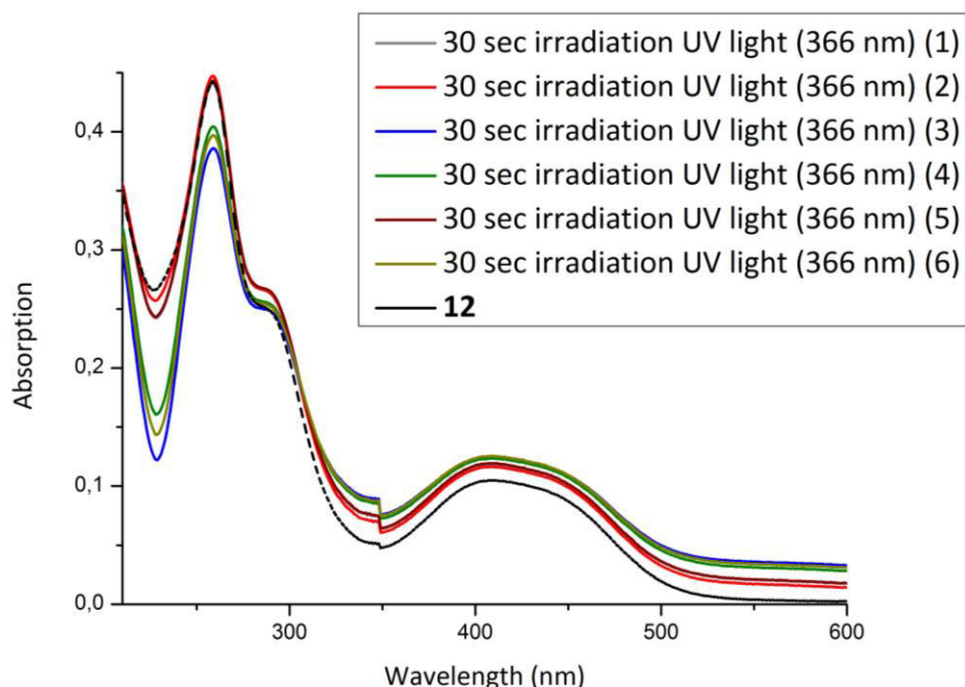


Figure 110: Irradiation with UV light (366 nm) of cyclohexene-Co(III)-complex **12** solved in ethanol, monitored via UV-vis spectroscopy ($7.5 \cdot 10^{-5}$ M, $d = 0.2$ cm).

It could be thinkable that this phenomenon and the structural modification undergone by the paramagnetic cyclohexene-Co(II)-complex **14** observed in ^{13}C -NMR (section 4.2.1, p. 82) are related. However, in this case the system changes in both directions in a very short period of time, while the evolution observed for complex **14** took hours and a backreaction could not be confirmed. Furthermore, complex **14** was not irradiated with UV light before the NMR-spectroscopic measurements. Therefore it cannot be concluded that these phenomena are related.

Finally, a last irradiation experiment was carried out. This time, complexes **11** and **12** were dissolved in acetone in a higher concentration than in the former irradiation experiments. The solutions were irradiated while stirring with light of 366 nm (8 W). While the cyclopentene-complex **11** did not undergo the photocyclization, at least in an appreciable yield, the cyclohexene complex **12** did undergo one complete switching-cycle (Figure 111). After inducing the photocyclization, the absorption decreased in the maximum at 407 nm, but it increased in the minimum at 345 nm and above 500 nm, which coincides with the

former irradiation experiments. The isosbestic points observed at 322 nm, 375 nm and 490 nm indicate that the complex is not decomposing upon irradiation. After the irradiation with visible light, the absorption of the large maximum increased again.

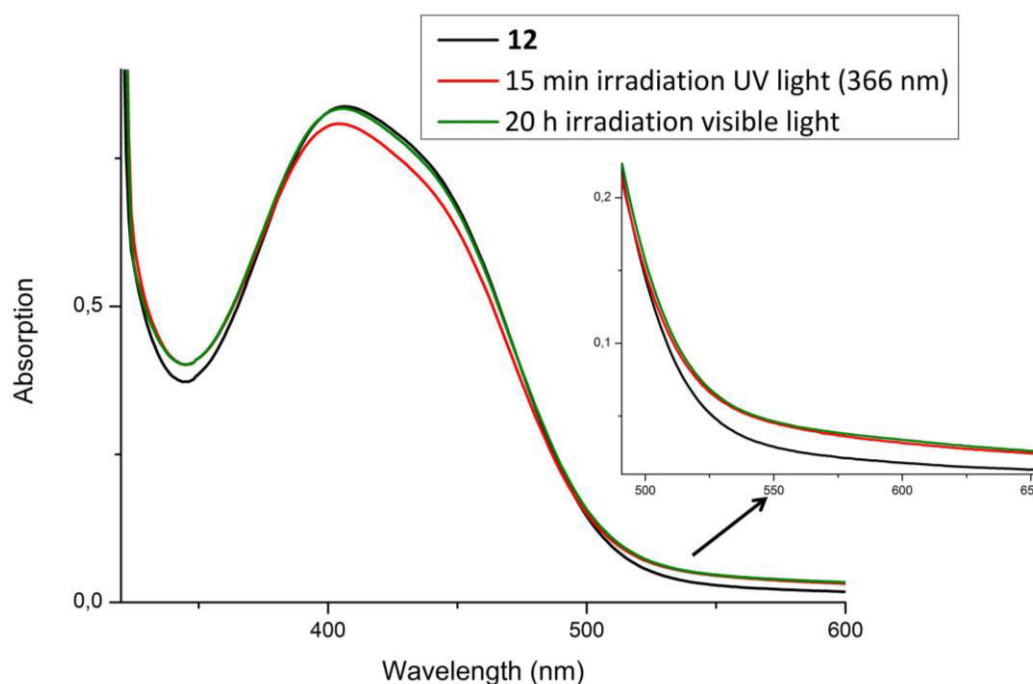


Figure 111: Irradiation experiments (366 nm, visible light) with the cyclohexene-Co(III)-complex **12** solved in acetone, monitored *via* UV-vis spectroscopy ($1.1 \cdot 10^{-4}$ M, $d = 1$).

Switching reaction monitored via $^1\text{H-NMR}$ spectroscopy

The cyclopentene-complex **11** was solved in acetonitrile- d_3 and the solution was irradiated with a LED lamp (385 nm, r.t.) for 3 h 30 min. The yellow solution turned brown during the process, but no new signals indicating the closed isomer of the molecular switch appeared in the $^1\text{H-NMR}$ spectrum.

Irradiation experiments with the paramagnetic Co(II)-complexes **13** and **14**

The cyclopentene-Co(II)-complex **13** and cyclohexene-Co(II)-complex **14**, both paramagnetic, are the target complexes of these doctor-thesis. With the aim of studying the magnetic coupling between the unpaired electrons of the cobalt centers when the molecular switch is found in the closed state, the switching reaction should be optimized and the closed isomer isolated. When the molecular switch is in the open state, the cobalt centers are not connected within a conjugated π -system, therefore no magnetic coupling was expected.

Due to the difficulty in exactly weighing small quantities with the standard Schlenk-technique, only approximate concentrations of the solutions of the Co(II)-complexes will be

given. As a consequence, the molar absorptivity coefficient ϵ values cannot be calculated and the next UV-vis spectra only offer qualitative information.

These complexes belong to the class represented in scheme 26, the sandwich units are bound to the molecular switch by an sp^2 carbon atom. When the molecular switch is found in the closed state, the cobalt centers are both connected to each other and to the molecular switch by a conjugated π -system. Therefore, the electron density of the metal center is expected to exert an influence in the switching reaction.

The first irradiation experiments were carried out with the cyclopentene-complex **13**. Before the exposure to the UV light (Figure 112, black) the complex was dissolved in pentane. The obtained UV-vis spectrum was difficult to assign to different maxima, so it was divided in three different parts. By comparing this complex with the paramagnetic dinuclear complexes of Pagels *et al.* ^[181] it was possible to relate transitions to each region. Below 300 nm π - π^* , M-Cp, M- π^* and π -M transitions could be found, being π and π^* orbitals of the organic molecular switch. Between 300 and 500 nm, M-Cp and d-d transitions of cobaltocene could be found. Between 500 and 700 nm, only M- π^* and d-d transitions were identified.

The solution was irradiated in the same quartz cuvette with a TL-lamp (350 nm, 8 W, r.t.) for 1 h. The absorption decreased in both maxima and the shoulder in the UV region and increased in the minimum about 440 nm (Figure 112, red). Afterwards the solution was irradiated again, but this time a LED lamp (532 nm) was employed. In order to avoid the warming of the solution, the whole system (the cuvette and the lamp) was cooled with an ice bad. After 1 h 45 min, the absorption in the maxima found in the UV region increased again, but the absorption at the shoulder and in the visible region did not change (Figure 112, green). Although the quantum yield is not as good as desired, these UV-vis-spectra show that the reversible switching reaction takes place.

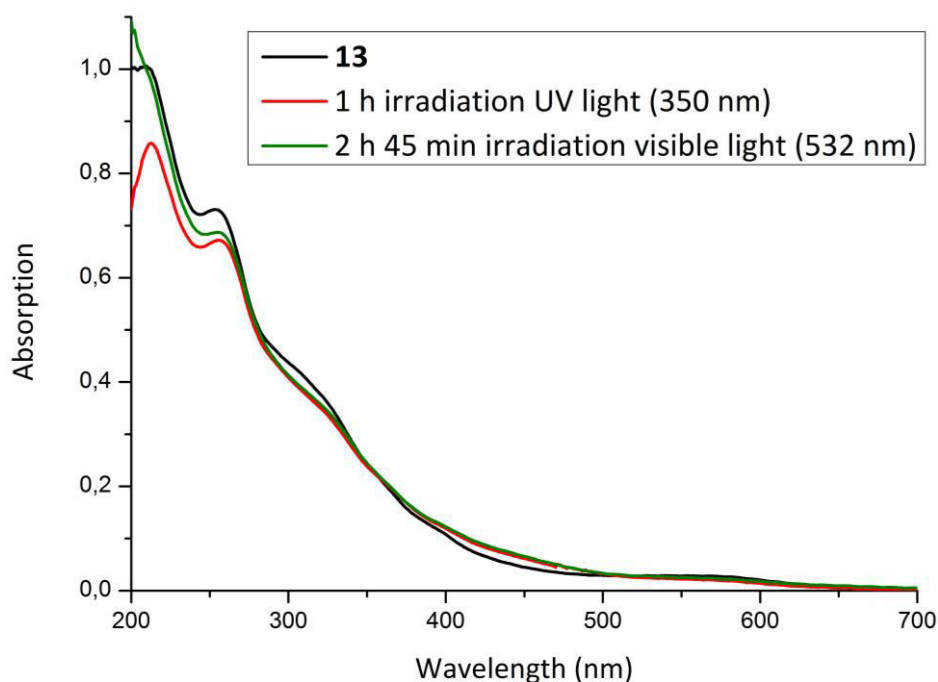


Figure 112: Irradiation experiments (350 nm, visible light) with the cyclopentene-Co(II)-complex **13** solved in pentane, monitored *via* UV-vis spectroscopy ($1.89 \cdot 10^{-6}$ M, $d = 1$).

When a more intensive lamp was employed for the irradiation (a mercury medium pressure lamp TQ-150, 365 nm, 25 W), the reaction times were shorter. The absorption in the maximum at 257 nm decreased while the absorption in the visible region increased, as in the former irradiation experiment. Nevertheless, this time the appearance of a new maximum at 410 nm was appreciated (Figure 113). As the evolution of the absorption values with the irradiation does not completely coincide with the spectra presented in figure 112 and the back reaction did not take place when irradiating with visible light (532 nm), a partially decomposition of the complex due to the high intensity of the irradiation cannot be excluded.

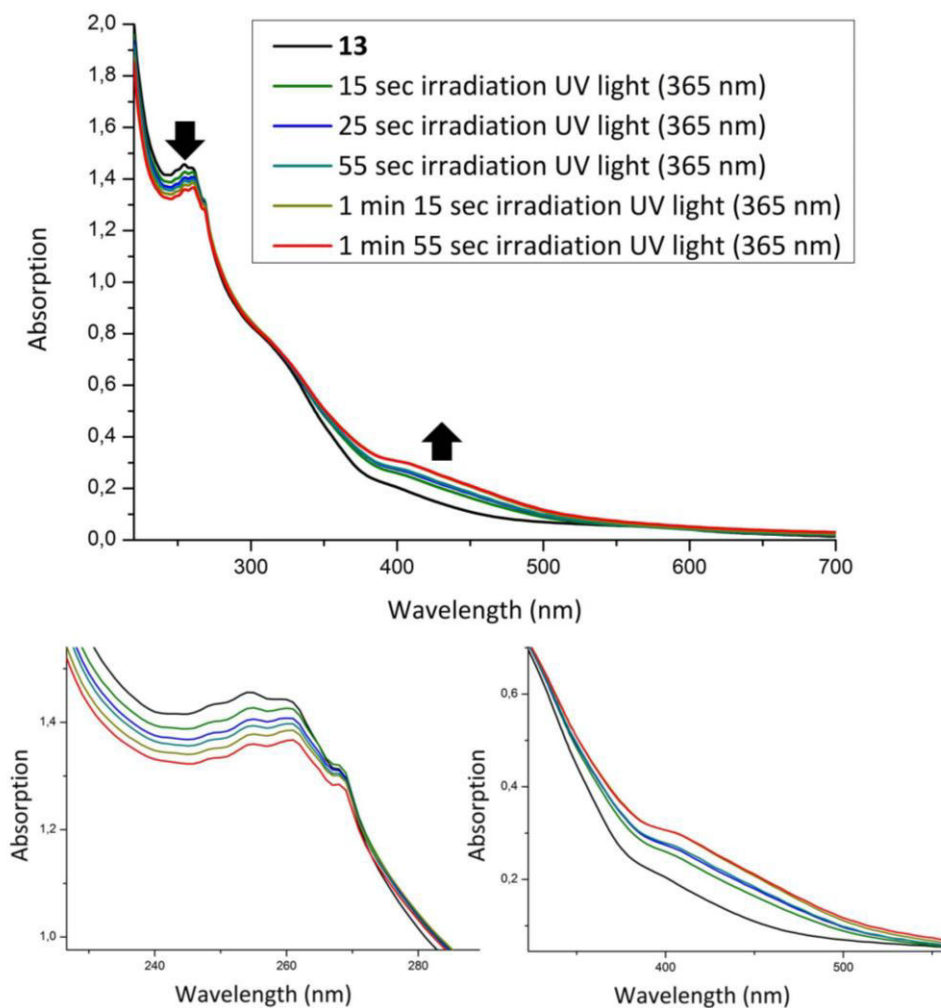


Figure 113: Irradiation experiments (mercury lamp TQ-150) with the cyclopentene-Co(II)-complex **13** solved in pentane, monitored *via* UV-vis spectroscopy (aprox. $4 \cdot 10^{-6}$ M, $d = 1$).

Consequently, with help of a XBO lamp 450 W/4 with a monochromator, where the intensity could be adjusted, a series of irradiations experiments were carried out. It was attempted to induce the photocyclization varying the wavelength from 320 nm to 400 nm in 10 nm intervals. An example is presented in figure 114: It can be seen that a reaction is taking place, and the isosbestic points coincide with the observed in figure 113. For the ring opening reaction wavelengths from 400 nm to 590 nm were used. However, in no case a ring closure reaction was observed.

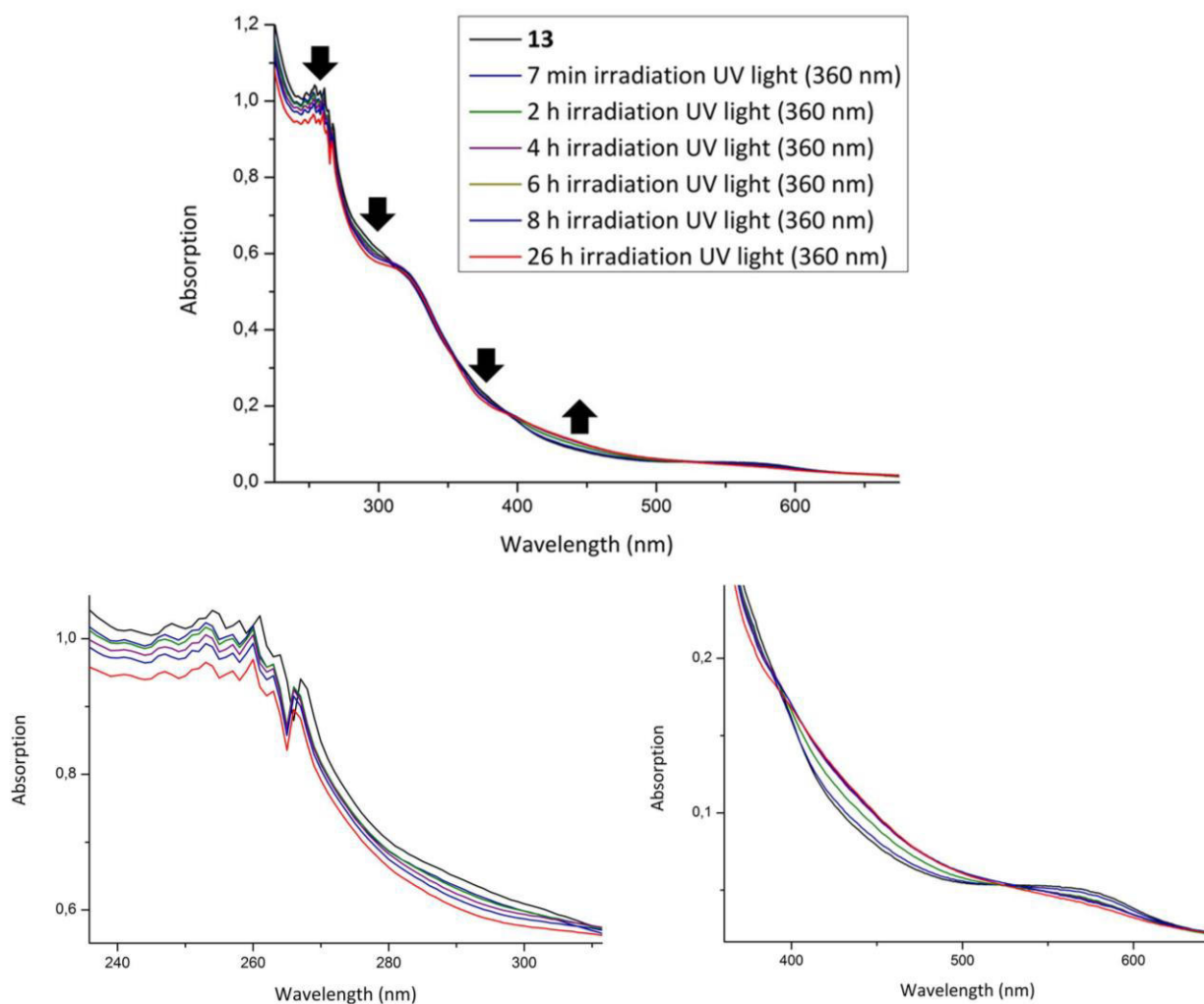


Figure 114: Irradiation experiments (XBO lamp 450 W/4 with a monochromator) with the cyclopentene-Co(II)-complex **13** solved in pentane, monitored *via* UV-vis spectroscopy (aprox. $3 \cdot 10^{-6}$ M, $d = 1$).

In a last attempt, complex **13**, solved in hexane, was irradiated with a laser of a wavelength of 374 nm, varying the intensity from 0.17 mW to 4 mW. It was expected that the compound would decompose almost immediately, as it presumably started to decompose when the TQ-150 lamp was employed. However, it did not occur. The complex apparently did undergo the photocyclization although the yield of the reaction was very poor.

It is worth to emphasize a big difference among the different lamps used to induce the switching cycle: the irradiated surface. While the TL- and the mercury lamps irradiate the whole surface of the cuvette where the solution is found, the XBO lamp and the laser irradiate only one point. Taking into account that the solutions were not stirred during the irradiation processes, it is expected for the reactions to take place very slowly or not take place at all. It explains why compound **13** did not react when the laser was used, while it presumably started to decompose when the Q-150 lamp (less intense) was used.

4. Results and Discussion

Finally, the UV-vis spectrum of the cyclohexene-complex **14** was recorded in hexane (Figure 115). As expected, it is similar to the UV-vis spectrum of complex **13** (Figure 112).

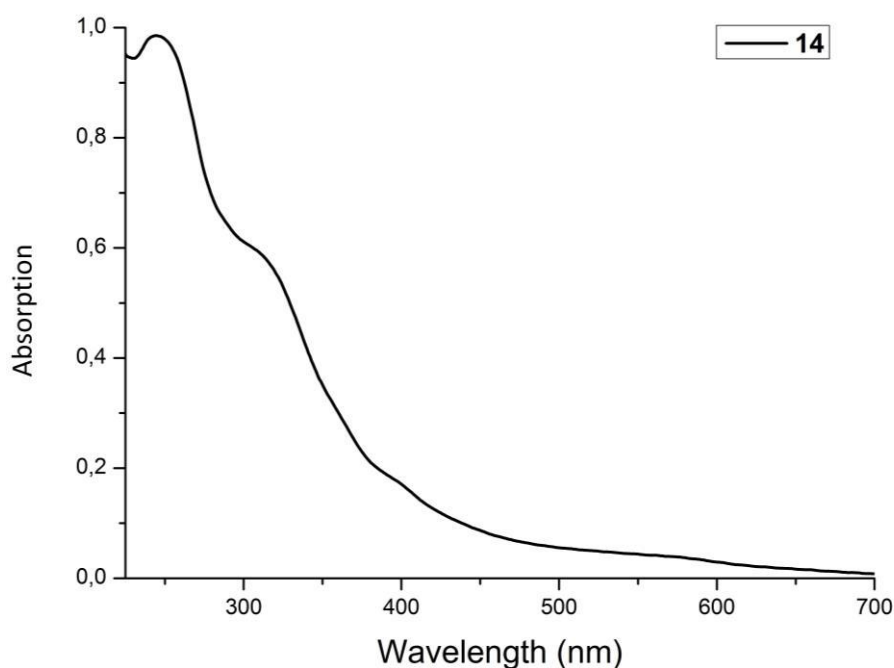


Figure 115: UV-vis spectrum of cyclohexene-Co(II)-complex **14** in pentane (aprox. 10^{-6} M, $d = 1$).

Complex **14** was irradiated with the TL-lamp (366 nm, 8 W, r.t.). At first sight no reaction was observed. It was necessary to prepare a more concentrated solution in order to be able to see that during the irradiation the absorption in the visible region increased (Figure 116).

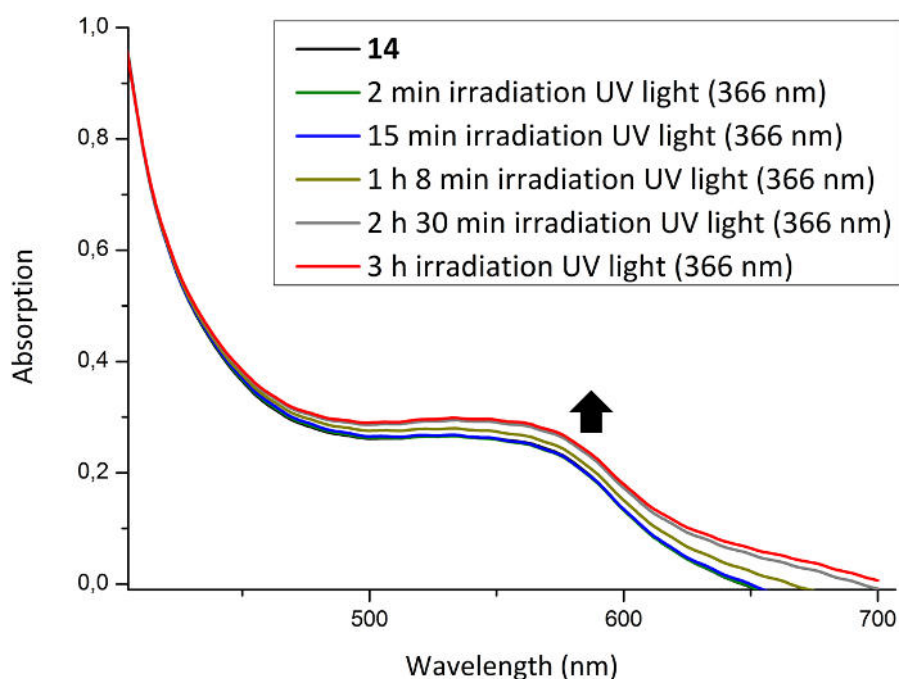


Figure 116: Irradiation experiments (366 nm) with the cyclohexene-Co(II)-complex **14** solved in pentane, monitored *via* UV-vis spectroscopy (aprox. 10^{-6} M, $d = 1$).

Unfortunately, the reverse reaction did not take place when the solution was irradiated with visible light.

4.5.2.2. Irradiation experiments with the iron complexes **17** and **18**

Both ferrocene complexes **17** and **18** were subjected to irradiation experiments in order to study their behaviour as molecular switches. Different organic solvents and light sources were employed.

In a first attempt, the complexes under study were solved in hexane and both solutions were irradiated with a TL-lamp (366 nm, 8 W).

According to Gordon *et al.*,^[237] who studied the behavior of different metallocenes in UV-vis spectroscopy, and by comparing with the spectrum of the organic molecular switch **1** (Figures 96 and 97), the transitions shown in figures 117 and 118 could be identified. The two maxima and the shoulder found in the UV region could be a mixture of π - π^* transitions of the organic molecular switch and two different Cp – M forbidden transitions of ferrocene. The shoulder at 350 nm and the wide maximum at 450 nm represent d-d transitions of ferrocene (Table 25).

The orange complex **17** solution turned pink when irradiated with UV light (366 nm, 8 W, r.t.). After the first minutes the change in UV-vis spectrum was very small but the followed tendency could be identified. After 1 h 49 min irradiation a significant amount of solvent was evaporated and, as a consequence, the absorption increased in the whole spectra. However, after this increase the UV-vis evolution could be more clearly seen: the absorption in both maxima and shoulder in UV region decreased during the irradiation while the opposite was true for the absorption in visible region (Figure 117).

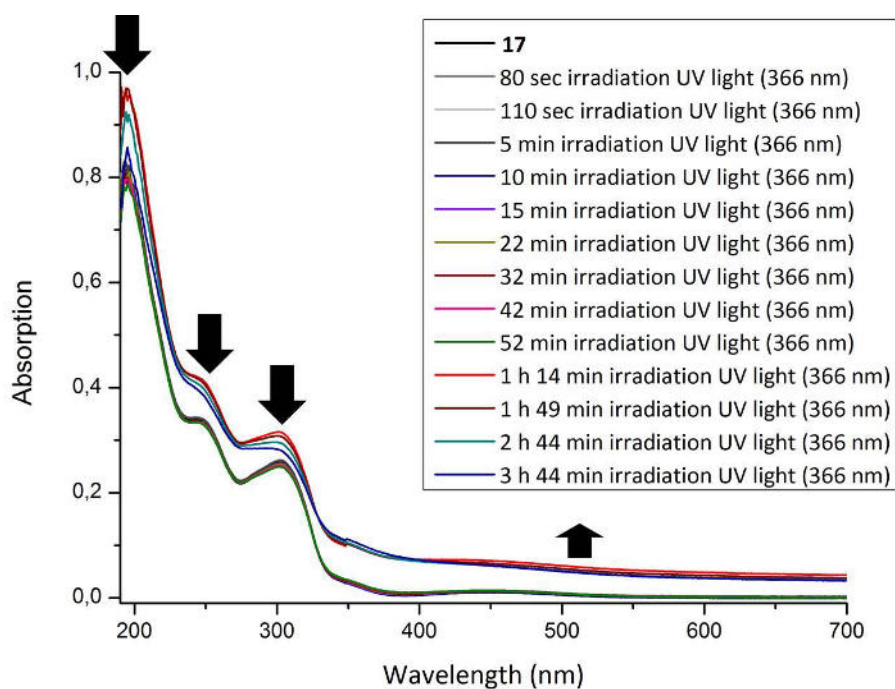


Figure 117: Irradiation of complex **17** in hexane with UV light ($6.85 \cdot 10^{-5}$ M, $d = 1$ cm).

The same experiments were carried out with the cyclohexene-complex **18** and, as in the case of the former complex, the orange solution turned pink during the irradiation with UV light (Figure 118).

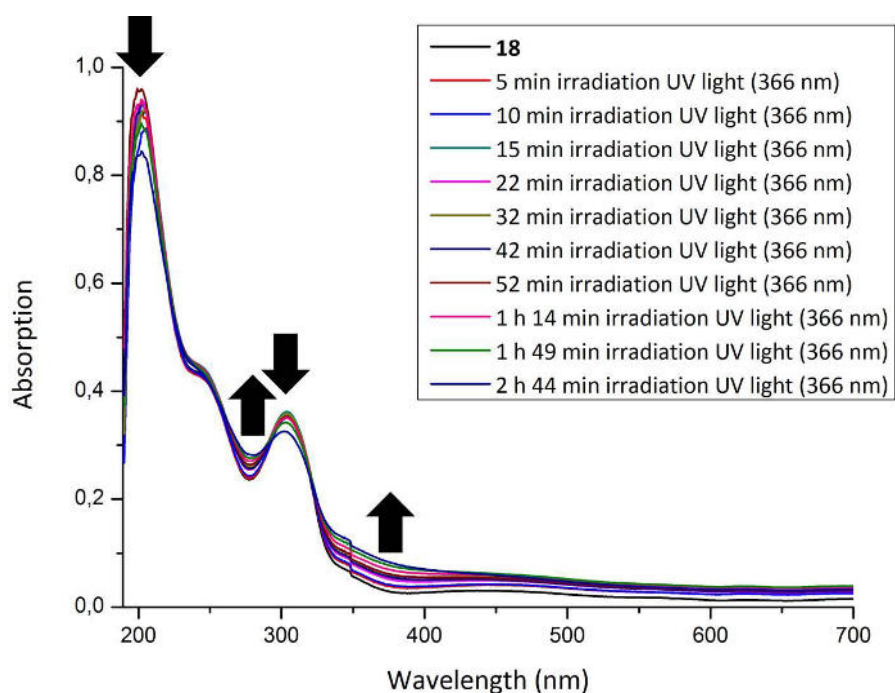


Figure 118: Irradiation of complex **18** in hexane with UV light ($7.47 \cdot 10^{-5}$ M, $d = 1$ cm).

The first measurements did not follow the expected tendency: the absorption in the maximum at 200 nm did not decrease but it slightly increased. However, when the

irradiation with UV light continued, the absorption at this band decreased with respect to the initial state. The same occurred to the absorption of the band at 300 nm. On the contrary, the absorption at the minimum around 280 nm and in the visible region, increased (Figure 118).

For both irradiation reactions defined isosbestic points are visible, what indicates that only one product is being formed. Nonetheless, when the samples were irradiated with visible light no significant reaction was detected. Although the pink colour almost disappeared and the solutions presented an orange colour again, these observations were not supported by changes in UV-vis spectroscopy.

In order to reduce the reaction times, a mercury medium pressure lamp TQ-150 (366 nm, 25 W, r.t.) was employed to induce the photocyclization reaction of the cyclopentene-derivative **17** (Figure 119). As expected, the absorption of the transition bands in the UV region decreased, the absorption in the visible region increased and an isosbestic point was found at 326 nm. Furthermore, the reaction took place faster (figures 117-119), due to the high power of the employed UV light source, more than three times higher than in the case of the TL-lamp.

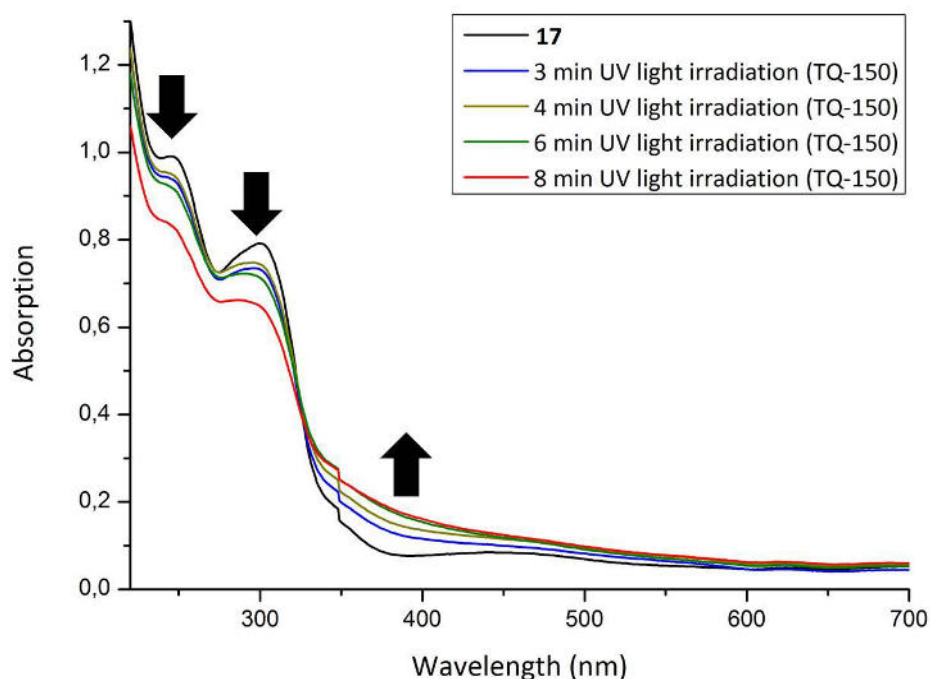


Figure 119: Irradiation of complex **17** in hexane with UV light ($5.4 \cdot 10^{-5}$ M, $d = 1$ cm).

4. Results and Discussion

In this case, the ring opening reaction was not observed when the sample was irradiated with visible light.

Other organic solvents, as THF or acetonitrile, different irradiation wavelengths (300 nm, 350 nm) and different UV light sources (Rayonet reactor, 365 nm, 16 W) were tested with similar results. In all cases the orange solution turned pink, but the absorption change in the visible region of the UV-vis spectra was not significant.

The colour alteration from orange to pink induced by the ring closure reaction seemed to be an unexplained phenomenon when looking at the visible region of the UV-vis spectra: no new transitions or significant shifts were visible. Nevertheless, in comparison with the absorption in the UV region, the absorption in the visible region of complexes **17** and **18** is very low. For this reason, more concentrated solutions were prepared in hexane and the irradiation experiments were repeated (Figures 120-123) using an TL-lamp (366 nm, 8 W, r.t.). Both solutions became light pink but the colour of the solution of complex **17** was more intensive than the corresponding solution of complex **18**. In both cases, the absorption increased through the whole visible range and this time a new maximum appeared around 560 nm, which represent the electronic interaction between the closed molecular switch and the ferrocene units (Table 25).

The analogous ethynylferrocene complex synthesized and investigated by Guirado^[78] (1,2-bis-(5'-ethynylferrocene-2'-methylthien-3'-yl)cyclopentene) presented a new maximum too, bathochromically shifted, when irradiated with UV light.

The assumption that the photocyclization took place by irradiating the samples with UV light was confirmed when the new maxima completely disappeared after irradiating the samples with visible light (Figures 120-123).

Table 25: UV-vis absorption spectroscopic data for complexes **17** and **18** in hexane.

λ , nm (ϵ , $M^{-1} cm^{-1}$)		
	Open Isomer	PSS
17	352 (sh, 2740); 449 (1185)	352 (sh, 3111); 449 (1333); 560 (325)
18	354 (sh, 3383); 450 (1555)	354 (sh, 3777); 450 (1851); 560 (251)

* sh = shoulder, PSS = photostationary state

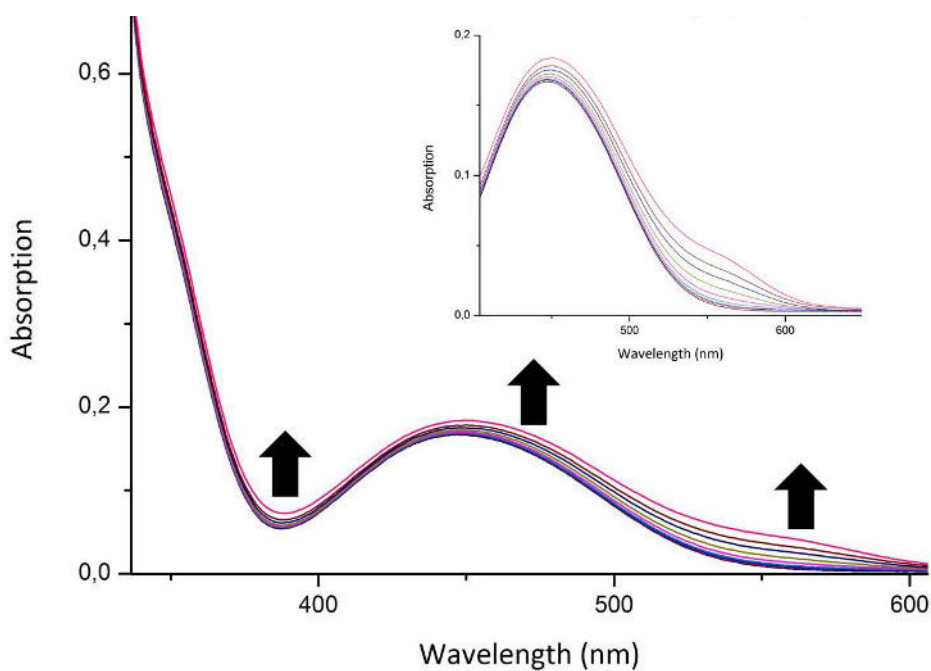


Figure 120: Irradiation of complex **17** with UV light in hexane ($1.35 \cdot 10^{-4}$ M, $d = 1$).

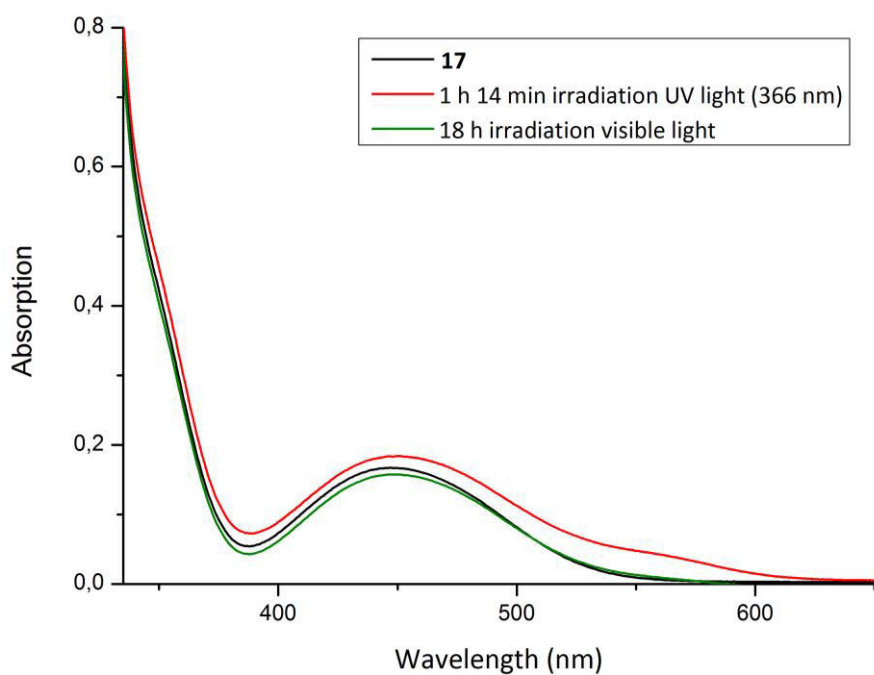


Figure 121: Switching cycle of complex **17** ($1.35 \cdot 10^{-4}$ M, $d = 1$) in hexane. Irradiation with UV light: 1 h 47 min; irradiation with visible light: 18 h

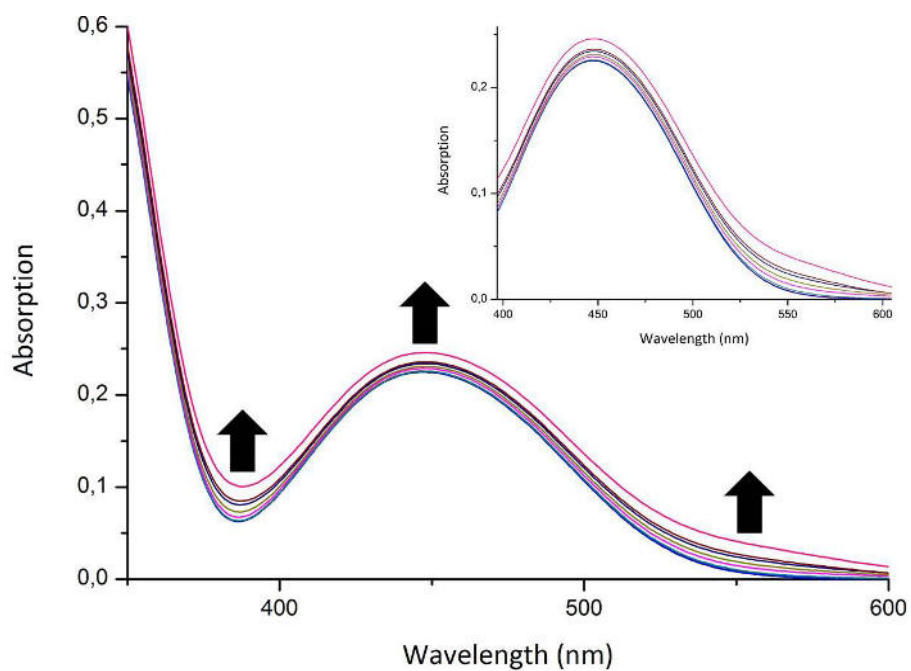


Figure 122: Irradiation of complex **18** with UV light in hexane ($1.33 \cdot 10^{-4}$ M, $d = 1$).

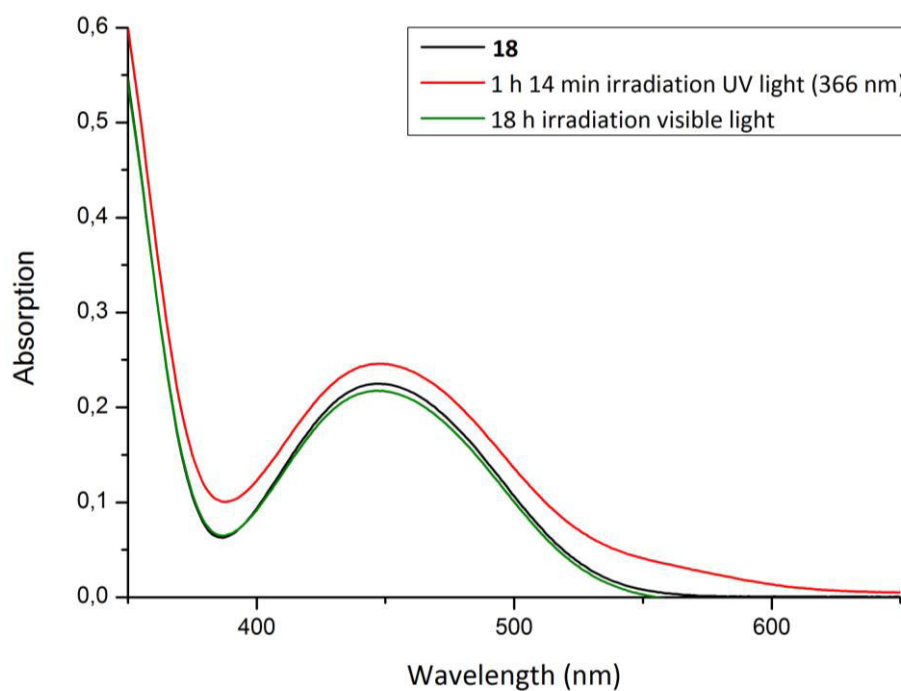


Figure 123: Switching cycle of complex **18** ($1.33 \cdot 10^{-4}$ M, $d = 1$) in hexane. Irradiation with UV light: 1 h 47 min; irradiation with visible light: 18 h.

Unfortunately, the resistance to fatigue of these complexes is not as good as desired. Only one switching cycle could be achieved for each complex.

Finally, theoretical UV-vis spectra were calculated. Two different possible structures for the antiparallel conformation were considered: the “in” and “out” isomers (see section 4.3.3). The obtained spectra are slightly different for both isomers, but it has to be kept in mind that in solution the metallocene moieties are not fixed in a certain position.

In all cases, not only the absorption in the UV region decreases, but a new maximum appears about 550 nm, which coincides with the former recorded spectra (Figures 120-123).

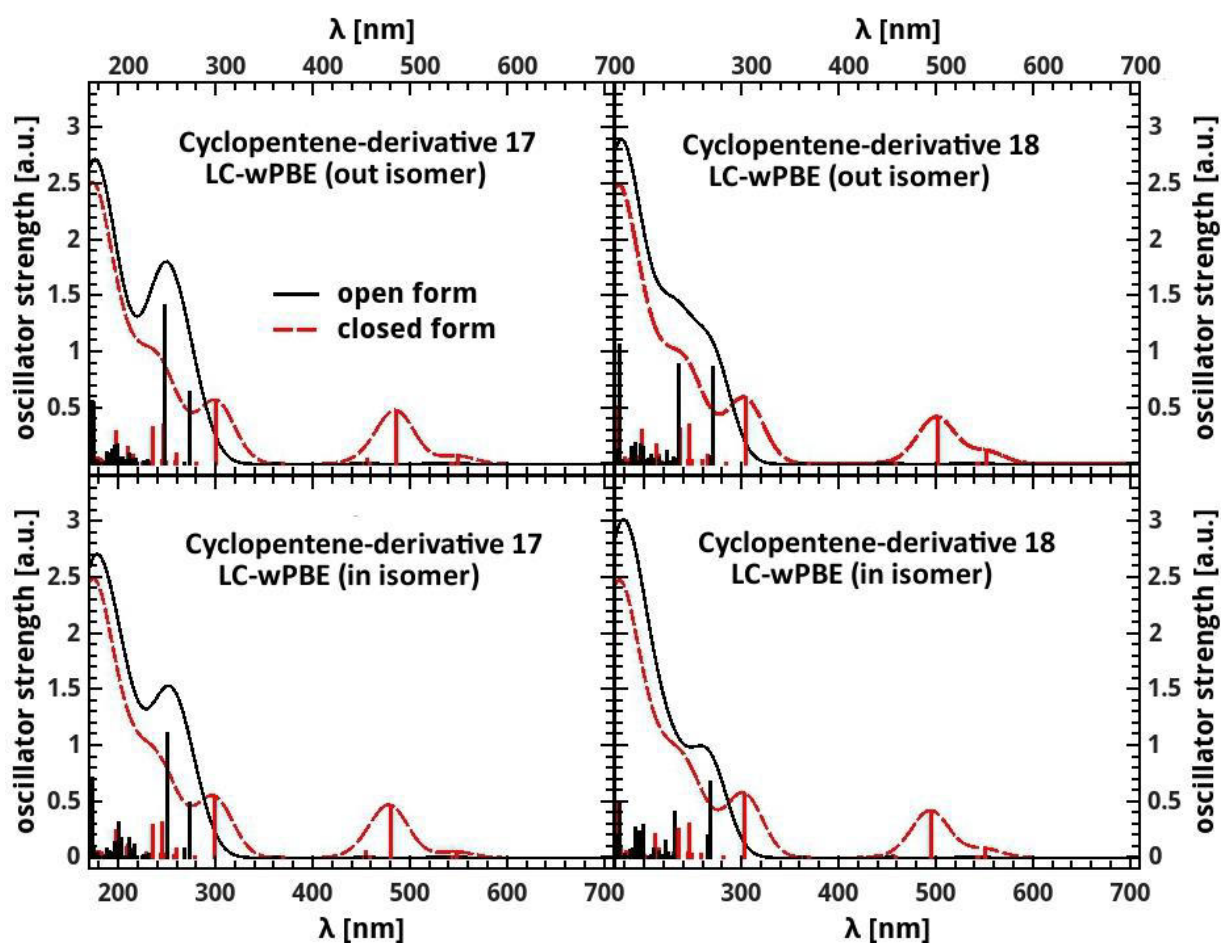


Figure 124: Calculated UV-vis spectra (Gaussian broadening with a half-width of 60 nm for the theoretical spectra) of compounds **17** and **18**. The spectra were calculated with LC- ω PBE (The stars denote the positions of the HOMO-LUMO transitions).

Switching reaction monitored *via* $^1\text{H-NMR}$ spectroscopy

Complexes **17** and **18** were solved in benzol- d_6 and the switching reaction was monitored *via* $^1\text{H-NMR}$ spectroscopy. After 5 h 30 min irradiation with a Rayonet reactor lamp (366 nm, 16 W, r.t.) and subsequent 35 h irradiation with a TL-lamp (366 nm, 8 W, r.t.), no new signals

appeared in the spectra. The starting and final $^1\text{H-NMR}$ spectra were exactly the same. Probably, the yield of the photocyclization was so poor, that the closed isomer could not be detected within this method.

Theoretical calculations

In order to understand the mechanism of the photocyclization, Torben Steenbock carried out the following theoretical Density Functional Theory (DFT) calculations employing the LC- ω PBE functional for single-point calculations and TDDFT calculations on structures optimized with BP86 (Basis set: def-TZVP).

The PES for the ferrocenyl-complex **17** (cyclopentene-derivative) as a function of the distance between the reactive carbon atoms participating in the switching reactions were calculated and compared with the PES for the analogous organic molecular switch **1** (Figure 125).

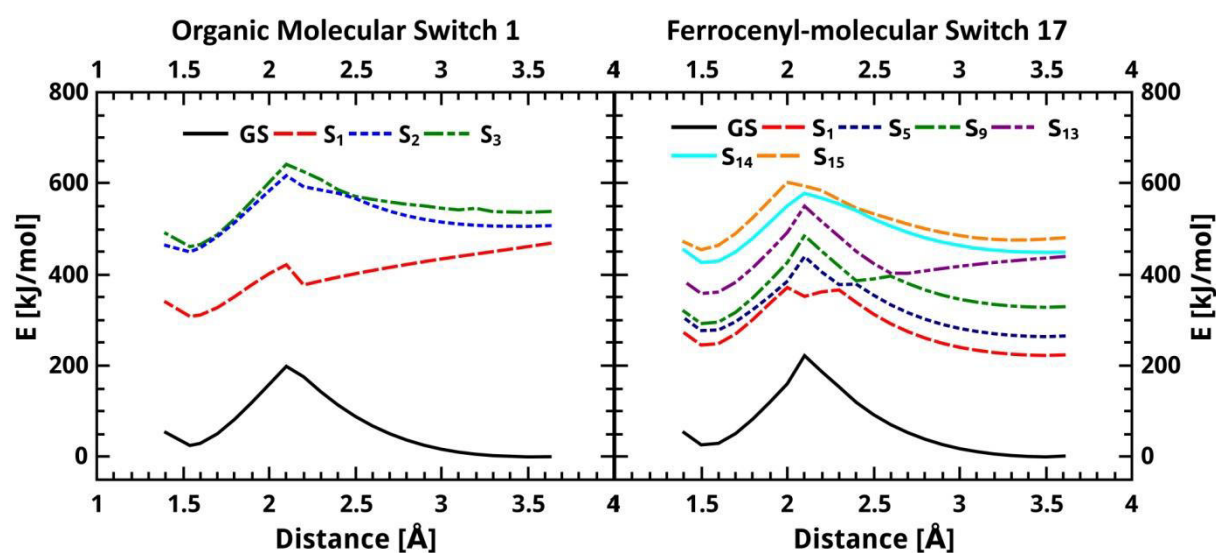


Figure 125: Potential energy surface for 1,2-bis(5-chloro-2-methylthien-3-yl)cyclopentene (**1**) (left) and for the analogous ferrocenyl-complex **17** (right) for LC- ω PEB /def-TZVP of the ground state and the excited singlet states as function of the C-C distance of the carbon atoms participating in the switching reaction.

Because of the system size, it was not possible to carry out calculations with post-Hartree Fock methods to locate conical intersections and the conclusions are only qualitative. Nevertheless, they shed light on the poor performance of these complexes as molecular switches.

In the case of the reference system, the cyclopentene-molecular switch **1**, only the HOMO-LUMO transition is important for the switching mechanism. This transition is

dominant in the state S_1 . The PES of the first excited state shows a global minimum at 1.5 Å which coincides with the minimum of the closed form in the ground state. A local minimum at 2.2 Å, which quite coincides with the transition state of the ground state, was also found. Other two excited states can be thought of participating in the reaction, the S_2 and S_3 singlet states.

The ring closure is an adiabatic photoreaction due to the small energy barrier in the first excited singlet state as already discussed by Staykov *et al.* [230,232] and by us. [220] After the excitation of the open form to the excited state S_1 (or even S_2 or S_3 and following relaxation to S_1 state), the energy decreases until reaching the local minimum. After overcoming the small energy barrier the molecular switch reaches the global minimum, where relaxes to the minimum on the ground state. On the contrary, the ring-opening reaction is a diabatic process (Figure 103). [220]

The choice of the singlet excited states for the ferrocenyl-complex **17** was done after seeing the calculated PES (Figure 125). Only the PES presenting a local minimum were selected, in order to obtain PES whose energies (almost) coincide at any point. The intensity of the transitions was also taken into account. It plays an important role in the excitation from the ground state.

The proposed mechanism of the closure reaction is presented in figure 126. The ferrocenyl-molecular switch **17** undergoes an excitation from the ground state to the S_{15} ($f=1.11$) and relaxes (possibly over the S_{14} state) to the S_{13} ($f=0.39$) excited state or is directly excited to the S_{13} excited state. The S_{13} state has mainly HOMO-LUMO character as already observed for the S_1 state of structure **1** and the shapes of the excited state PESs are similar, although the energetic barrier in the S_{13} state (compound **17**) is much higher than for the S_1 state of **1**. As a consequence, the molecule rather relaxes radiationless to the S_9 state, which nearly becomes energetically degenerate with the S_{13} state at 2.6 Å, than overcoming the high energetic barrier on the PES of S_{13} .

Ring Closure Mechanism - Ferrocenyl-complex **17**

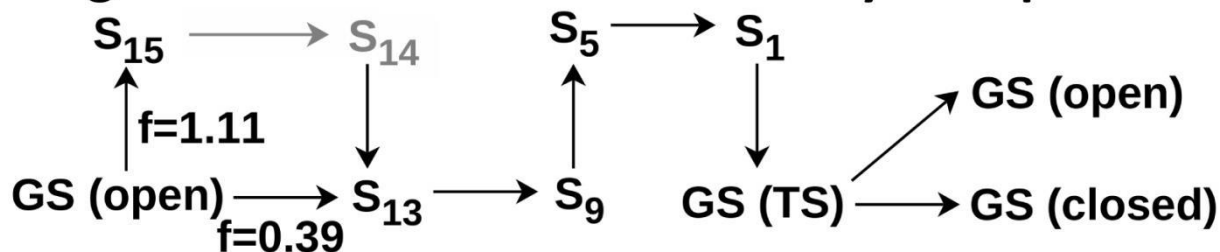


Figure 126: Ring closure mechanism for the ferrocenyl-complex **17** (f = Oscillator strength, GS = Ground state, TS = Transition state).

The same situation occurs on the PES of S_9 at 2.4 Å, where it nearly touches the PES of the S_5 state. Finally, the molecular switch relaxes to the S_1 excited state. It should be noticed that the energy barriers between the local minima and the local minimum referring to the closed isomer decreases from S_{13} , S_9 and S_5 to S_1 . In S_1 the energetic barrier is the smallest and the molecule can easily overcome it to reach the minimum of the closed isomer in the first excited state and then relaxes to the ground state.

In contrast to **1** where the reaction mainly involves one excited state (S_1) due to the small energetic barrier for the cyclization, the higher energetic barriers on the PESs of the different excited states for **17** suggest a transition between different excited states to finally reach the closed form. We further assume that only a part of the molecules is following the reaction coordinate towards the closed state at each transition between two PESs, while the other part reacts back to the open state. In consequence only a small fraction of the molecules reach the closed state. Another bottleneck for the inefficient ring closure might also be connected with the transition probabilities between the different excited states, which could not be calculated within the DFT/TDDFT calculations.

4.5.2.3. Conclusions (IV)

After investigating the behaviour as molecular switches of the cobalt(I) (**9** and **10**), cobalt(III) (**11** and **12**), cobalt(II) (**13** and **14**) and iron(II) (**17** and **18**) sandwich complexes and comparing it with the organic compounds **1** and **5**, it becomes obvious that the presence of the metal atoms exert great influence in the switching reaction.

In the case of the cobalt(I) complexes **9** and **10** the sandwich units are connected to the switching core by a sp^3 carbon atom (Scheme 25) which act as an insulator and therefore the cobalt atoms do not influence the molecular switch unit. These complexes displayed a distinct reversible switching reaction in a considerable yield.

The electronic situation of the compounds wherein the sandwich units are directly coupled to the molecular switch is quite different. The metal atoms are connected to the switching core by means of a conjugated π -system. This fact is vitally important as was illustrated by the irradiation experiments carried out with the complexes **11-14** and **17-18**. The yields of the photocyclization were very poor and in some occasions the ring opening reaction was even not observed.

As similar results were obtained by irradiating the cobalt(III) complexes **11** and **12**, which contain an acceptor substituent attached to the thiophene rings, and the cobalt(II) complexes **13** and **14**, the idea of the acceptor character of the cobaltocenium units being responsible of the failure of the cyclization reaction, as Guirado and coworkers^[78] postulated, can be dismissed.

As the theoretical calculations for the photocyclization mechanism for the ferrocenyl-complex **17** illustrated, the large number of excited states involved in the photoreaction could be responsible of its observed poor yield. Contrary to the organic molecular switches **1** and **5**, the ring closure reaction follows a diabatic process. Therefore, in each transition (between excited states) a certain part of the molecules react back to the initial situation, the open state of the molecular switch. As the number of transitions is high, only a small fraction of the molecules reaches the closed state. Although the same calculations were not performed for the other synthesized complexes, it can be assumed that the situation is quite comparable.

When both connecting switching cores (cyclopentene- and cyclohexene-backbone) were compared, it was observed that the resistance to fatigue presented by the cobalt(I)-complex **9** was better than for the analogous complex **10**. In addition, depending on the employed solvent, the yield of the photocyclization reactions slightly varied from one molecular switch to the other in almost all cases. However, these little differences were not enough to determinate that one molecular switch backbone presents better switching properties than the other, as it was expected (see section 4.5.1.1).^[220]

Concluding, on the basis of the presented results, except for the cobalt(I)- complexes **9** and **10**, where the metal centers are “independent” from the switching core, the presence of the metal centers is not advantageous for the switching reaction. The observed reaction yields are poor, also is the resistance to fatigue. These facts prevent these complexes from presenting the required efficiency needed in molecular switch devices.

5. Summary

The aim of this thesis was the synthesis of paramagnetic complexes where two sandwich units (cobaltocene or ferrocenium) are connected by a dithienylethene molecular switch and the study of their behaviour as molecular switches as well as their magnetic properties.

To achieve this target two different dithienylethene derivatives were employed as connecting units: the well known 1,2-dithienylcyclopentene and the almost not mentioned in the literature 1,2-dithienylcyclohexene. The latter was synthesized in good yield by means of a McMurry reaction. Single crystals were obtained from the iodo derivative **6**. Both possible conformations (parallel and antiparallel) were found in the crystal packing.

Nine new bismetalocene complexes (Figure 127) were synthesized and characterized. It is worth mentioning that ^{13}C - and two-dimensional NMR experiments were recorded for the paramagnetic cobaltocene complex **14**, measurements which are not often found in the literature for this type of compounds.

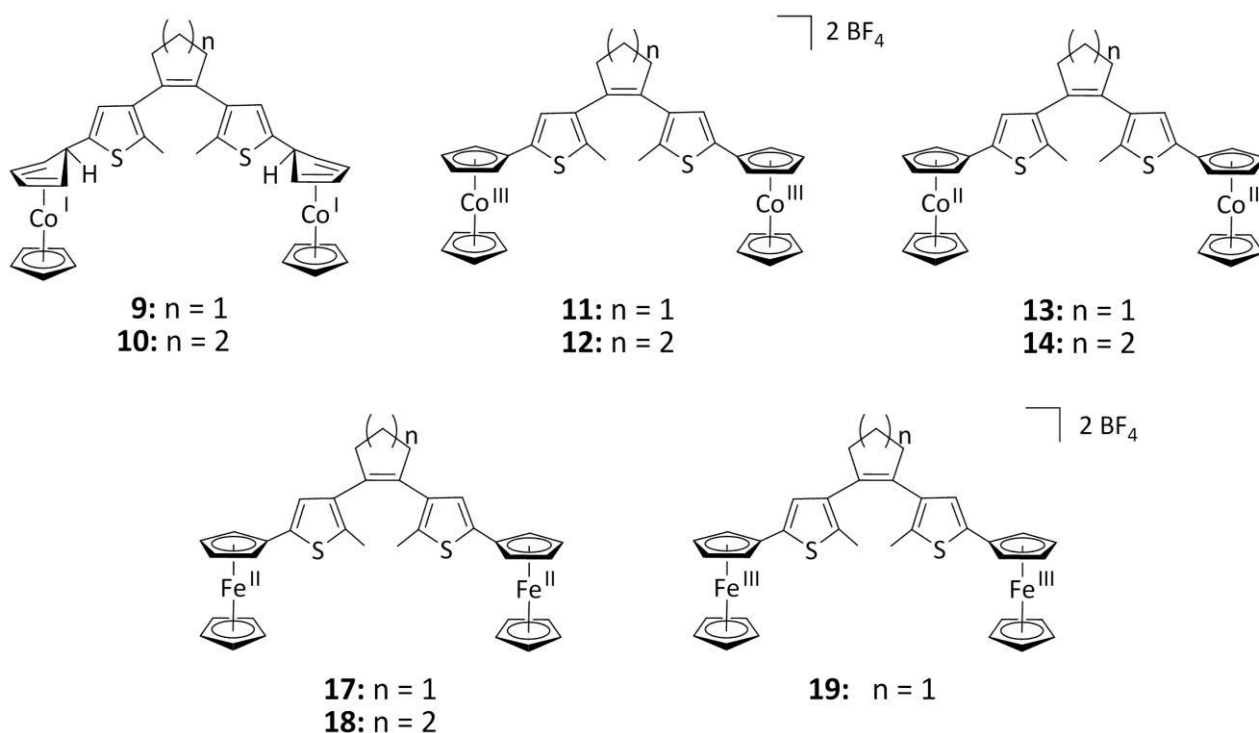


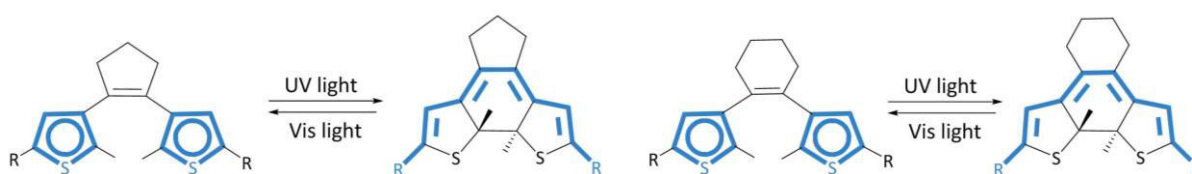
Figure 127: Synthesized metal complexes.

The molecular structures of all diamagnetic complexes (**9-12**, **17**, **18**) were achieved. Contrary to the 1,2-bis(5-iodo-2-methylthien-3-yl)cyclohexene (**6**), for these complexes only the antiparallel conformation was found, which is the only conformer to be capable for cyclization reaction.^[70] In addition, in all cases the distance between the methylated carbon

atoms was shorter than 420 pm, so the switching reaction should be possible even in the solid state. [95]

The redox behaviour of these complexes when the molecular switch is found in the open state was also investigated. For the cobaltocenium complexes **11** and **12**, two two-electrons waves were observed, indicating that an electronic communication does not occur substantially between the metal centers. The same was concluded for the ferrocene complexes **17** and **18**, which displayed only one two-electrons redox wave.

Irradiation experiments, monitored by means of UV-vis spectroscopy, were carried out with the chloro-substituted organic molecular switches **1** and **5** (Scheme 27). In both cases several switching cycles could be performed. Theoretical calculations confirmed that the switching properties of both molecular switches (**1** and **5**) are very similar.



Scheme 27: Switching reactions for the diarylethene molecular switches chosen for this thesis.

The same experiments were repeated with the bimetalloocene complexes, excepting for the ferrocenium complex **19**. The cobalt(I)-complexes **9** and **10**, where the carbon atom connects the sandwich units to the switching core displays a sp^3 hybridization, underwent the reversible switching reaction in measurable yield. On the contrary, the cobaltocenium (**11**, **12**), cobaltocene (**13**, **14**) and ferrocene (**17**, **18**) complexes presented only poor yields for the ring-closure and ring-opening reactions. This fact reveals that the presence of metallocene complexes direct attached to the switching clamp forming a conjugated π -system, is not advantageous for the switching reaction.

It was also attempted to monitor the switching reaction by means of cyclic voltammetry and NMR-spectroscopy. Unfortunately, the closed isomers could not be detected by either of these methods.

The theoretical calculations for the ferrocenyl complex **17** indicated that a possible reason for the poor yield of the photocyclization in these complexes could be the high number of single excited states involved in the reaction. In contrast to the organic molecular switches (**1**, **5**), the photocyclization of complex **17** follows a diabatic process. Due to the high number of transitions between single excited states and the fact that during each transition a certain

percentage of the molecules reacts back to the open state, only a small fraction of them reaches the closed state.

The poor yields of the ring-closure and ring-opening reactions and the low resistance to fatigue displayed by these complexes, prevent them from presenting the properties required for being used in molecular switch devices.

VT-NMR measurements were carried out with the paramagnetic cobaltocene complexes **13** and **14**. While the most of the signals followed the Curie Law in the measured temperature range, the signals corresponding to the protons in the α and β positions of the substituted Cp rings presented the already known "Cobaltocene Anomaly".^[148,149]

Finally, the magnetic coupling between the unpaired electrons of the connected cobaltocene units was not investigated. Taking into account the results of the cyclic voltammetric experiments, no magnetic coupling was expected when the molecular switch is found in the open state; and due to the poor yield of the photocyclization reaction, the closed isomer of the paramagnetic complexes could not be isolated.

6. Zusammenfassung

Das Ziel dieser Arbeit war die Synthese von paramagnetischen Komplexen, in welchen zwei Sandwich-Einheiten (Cobaltocen oder Ferrocenium) durch einen molekularen Dithienylethen-Schalter verbunden sind. Weiterhin sollte ihre Schaltfähigkeit sowie ihre magnetischen Eigenschaften untersucht werden.

Um dieses Ziel zu erreichen, wurden zweierlei Dithienylethen-Derivate als Verbindungseinheiten verwendet: das bereits bekannte 1,2-Dithienylcyclopenten und das in der Literatur kaum erwähnte 1,2-Dithienylcyclohexen. Letzteres wurde mit guter Ausbeute durch eine McMurry-Reaktion synthetisiert. Dabei wurden Einkristalle des Iododerivates **6** erhalten und beide möglichen Konformere (parallel und antiparallel) in der Kristallpackung gefunden.

Weiterhin wurden neun neue Bismetallocen-Komplexe (Abbildung 1) synthetisiert und charakterisiert. Für den paramagnetischen Cobaltocen-Komplex **14** wurden ^{13}C - und zweidimensionale NMR-Experimente durchgeführt. Derartige Untersuchungen sind in der Literatur bisher kaum bekannt.

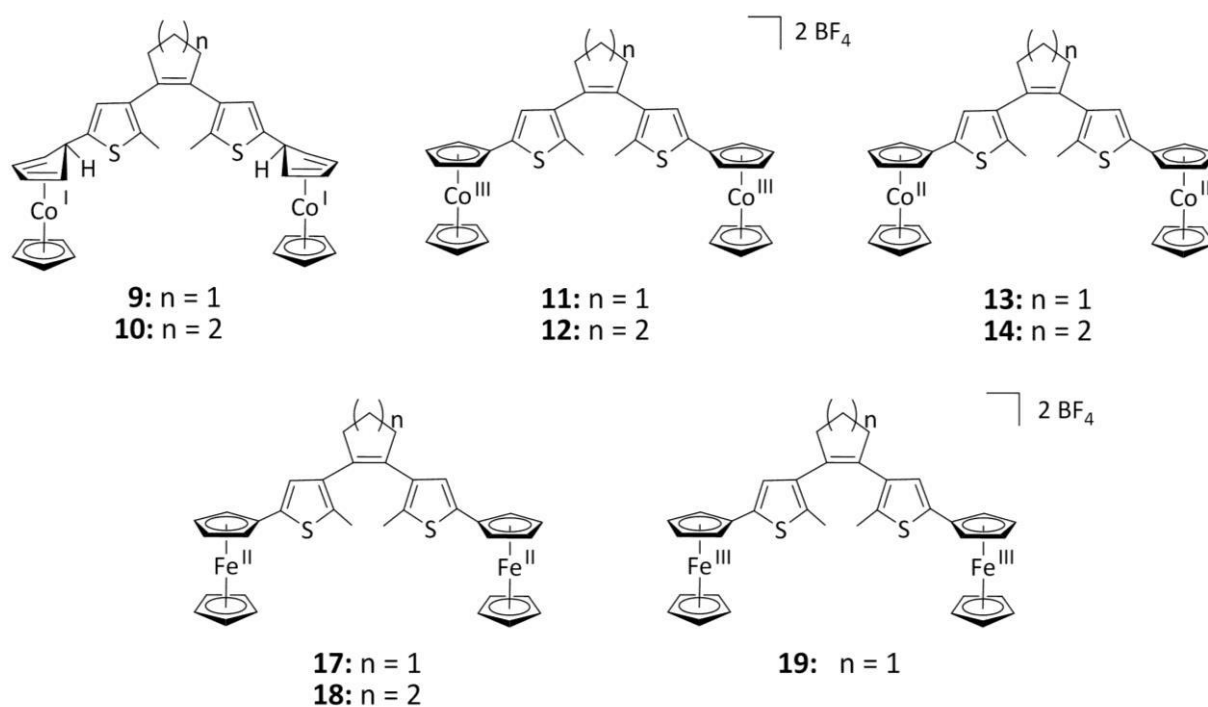


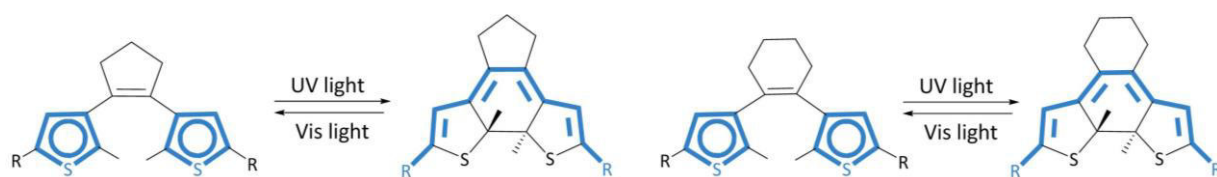
Abbildung 1: Synthetisierte Metallkomplexe.

6. Zusammenfassung

Die Molekülstrukturen aller diamagnetischen Komplexe (**9-12**, **17**, **18**) konnten erhalten werden. Im Gegensatz zu dem 1,2-Bis(5-iodo-2-methylthien-3-yl)cyclohexen (**6**) wurden dabei in allen Fällen nur die jeweils antiparallelen Konformere gefunden. Nur diese Konformation kann eine Photozyklisierung eingehen.^[70] Weiterhin beträgt der Abstand zwischen den methylierten Kohlenstoff-Atomen in allen Komplexen weniger als 420 pm, woraus sich ergibt, dass der Schaltvorgang auch im Feststoff stattfinden können sollte.^[95]

Die Untersuchung des Redox-Verhaltens der Komplexe bei geöffnetem molekularen Schalter ergab zwei Zwei-Elektronen-Wellen für die Cobaltocenium-Komplexe **11** und **12**. Dies deutet darauf hin, dass zwischen den Metallzentren keine elektronische Kommunikation existiert. Gleiches gilt für die Ferrocenyl-Komplexe, da hier nur eine Zwei-Elektronen-Welle gefunden wurde.

Mit den organischen molekularen Schaltern **1** und **5** wurden Bestrahlungsexperimente durchgeführt und diese UV-vis spektroskopisch verfolgt. In beiden Fällen wurden mehrere Schaltzyklen beobachtet (Schema 1). Die ähnlichen Eigenschaften beider molekularen Schalter (**1** und **5**) wurden durch theoretische Berechnungen bestätigt.



Schema 1: Schaltreaktionen der für diese Arbeit ausgewählten molekularen Schalter .

Abgesehen vom Ferrocenium-Komplex **19** wurden identische Bestrahlungsexperimente mit den Bismetallocen-Komplexen durchgeführt. Im Fall der Cobalt(I)-Komplexe, ist das Kohlenstoff-Atom, welches den Sandwich-Komplex mit dem molekularen Schalter verbindet, sp^3 -hybridisiert. Der Schaltvorgang fand hier mit hoher Ausbeute statt. Im Gegensatz dazu, war die Ausbeute der Photozyklisierung und der Ringöffnungsreaktion bei den Cobaltocenium- (**11**, **12**), Cobaltocen- (**13**, **14**) und Ferrocen- (**17**, **18**) Komplexen sehr niedrig. Daraus folgt, dass die Anwesenheit von Metallocen-Komplexen, welche direkt mit dem molekularen Schalter verbunden sind und dabei ein konjugiertes π -System bilden, nicht vorteilhaft für den Schaltvorgang ist.

Es wurde versucht, den Schaltvorgang mit Hilfe der NMR-Spektroskopie und Cyclovoltammetrie zu verfolgen. Leider konnten keine Signale geschlossener Isomere mit beiden Methoden detektiert werden.

Die schlechte Ausbeute der Zyklisierungsreaktion des Ferrocenyl-Komplex **17** resultiert laut theoretischen Berechnungen aus der hohen Anzahl angeregter Zustände, welche an der Photoreaktion teilnehmen. Im Unterschied zu den organischen molekularen Schaltern **1** und **5**, erfolgt die Photozyklisierung von **17** in einem diabatischen Prozess. Aufgrund der Vielzahl von Übergängen zwischen den einfach angeregten Zuständen und der Tatsache, dass außerdem bei jedem Übergang ein bestimmter Prozentsatz Moleküle zum offenen Zustand zurückreagiert, erreicht nur ein kleiner Teil der Moleküle den geschlossenen Zustand. Die daraus resultierende niedrige Ausbeute der Zyklisierung und der Ringöffnungsreaktionen sowie die schlechte Ermüdungsresistenz verhindern die Nutzung dieser Komplexe als molekulare Schalter.

Mit den Komplexen **13** und **14** wurden temperaturabhängige NMR-Messungen durchgeführt. Mit Ausnahme der Signale der Wasserstoff-Atome an den α - und β -Positionen der substituierten Cp-Ringe, welche die schon bekannte „Anomalie von Cobaltocenen“ zeigen, folgen die Signale dem Curie-Gesetz. ^[148,149]

Die magnetische Kopplung zwischen den ungepaarten Elektronen der verbundenen Cobaltocene wurde nicht untersucht. Jedoch wird unter Berücksichtigung der Ergebnisse der Cyclovoltammetrie keine magnetische Kopplung für die molekularen Schalter im offenen Zustand erwartet. Weiterhin konnte das geschlossene Isomer der paramagnetischen Komplexe aufgrund der niedrigen Ausbeute der Photozyklisierungs-Reaktion nicht isoliert werden.

7. Experimental Section

7.1. General

Unless otherwise noted, the reactions were carried out under dry nitrogen atmosphere using standard Schlenk techniques. The used solvents were saturated with nitrogen, dried with the adequate drying agent and distilled before used. Hexane, pentane and diethylether were dried with sodium-potassium alloy, THF and DME with potassium, toluene with sodium and DCM and acetonitrile with CaH₂. When alkali metals were employed, benzophenone was added as indicator. Tetramethylcyclopent-2-en-1-one was dried with CaH₂, condensed at low pressure and degased. The following chemicals were synthesized according to the literature: 1,2-bis(5-bromo-2-methylthien-3-yl)cyclopentene, ^[73] cobaltocenium iodide, decamethylcobaltocene ^[194] and 1,5-bis(5-chloro-2-methylthien-3-yl)hexane-1,6-dione **4**. ^[189]

7.2. Analytical methods

NMR-Spectroscopy

Brucker Fourier300

Varian Gemini 2000

Brucker Avance 400

The NMR measurements were carried out at room temperature and referenced to the solvent. When possible, multiplicities of higher order were evaluated according to first order and are marked with the prefix "m~". Following abbreviations were used to express the multiplicity of the signals: s (singlet), d (doublet), t (triplet), q (quartet), quin (quintuplet), m (multiplet)

Mass-spectroscopy

Agilent ESI-TOF 6224 (ESI)

Finnigan MAT 311 A (EI)

VG Analytical 70-250 S

The measurements were carried out in the Department of Organic Chemistry in the University of Hamburg.

UV-vis spectroscopy

Varian Cary 5e UV/vis–NIR spectrophotometer

Perkin Elmer Lambda 25 UV-vis-Spektrometer

Elemental Analysis

Carlo Erba1108 CHNS-O

The measurements were carried out in the Department of Analytical Chemistry in the University of Hamburg.

Column and thin-layer chromatography

Silica 660 (Merck), (0.063-0.200 mm), Aluminiumoxid 90 (Merck), neutral (0.063-0.200 mm)

TLC-plate Silica 60, WF_{254S} (Macherei-Nagel), TLC-plate Aluminiumoxid 60, WF_{254S} (Macherei-Nagel)

X-Ray structure analysis

The crystals were transferred to Polyalphaolefin oil. The best one was selected with the help of a petrographic microscope and it was situated on the goniometer with a glass filament. The whole system was refrigerated with nitrogen stream-cooling. The oil froze and the measurement took place at 100 K. The measurement of the intensity of the reflexes was carried out with a single crystal diffractometer developed by Bruker (AXS Smart APEX) with an area detector system (Smart CCD) with Molybdenum-K α -irradiation ($\lambda = 0.71073 \text{ \AA}$) or a Supernova Oxford Diffraction diffractometer made by Agilent Technologies with Mo-K α - or Copper-K α -irradiation ($\lambda = 1.54178 \text{ \AA}$). The determination of the intensity of the reflexes from the collected frames was done employing the program SAINT^[238] and the absorption effects were corrected with the help of the program SADABS.^[239] For the evaluation of the measurement, SHELXTL^[240] was used. The space group was investigated with the program XPREP. The phase problem was solved with the program SHELXS-97^[241] by Patterson and direct methods. SHELXL-97^[242] was employed for the refinement of the final structure. The refinement of the atoms (except hydrogen atoms) was done with anisotropic temperature factors (Refinement method: Full-matrix least-squares on F^2). Hydrogen-atoms were handled with the help of the Reiter-model.

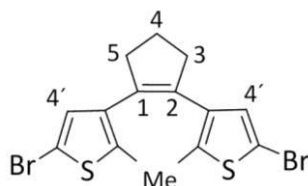
The parameters $R1$, $wR2$ and GOF were calculated employing following equations:

$$R1 = \frac{\sum[|F_o| - |F_c|]}{\sum|F_o|} \quad wR2 = \sqrt{\frac{\sum w(F_o^2 - F_c^2)^2}{\sum w(F_o^2)}} \quad GOF = \sqrt{\frac{\sum w(F_o^2 - F_c^2)^2}{n-p}}$$

The figures were done with the help of the program Mercury 1.4.2.

7.3. Synthesis and characterization

7.3.1. 1,2-Bis(5-bromo-2-methylthien-3-yl)cyclopentene (2)

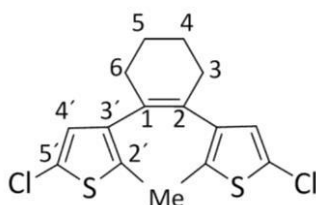


1,2-Bis(5-chloro-2-methylthien-3-yl)cyclopentene (**1**) (1.90 g, 5.78 mmol) was dissolved in THF (150 mL) and *n*-butyllithium (6.6 mL, 10.6 mmol, 1.6 M in hexane) was added at $-78\text{ }^{\circ}\text{C}$. After stirring the solution for 5 min at this temperature, it was allowed to warm to room temperature in the darkness (2 h). Afterwards the grey suspension was cooled again ($-78\text{ }^{\circ}\text{C}$) and 1,1,2,2-tetrabromethane (1.8 mL, 5.5 g, 16 mmol) was added. The reaction mixture was stirred for two hours at room temperature. The product was purified by column chromatography (silica, PE) (600 mg, 1.43 mmol, 25 %).

$^1\text{H-NMR}$ (200 MHz, Chloroform- d_1 , 298 K): δ [ppm] = 6.71 (s, 2H, 4'-H), 2.72 (t, $J = 7.4$ Hz, 4H, 3-H, 5-H), 2.02 (m-quin, $J = 7.1$ Hz, 2H, 4-H), 1.88 (s, 6H, Me-H).

The characterization agrees with the published literature. ^[186]

7.3.2. 1,2-Bis(5-chloro-2-methylthien-3-yl)cyclohexene (5)



$\text{TiCl}_3(\text{THF})_3$ (9.33 g, 25.2 mmol) was suspended in DME (300 mL) and the suspension was refluxed for three days. Afterwards Zn-Cu couple (7.23 g) was added to the deep green solution at room temperature. The reaction mixture was refluxed for another three hours and a black suspension was yielded. After cooling it at room temperature 1,5-bis(5-chloro-2-

methylthien-3-yl)hexane-1,5-dione (**4**) (1.21 g, 3.23 mmol) was added and the suspension was refluxed overnight. The resulting slurry was filtered in the air and washed with DCM. The solid residue on the filter was washed carefully with water, in order to avoid its spontaneous ignition. After removing the solvent in vacuum, the crude product was dissolved in DCM (100 mL) and washed with water (3*50 mL). The combined aqueous phases were washed with DCM (1*50 mL) and then the combined organic phases were dried (Na_2SO_4), filtered and the solvent evaporated to yield a brown tar, which was purified by column chromatography (Al_2O_3 , PE) to afford a pure product as colourless oil, which after twelve hours became a colourless solid (670 mg, 1.96 mmol, 61 %).

$^1\text{H-NMR}$ (300 MHz, Chloroform- d_1 , 298 K): δ [ppm] = 6.49 (s, 2H, 4'-H), 2.26 (m-quin, $J = 3.7$ Hz, 4H, 3-H, 6-H), 1.96 (s, 3H, Me-H), 1.77 (m-quin, $J = 3.7$ Hz, 4H, 4-H, 5-H).

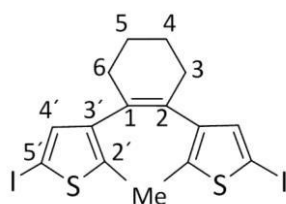
$^{13}\text{C-NMR}$ (101 MHz, Chloroform- d_1 , 298 K): δ [ppm] = 139.36 (2'-C), 132.38 (5'-C), 131.64 (1-C, 2-C), 127.15 (4'-C), 124.26 (3'-C), 31.54 (3-C, 6-C), 23.06 (4-C, 5-C), 14.19 (Me-C).

HRMS (ESI): $m/z = 343.0126$ ($[\text{M-H}]^+$), calculated: 343.0070

Elemental analysis [%]: $\text{C}_{16}\text{H}_{16}\text{Cl}_2\text{S}_2$ calculated: C 55.97, H 4.70, S 18.68

experimental: C 56.19, H 4.79, S 18.51

7.3.3. 1,2-Bis(5-iodo-2-methylthien-3-yl)cyclohexene (**6**)



1,2-Bis(5-chloro-2-methylthien-3-yl)cyclohexene (**2**) (1.48 g, 4.33 mmol) was charged in a Schlenk-flask and dissolved in THF (200 mL). *n*-Butyllithium (6.5 mL, 1.6 M in hexane, 10.4 mmol) was carefully added at -78 °C and the solution was stirred for one hour at that temperature and it turned red. Afterwards the solution was allowed to warm to room temperature and was stirred for an additional hour. To the brown mixture iodine (2.65 g, 10.43 mmol) was added and the solution was stirred for four hours. The reaction was quenched with saturated aqueous $\text{Na}_2\text{S}_2\text{O}_3$ (75 mL) and for additional 15 min stirred. The product was extracted with Et_2O (100 mL) and the organic phase was washed with saturated

$^1\text{H-NMR}$ (400 MHz, Benzene- d_6 , 298 K): δ [ppm] = 6.28 (s, 2H, 4'-H), 5.09-5.04 (m-t, $J = 2.0$ Hz, 4H, β -H), 4.51 (s, 10H, Cp-H), 3.90-3.86 (m-t, $J = 2.4$ Hz, 2H, 5''-H), 2.81-2.79 (m, 4H, α -H), 2.64 (t, $J = 7.45$ Hz, 4H, 3-H, 5-H), 1.90 (s, 6H, Me-H), 1.83-1.76 (m, 2H, 4-H).

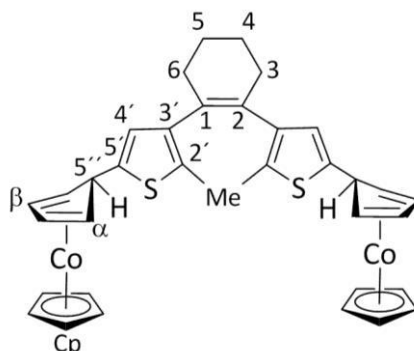
$^{13}\text{C-NMR}$ (75 MHz, Benzene- d_6 , 298 K): δ [ppm] = 147.00 (5'-C), 135.29 (2'-C), 134.79 (3'-C), 131.67 (1-C, 2-C), 121.83 (4'-C), 79.48 (Cp-C), 74.81 (β -C), 51.21 (5''-C), 45.52 (α -C), 38.63 (3-C, 5-C), 23.30 (4-C), 14.40 (Me-C).

MS (EI): m/z = 636 $[\text{M}]^+$, 634 $[\text{M}-2\text{H}]^+$, 511 $[\text{M}-\text{CoCp}]^+$, 445 $[\text{M}-\text{CoCp}_2]^+$, 220, 205, 189 $[\text{CoCp}_2]^+$, 124 $[\text{CoCp}]^+$, 98, 66 $[\text{Cp}]^+$, 59 $[\text{SCCH}_3]^+$

HRMS (ESI): m/z = 637.0816 ($[\text{M}+\text{H}]$), calculated: 637.0844

Elemental analysis [%]: $\text{C}_{35}\text{H}_{34}\text{Co}_2\text{S}_2$ calculated: C 66.03, H 5.38, S 10.07
 experimental: C 66.12, H 5.96, S 9.55

7.3.5. 1,2-Bis(2'-methyl-5'-[(η^5 -cyclopentadienyl)(η^4 -1'',3''-cyclopentadien-5''-yl)cobalt(I)]-thiophen-3'-yl)cyclohexen-1-en (10)



1,2-Bis(5-chloro-2-methylthien-3-yl)cyclohexene (**2**) (0.225 g, 0.658 mmol) was solved in THF (140 mL) and *n*-butyllithium (0.98 mL, 1.6 M in hexane, 1.57 mmol) was carefully added at -78 °C. The next two hours the suspension was allowed to warm at -10 °C. Afterwards cobaltocenium iodide (0.607 g, 1.92 mmol) was added at -30 °C and the solution turned red. The reaction mixture was stirred for three hours at that temperature and at room temperature overnight. The reaction was quenched with 10 mL water and after adding 100 mL toluene the mixture was washed with water (3*50 mL). The organic phase was dried with NaSO_4 and filtered. The solvent was evaporated in vacuum and the crude product was recrystallized with absolute DME under nitrogen atmosphere. The complex precipitated in form of air stable red crystals suitable for X-ray analysis (347 mg, 0.53 mmol, 81 %).

7. Experimental Section

$^1\text{H-NMR}$ (300 MHz, Toluene- d_8 , 298 K): δ [ppm] = 6.06 (s, 2H, 4'-H), 5.09-5.01 (m, 4H, β -H), 4.53 (s, 10H, Cp-H), 3.84 (m-t, $J = 2.4$ Hz, 2H, 5''-H), 2.79 (q, $J = 2.4$ Hz, 4H, α -H), 2.26-2.17 (m-p, $J = 3.2$ Hz, 4H, 3-H, 6-H), 1.88 (s, 6H, Me-H), 1.64-1.54 (m-p, $J = 3.2$ Hz, 4H, 4-H, 5-H).

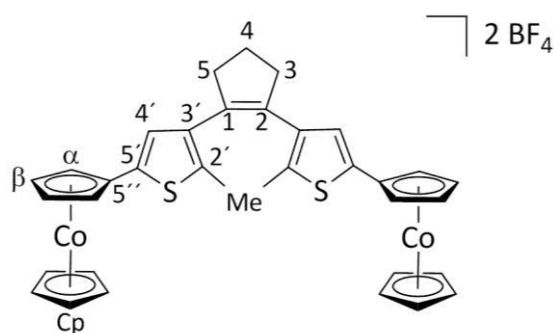
$^{13}\text{C-NMR}$ (101 MHz, Pyridine- d_5 , 298 K): δ [ppm] = 146.43 (5'-C), 140.22 (2'-C), 132.13 (3'-C), 130.68 (1-C, 2-C), 122.86 (4'-C), 80.11 (Cp-C), 75.36 (β -C), 51.52 (5''-C), 46.01 (α -C), 32.18 (3-C, 6-C), 23.79 (4-C, 5-C), 14.67 (Me-C).

HRMS (ESI): $m/z = 651.0976$ ([M+H]), calculated: 651.1001

Elemental analysis [%]: $\text{C}_{36}\text{H}_{36}\text{Co}_2\text{S}_2$ calculated: C 66.45, H 5.58, S 9.86

experimental: C 66.00, H 5.59, S 9.21

7.3.6. 1,2-Bis(2'-methyl-5'-[bis(η^5 -cyclopentadienyl)cobalt(III)]-thiophen-3'-yl)-cyclopent-1-en-bis(tetrafluoroborate) (11)



1,2-Bis{2'-methyl-5'-[$(\eta^5$ -cyclopentene)(η^4 -1'',3''-cyclopentadien-5''-yl)cobalt(I)]-thiophen-3'-yl}cyclopent-1-en (**9**) (0.16 g, 0.25 mmol) was dissolved in DCM (15 mL). To this solution, tritylium tetrafluoroborate (0.19 g, 0.57 mmol) dissolved in DCM (20 mL) was added. The reaction mixture was stirred overnight. The obtained brown suspension was filtered and the solvent was removed in vacuum. The product was dissolved in DCM (20 mL) and filtered again. Toluene (50 mL) was slowly added and the two phase system was kept at -18 °C overnight. The mother liquor was decanted, the solvent was evaporated and the procedure was repeated yielding additional product. The orange crystals were dissolved in Et_2O , the yellow solution was cooled with liquid nitrogen and Et_2O was added until precipitation began. The suspension was kept at -18 °C overnight and the product was obtained as orange crystals (109 mg, < 54 %). In order to obtain crystals suitable for X-ray analysis, the complex was dissolved in acetone and benzene gas was diffused slowly until the product precipitated.

second solution was added to the first solution and the reaction mixture was stirred for four hours. Then the solvent was removed in vacuum and the product was extracted with *n*-pentane (120 mL). The suspension was filtered under nitrogen and the solvent was evaporated (212 mg, < 53 %).

When the product was not found in ESI-mass-spectroscopy, a small aliquot was solved in THF-degassed water mixture (1/1 v/v) and stirred for 30 min under nitrogen atmosphere. Afterwards, the Schlenk-flask was opened and the solution stirred for another 15 minutes. $\text{NH}_4\text{BF}_4(\text{aq})$ was added and the solution was washed with chloroform. A yellow coloured organic phase was obtained. After removing the solvent an ESI-mass spectrum was recorded and the desired cobaltocenium complex **11** was found.

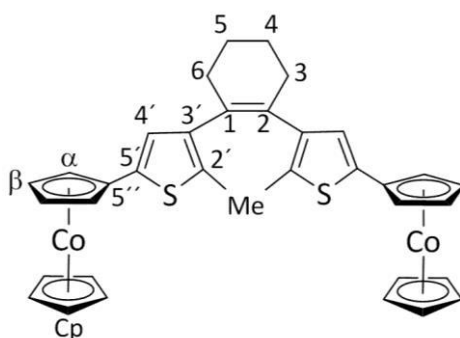
$^1\text{H-NMR}$ (400 MHz, Benzene- d_6 , 298 K): δ [ppm]= 24.71 (s, 6H, Me-H), 2.50 (t, $J = 7.4$ Hz, 4H, 3-H, 5-H), 1.93 (p, $J = 7.1$ Hz, 2H, 4-H), -23.95 (s, 2H, 4'-H), -24.06 (s, 4H, β -H or α -H), -50.00 (s, 4H, β -H or α -H), -50.33 (s, 10H, Cp-H).

$^1\text{H-NMR}$ (400 MHz, Toluene- d_8 , 298 K): δ [ppm]= 24.38 (s, 6H, Me-H), 2.49 (t, $J = 7.3$ Hz, 4H, 3-H, 5-H), 2.02-1.87 (m, 2H, 4-H), -23.66 (s, 2H, 4'-H), -24.60 (s, 4H, β -H or α -H), -49.95 (s, 4H, β -H or α -H), -50.38 (s, 10H, Cp-H).

MS (EI): $m/z = 634$ $[\text{M}]^+$, 317 $[\text{M}]^{2+}$, 189 $[\text{CoCp}_2]^+$, 124 $[\text{CoCp}]^+$, 66 $[\text{Cp}]^+$

HRMS (ESI): $m/z = 317.032$ ($[\text{M}]^{2+}$), calculated: 317.0304

7.3.10. 1,2-Bis{2'-methyl-5'-[bis(η^5 -cyclopentadienyl)cobalt(II)]-thiophen-3'-yl}-cyclohex-1-en (14)



1,2-Bis{2'-methyl-5'-[bis(η^5 -cyclopentene)cobalt(III)]-thiophen-3'-yl}-cyclopent-1-en-bis-(tetrafluoroborate) (**12**) (84 mg, 0.10 mmol) and 1,2-bis{2'-methyl-5'-[bis(η^5 -cyclohexene)cobalt(III)]-thiophen-3'-yl}-cyclopent-1-en-bis(hexafluorophosphate) (**12b**) (98 mg,

7. Experimental Section

0.10 mmol) were suspended in THF (40 mL). Decamethylcobaltocene (96 mg, 0.29 mmol) was solved in THF (20 mL) and added to the orange solution. The reaction mixture was stirred for seven hours. Then the solvent was removed in vacuum and the violet product was extracted with toluene (40 mL). The suspension was filtered under nitrogen and the solvent was evaporated. The black powder was suspended in *n*-pentane (40 mL) and again filtered. After evaporation of the solvent the product was obtained as a black powder (24 mg, 25 %).

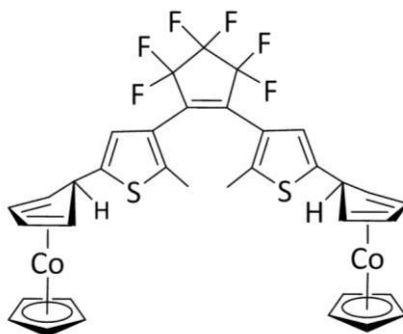
When the product was not found in ESI-mass-spectroscopy, a small aliquot was solved in THF-degassed water mixture (1/1 v/v) and stirred for 30 min under nitrogen atmosphere. Afterwards, the Schlenk-flask was opened and the solution stirred for another 15 minutes. $\text{NH}_4\text{BF}_4(\text{aq})$ was added and the solution was washed with chloroform. A yellow coloured organic phase was obtained. After removing the solvent an ESI-mass spectrum was recorded and the desired cobaltocenium complex **12** was found.

$^1\text{H-NMR}$ (400 MHz, Toluene- d_8 , 298 K): δ [ppm]= 23.53 (s, 6H, Me-H), 2.55 (2, 4H, 4-H, 5-H), 1.84 (s, 4H, 3-H, 6-H), -21.60 (s, 2H, 4'-H), -26.93 (s, 4H, β -H or α -H), -48.74 (s, 4H, β -H or α -H), -49.70 (s, 10H, Cp-H).

$^{13}\text{C-NMR}$ (101 MHz, Toluene- d_8 , 298 K): δ [ppm] = 604.63, 589.98 (Cp-C), 390.57, 353.27 (4'-C), 272.18, 132.91 (1-C, 2-C), 31.02, 23.32 (3-C, 6-C), 18.88 (2-C, 5-C), 18.19 (3'-C), -22.79-(-26.45) (q, Me-C), -214.6.

HRMS (ESI): $m/z = 324.0398$ ($[\text{M}]^{2+}$), calculated: 324.0383

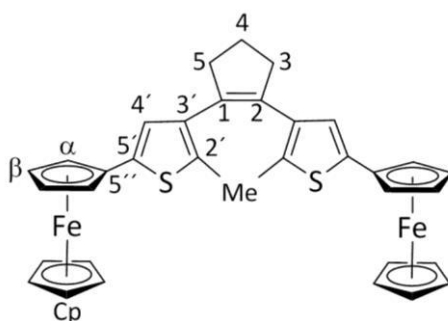
7.3.11. Attempt to the synthesis of 1,2-bis{2'-methyl-5'-[(η^5 -cyclopentadienyl)(η^4 -1'',3''-cyclopentadien-5''-yl)cobalt(I)]-thiophen-3'-yl}perfluorocyclopent-1-en (**16**)



1,2-Bis(5-chloro-2-methylthien-3-yl)hexafluorocyclopent-1-en (**15**) (46.6 mg, 0.107 mmol) was dissolved in 10 mL THF and cooled at -78°C . *n*-Butyllithium (0.18 mL, 1.6 M in hexane,

0.11 mmol) was slowly added to the colourless solution and it turned red. The solution was allowed to warm to room temperature (90 min) and it turned green. Cobaltocenium iodide powder (85 mg, 0.26 mmol) was given direct to the reaction mixture and a brown suspension was obtained, which was stirred for 17 h. After quenching the reaction with distilled water (0.3 mL) the suspension was filtered and the solvent evaporated. The brown product was dissolved in toluene (25 mL) and washed with a saturated NaCl solution (1*10 mL) and with water (2*10 mL). After eliminating the solvent a red solid was obtained, which could not be identified.

7.3.12. 1,2-Bis(2'-methyl-5'-[bis(η^5 -cyclopentadienyl)iron(II)]-thiophen-3'-yl)-cyclopent-1-en (17)



Ferrocene (12.24 g, 65.79 mmol) and KOtBu (2.03 g, 18.09 mmol) were charged in a Schlenk-flask and solved in THF (130 mL). The solution was cooled at $-70\text{ }^{\circ}\text{C}$ and *n*-butyllithium (43.5 mL, 1,7 M in pentane, 73.95 mmol) was added dropwise. The orange suspension was stirred for one hour at this temperature and then it was warmed to $-50\text{ }^{\circ}\text{C}$. ZnCl₂.THF (20.99 g, 74.83 mmol) was added and the reaction mixture was kept one hour at this temperature, and another hour at room temperature. To the orange solution 1,2-bis(5-iodo-2-methylthien-3-yl)cyclopentene (**3**) (3.14 g, 6.14 mmol) solved in 15 mL THF and [Pd(PPh₃)₄] (2.80 g, 2.42 mmol) as powder was added. Afterwards, the deep red solution was stirred at $60\text{ }^{\circ}\text{C}$ for 19 h. After evaporation of the solvent, the crude product was suspended in DCM (200 mL) and washed with water (5*75 mL) and with a saturated NaCl solution (1*100 mL). After drying the organic phase with Na₂SO₄, the remaining product was purified by column chromatography on silica (PE/ PE:DCM 9:1 (v/v)). After removing the solvent the product was yielded in form of orange crystals (2.18 g, 3.47 mmol, 56 %). Suitable crystals for X-ray structure analysis were obtained by solving the product in boiling DMC and cooling the solution very slowly to $-4\text{ }^{\circ}\text{C}$.

7. Experimental Section

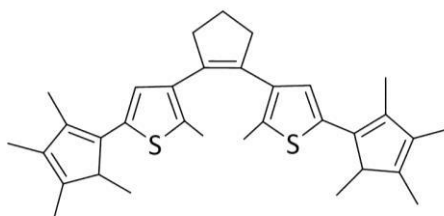
product was found in the mother liqueur. After evaporating the solvent under vacuum, the product was found in form of a navy blue powder. An aliquot was solved in DCM and pentane was diffused slowly as gas, and crystals suitable for X-ray analysis were obtained.

$^1\text{H-NMR}$ (400 MHz, Dichlormethane- d_2 , 298 K): δ [ppm]= 42.61 (s, β -H and α -H), 30.49 (s, Cp-H), 25.70 (s, Me-H), -23.47 (s, 4'-H)

MS (EI): $m/z = 628$ $[\text{M}]^+$, 314 $[\text{M}]^{2+}$

MS (FAB+): $m/z = 628.1$ $[\text{M}]^+$

7.3.15. 1,2-Bis(2,3,4,5-tetramethylcyclopentadienyl)-cyclopent-1-en (22)



1,2-Bis(5-chloro-2-methylthien-3-yl)cyclopentene (**2**) (390 mg, 118 mmol) was dissolved in Et_2O (30 mL) and *n*-butyllithium (0.8 mL, 1.6 M in hexane, 1.3 mmol) was added and the solution turned orange. After 25 min stirring, anhydrous 2,3,4,5-tetramethylcyclopent-2-en-1-one (0.2 mL, 183 mg, 1.3 mmol) was given to the solution, and it was refluxed for 1 h. After allowing the reaction mixture to warm to room temperature, *n*-butyllithium (0.8 mL, 1.6 M in hexane, 1.3 mmol) was added and the solution was stirred for 1 h. Afterwards, 2,3,4,5-tetramethylcyclopent-2-en-1-one (0.2 mL, 183 mg, 1.3 mmol) was added and the solution was stirred for 1 h. The solution was quenched with a saturated NH_4Cl solution and the layers were separated. The aqueous phase was then washed with Et_2O (1*10 mL) and the organic phase with water (1*10 mL). To the ethereal phase *p*-toluenesulfonic acid (50 mg) was given and after 10 min the formation of a solid was observed, which was solved again when Et_2O (10 mL) was added. The solution was washed again with water (3*5 mL), dried with NaSO_4 and filtered. Finally, the solvent was evaporated.

HRMS (ESI): $m/z = 501.0819$ ($[\text{M}+\text{H}]$), calculated: 501.257

8. Literature

- [1] Konrad Zuse, *www.Konrad-Zuse.de*. (09.03.2015).
- [2] Universidad de Castilla-La Mancha, *www.uclm.es/profesorado/ricardo/WEBNNTT/Bloque%201/Historia.htm*. (24.01.2015).
- [3] IBM, *www-03.ibm.com/ibm/history/exhibits/650/650_pr2.html*. (24.01.2015).
- [4] Motorola, *https://www.motorola.com/us/consumers/about-motorola-us/About_Motorola-History-Timeline/About_Motorola-History-Timelin*. (24.01.2015).
- [5] M. Johnson, *J. Phys. Chem. B* **2005**, *109*, 14278–14291.
- [6] a) G. M. Tsivgoulis, J.-M. Lehn, *Adv. Mater.* **1997**, *9*, 39–42; b) G. M. Tsivgoulis, J.-M. Lehn, *Chem. Eur. J.* **1996**, 1399–1406; c) D. M. Eigler, C. P. Lutz, W. E. Rudge, *Nature* **1991**, *352*, 600–603; d) P. Ball, L. Garwin, *Nature* **1992**, *355*, 761–766.
- [7] D. Baylor, *Proc. Natl. Acad. Sci. U.S.A.* **1996**, *93*, 560–565.
- [8] H. Rau in *Photochromism. Molecules and Systems*. (Ed.: H. Dürr, H. Bouas-Laurent), rev. ed. Elsevier, Amsterdam, **2006**.
- [9] Y. Kim, T. J. Hellmuth, D. Sysoiev, F. Pauly, T. Pietsch, J. Wolf, A. Erbe, T. Huhn, U. Groth, U. E. Steiner, *Nano Lett.* **2012**, *12*, 3736–3742.
- [10] M. Stein, S. J. Middendorp, V. Carta, E. Pejo, D. E. Raines, S. A. Forman, E. Sigel, D. Trauner, *Angew. Chem. Int. Ed.* **2012**, *51*, 10500–10504.
- [11] J. Griffiths, *Chem. Soc. Rev.* **1972**, *1*, 481–493.
- [12] U. Al-Atar, R. Fernandes, B. Johnsen, D. Baillie, N. R. Branda, *J. Am. Chem. Soc.* **2009**, *131*, 15966–15967.
- [13] L. Sheng, M. Li, S. Zhu, H. Li, G. Xi, Y.-G. Li, Y. Wang, Q. Li, S. Liang, K. Zhong, *Nat. Comms.* **2014**, *5*, 1–8.
- [14] Entire volume dedicated to "Molecular Switches", *Chem. Rev.* **2000**, *100*.
- [15] G. Schulze, J. Simon (Eds.) *Jander- Jahr. Maßanalyse. Theorie und Praxis der Titrationsen mit chemischen und physikalischen Indikationen.*, 16. Aufl., Walter de Gruyter, Berlin - New York, **2003**.
- [16] H. Bouas-Laurent, H. Duerr, *Pure Appl. Chem.* **2001**, *73*, 639–665.
- [17] GESTIS-Stoffdatenbank, *http://www.dguv.de/ifa/Gefahrstoffdatenbanken/GESTIS-Stoffdatenbank/index.jsp*. (30-07-2014).
- [18] H. Gobin Khorana, *J. Biol. Chem.* **1992**, *267*, 1–4.
- [19] P. S. Deigner, W. C. Law, F. J. Canada, R. R. Rando, *Science* **1989**, *244*, 968–971.
- [20] A. Petitjean, R. G. Houry, N. Kyritsakas, J.-M. Lehn, *J. Am. Chem. Soc.* **2004**, *126*, 6637–6647.
- [21] P. M. Monk, R. J. Mortimer, D. R. Rosseinsky, *Electrochromism: Fundamentals and Applications*, 1st Edition, VCH Publ., Weinheim, **1995**.
- [22] S. P. Semproni, D. J. Knobloch, C. Milsman, P. J. Chirik, *Angew. Chem. Int. Ed.* **2013**, *52*, 5372–5376.
- [23] P. W. Atkins, *Physikalische Chemie*, 3. Aufl., VHC, Weinheim, **1990**.
- [24] M. Irie, *Chem. Rev.* **2000**, *100*, 1685–1716.

- [25] H. Dürr, *Angew. Chem.* **2004**, *116*, 3404–3418.
- [26] J. Fritzsche, *C. R. Hebd. Seances Acad. Sci.* **1867**, *69*, 1035.
- [27] E. ter Meer, *Justus Liebigs Ann. Chem.* **1876**, *181*, 1–22.
- [28] T. L. Phipson, *Chem. News* **1899**, *43*, 283.
- [29] Y. Hirshberg, *C. R. Hebd. Seances Acad. Sci.* **1950**, *231*, 903–904.
- [30] a) G. Berkovic, V. Krongauz, V. Weiss, *Chem. Rev.* **2000**, *100*, 1741–1754; b) B. S. Lukyanov, M. B. Lukyanova, *Chem. Hetrocycl. Compd.* **2005**, *41*, 281–311; c) J. T. Wojtyk, P. M. Kazmaier, E. Buncel, *Chem. Commun.* **1998**, 1703–1704.
- [31] X. Guo, D. Zhang, G. Yu, M. Wan, J. Li, Y. Liu, D. Zhu, *Adv. Mater.* **2004**, *16*, 636–640.
- [32] B. Schaudel, C. Guerneur, C. Sanchez, K. Nakatani, J. A. Dalairé, *J. Mater. Chem.* **1997**, *7*, 61–65.
- [33] T. Suzuki, F.-T. Lin, S. Priyadashy, S. G. Weber, *Chem. Commun.* **1998**, 2685–2686.
- [34] S. Zhang, Q. Zhang, B. Ye, X. Li, X. Zhang, Y. Deng, *J. Phys. Chem. B* **2009**, *113*, 6012–6019.
- [35] V. I. Minkin, *Chem. Rev.* **2004**, *104*, 2751–2776.
- [36] V. I. Minkin in *Molecular Switches*. (Eds.: B. Feringa, W. R. Browne), 2., completely rev. and enl. ed., Wiley-VCH GmbH & Co. KGaA., Weinheim, **2011**.
- [37] H. Decker, H. Fellenberg, *Liebigs Ann. Chem.* **1909**, *364*, 1–44.
- [38] a) W. Dilthey, *Chem. Ber.* **1926**, *59*, 1856–1858; b) A. Loewenbein, W. Kats, *Chem. Ber.* **1926**, *59*, 1377–1383; c) W. Dilthey, C. Berres, E. Holterhoff, H. Wuebken, *J. Prakt. Chem.* **1926**, *114*, 179–198.
- [39] E. Fischer, Y. Hirshberg, *J. Chem. Soc. (resumed)* **1952**, 4522–4524.
- [40] L. M. Trefonas, J. Schneller, A. I. Meyers, *Tetrahedron Lett.* **1961**, *2*, 785–790.
- [41] R. Gugliemetti in *Photochromism. Molecules and Systems*. (Ed.: H. Dürr, H. Bouas-Laurent), rev. ed. Elsevier, Amsterdam, **2006**.
- [42] J. T. Wojtyk, P. M. Kazmaier, E. Buncel, *Chem. Mater.* **2001**, *13*, 2547–2551.
- [43] N. Andersson, P. Alberius, J. Örtengren, M. Lindgren, L. Bergström, *J. Mater. Chem.* **2005**, *15*, 3507.
- [44] N. Y. C. Chu in *Photochromism. Molecules and Systems*. (Ed.: H. Dürr, H. Bouas-Laurent), rev. ed. Elsevier, Amsterdam, **2006**.
- [45] Y. Yokoyama, T. Gushiken, T. Ubukata in *Molecular Switches*. (Eds.: B. Feringa, W. R. Browne), 2., completely rev. and enl. ed., Wiley-VCH GmbH & Co. KGaA., Weinheim, **2011**.
- [46] Y. Yokoyama, *Chem. Rev.* **2000**, *100*, 1717–1740.
- [47] a) H. Stobbe, *Chem. Ber.* **1905**, *40*, 3372–3382; b) H. Stobbe, *Chem. Ber.* **1905**, *38*, 3673–3682; c) H. Stobbe, *Liebigs Ann.* **1911**, *380*, 1–2.
- [48] A. Santiago, R. S. Becker, *J. Am. Chem. Soc.* **90**, 3654–3658.
- [49] a) H. G. Heller, K. Salisbury, *J. Chem. Soc. (C)* **1967**, 1552–1554; b) H. G. Heller, D. Auld, K. Salisbury, *J. Chem. Soc. (C)* **1967**, 682–685; c) H. G. Heller, D. Auld, K. Salisbury, *J. Chem. Soc. (C)* **1967**, 2457–2459; d) H. G. Heller, K. Salisbury, *J. Chem. Soc. (C)* **1970**, 873–874; e) H. G. Heller, K. Salisbury, *J. Chem. Soc. (C)* **1970**, 1997–2000; f) H. G. Heller, K. Salisbury, *J. Chem. Soc. (C)* **1970**, 399–402; g) S. Hastings, H. G. Heller, *J. Chem. Soc.*,

- Perkin Trans. 1* **1972**, 1839–1842; h) R. J. Hart, H. G. Heller, *J. Chem. Soc., Perkin Trans. 1* **1972**, 1321–1323; i) H. G. Heller, M. Szewczyk, *J. Chem. Soc., Perkin Trans. 1* **1974**, 1487–1492; j) H. G. Heller, R. M. Megit, *J. Chem. Soc., Perkin Trans. 1* **1974**, 923–927; k) S. Hastings, H. G. Heller, H. Tucker, *J. Chem. Soc., Perkin Trans. 1* **1975**, 1545–1548; l) S. Hastings, H. G. Heller, K. Salisbury, *J. Chem. Soc., Perkin Trans. 1* **1975**, 1995–1998; m) P. J. Darcy, R. J. Hart, H. G. Heller, *J. Chem. Soc., Perkin Trans. 1* **1978**, 571–576; n) H. G. Heller, D. Piggott, *J. Chem. Soc., Perkin Trans. 1* **1978**, 989–994.
- [50] O. Crescente, H. G. Heller, S. Oliver, *J. Chem. Soc., Perkin Trans. 1* **1979**, 150–153.
- [51] a) J. Whittal in *Photochromism. Molecules and Systems*. (Ed.: H. Dürr, H. Bouas-Laurent), rev. ed. Elsevier, Amsterdam, **2006**; b) H. G. Heller, S. Oliver, M. Shawe, *J. Chem. Soc., Perkin Trans. 1* **1979**, 154–157.
- [52] H. G. Heller, S. Oliver, *J. Chem. Soc., Perkin Trans. 1* **1981**, 197–201.
- [53] P. J. Darcy, H. G. Heller, P. J. Strydom, J. Whittal, *J. Chem. Soc., Perkin Trans. 1* **1981**, 202–205.
- [54] Y. Yokoyama, T. Goto, T. Inoue, M. Yokoyama, Y. Kurita, *Chem. Lett.* **1988**, *17*, 1049–1052.
- [55] H. Rau, *Angew. Chem. Int. Ed.* **1973**, *12*, 224–235.
- [56] F. Krollpfeiffer, C. Mühlhausen, G. Wolf, *Liebigs Ann. Chem.* **1934**, 39–51.
- [57] G. S. Hartley, *Nature* **1937**, *140*, 281.
- [58] a) T. Avellini, H. Li, A. Coskun, G. Barin, A. Trabolsi, A. N. Basuray, S. K. Dey, A. Credi, S. Silvi, J. F. Stoddart et al., *Angew. Chem. Int. Ed.* **2012**, *51*, 1611–1615; b) B. J. Coe, *Chem. Eur. J.* **1999**, *9*, 2464–2471; c) L. Fang, S. Chen, Y. Zhang, H. Zhang, *J. Mater. Chem.* **2011**, *21*, 2320–2329; d) M. Han, T. Hirade, M. Hara, *New J. Chem.* **2010**, *34*, 2887–2891; e) M. Han, T. Honda, D. Ishikawa, E. Ito, M. Hara, Y. Norikane, *J. Mater. Chem.* **2011**, *21*, 4696–4702; f) C.-C. Ko, V. Wing-Wah Yam, *J. Mater. Chem.* **2010**, *20*, 2063–2070; g) Y. J. Liu, H. T. Dai, X. W. Sun, *J. Mater. Chem.* **2011**, *21*, 2982–2986; h) R. Reuter, H. A. Wegner, *Chem. Commun.* **2011**, *47*, 12267–12276; i) S. Tamesue, Y. Takashima, H. Yamaguchi, S. Shinkai, A. Harada, *Angew. Chem. Int. Ed. Engl.* **2010**, *49*, 7461–7464; j) Y. Wang, G. Ye, X. Wang, *J. Mater. Chem.* **2012**, *22*, 7614–7621; k) X. Jia, D. Chao, E. B. Berda, S. Pei, H. Liu, T. Zheng, C. Wang, *J. Mater. Chem.* **2011**, *21*, 18317–18324; l) P. Wolfer, H. Audorff, K. Kreger, L. Kador, H.-W. Schmidt, N. Stingelin, P. Smith, *J. Mater. Chem.* **2011**, *21*, 4339–4345; m) C. R. Zhang, W. P. Yan, M. G. Fan, *Chin. Chem. Lett.* **2007**, *18*, 519–522.
- [59] T. Okeda, O. Tsutsumi, *Science* **1995**, *268*, 1873–1875.
- [60] S. Shinkai, T. Najaki, Y. Nishida, T. Ogawa, O. Manabe, *J. Am. Chem. Soc.* **1980**, *102*, 5860–5865.
- [61] M. Kurihara, T. Matsuda, A. Hirooka, T. Yutaka, H. Nishihara, *J. Am. Chem. Soc.* **2000**, *122*, 12373–12374.
- [62] C. Vanlersberghe, F. Camu, *Handb. Exo. Pharmacol.* **2008**, *182*, 227–252.
- [63] K. A. Muskat, S. Ozeri-Sharafi, G. Seger, T. A. Pakkanen, *J. Chem. Soc., Perkin Trans. 2* **1975**, 1515–1520.

- [64]a) T. J. Cuppen, W. H. Laarhoven, *J. Am. Chem. Soc.* **1972**, *94*, 5914–5915; b) C. Goedicke, H. Stegemeyer, *Chem. Phys. Lett.* **1972**, *17*, 492–494.
- [65]W. H. Laarhoven in *Photochromism. Molecules and Systems*. (Ed.: H. Dürr, H. Bouas-Laurent), rev. ed. Elsevier, Amsterdam, **2006**.
- [66]M. Irie, M. Mohri, *J. Org. Chem.* **1988**, *53*, 803–808.
- [67]R. M. Kellogg, M. B. Groen, H. Wynberg, *J. Org. Chem.* **1967**, *32*, 3093–3100.
- [68]R. B. Woodward, R. Hoffmann, *Angew. Chem. Int. Ed.* **1969**, *8*, 781–932.
- [69]R. B. Woodward, R. Hoffmann, *J. Am. Chem. Soc.* **1965**, *87*, 395–397.
- [70]S. Nakamura, M. Irie, *J. Org. Chem.* **1988**, *53*, 6136–6138.
- [71]M. Hanazawa, R. Sumiya, Y. Horikawa, M. Irie, *J. Am. Chem. Soc., Chem. Commun.* **1992**, *3*, 206–207.
- [72]M. M. Krayushkin, L. G. Vorontsova, V. N. Yarovenko, I. V. Zavarzin, V. N. Bulgakova, Z. A. Starikova, V. A. Barachevskii, *Russ. Chem. Bull. Int. Ed.* **2008**, *57*, 2402–2404.
- [73]L. N. Lucas, J. de Jong, J. van Esch, R. M. Kellogg, B. L. Feringa, *Eur. J. Org. Chem.* **2003**, *1*, 155–166.
- [74]H. Lin, W. Xu, D. Zhu, *J. Mater. Chem.* **2010**, *20*, 884–890.
- [75]V. A. Migulin, M. M. Krayushkin, V. A. Barachevsky, O. I. Kobeleva, T. M. Valova, K. A. Lyssenko, *J. Org. Chem.* **2012**, *77*, 332–340.
- [76]V. P. Rybalkin, E. N. Shepelenko, L. L. Popova, A. D. Dubonosov, A. V. Metelitsa, N. I. Makarova, V. A. Bren, V. I. Minkin, *Russ. J. Org. Chem.* **2006**, *142*, 619–621.
- [77]G. Hohlneicher, M. Müller, M. Demmer, J. Lex, J. H. Penn, L.-x. Gan, P. D. Loesel, *J. Am. Chem. Soc.* **1988**, *110*, 4483–4494.
- [78]G. Guirado, C. Coudret, J.-P. Launay, *J. Phys. Chem. C* **2007**, *111*, 2770–2776.
- [79]C. C. Warford, V. Lemieux, N. Branda in *Molecular Switches*. (Eds.: B. Feringa, W. R. Browne), 2., completely rev. and enl. ed., Wiley-VCH GmbH & Co. KGaA., Weinheim, **2011**.
- [80]M. Irie, K. Sakemura, M. Okinaka, K. Uchida, *J. Org. Chem.* **1995**, *60*, 8305–8309.
- [81]S. L. Gilat, S. H. Kawai, J.-M. Lehn, *J. Chem. Soc., Chem. Commun.* **1993**, 1439–1442.
- [82]S. L. Gilat, S. H. Kawai, J.-M. Lehn, *Chem. Eur. J.* **1995**, *1*, 275–284.
- [83]a) M. Takeshita, C. N. Choi, M. Irie, *Chem. Commun.* **1997**, *62*, 2265–2266; b) M. Takeshita, N. Kato, S. Kawauchi, T. Imase, J. Watanabe, M. Irie, *J. Org. Chem.* **1998**, *63*, 9306–9313.
- [84]K. Uchida, E. Tsuchida, Y. Aoi, S. Nakamura, M. Irie, *Chem. Lett.* **1999**, *26*, 63–64.
- [85]F. Stellace, C. Bertarelli, *Adv. Mater.* **1999**, *11*, 292–295.
- [86]M. Takeshita, M. Nagai, T. Yamato, *Chem. Commun.* **2003**, 1496–1497.
- [87]M. Irie, K. Uchida, T. Eriguchi, H. Tsuzuki, *Chem. Lett.* **1995**, 899–900.
- [88]M. Kamrul Hossain, M. Takeshita, T. Yamato, *Eur. J. Org. Chem.* **2005**, *2005*, 2771–2776.
- [89]R. Göstl, B. Kobin, L. Grubert, M. Pätzl, S. Hecht, *Chem. Eur. J.* **2012**, *18*, 14282–14285.
- [90]M. Irie, T. Lifka, K. Uchida, S. Kobatake, Y. Shindo, *Chem. Commun.* **1999**, 747–750.
- [91]J. C. Owrutsky, H. H. Nelson, A. P. Baronavski, O.-K. Kim, G. M. Tsivgoulis, *Chem. Phys. Lett.* **1998**, *293*, 555–563.

- [92] V. Ramamurthy in *Photochemistry in Organized & Constrained Media* (Eds.: J. R. Scheffer, P. R. Pokkuluri), VCH Publ., New York, **1991**.
- [93] S. Kobatake, T. Yamada, K. Uchida, N. Kato, M. Irie, *J. Am. Chem. Soc.* **1999**, *121*, 2380–2386.
- [94] S. Kobatake, M. Irie, *Bull. Chem. Soc. Jpn.* **2004**, *77*, 195–210.
- [95] S. Kobatake, K. Uchida, E. Tsuchida, M. Irie, *Chem. Commun.* **2002**, 2804–2805.
- [96] G. M. Ó Máille, S. M. Draper, *Spectrosc. Prop. Inorg. Organomet. Compd.* **2012**, *43*, 166–215.
- [97] V. Adamo, P. Belser, *Chimia* **2003**, *57*, 169–172.
- [98] P. Belser, L. de Cola, F. Hartl, V. Adamo, B. Bozic, Y. Chriqui, V. M. Iyer, R. T. Jukes, J. Kühni, M. Querol et al., *Adv. Funct. Mater.* **2006**, *16*, 195–208.
- [99] R. T. Jukes, V. Adamo, F. Hartl, P. Belser, L. de Cola, *Inorg. Chem.* **2004**, *43*, 2779–2792.
- [100] a) A. C. Jacko, R. H. McKenzie, B. J. Powell, *J. Mater. Chem.* **2010**, *20*, 10301–10320; b) M. Schwalbe, M. Karnahl, S. Tschierlei, U. Uhlemann, M. Schmitt, B. Dietzek, J. Popp, R. Groake, J. G. Vos, S. Rau, *Dalton Trans.* **2010**, *39*, 2768–2771; c) A. O. Tolpygin, A. V. Cherkasov, G. K. Fukin, A. A. Trifonov, *Inorg. Chem.* **2014**, *53*, 1537–1543; d) O. S. Wenger, *Chem. Soc. Rev.* **2012**, *41*, 3772–3779; e) O. Sato, *Proc. Jpn. Acad., Ser. B* **2012**, *88*, 213–225; f) Y. Lin, J. Yin, J. Yuan, M. Hu, Z. Li, G.-A. Yu, S. H. Liu, *Organometallics* **2010**, *29*, 2808–2814.
- [101] K. Motoyama, T. Koike, M. Akita, *Chem. Commun.* **2008**, 5812–5814.
- [102] Y.-W. Zhong, N. Vila, J. C. Henderson, H. D. Abruña, *Inorg. Chem.* **2009**, *48*, 991–999.
- [103] Y.-W. Zhong, N. Vila, J. C. Henderson, S. Flores-Torres, H. D. Abruña, *Inorg. Chem.* **2007**, *46*, 10470–10472.
- [104] Y. Lin, J. Yuan, M. Hu, J. Cheng, J. Yin, S. Jin, S. H. Liu, *Organometallics* **2009**, *28*, 6402–6409.
- [105] Y.-W. Zhong, N. Vilà, J. C. Henderson, H. D. Abruña, *Inorg. Chem.* **2009**, *48*, 7080–7085.
- [106] O. Sato, *Proc. Jpn. Acad., Ser. B* **2012**, *88*, 213–225.
- [107] Á. Fernández-Acebes, J.-M. Lehn, *Adv. Mater.* **1998**, *10*, 1519–1522.
- [108] a) G. M. Tsivgoulis, J.-M. Lehn, *Chem. Eur. J.* **1996**, 1399–1406; b) G. M. Tsivgoulis, J.-M. Lehn, *Angew. Chem. Int. Ed.* **1995**, *34*, 1119–1122.
- [109] P. H.-M. Lee, C.-C. Ko, N. Zhu, V. W.-W. Yam, *J. Am. Chem. Soc.* **2007**, *129*, 6058–6059.
- [110] M. Malaun, Z. R. Reeves, R. L. Paul, J. C. Jeffery, J. A. McCleverty, M. D. Ward, I. Asselberghs, K. Clays, A. Persoons, *Chem. Commun.* **2001**, 49–50.
- [111] G. Guirado, C. Coudret, M. Hliwa, J.-P. Launay, *J. Phys. Chem. B* **2005**, *109*, 17445–17459.
- [112] K. Uchida, A. Inagaki, M. Akita, *Organometallics* **2007**, *26*, 5030–5041.
- [113] S. Fraysse, C. Coudret, J.-P. Launay, *Eur. J. Inorg. Chem.* **2000**, 1581–1590.
- [114] Y. Tanaka, A. Inagaki, M. Akita, *Chem. Commun.* **2007**, 1169–1171.

- [115] Y. Tanaka, T. Ishisaka, A. Inagaki, T. Koike, C. Lapinte, M. Akita, *Chem. Eur. J.* **2010**, *16*, 4762–4776.
- [116] J.-M. Lehn, Á. Fernández-Acebes, *Chem. Eur. J.* **1999**, *5*, 3285–3292.
- [117] M. Akita, *Organometallics* **2011**, *30*, 43–51.
- [118] a) X.-H. Zhou, F.-S. Zhang, P. Yuan, F. Sun, S.-Z. Pu, F.-Q. Zhao, C.-H. Tung, *Chem. Lett.* **2004**, *33*, 1006–1007; b) Y. Moriyama, K. Matsuda, N. Tanifuji, S. Irie, M. Irie, *Org. Lett.* **2005**, *7*, 3315–3318; c) A. Peters, N. R. Branda, *J. Am. Chem. Soc.* **2003**, *125*, 3404–3405; d) A. Peters, N. R. Branda, *Chem. Commun.* **2003**, 954–955; e) T. Koshido, T. Kawai, K. Yoshino, *J. Phys. Chem.* **1995**, *99*, 6110–6114.
- [119] E. C. Harvey, J. Areephong, A. A. Cafolla, C. Long, W. R. Browne, B. L. Feringa, M. T. Pryce, *Organometallics* **2014**, *33*, 447–456.
- [120] A. Weiss, H. Witte, *Magnetochemie. Grundlagen und Anwendungen*, 1. Aufl., Chemie GmbH, Weinheim, **1973**.
- [121] O. Kahn, *Molecular Magnetism-Olivier Kahn*, 1 st Edition, VCH Publishers, Inc., New York, **1993**.
- [122] E. Riedel (Ed.) *Moderne Anorganische Chemie*, 3. Aufl., Walter de Gruyter, Berlin, **2007**.
- [123] B. Weber, *Skript zur Vorlesung "Molekulare Magneten"*, Ludwig-Maximilians-Universität München, **2009**.
- [124] I. Bertini, C. Luchinat, G. Parigi, *Solution NMR of Paramagnetic Molecules. Applications to Metallobiomolecules and Models*, 1 st Edition, Elsevier, Amsterdam, **2001**.
- [125] J. S. Miller, A. J. Epstein, *Angew. Chem. Int. Ed.* **1994**, *33*, 385–415.
- [126] B. Bechlars, D. M. D'Alessandro, D. M. Jenkins, A. T. Lavarone, S. D. Glover, C. P. Kubiak, J. R. Long, *Nat. Chem.* **2010**, *2*, 362–368.
- [127] J. S. Miller, D. T. Glatzhofer, R. Laversanne, T. B. Brill, M. D. Timken, C. J. O'Connor, J. H. Zhang, J. C. Calabrese, A. J. Epstein, S. Chittipeddi, *Chem. Mater.* **1990**, *2*, 60–69.
- [128] a) S. A. Miller, J. A. Tebboth, J. F. Tremaine, *J. Chem. Soc.* **1952**, 632–635; b) T. J. Kealy, P. L. Pauson, *Nature* **1951**, *168*, 1039–1040.
- [129] G. Wilkinson, M. Rosenblum, M. C. Whiting, R. B. Woodward, *J. Am. Chem. Soc.* **1952**, *74*, 2125–2126.
- [130] W. Pfab, E. O. Fischer, *ZAAC* **1953**, *274*, 316–322.
- [131] G. Wilkinson, *J. Am. Chem. Soc.* **1952**, *74*, 6148–6149.
- [132] a) E. O. Fischer, R. Jira, *Z. Naturforsch.* **1953**, *8b*, 1–2; b) E. O. Fischer, R. Jira, *Z. Naturforsch.* **1953**, *5b*, 327–328.
- [133] C. Rieker, G. Ingram, P. Jaitner, H. Schottenberger, K. E. Schwarzhan, *J. Organomet. Chem.* **1990**, *381*, 127–133.
- [134] a) W. E. Geiger, Bowden, William, L., N. El Murr, *Inorg. Chem.* **1979**, *18*, 2358–2361; b) J. A. Bard, E. García, *Inorg. Chem.* **1993**, *32*, 3528–3531.
- [135] N. El Murr, E. Laviro, *Tetrahedron Lett.* **1975**, *16*, 875–878.
- [136] J. H. Ammeter, J. M. Brom, *Chem. Phys. Lett.* **1974**, *27*, 380–384.

- [137] a) C. Cauletti, J. C. Green, M. Kelly, P. Powell, J. van Tilborg, J. Robbins, J. Smart, *J. Electron. Spectrosc. Relat. Phenom.* **1980**, *19*, 327–353; b) H. Eicher, *Phys. Rev. A* **1989**, *40*, 1637–1639; c) G. Fronzoni, M. Stener, S. Furlan, P. Decleva, *Chem. Phys.* **2001**, *273*, 117–133; d) J. Brennan, G. Cooper, J. C. Green, M. P. Payne, C. M. Redfern, *J. Electron. Spectrosc. Relat. Phenom.* **1993**, *66*, 101–115.
- [138] K. R. Gordon, K. D. Warren, *J. Organomet. Chem.* **1976**, *117*, C27–C29.
- [139] J. Weber, A. Goursot, E. Pénigault, J. H. Ammeter, J. Bachmann, *J. Am. Chem. Soc.* **1982**, *104*, 1491–1506.
- [140] E. König, R. Schnakig, S. Kremer, B. Kanellakopoulos, R. Klenze, *Chem. Phys.* **1978**, *27*, 331–344.
- [141] J. D. Dunitz, L. E. Orgel, A. Rich, *Acta Cryst.* **1956**, *9*, 373–375.
- [142] G. L. Hardgrove, D. H. Templeton, *Acta Cryst.* **1959**, *12*, 28–32.
- [143] P. Zanello, *Inorganic Electrochemistry. Theory, Practice und Application.*, Edition: 2003, Royal Society of Chemistry, Cambridge, **2003**.
- [144] J. H. Ammeter, *J. Chem. Phys.* **1972**, *57*, 678–698.
- [145] J. H. Ammeter, *J. Magn. Reson. (1969)* **1978**, *30*, 299–325.
- [146] F. H. Köhler, *J. Organomet. Chem.* **1976**, *110*, 235–246.
- [147] a) F. H. Köhler, *J. Organomet. Chem.* **1975**, *91*, 57–64; b) F. H. Köhler, W. Prössdorf, *J. Am. Chem. Soc.* **1978**, *100*, 5970–5972; c) F. H. Köhler, W. Proessdorf, *J. Am. Chem. Soc.* **1978**, *100*, 5970–5972; d) F. H. Köhler, K. H. Doll, W. Prössdorf, *J. Organomet. Chem.* **1982**, *224*, 341–353; e) N. Hebindanz, F. H. Köhler, F. Scherbaum, B. Schlesinger, *Magn. Reson. Chem.* **1989**, *27*, 798–802; f) J. Bluemel, P. Hofmann, F. H. Köhler, *Magn. Reson. Chem.* **1993**, *31*, 1–6; g) H. Hilbig, F. H. Köhler, *New J. Chem.* **2001**, *25*, 1152–1162; h) H. Heise, F. H. Köhler, M. Herker, W. Hiller, *J. Am. Chem. Soc.* **2002**, *124*, 10823–10832.
- [148] F. H. Köhler, *J. Organomet. Chem.* **1976**, *121*, C61–C62.
- [149] F. H. Köhler, *J. Organomet. Chem.* **1978**, *160*, 299–306.
- [150] S. Altmannshofer, E. Herdtweck, F. H. Köhler, R. Miller, R. Mölle, E.-W. Scheidt, W. Scherer, C. Train, *Chem. Eur. J.* **2008**, *14*, 8013–8024.
- [151] K. Eberl, F. H. Köhler, L. Mayring, *Angew. Chem.* **1976**, *88*, 544–545.
- [152] U. Kölle, F. Khouzami, *Angew. Chem.* **1980**, *92*, 658–659.
- [153] J. L. Robbins, N. Edelstein, B. Spencer, J. C. Smart, *J. Am. Chem. Soc.* **1982**, *104*, 1882–1983.
- [154] Zoller L., E. Moser, J. H. Ammeter, *J. Phys. Chem.* **1986**, *90*, 6632–6638.
- [155] V. Maryin, P. V. Petrovskii, *J. Organomet. Chem.* **1992**, *441*, 125–141.
- [156] H. Eicher, F. H. Köhler, *Chem. Phys.* **1988**, *128*, 297–309.
- [157] E. König, V. P. Desai, B. Kanellakopoulos, F. H. Köhler, *Chem. Phys.* **1983**, *80*, 263–272.
- [158] F. H. Köhler in *Magnetism: Molecules to Materials. Models and Experiments* (Eds.: J. S. Miller, M. Drillon), 1st Edition, Wiley-VCH GmbH & Co. KGaA., Weinheim, **2001**.
- [159] P. Hudeczek, F. H. Köhler, *Organometallics* **1992**, *11*, 1773–1775.
- [160] G. E. McManis, R. M. Nielson, M. J. Weaver, *Inorg. Chem.* **1988**, *27*, 1827–1829.

- [161] H. Hilbig, P. Hudeczek, F. H. Köhler, X. Xie, P. Bergerat, O. Kahn, *Inorg. Chem.* **1998**, *37*, 4246–4257.
- [162] P. Hudeczek, F. H. Köhler, P. Bergerat, O. Kahn, *Chem. Eur. J.* **1999**, *5*, 70–78.
- [163] J. M. Manriquez, M. D. Ward, W. M. Reiff, J. C. Calabrese, N. L. Jones, P. J. Carrol, E. E. Bunel, J. S. Miller, *J. Am. Chem. Soc.* **1995**, *117*, 6182–6193.
- [164] J. M. Manriquez, M. D. Ward, J. C. Calabrese, P. J. Fagan, A. J. Epstein, J. S. Miller, *Mol. Cryst. Liq. Cryst.* **1989**, *176*, 527–534.
- [165] a) M.-T. Lee, B. M. Foxman, M. Rosenblum, *Organometallics* **1985**, *4*, 539–547; b) R. Arnold, S. A. Matchett, M. Rosenblum, *Organometallics* **1988**, *7*, 2261–2266; c) R. D. Hudson, B. M. Foxman, M. Rosenblum, *Organometallics* **2000**, *19*, 469–474.
- [166] N. Pagels, *Dissertation*, Universität Hamburg, Hamburg, **2011**.
- [167] S. Barlow, D. O'Hare, *Chem. Soc. Rev.* **1997**, *97*, 637–669.
- [168] J. Heinze, *Angew. Chem.* **1984**, *96*, 823–916.
- [169] P. Day, N. S. Hush, R. J. Clark, *Philos Trans A Math Phys Eng Sci* **2008**, *366*, 5–14.
- [170] J. P. Fackler, *Mixed Valence Compounds*, John Wiley & Sons, Ltd, Hoboken, **2006**.
- [171] L.-A. Alcaraz Mas, A. González Donaire, *An. Quím.* **2006**, *102*, 27–33.
- [172] H. Jaffe, M. Orchin, *Theory and Applications of Ultraviolet Spectroscopy*, 1st Edition, John Wiley & Sons, Ltd, Hoboken, **1962**.
- [173] A. Beer, *Ann. Physik Chem. (2)* **1852**, *86*, 78–88.
- [174] H. G. Becker (Ed.) *Einführung in der Photochemie*, 1. Aufl., VEB Deutscher Verlag der Wissenschaften, Berlin, **1975**.
- [175] F. Würthner, S. Yao, *Angew. Chem.* **2000**, *112*, 2054–2057.
- [176] G. Szalóki, J.-L. Pozzo, *Chem. Eur. J.* **2013**, *19*, 11124–11132.
- [177] a) X. Piao, Y. Zou, J. Wu, C. Li, T. Yi, *Org. Lett.* **2009**, *11*, 3818–3821; b) H. Tian, S. Wang, *Chem. Commun.* **2007**, 781–792; c) T. B. Norsten, N. R. Branda, *J. Am. Chem. Soc.* **2001**, *123*, 1784–1785.
- [178] a) W. Tan, Q. Zhang, J. Zhang, H. Tian, *Org. Lett.* **2009**, *11*, 161–164; b) Y. Lin, J. Yin, J. Yuan, M. Hu, Z. Li, G.-A. Yu, S. H. Liu, *Organometallics* **2010**, *29*, 2808–2814; c) S. Kume, H. Nishihara, *Dalton Trans.* **2008**, 3260–3271.
- [179] a) Y. Chen, D. X. Zeng, M. G. Fan, *Org. Lett.* **2003**, *5*, 1435–1437; b) Z.-N. Huang, B.-A. Xu, S. Jin, M.-G. Fang, *Synthesis* **1998**, *8*, 1092–1095.
- [180] a) W. Yueh, N. L. Bauld, *J. Chem. Soc., Perkin Trans. 2* **1996**, 1761–1766; b) P. Raster, A. Schmidt, M. Rambow, N. Kuzmanovic, B. König, G. Hilt, *Chem. Commun.* **2014**, *50*, 1864–1866.
- [181] N. Pagels, O. Albrecht, D. Görlitz, A. Y. Rogachev, M. H. Prosenc, J. Heck, *Chem. Eur. J.* **2011**, *17*, 4166–4176.
- [182] N. Pagels, J. Heck, *J. Organomet. Chem.* **2008**, *693*, 241–246.
- [183] S. Trtica, M. H. Prosenc, M. Schmidt, J. Heck, O. Albrecht, D. Görlitz, F. Reuter, E. Rentschler, *Inorg. Chem.* **2010**, *49*, 1667–1673.

- [184] a) N. Tanifuji, M. Irie, K. Matsuda, *J. Am. Chem. Soc.* **2005**, *127*, 13344–13353; b) S. Venkataramani, U. Jana, M. Dommaschk, F. D. Sönnichsen, F. Tuczek, R. Herges, *Science* **2011**, *331*, 445–448.
- [185] D. R. Arnold, C. P. Hadjiantoniou, *Can. J. Chem.* **1978**, *56*, 1970–1984.
- [186] D. Wilson, N. R. Branda, *Angew. Chem. Int. Ed. Engl.* **2012**, *51*, 5431–5434.
- [187] E. Prestsch, P. Bühlmann, C. Affolter, A. Herrera, R. Martínez, *Determinación estructural de compuestos orgánicos*, Edición 2002, Masson, Barcelona, **2002**.
- [188] R. J. Abraham, M. Mobli, R. J. Smith, *Magn Reson Chem* **2004**, *42*, 436–444.
- [189] N. Branda, WO 2006/125317, **2006**.
- [190] J. E. McMurry, T. Lectka, J. G. Rico, *J. Org. Chem.* **1989**, *54*, 3748–3749.
- [191] E. O. Fischer, G. E. Herberich, *Chem. Ber.* **1961**, *94*, 1517–1523.
- [192] G. E. Herberich, E. Bauer, J. Schwarzer, *J. Organomet. Chem.* **1969**, *17*, 445–452.
- [193] M. L. Green, L. Pratt, G. Wilkinson, *J. Chem. Soc.* **1959**, 3753–3767.
- [194] N. G. Connelly, W. E. Geiger, *Chem. Rev.* **1996**, *96*, 877–910.
- [195] S. Vanicek, H. Kopacka, K. Wurst, T. Müller, H. Schottenberger, B. Bildstein, *Organometallics* **2014**, *33*, 1152–1156.
- [196] C. Strohecker, *Diplomarbeit*, Universität Hamburg, Hamburg, **2011**.
- [197] G. M. Tsivgoulis, J.-M. Lehn, *Chem. Eur. J.* **1996**, 1399–1406.
- [198] A. Hildebrandt, T. Ruffer, E. Erasmus, J. C. Swarts, H. Lang, *Organometallics* **2010**, *29*, 4900–4905.
- [199] M. Schlosser, *J. Organomet. Chem.* **1967**, *8*, 9–16.
- [200] S. Scholz, M. Scheibitz, F. Schödel, M. Bolte, M. Wagner, H.-W. Lerner, *Inorg. Chim. Acta* **2007**, *360*, 3323–3329.
- [201] E. W. Neuse, M. S. Loonat, *J. Organomet. Chem.* **1985**, *286*, 329–341.
- [202] P. Zanello, A. Cinquantini, S. Mangani, G. Opromolla, L. Pardi, C. Janiak, M. D. Rausch, *J. Organomet. Chem.* **1994**, *471*, 171–177.
- [203] F. H. Köhler, *J. Organomet. Chem.* **1974**, *69*, 145–150.
- [204] E. W. Neuse, F. B. Khan, M. G. Meirim, *Appl. Organomet. Chem.* **1988**, 129–141.
- [205] E. E. Bunel, P. Campos, J. Ruz, L. Valle, *Organometallics* **1988**, *7*, 474–476.
- [206] N. Pagels, M. H. Prosenc, J. Heck, *Organometallics* **2011**, *30*, 1968–1974.
- [207] I. Gattinger, M. A. Herker, W. Hiller, F. H. Köhler, *Inorg. Chem.* **1999**, *38*, 2359–2368.
- [208] L. Xu, Z.-j. Zhao, Y.-j. Xing, P. Lu, *J. Zhejiang Univ. Sci. A* **2008**, *9*, 1590–1594.
- [209] M. Irie, M. Mohri, *J. Org. Chem.* **1988**, *53*, 803–808.
- [210] K. Uchida, Y. Nakayama, M. Irie, *Bull. Chem. Soc. Jpn.* **1990**, *63*, 1311–1315.
- [211] F. L. Anet, M. Z. Haq, *J. Am. Chem. Soc.* **1965**, *87*, 3147–3150.
- [212] V. O. Dashevsky, A. A. Lugovskoy, *J. Mol. Struct.* **1972**, *12*, 39–43.
- [213] S. K. Collins, Y. El-Azizi, A. R. Schmitzer, *J. Org. Chem.* **2007**, *72*, 6397–6408.
- [214] a) C. Janiak, *J. Chem. Soc., Dalton Trans.* **2000**, 3885–3896; b) M. O. Sinnokrot, E. F. Valeev, C. D. Sherrill, *J. Am. Chem. Soc.* **2002**, *124*, 10887–10893.
- [215] H. Liu, S. Kang, J. Y. Lee, *J. Phys. Chem. B* **2011**, *115*, 5113–5120.
- [216] M. F. Rettig, R. S. Drago, *J. Am. Chem. Soc.* **1969**, *91*, 3432–3441.

- [217] a) I. R. Lyatifov, S. P. Solodovnikov, V. N. Babin, R. B. Materikova, *Z. Naturforsch B* **1979**, *34*, 863–866; b) R. B. Materikova, V. N. Babin, S. P. Solodovnikov, I. R. Lyatifov, P. V. Petrovskii, E. I. Fedin, *Z. Naturforsch B* **1980**, *35*, 1415–1419.
- [218] J. Wissler, A. Mulder, R. Tampé, M. Bolte, *Acta Crystallogr E Struct Rep Online* **2006**, *62*, o5649–o5650.
- [219] S. Grimme, *J. Comput. Chem* **2006**, *27*, 1787–1799.
- [220] T. Steenbock, A. Escribano, J. Heck, C. Herrmann, *Chem. Phys. chem.* **2015**, *16*, 1491–1501.
- [221] R. S. Stojanovic, A. M. Bond, *Anal. Chem.* **1993**, *65*, 56–64.
- [222] J. Heinze, *Angew. Chem. Int. Ed. Engl.* **1984**, *96*, 823–916.
- [223] C. Levanda, K. Bechgaard, D. O. Cowan, *J. Org. Chem.* **1976**, 2700–2704.
- [224] a) D. S. Polcyn, I. Shain, *Anal. Chem.* **1966**, *38*, 370–375; b) F. Ammar, J. M. Savéant, *J. Electroanal. Chem. Interfacial Electrochem.* **1973**, *47*, 215–221.
- [225] a) J. P. Perdew, *Phys. Rev. B* **1986**, *34*, 7406; b) A. D. Becke, *Phys. Rev. A* **1988**, *38*, 3098–3100.
- [226] a) K. Kim, K. D. Jordan, *J. Phys. Chem. A* **1994**, *98*, 10089–10094; b) P. J. Stephens, F. J. Devlin, C. F. Chabalowski, M. J. Frisch, *J. Phys. Chem.* **1994**, *98*, 11623–11627.
- [227] a) A. Schaefer, H. Horn, R. Ahlrichs, *J. Chem. Phys.* **1992**, *97*, 2571–2577; b) A. Schaefer, C. Huber, R. Ahlrichs, *J. Chem. Phys.* **1994**, *100*, 5829–5835.
- [228] R. V. Concepcion, J. J. Breyear, J. G. Jewett, C. H. Bushweller, *J. Phys. Org. Chem.* **1998**, *11*, 84–90.
- [229] a) B. Shapiro, M. Johnston, J. Hlubucek, G. Sullivan, G. Stroebel, *J. Magn. Reson. (1969)* **1973**, *9*, 411–421; b) F. R. Jensen, D. S. Noyce, C. H. Sederholm, A. J. Berlin, *J. Am. Chem. Soc.* **1960**, *82*, 1256–1257.
- [230] A. Staykov, K. Yoshizawa, *J. Phys. Chem. C* **2008**, *113*, 3826–3834.
- [231] D. Guillaumont, T. Kobayashi, K. Kanda, H. Miyasaka, K. Uchida, S. Kobatake, K. Shibata, S. Nakamura, M. Irie, *J. Phys. Chem. A* **2002**, *106*, 7222–7227.
- [232] A. Staykov, K. Yoshizawa, *J. Chem. Phys. C* **2009**, *113*, 3826–3834.
- [233] N. J. Turro, *Modern Molecular Photochemistry*, University Science Books, Sausalito, **1991**.
- [234] J. Ern, A. T. Bens, H.-D. Martin, S. Mukamel, D. Schmid, S. Tretiak, E. Tsiper, C. Kryschi, *Chem. Phys.* **1999**, *246*, 115–125.
- [235] M. Irie, O. Miyatake, K. Uchida, T. Eriguchi, *J. Am. Chem. Soc.* **1994**, *116*, 9894–9900.
- [236] S. Meng, J. Ma, *J. Phys. Chem. A* **2012**, *116*, 913–923.
- [237] K. R. Gordon, K. D. Warren, *Inorg. Chem.* **1978**, *17*, 987–994.
- [238] *SAINT 6.02. Program for Data Reduction*, Bruker Industrial Automation, **2000**.
- [239] *SADABS. Program for area detector absorption corrections*, Siemens Analytical X-Ray.
- [240] G. Sheldrick, *SHELXS-NT V5.1*, Bruker Crystallographic Research Systems, Bruker Analytical X-Ray Instruments Inc., Madison, Wisconsin, USA, **1997**.
- [241] G. Sheldrick, *SHELXS-97, Program for crystal structure solution by Patterson and direct*.

- [242] G. Sheldrick, *SHELXL-97. Program for crystal structure refinement*, Universität Göttingen, **1997**.
- [243] a) Sigma-Aldrich, <https://www.sigmaaldrich.com/germany.html>. **(11-04-2015)**; b) GESTIS-Stoffdatenbank, <http://www.dguv.de/ifa/Gefahrstoffdatenbanken/GESTIS-Stoffdatenbank/index.jsp>. **(11-04-2015)**.

9. List of Chemicals

Table 26: Employed chemical products. ^[243]

Name	H-phrases	P-phrases	GHS
Acetone	H225, H319, H336, EUH066	P210, P261, P305+P351+P338	
Acetonitrile	H225, H332, H302, H312, H319	P210, P305+P351+P338, P403+P235	
Adipoyl chloride	H314	-	
Aluminium oxide	-	-	-
Ammonium chloride	H302, H319	P305+P351+P338	
Benzene	H225, H350, H340, H372, H304, H319, H315	P201, P210, P308+P313, P301+P310, P331, P305+P351+P338, P302+P352	
Benzophenone	H373, H412	P260, P273, P281, P308+P313, P391	
<i>n</i>-Butyllithium 1.6 M (in hexane)	H225, H250, H261, H304, H314, H336, H361f, H373, H411, EUH014	P210, P222, P231+P232, P262, P273, P422	
<i>tert</i>-Butyllithium 1.7 M (in pentane)	H225, H250, H260, H304, H314, H336, H411	P210, P222, P223, P231+P232, P370+P378, P422	
Calcium hydride	H260	P223, P231+P232, P370+P378, P422	
Chloroform	H351, H361d, H331, H302, H372, H319,		

Name	H-phrases	P-phrases	GHS
<i>n</i>-Chlorosuccinimide	H302, H314	P280, P305+P351+P338, P310	
Cobalt(II)-chloride	H302, H317, H318, H334, H341, H350i, H360F, H410	P201, P261, P273, P280, P284	
Cobaltocene	H228, H317, H334, H341, H351	P210, P261, P280, P3432+P311	
Cobaltocenium hexafluorophosphate	H302+H312+H332, H315, H319, H335	P261, P280, P305+P351+P338	
Copper(II)-sulfate pentahydrate	-	-	-
Decamethylcobalto- cene	No data available	No data available	No data available
Dichloromethane	H315, H319, H335, H336, H351, H373	P261, P281, P305+P351+P338	
Dicyclopentadiene	H226, H302, H315, H319, H330, H335, H411	P260, P273, P284, P305+P351+P338, P310	
Diethylether	H224, H302, H336, EUH019, EUH066	P210, P240, P403+P235	
Dimethoxyethane	H225, H336, H304, H411, EUH066	P273, P301+P310, P331, P403+P235	
Ferrocene	H228, H302, H411	P210, P260, P273	
Glutaryl chloride	H301, H314	P280, P301+P310, P305+P351+P338, P310	

9. List of Chemicals

Name	H-phrases	P-phrases	GHS
<i>n</i>-Hexane	H225, H304, H361f, H373, H315, H336, H411	P210, P240, P273, P301+P310, P331, P302+P352, P403+P235	
Iodine	H312+H332, H319, H335, H400	H315, H372, P273, P302+P352, P305+P351+P338, P314	
2-Methylthiophene	H225	P210	
Nitromethane	H226, H302	P210	
Nitrosyl tetrafluoroborate	H314	P280, P305+P351+P338, P310	
1,2,3,4,5-Pentamethylcyclopentadiene	H226	-	
<i>n</i>-Pentane	H225, H336, H304, H411, EUH066	P273, P301+P310, P331, P403+P235	
Petroleum ether	H225, H304, H315, H336, H361f, H373, H411	P201, P210, P301+P310, P331, P370+P378, P501	
Potassium	H260, H314, EUH014	P280, P301+P330+P331, P305+P351+P338, P309+P310, P402+P404	
Potassium <i>tert</i>-butoxyde	H228, H252, H314, EUH014	P210, P235+P410, P280, P310, P305+P351+P338,	

Name	H-phrases	P-phrases	GHS
Pyridine-d₅	H225, H302+H312+H332, H315, H319	P210, P280, P305+P351+P338	
Silica gel	-	-	-
Silver tetrafluoroborate	H314	P280, P310, P305+P351+P338	
Sodium	H260, H314, EUH014	P280, P301+P330+P331, P305+P351+P338, P309+P310, P370+P378, P422	
Sodium chloride	-	-	-
Sodium sulfate	-	-	-
Sodium thiosulfate	-	-	-
1,1,2,2-Tetrabromoethane	H302, H315, H319, H330, H412	P260, P273, P284, P305+P351+P338, P310	
Tetrahydrofurane	H225, H302, H319, H335, H351 EUH019	P210, P233, P280, P370+P378, P501	
Tetrakis(triphenylphosphine)palladium (0)	-	-	-
Titanium(III)-chloride Tetrahydrofurane complex	H228, H314	P210, P280, P305+P351+P338	
Titanium(IV)-chloride	H314, H330, H370, H372, EUH014, EUH071	P260, P280, P284, P305+P351+P338, P310	

9. List of Chemicals

Name	H-phrases	P-phrases	GHS
Toluene	H225, H361d, H304, H373, H315, H336	P210, P301+P310, P331, P302+P352	
Triphenylcarbenium tetrafluoroborate	H314, EUH014	P280, P305+P351+P338, P310	
Zinc	H250, H260, H410	P222, P223, P231+P232, P273, P370+P378, P422	

10. Supporting Information

10.1. ^1H - and ^{13}C -Spectra of the synthesized compounds

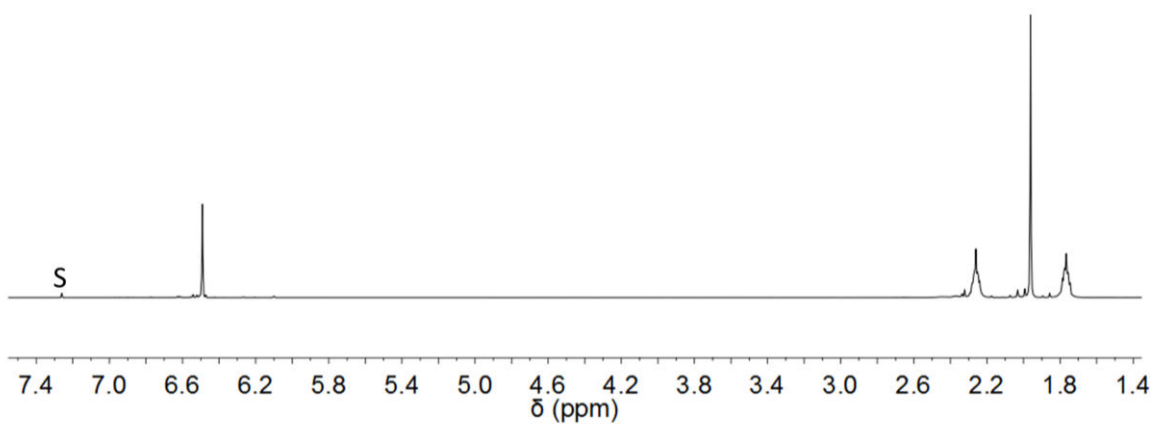


Figure 128: ^1H -NMR-spectrum of **5** in chloroform- d_1 (S = solvent).

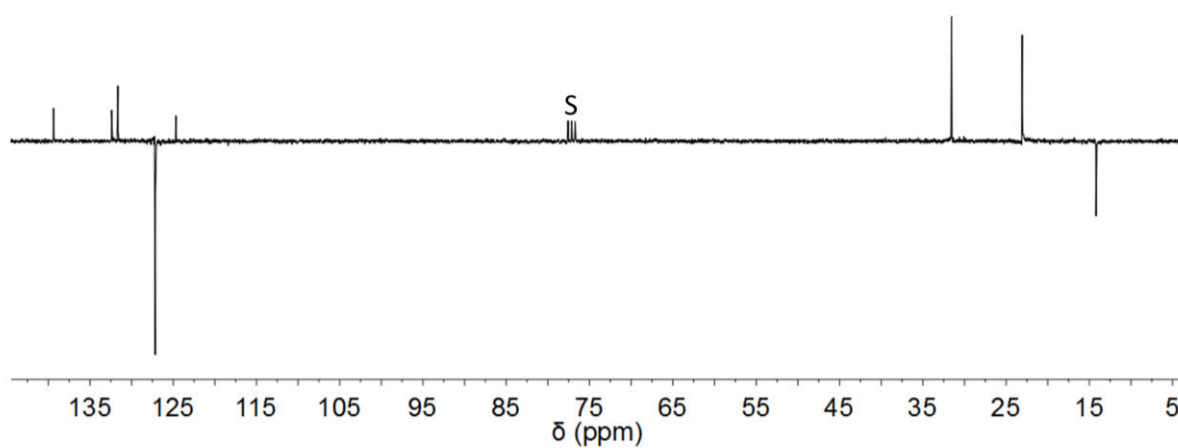


Figure 129: ^{13}C -NMR-spectrum of **5** in chloroform- d_1 (S = solvent)

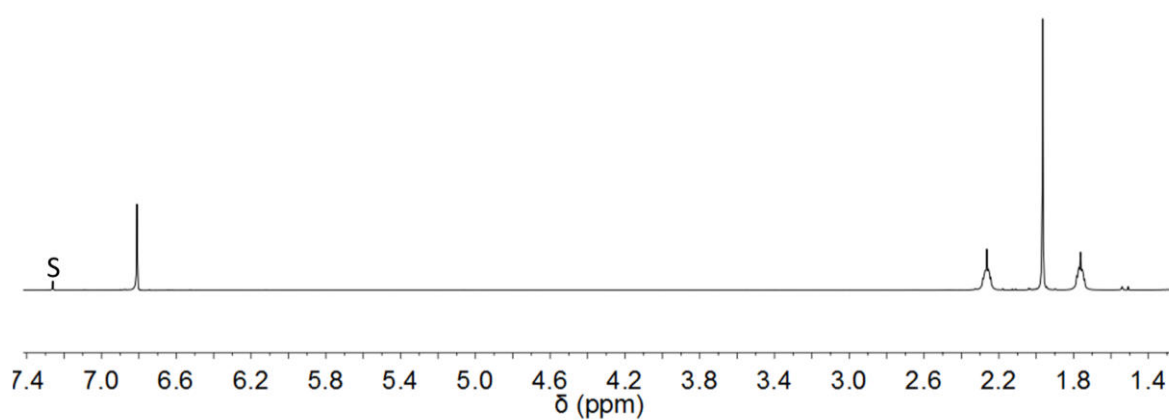


Figure 130: ^1H -NMR-spectrum of **6** in chloroform- d_1 (S = solvent).

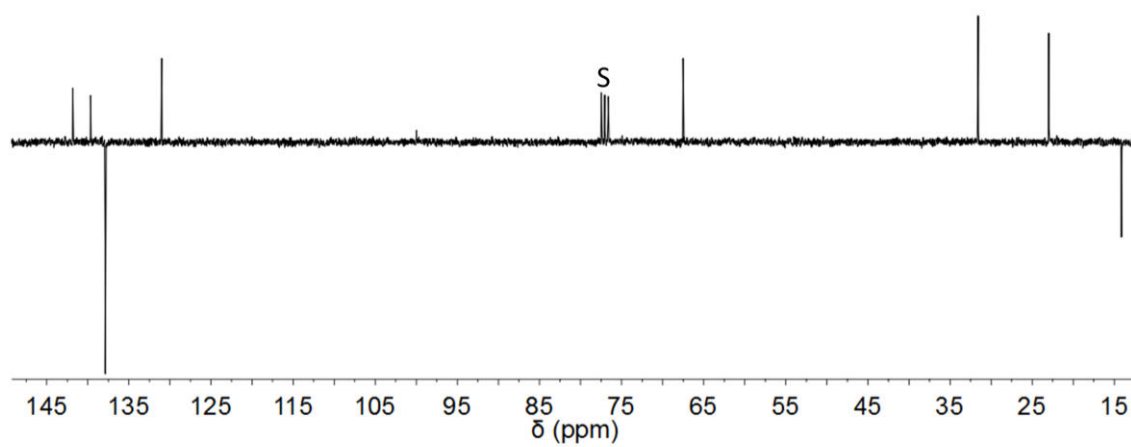


Figure 131: ^{13}C -NMR-spectrum of **6** in chloroform- d_1 (S = solvent).

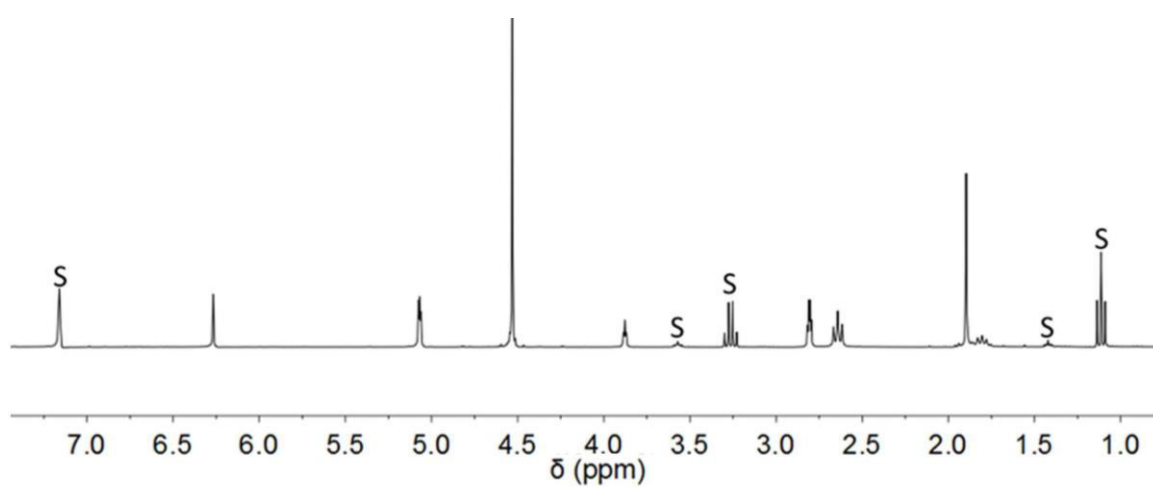


Figure 132: ^1H -NMR-spectrum of **9** in benzene- d_6 (S = solvent).

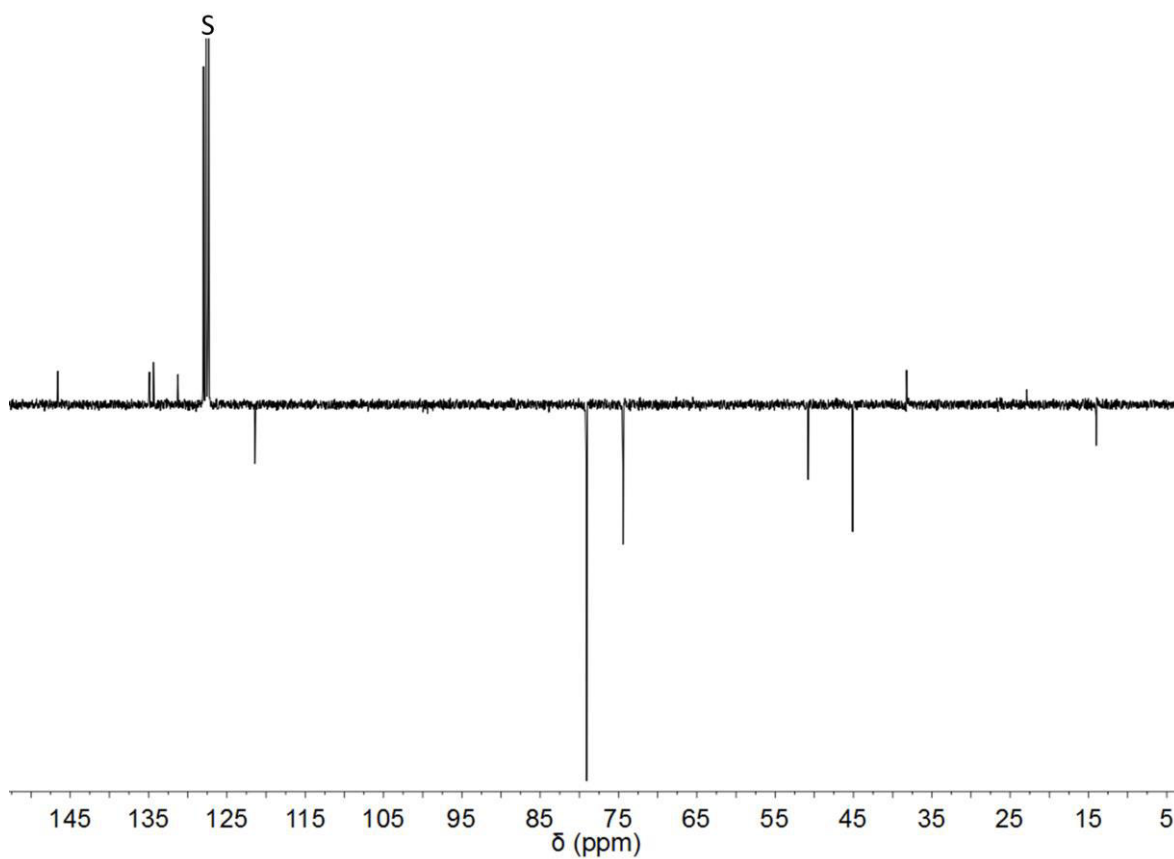


Figure 133: ^{13}C -NMR-spectrum of **9** in benzene- d_6 (S = solvent).

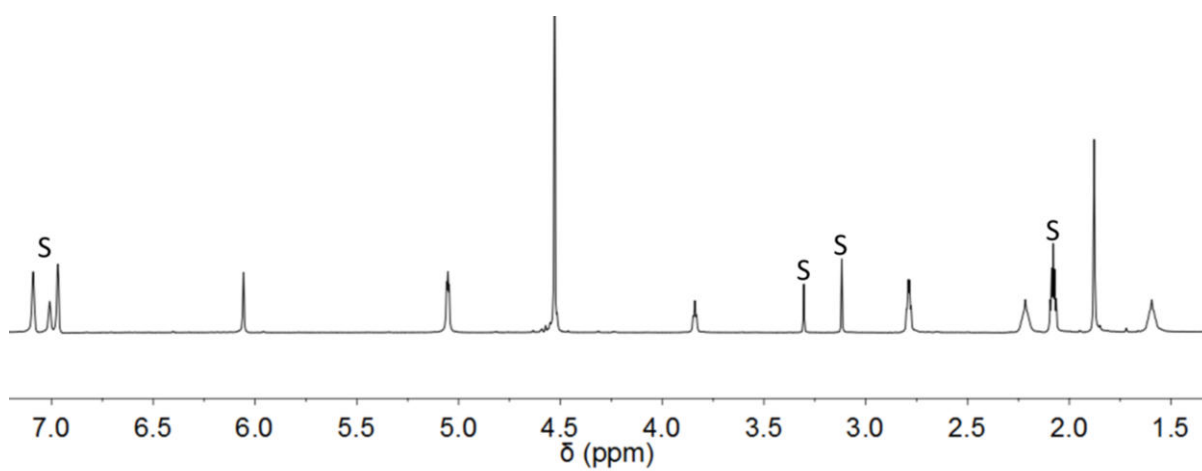


Figure 134: ^1H -NMR-spectrum of **10** in toluene- d_8 (S = solvent).

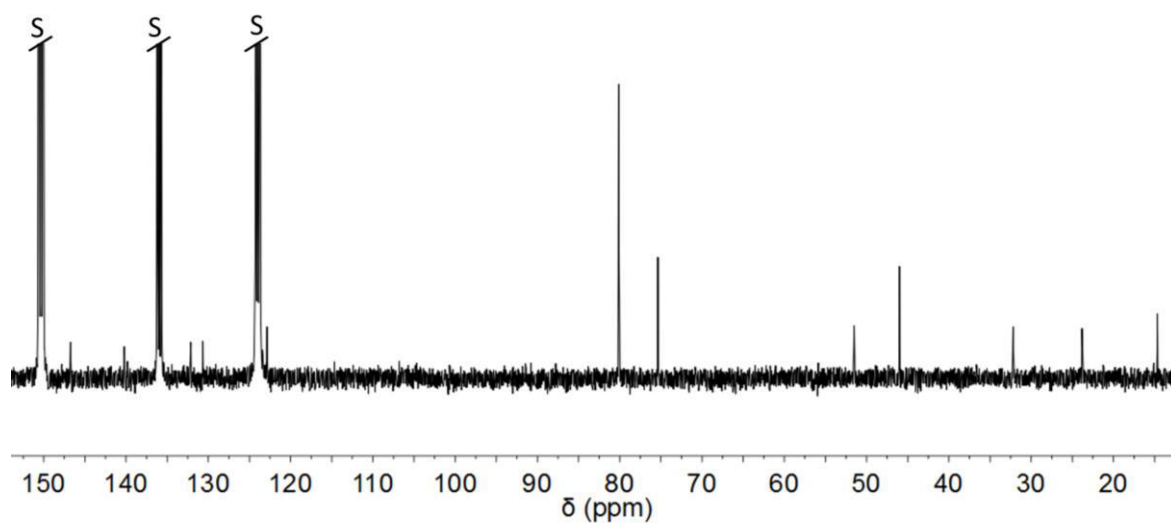


Figure 135: ^{13}C -NMR-spectrum of **10** in pyridine- d_5 (S = solvent).

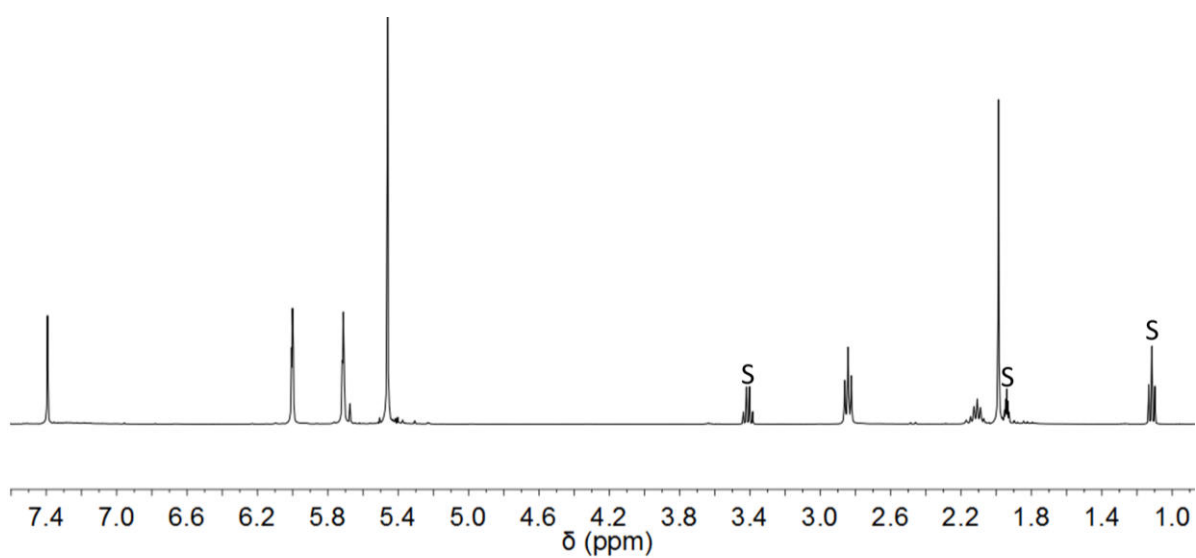


Figure 136: ^1H -NMR-spectrum of **11** in acetonitrile- d_3 (S = solvent).

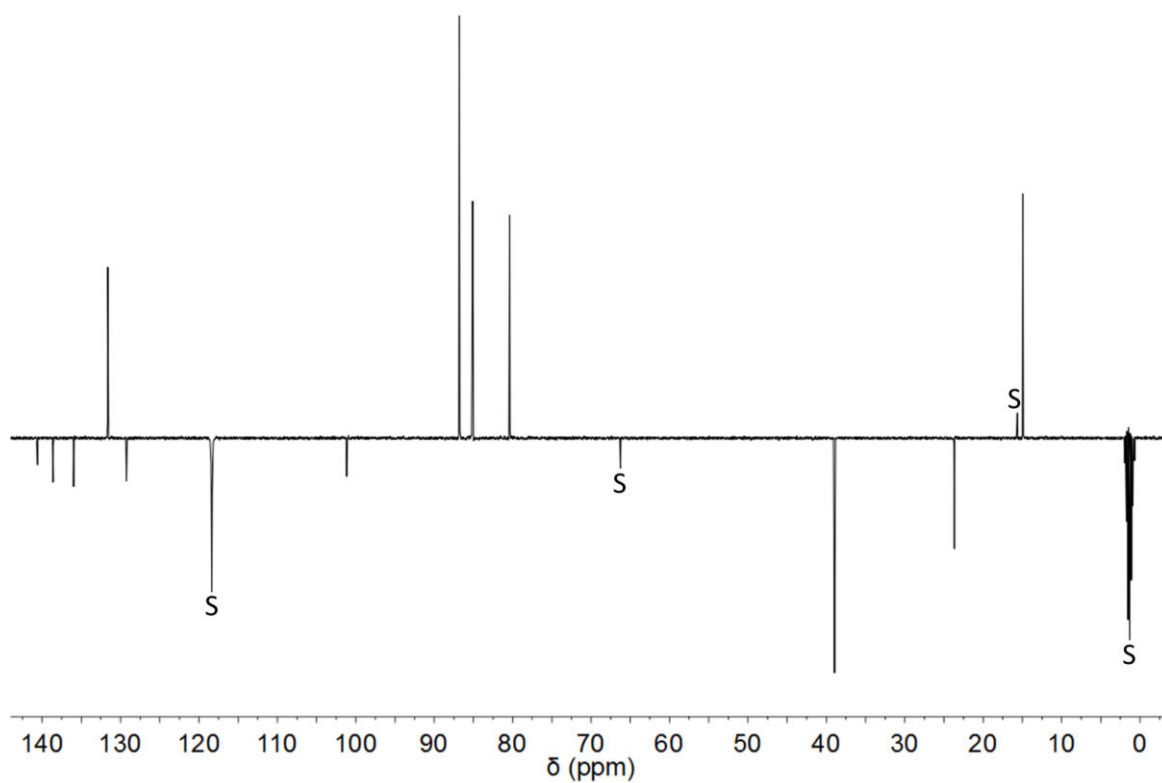


Figure 137: ^{13}C -NMR-spectrum of **11** in acetonitrile- d_3 (S = solvent).

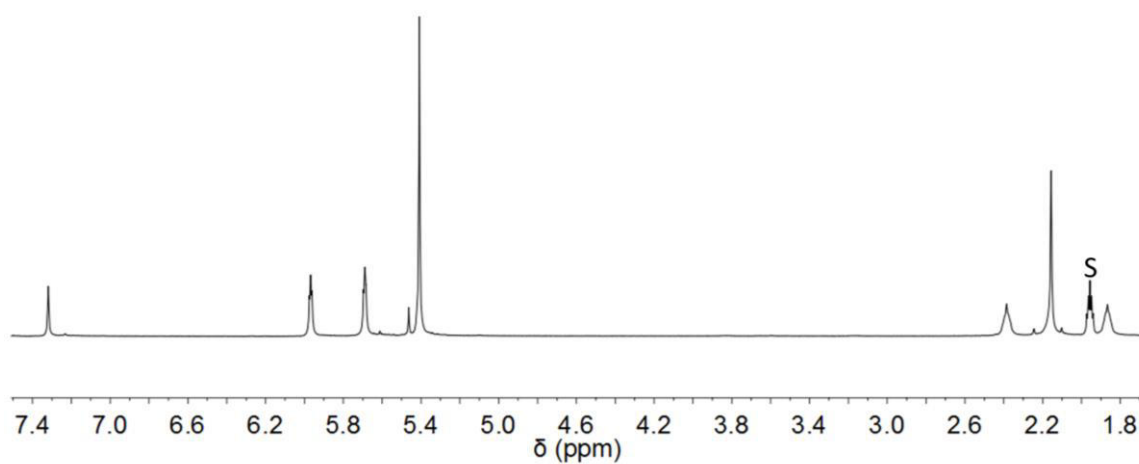


Figure 138: ^1H -NMR-spectrum of **12** in acetonitrile- d_3 (S = solvent).

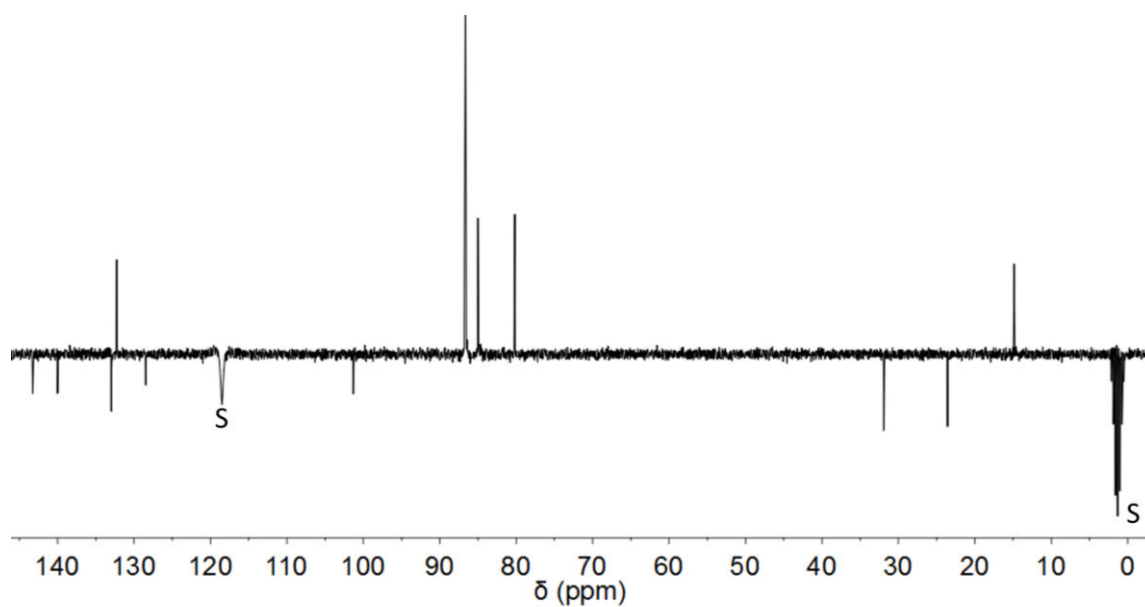


Figure 139: ^{13}C -NMR-spectrum of **12** in acetonitrile- d_3 (S = solvent).

Complex **13**, ^1H -NMR-spectrum: Figure 61.

Complex **14**, ^1H -NMR-spectrum: Figure 62.

Complex **14**, ^{13}C -NMR-spectrum: Figure 63.

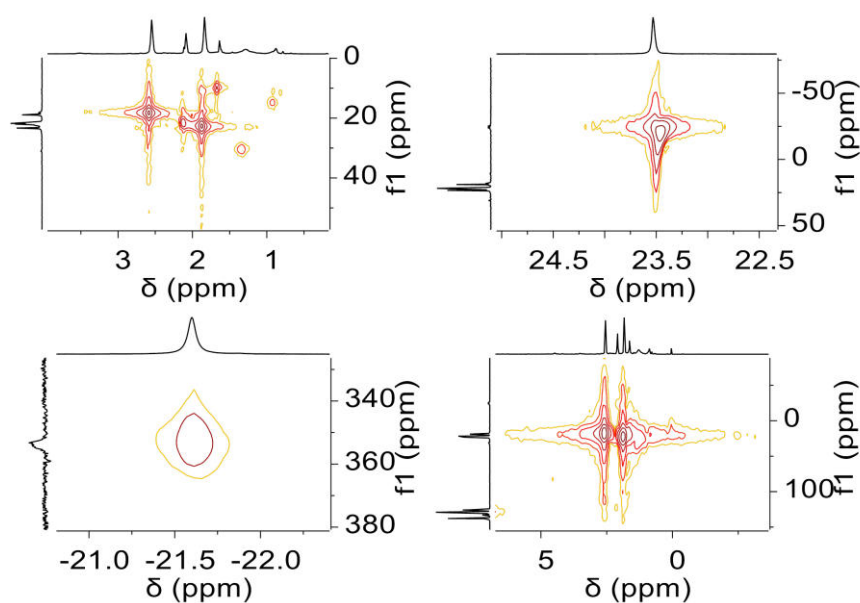


Figure 140: Cuts from the HMQC-spectrum of complex **14** in toluene- d_8 .

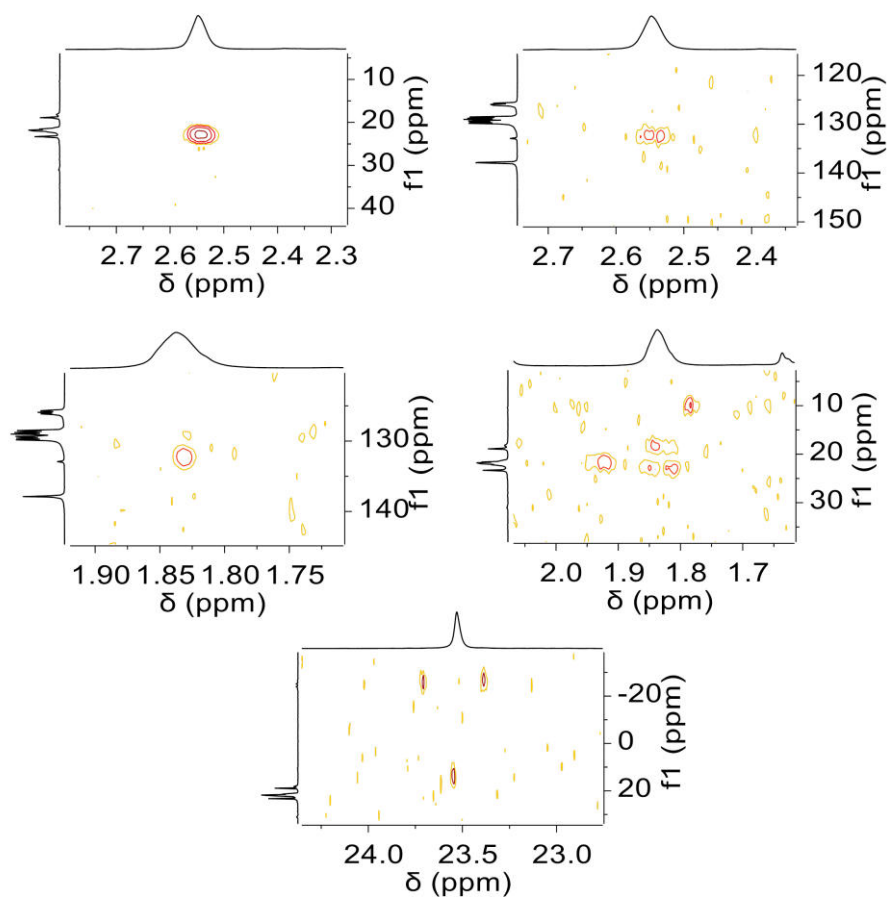


Figure 141: Cuts from the HMBC-spectrum of complex **14** in toluene- d_8 .

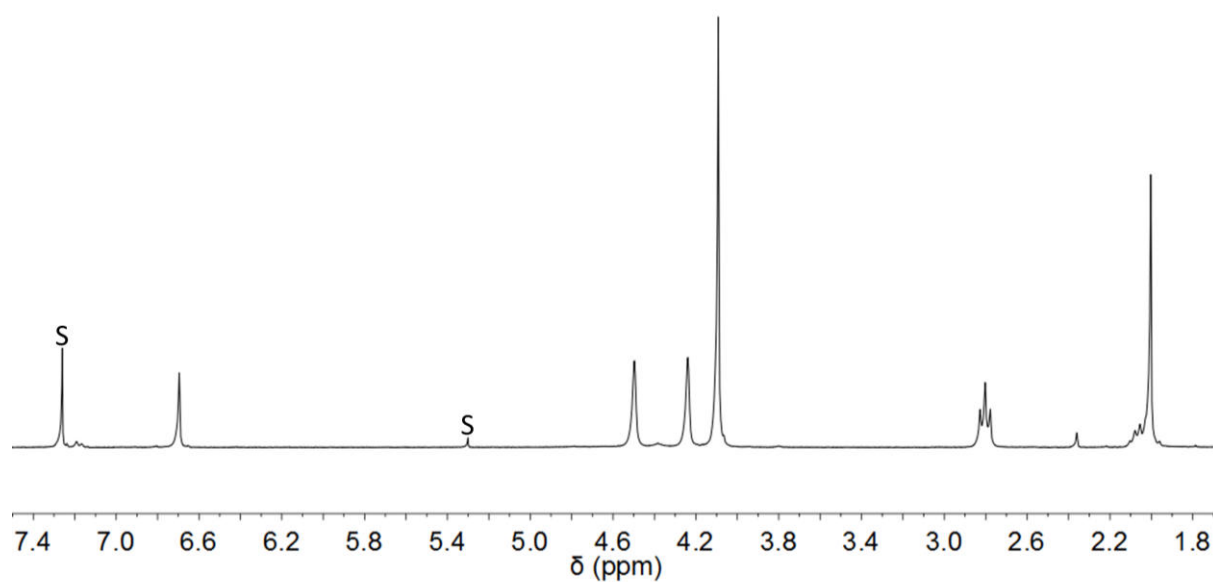


Figure 142: ^1H -NMR-spectrum of **17** in chloroform- d_1 (S = solvent).

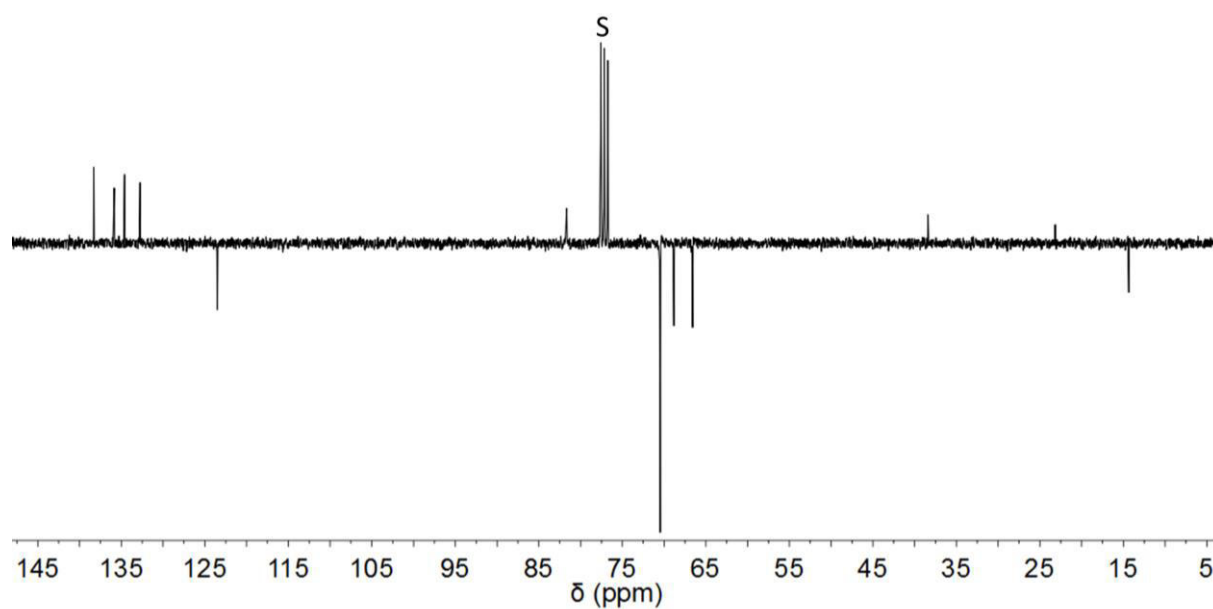


Figure 143: ^{13}C -NMR-spectrum of **17** in chloroform- d_1 (S = solvent).

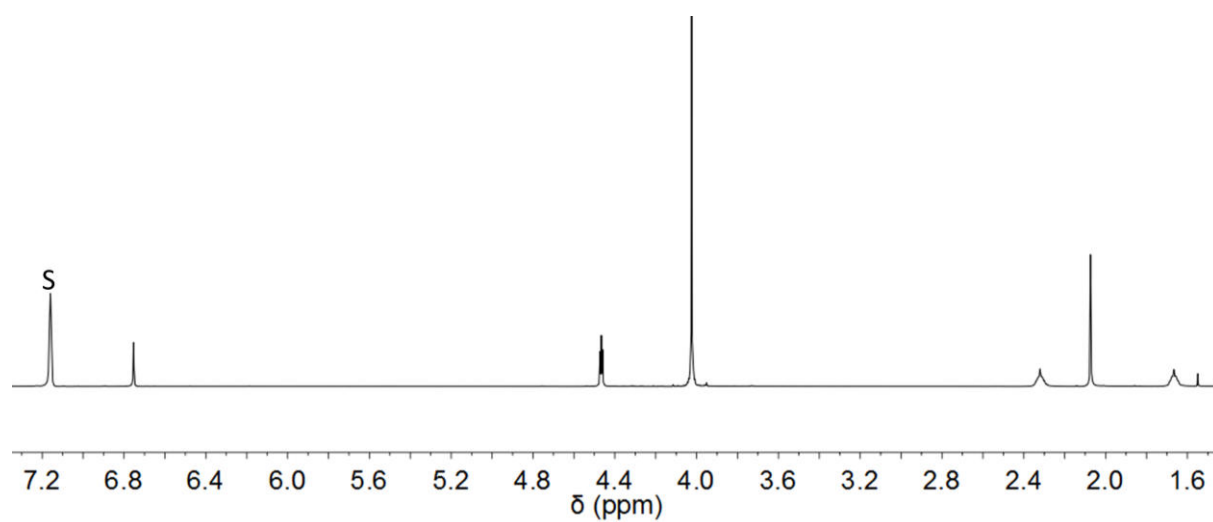


Figure 144: ^1H -NMR-spectrum of **18** in benzene- d_6 (S = solvent).

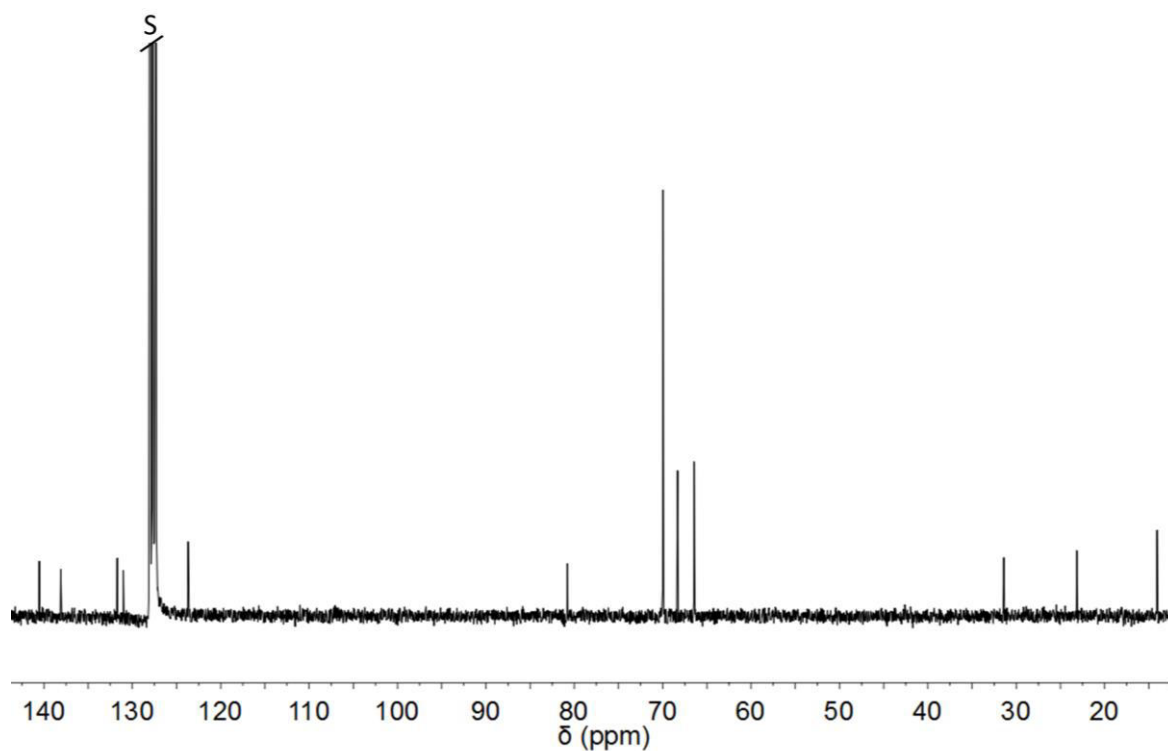


Figure 145: ^{13}C -NMR-spectrum of **18** in benzene- d_6 (S = solvent).

Complex **19**, ^1H -NMR-spectrum: Figure 60.

10.2. Crystallographic Data

Table 27: Crystallographic data for compounds **4** and **6**.

Compound	4	6
Empirical Formula	C ₁₆ H ₁₆ Cl ₂ O ₂ S ₂	C ₁₆ H ₁₆ I ₂ S ₂
Molecular weight [g/mol]	374.00	525.88
Temperature [K]	100(2)	100(2)
Wavelength [pm]	71.073	71.073
Crystal System	monoclinic	monoclinic
Space group	<i>P2₁/c</i>	<i>C2/c</i>
a, b, c [Å]	7.91890(10), 9.84320(10), 10.71330(10)	37.3853(11), 8.8061(2), 16.1944(3)
α, β, γ [°]	90.00, 93.9220(10), 90.00	90.00, 104.775(3), 90.00
Volume [Å³]	833.117(16)	5155.2(2)
Z	1	2
Density (calculated) [mg/mL]	1.496	2.373
Absorption coefficient	0.643	4.540
F(000)	388	3500
Crystal size [mm³]	1.14*1.08*0.96	0.12*0.08*0.03
θ-Range for data collection	3.31 ° to 35.00 °	2.86 ° to 29.15 °
Index ranges	-12 ≤ <i>h</i> ≤ 12 -15 ≤ <i>k</i> ≤ 15 -17 ≤ <i>l</i> ≤ 17	-50 ≤ <i>h</i> ≤ 50 -11 ≤ <i>k</i> ≤ 11 -22 ≤ <i>l</i> ≤ 21
Number of reflections collected	23412	35436
Number of independent reflections (<i>I</i> > 2σ(<i>I</i>))	3256	5280
Completeness [%]	99.9	92.9

Compound	4	6
Data/restraints/parameters	3663 /0/101	6461/0/272
Goodnes-of-fit on F^2	1.078	1.077
Final R indices [$I > 2\sigma(I)$]	$R_1 = 0.0255$, $wR_2 = 0.0712$	$R_1 = 0.0356$, $wR_2 = 0.0810$
R_1 , wR_2 (all data)	$R_1 = 0.0304$, $wR_2 = 0.0712$	$R_1 = 0.0493$, $wR_2 = 0.0870$
CCDC-Nr	1044481	1044506

Table 28: Crystallographic data for compounds 9 and 10.

Compound	9	10
Empirical Formula	$C_{35}H_{34}CO_2S_2$	$C_{36}H_{36}CO_2S_2$
Molecular weight [g/mol]	636.08	650.09
Temperature [K]	100(2)	100(2)
Wavelength [pm]	71.073	154.184
Crystal System	monoclinic	monoclinic
Space group	Pc	$P2_1/n$
a, b, c [Å]	13.4734(15), 12.4692(14), 18.407(2)	14.8756(2), 12.17150(10), 17.2963(2)
α , β , γ [°]	90.00, 99.8560(10), 90.00	90.00, 110.6720(10), 90.00
Volume [Å ³]	3046.7(6)	2930.01(6)
Z	4	4
Density (calculated) [mg/mL]	1.469	1.475
Absorption coefficient	1.254	10.375
F(000)	1404	1352
Crystal size [mm ³]	0.12*0.14*0.48	0.30*0.20*0.14
Θ -Range for data collection	1.63 ° to 27.50 °	3.38 ° to 74.99 °

10. Supporting Information

Compound	9	10
Index ranges	-17 ≤ <i>h</i> ≤ 17 -16 ≤ <i>k</i> ≤ 16 -23 ≤ <i>l</i> ≤ 23	-18 ≤ <i>h</i> ≤ 18 -15 ≤ <i>k</i> ≤ 15 -21 ≤ <i>l</i> ≤ 21
Number of reflections collected	31850	60398
Number of independent reflections (<i>I</i> > 2σ(<i>I</i>))	11706	5513
Completeness [%]	99.4	100
Data/ restraints/parameters	13729/2/755	6039/17/379
Goodnes-of-fit on <i>F</i>²	1.052	1.044
Final R indices [<i>I</i> > 2σ(<i>I</i>)]	<i>R</i> ₁ = 0.0386 , <i>wR</i> ₂ = 0.0876	<i>R</i> ₁ = 0.0429 , <i>wR</i> ₂ = 0.1036
<i>R</i>₁, <i>wR</i>₂ (all data)	<i>R</i> ₁ = 0.0492 , <i>wR</i> ₂ = 0.0931	<i>R</i> ₁ = 0.0475 , <i>wR</i> ₂ = 0.1076

Table 29: Crystallographic data for compounds **11** and **12**.

Compound	11	12
Empirical Formula	C ₃₅ H ₃₂ B ₂ CO ₂ F ₈ S ₂	C ₃₆ H ₃₄ B ₂ CO ₂ F ₈ S ₂
Molecular weight [g/mol]	808.07	822.08
Temperature [K]	100(2)	100(2)
Wavelength [pm]	154.178	154.178
Crystal System	monoclinic	orthorhombic
Space group	<i>P</i> 2 ₁ / <i>c</i>	<i>F</i> dd2
a, b, c [Å]	14.0614(2), 19.6971(2), 13.8801(2)	24.2192(2), 29.9190(3), 9.44750(10)
α, β, γ [°]	90.00, 105.3300(10), 90.00	90.00, 90.00, 90.00
Volume [Å³]	3707.57(8)	6845.79(11)
Z	4	8

Compound	11	12
Density (calculated) [mg/mL]	1.552	1.596
Absorption coefficient	8.691	9.356
F(000)	1768	3344
Crystal size [mm ³]	0.10* 0.10* 0.30	0.16* 0.05* 0.02
Θ -Range for data collection	2.5 ° to 72 °	4.70 ° to 75.96 °
Index ranges	-17 ≤ <i>h</i> ≤ 16 -24 ≤ <i>k</i> ≤ 24 -16 ≤ <i>l</i> ≤ 16	-30 ≤ <i>h</i> ≤ 30 -37 ≤ <i>k</i> ≤ 37 -11 ≤ <i>l</i> ≤ 11
Number of reflections collected	70276	28183
Number of independent reflections (<i>I</i> > 2σ(<i>I</i>))	6430	3440
Completeness [%]	98.9	99.6
Data/restraints/parameters	6952/0/482	3535/1/227
Goodnes-of-fit on <i>F</i> ²	2.294	1.073
Final R indices [<i>I</i> > 2σ(<i>I</i>)]	<i>R</i> ₁ = 0.0608, <i>wR</i> ₂ = 0.1630	<i>R</i> ₁ = 0.0264, <i>wR</i> ₂ = 0.0676
<i>R</i> ₁ , <i>wR</i> ₂ (all data)	<i>R</i> ₁ = 0.0693, <i>wR</i> ₂ = 0.1640	<i>R</i> ₁ = 0.0274, <i>wR</i> ₂ = 0.0682

Table 30: Crystallographic data for compounds **17** and **18**.

Compound	17	18
Empirical Formula	C ₃₅ H ₃₂ Fe ₂ S ₂	C ₃₆ H ₃₄ Fe ₂ S ₂
Molecular weight [g/mol]	628.06	642.08
Temperature [K]	100(2)	100(2)
Wavelength [pm]	71.073	71.073
Crystal System	orthorhombic	monoclinic
Space group	P2 ₁ 2 ₁ 2	P2 ₁ /c

10. Supporting Information

Compound	17	18
a, b, c [Å]	10.0629(2), 19.4763(5), 7.94240(10)	12.91950(10), 12.81980(10), 17.6591(2)
α, β, γ [°]	90.00, 90.00, 90.00	90.00, 91.1570(10), 90.00
Volume [Å ³]	1556.62(5)	2924.20(5)
Z	2	1
Density (calculated) [mg/mL]	1.516	1.459
Absorption coefficient	1.263	1.160
F(000)	730	1336
Crystal size [mm ³]	0.20*0.20*0.03	
Θ -Range for data collection	2.91 ° to 27.99 °	2.80 ° to 28.00 °
Index ranges	-13 ≤ h ≤ 13 -25 ≤ k ≤ 25 -10 ≤ l ≤ 9	-17 ≤ h ≤ 17 -16 ≤ k ≤ 16 -22 ≤ l ≤ 22
Number of reflections collected	20802	38879
Number of independent reflections ($I > 2\sigma(I)$)	3044	5895
Completeness [%]	99.0	98.4
Data/ restraints/parameters	3674/0/192	6938/0/363
Goodnes-of-fit on F^2	1.059	1.053
Final R indices [$I > 2\sigma(I)$]	$R_1 = 0.0432, wR_2 = 0.0817$	$R_1 = 0.0313, wR_2 = 0.0718$
R1, wR2 (all data)	$R_1 = 0.0626, wR_2 = 0.0903$	$R_1 = 0.0406, wR_2 = 0.0761$

The CIF's files are in possession of Prof. Dr. Jürgen Heck.

11. Curriculum Vitae

Personal Information

Name	Alejandra Escribano Sanvicente
Address	
Date and Place of Birth	08.01.1985 in Vitoria, Spain
Nationality	Spanish

Education

07/2015	End of the Ph-D studies
10/2009	Start of the Ph-D studies in the research group of Prof. Dr. J. Heck (“Molecular Switches Connecting Paramagnetic Metallocenes”)
09/2003 – 07/2009	Academic studies at the University of Zaragoza (Spain) Diploma in Chemistry
10/2008 – 07/2009	Academic studies at the Westfälische Wilhelms-Universität Münster (Germany) with the financial support of the “Socrates-Erasmus Program” Diploma thesis in the research group of Prof. Dr. W. Seidel: “Coordination Chemistry of Sulfur- and Phosphorusubstituted Alkynes”
09/2007 – 07/2008	Academic studies at the University of Granada (Spain) with the financial support of the “Programa Séneca”
09/1999 – 05/2003	University entrance qualification at “Colegio Santa María – Marianistas” in Vitoria, Spain

Professional Experience

since 10/2009	Research assistant at the Institute of Inorganic and Applied Chemistry, University of Hamburg <ul style="list-style-type: none"> - Laboratory and research laboratory assistance (chemistry and biology students) - Seminars, exercise courses - Exams and laboratory reports correction
03/2000 – 09/2003	Riding instructor (Children: 4 – 10 years) in „Club Hípico Gopegi“ in Vitoria, Spain

Stays Abroad

07/1999	Four weeks in Nottingham (England) living with a host family
05/2000	One week in Paris (France) living with a host family (" <i>Santa María – Marianistas</i> School Exchange Program")
07/2000	Four weeks in Torquay (England) living with a host family
since 09/2008	Studies in Germany

Participations at Conferences

08/2010	"3 rd EuCheMS Chemistry Congress" in Nürnberg, Germany (Poster)
03/2011	"13 th JCF-Frühjahrssymposium" in Erlangen, Germany (Poster)
09/2011	"2 nd Status-Workshop of the LEXI-Cluster "Nano-Spintronics" in Hamburg, Germany (Presentation: "Optical Switches in Molecular Magnets")
09/2011	"14 th Norddeutsches Doktorandenkolloquium" in Walsrode, Germany (Presentation: " <i>Molekulare Schalter in Molekularen Magneten</i> ")
02/2012	"10 th Ferrocene Colloquium" in Braunschweig, Germany (Poster)
09/2012	"25 th International Conference on Organometallic Chemistry" in Lissabon, Portugal (Poster)
09/2012	"International Workshop: Contacts to and within Molecules" in Hamburg, Germany (Presentation: "Photochromic Switches Connecting Paramagnetic Metallocenes")

Publications

2015	T. Steenbock, A. Escribano, J. Heck, C. Herrmann, <i>Chem. Phys. chem.</i> 2015 , <i>16</i> , 1491–1501.
------	---

Additional Skills and Competences

Foreign Languages	Spanish:	First language
	German:	Fluent
	English:	Good knowledge

Computer Skills	Very good knowledge in Windows-Office-Package Very good knowledge in Nuts, MestReNova, Nova, Origin 11.0 Chem Draw 11.0
-----------------	---

Personal Interest

Leisure Time Activities	Reading historical novels, fishkeeping
-------------------------	--

Driving License	Class B
-----------------	---------

Hamburg, 15.07.2015